forests

IMPACT FACTOR 2.221

Fine Root and Soil Nitrogen Dynamics during Stand Development Following Shifting Agriculture in Northeast India

Volume 11 · Issue 12 | December 2020

MDPI

mdpi.com/journal/forests
ISSN 1999-4907

IMPACT FACTOR 2.221

forests

Submit to Forests

Review for Forests

Journal Menu

- Forests Home
- Aims & Scope
- Editorial Board
- Reviewer Board
- Topics Board
- Instructions for Authors
- Special Issues
- Sections & Collections
- Article Processing Charge
- Indexing & Archiving
- Editor's Choice Articles
- Most Cited & Viewed
- Journal Statistics
- Journal History
- Journal Awards
- Editorial Office

Journal Browser

Volume

Issue

Go

Forthcoming issue

Current issue

Vol. 12 (2021) Vol. 6 (2015)
Vol. 11 (2020) Vol. 5 (2014)
Vol. 10 (2019) Vol. 4 (2013)
Vol. 9 (2018) Vol. 3 (2012)
Vol. 8 (2017) Vol. 2 (2011)
Vol. 7 (2016) Vol. 1 (2010)

Editorial Board

- Editorial Board
- Forest Ecology and Management Section
- Forest Ecophysiology and Biology Section
- Forest Economics, Policy, and Social Science Section
- Forest Inventory, Modeling and Remote Sensing Section
- Wood Science and Forest Products Section
- Genetics and Molecular Biology Section

Editors (12)

Prof. Dr. Timothy A. Martin Website SciProfiles
Editor-in-Chief
School of Forest Resources and Conservation, PO Box 110410, University of Florida, Gainesville, Florida, 32611-0410, USA
Interests: tree ecophysiology; forest biology; silviculture; stand dynamics; carbon sequestration; water relations
Special Issues and Collections in MDPI journals

Dr. Carol A. Loopstra Website SciProfiles
Section Editor-in-Chief
Department of Ecosystem Science and Management, Texas A&M University, MS 2138, College Station, TX 77843-2138, USA
Interests: conifer genomics; tree improvement; drought resistance; gene expression; wood development; dendroecology
Special Issues and Collections in MDPI journals

Dr. Olga Viedma Website SciProfiles
Section Editor-in-Chief
Department of Environmental Sciences, University of Castilla-La Mancha, Avda. Carlos III, 45071 Toledo, Spain
Interests: remote sensing; Lidar; forest fires; land use-land cover changes; statistical models
Special Issues and Collections in MDPI journals

Dr. Angela Lo Monaco Website SciProfiles
Section Editor-in-Chief
Department of Agriculture and Forest Science, University of Tuscia, Via San Camillo de Lellis snc, 01100 Viterbo, Italy
Interests: wood characterisation; wood anatomy; wood modification; wood coating; mechanical testing; physical testing; wood properties; wood quality; tree growth; forest products; forest resource management; sustainability; wood in cultural heritage; wood in religious art
Special Issues and Collections in MDPI journals

Prof. Dr. Luis Diaz-Balteiro Website SciProfiles
Section Editor-in-Chief
Department of Forest and Environmental Engineering and Management, Universidad Politécnica de Madrid, Madrid, Spain
Interests: forest management; forest sustainability; multi-criteria decision-making techniques
Special Issues and Collections in MDPI journals

Dr. L. Monika Moskal Website SciProfiles
Section Editor-in-Chief
School of Environmental and Forest Sciences, College of the Environment, University of Washington (UW), Director, UW Precision Forestry Cooperative and Remote Sensing and Geospatial Analysis Laboratory, Washington, Box 352100, Seattle WA 98195-2100, USA
Interests: ALT; TLS; MLS; lidar precision forestry; hyper-resolution (spatial, temporal, spectral) remote sensing; ecosystem services
Special Issues and Collections in MDPI journals

Dr. Cate Macinnis-Ng Website SciProfiles
Section Editor-in-Chief
Department of Biological Sciences, Faculty of Science, University of Auckland, Private Bag 92019, Auckland 1142, New Zealand
Interests: plant ecophysiology; carbon and water cycles; forest function; global change
Special Issues and Collections in MDPI journals

Prof. Dr. Stefan Arndt Website SciProfiles
Section Editor-in-Chief
School of Ecosystem and Forest Sciences, The University of Melbourne, 500 Yarra Boulevard, Richmond, 3121, Victoria, Australia
Interests: plant ecophysiology; stress physiology; drought tolerance; water relations; forest growth and carbon balance; trace gas emissions

Dr. Damian C. Adams Website SciProfiles
Section Editor-in-Chief
School of Forest Resources and Conservation, University of Florida, 355 Newins-Ziegler Hall, Gainesville, FL 32611-0410, USA
Interests: nonmarket valuation; economic analysis; ecosystem services; invasive species; policy analysis; choice modeling; survey methods; bioeconomic modeling
Special Issues and Collections in MDPI journals

Prof. Dr. Eric J. Jokela Website SciProfiles
Founding Editor-in-Chief
School of Forest Resources and Conservation, University of Florida, 353 Newins-Ziegler Hall, PO Box 110410, Gainesville, FL 32611-0410, USA
Interests: tree nutrition; production ecology; nutrient cycling; forest soil carbon management; silvicultural management systems
Special Issues and Collections in MDPI journals

Dr. Libby Pinkard * Website SciProfiles
Founding Section Editor-in-Chief
CSIRO Land and Water, Private Bag 12, Hobart 7000, TAS, Australia
Interests: tree physiology; climate change; environmental stress; forest management; pests and diseases
* Section Forest Ecology and Management

Prof. Dr. Dave Verbyla * Website SciProfiles
Founding Section Editor-in-Chief
Department of Forest Sciences, School of Natural Resources and Agricultural Sciences, University of Alaska Fairbanks, Fairbanks, AK 99775-7200, USA
Interests: remote sensing; geographic information systems; spatial analysis; multi-temporal trends in boreal forests; boreal wildfire severity; bias in change detection estimates; GIS analysis techniques
* Section Forest Inventory, Quantitative Methods and Remote Sensing
Special Issues and Collections in MDPI journals

Editorial Board Members (425)

Filter Editorial Board Members Filter

Dr. Mauricio Acuna Website SciProfiles
Forest Research Institute, University of the Sunshine Coast, Locked Bag 4, Maroochydore DC, QLD 4558, Australia
Interests: wood and biomass supply chain optimization; sensor technology; transport optimization; forest planning
Special Issues and Collections in MDPI journals:
Special Issue in *Forests*: Supply Chain Optimization for Biomass and Biofuels
Special Issue in *Forests*: Operations Research and Optimisation Techniques in Forest Management and Operations

Special Issue in *Sustainability*: Forest Engineering and Sustainable Forest Bioenergy

Dr. Bartosz Adamczyk Website
Natural Resources Institute Finland (Luke), Latokartanonkaari 9, 00790 Helsinki, Finland
Interests: plant and soil biochemistry; plant-soil-microbial interactions; climate change; plant secondary compounds; chromatography; isotopes; plant biochemistry; plant physiology; greenhouse gases; carbon sequestration; soil organic matter; boreal forests

Prof. Dr. Francisca C. Aguiar Website SciProfiles
Centro de Estudos Florestais, Instituto Superior de Agronomia, Universidade de Lisboa, Tapada da Ajuda, 1349-017, Lisbon, Portugal
Interests: riparian forests; macrophytes; ecosystem services; biogeography; functional ecology; adaptation to climate change; effects of land-use and stream flow regulation; indicators of ecological quality; weeds; invasive alien plants
Special Issues and Collections in MDPI journals:
Special Issue in *Forests*: Spatial and Temporal Patterns and Ecosystem Services of Riparian Forests
Special Issue in *Water*: Vulnerability and Conservation of Freshwater Biodiversity

Dr. Iciar Alberdi Website SciProfiles
National Institute of Agricultural Research, Centre for Forest Research, La Coruña km 7.5 28040 Madrid, Spain
Interests: forest monitoring; National Forest Inventory; conservation; natural resources management; forest biodiversity indicators; forest information harmonization
Special Issues and Collections in MDPI journals:
Special Issue in *Forests*: Forest Resources Assessments: Mensuration, Inventory and Planning

Dr. Auro C. Almeida Website SciProfiles
Commonwealth Scientific and Industrial Research Organisation (CSIRO), Private Bag 12, Hobart TAS 7001, Australia
Interests: tree ecophysiology; forest hydrology; process-based modelling; water relations; catchment and basin management; climate change adaptation

Dr. Pedro Álvarez-Álvarez Website SciProfiles
Department of Organisms and Systems Biology, Polytechnic School of Mieres, University of Oviedo, E-33600 Mieres, Asturias, Spain
Interests: forest ecosystems; ecosystems services; spatial patterns; ecological process; multi-scale
Special Issues and Collections in MDPI journals:
Special Issue in *Forests*: Patterns and Processes of Forest Ecosystem Services
Special Issue in *Environments*: Soil Nutrient Dynamics and Plant Response

Prof. Dr. Artur Alves Website SciProfiles
Centro de Estudos do Ambiente e do Mar, Departamento de Biologia, Universidade de Aveiro, Campus Universitário de Santiago, 3810-193 Aveiro, Portugal
Interests: plant pathology; fungi; taxonomy; biological control; plant-microbe interactions

Prof. Dr. Arild Angelsen Website SciProfiles
School of Economics and Business, Norwegian University of Life Sciences (NMBU), P.O. Box 5003, 1432 Ås, Norway
Interests: climate and forest (REDD); environmental income; international climate policy; poverty analysis; tropical deforestation

Dr. Cristina Aponte Website SciProfiles
National Institute for Research and Development in Forestry "Marin Drăcea", 128 Blvd. Eroilor, Voluntari 077190, Ilfov, Romania
Interests: plant-soil interactions; climate change; forest fires; functional ecology; mycorrhizal ecology; forest ecology; remote sensing; forest management; forest modeling; forest carbon; forest disturbances

Dr. José Aranha Website SciProfiles
Department of Forestry Sciences and Landscape Architecture (CIFAP), University of Trás-os-Montes and Alto Douro, 5001-801 Vila Real, Portugal
Interests: forestry inventory; spatial analysis; biomass; wild fires; ecosystem services
Special Issues and Collections in MDPI journals:
Special Issue in *Forests*: Applications of Remote Sensing Data in Mapping of Forest Growing Stock and Biomass

MDPI

Subscribe to receive issue release notifications and newsletters from MDPI journals

Acoustics
Actuators
Administrative Sciences
Adolescents

Enter your email address...

Subscribe

Further Information
Article Processing Charges
Pay an Invoice
Open Access Policy
Contact MDPI
Jobs at MDPI

Guidelines
For Authors
For Reviewers
For Editors
For Librarians
For Publishers
For Societies

MDPI Initiatives
Institutional Open Access Program (IOAP)
Sciforum
Preprints
Scilit
SciProfiles
MDPI Books
Encyclopedia
JAMS
Proceedings
MDPI Blog

Follow MDPI
LinkedIn
Facebook
Twitter

© 1996-2021 MDPI (Basel, Switzerland) unless otherwise stated Disclaimer Terms and Conditions Privacy Policy

IMPACT FACTOR 2.633 CITESCORE 3.3 SCOPUS

forests

Submit to *Forests*

Review for *Forests*

Edit a Special Issue

Journal Menu

- *Forests* Home
- Aims & Scope
- Editorial Board
- Reviewer Board
- Topical Advisory Panel
- Instructions for Authors
- Special Issues
- Sections & Collections
- Article Processing Charge
- Indexing & Archiving
- Editor's Choice Articles
- Most Cited & Viewed
- Journal Statistics
- Journal History
- Journal Awards
- Editorial Office

Journal Browser

volume

issue

Go

Forthcoming issue
Current issue

Vol. 12 (2021) Vol. 6 (2015)
Vol. 11 (2020) Vol. 5 (2014)
Vol. 10 (2019) Vol. 4 (2013)
Vol. 9 (2018) Vol. 3 (2012)
Vol. 8 (2017) Vol. 2 (2011)
Vol. 7 (2016) Vol. 1 (2010)

Special Issue "Timber and Construction Structure"

- Print Special Issue Flyer
- Special Issue Editors
- Special Issue Information
- Keywords
- Published Papers

A special issue of *Forests* (ISSN 1999-4907). This special issue belongs to the section "Wood Science and Forest Products".

Deadline for manuscript submissions: **closed (10 March 2021)**.

Share This Special Issue

Special Issue Editors

Prof. Dr. Miroslav Premrov E-Mail Website SciProfiles
Guest Editor
Faculty of Civil Engineering, Transportation Engineering and Architecture, University of Maribor, Smetanova ulica 17, 2000, Maribor, Slovenia
Interests: timber structures; composite structures; timber–glass buildings; structural analysis; energy-efficient timber buildings

Prof. Dr. Vesna Žegarac Leskovar E-Mail Website SciProfiles
Guest Editor
Faculty of Civil Engineering, Transportation Engineering and Architecture, University of Maribor, Smetanova ulica 17, 2000, Maribor, Slovenia
Interests: architecture; sustainable building design; timber–glass buildings, energy-efficient timber buildings; LCA

Special Issue Information

Dear Colleagues,

As a natural raw material, timber shows indisputable environmental excellence and is undoubtedly one of the best choices for sustainable construction. Timber has good mechanical properties and ensures a comfortable indoor climate in addition to playing an important role in the reduction of CO_2 emissions. Besides the ecological benefits, there are currently further additional strong arguments in favor of building timber structures. Brand new and improved features introduced in the early 1980s brought about a significant expansion in timber buildings all over the world. Moreover, the development of new timber products in the last few decades (cross-laminated timber, for instance, at the beginning of the 1990s) encouraged advances in the form and especially the height of timber buildings, which made timber structures competitive with other structures built with classical building materials. Today, timber buildings with a height up to 20 stories can be built in a cross-laminated structural system. Furthermore, combining timber structural elements with other building materials (for instance, with glass, brick, concrete, or steel) can open new perspectives on attractive architectural forms of such hybrid timber buildings.

This Special Issue of *Forests* will present current research from different fields of timber buildings, such as experimental and numerical analysis on the structural stability of multi-story and hybrid timber buildings and structural modeling of composite timber elements, as well as strengthening methods of old timber structures. The second aim of this Special Issue is to emphasize the importance of interdisciplinary and integrative approaches when considering the issue of timber building design. Therefore, topics relating to various architectural aspects of the design of highly attractive timber structures, considering energy efficiency, daylighting, indoor environmental quality, life-cycle assessment, and other parameters, are also welcome.

Prof. Dr. Miroslav Premrov
Prof. Dr. Vesna Žegarac Leskovar
Guest Editors

Manuscript Submission Information

Manuscripts should be submitted online at www.mdpi.com by registering and logging in to this website. Once you are registered, click here to go to the submission form. Manuscripts can be submitted until the deadline. All papers will be peer-reviewed. Accepted papers will be published continuously in the journal (as soon as accepted) and will be listed together on the special issue website. Research articles, review articles as well as short communications are invited. For planned papers, a title and short abstract (about 100 words) can be sent to the Editorial Office for announcement on this website.

Submitted manuscripts should not have been published previously, nor be under consideration for publication elsewhere (except conference proceedings papers). All manuscripts are thoroughly refereed through a single-blind peer-review process. A guide for authors and other relevant information for submission of manuscripts is available on the Instructions for Authors page. *Forests* is an international peer-reviewed open access monthly journal published by MDPI.

Please visit the Instructions for Authors page before submitting a manuscript. The Article Processing Charge (APC) for

publication in this open access journal is 1800 CHF (Swiss Francs). Submitted papers should be well formatted and use good English. Authors may use MDPI's English editing service prior to publication or during author revisions.

Keywords

- Wood as a structural material
- New wood products
- Multi-story timber buildings
- Hybrid timber buildings
- Structural modeling
- Structural analysis
- Energy-efficient timber buildings
- LCA of timber buildings

Published Papers (8 papers)

Download All Papers

Order results: Content type

Result details: Normal

Show export options

Research

Jump to: Review

Open Access Article

Defect Index of Timberwork in House, Korea

by Junmo Park and Deokseok Seo

Forests 2021, *12*(7), 896; https://doi.org/10.3390/f12070896 - 08 Jul 2021

Viewed by 374

Abstract Wood is a material that is familiar to humans and environment-friendly, and it is used widely as a building material. However, as the dispute over housing defects have increased in Korea, various defects have occurred in timberwork and have become disputes. Notwithstanding, efforts [...] Read more.

(This article belongs to the Special Issue Timber and Construction Structure)

► Show Figures

Open Access Article

Analytical and Numerical Verification of Vibration Design in Timber Concrete Composite Floors

by Nikola Perković, Vlatka Rajčić and Jure Barbalić

Forests 2021, *12*(6), 707; https://doi.org/10.3390/f12060707 - 29 May 2021

Viewed by 702

Abstract The TCC concept has been studied and developed over the past decades. The variety of solutions shows the meaningfulness and functionality of this system, as well as the continuous work of scientists over time. To benefit from these advantages, the composite needs to [...] Read more.

(This article belongs to the Special Issue Timber and Construction Structure)

► Show Figures

Open Access Article

Ultrasonic Signal Transmission Performance in Bolted Connections of Wood Structures under Different Preloads

by Zilong Zhuang, Yabin Yu, Ying Liu, Jiawei Chen and Zhengguang Wang

Forests 2021, *12*(6), 652; https://doi.org/10.3390/f12060652 - 21 May 2021

Viewed by 396

Abstract In industrial applications, bolt connections are simple and economical, contributing to their popularity for use in wood packing boxes. However, they can easily fail when subjected to a continuous vibrational load under usual working conditions such as transportation and hoisting. Based on an [...] Read more.

(This article belongs to the Special Issue Timber and Construction Structure)

► Show Figures

Open Access Article

The Prediction of Stiffness Reduction Non-Linear Phase in Bamboo Reinforced Concrete Beam Using the Finite Element Method (FEM) and Artificial Neural Networks (ANNs)

by Muhtar

Forests 2020, *11*(12), 1313; https://doi.org/10.3390/f11121313 - 10 Dec 2020

Viewed by 500

Abstract This paper discusses the reduction of the stiffness of bamboo reinforced concrete (BRC) beams to support the use of bamboo as an environmentally friendly building material. Calculation of cross-section stiffness in numerical analysis is very important, especially in the non-linear phase. After the [...] Read more.

(This article belongs to the Special Issue Timber and Construction Structure)

► Show Figures

Open Access Article

Loosening of Bolted Connections under Transverse Loading in Timber Structures

by Jiawei Chen, Honghong Wang, Yabin Yu, Ying Liu and Dong Jiang
Forests 2020, *11*(8), 816; https://doi.org/10.3390/f11080816 - 28 Jul 2020
Cited by 2 | Viewed by 856

Abstract Bolted joints are widely used in timber structures, and the loosening of bolt connections will reduce the structural performance. In this paper, a mechanical model of bolt connection for timber structures is established, and the process of bolt loosening under a transverse load [...] Read more.
(This article belongs to the Special Issue Timber and Construction Structure)

► Show Figures

Open Access Article

Influence of Board Density on the Physical and Mechanical Properties of Bamboo Oriented Strand Lumber

by Yuhui Sun, Yahui Zhang, Yuxiang Huang, Xiaoxin Wei and Wenji Yu
Forests 2020, *11*(5), 567; https://doi.org/10.3390/f11050567 - 18 May 2020
Cited by 2 | Viewed by 850

Abstract The process of bamboo-oriented strand lumber (BOSL) represents one of the best opportunities for automation, property control and consistency, and high utilization of material from abundant, fast-growing, and sustainable bamboo. In this study, BOSLs were prepared, with reference to the preparation process of [...] Read more.
(This article belongs to the Special Issue Timber and Construction Structure)

► Show Figures

Review

Jump to: Research

Open Access Review

A Review of Architectural and Structural Design Typologies of Multi-Storey Timber Buildings in Europe

by Vesna Žegarac Leskovar and Miroslav Premrov
Forests 2021, *12*(6), 757; https://doi.org/10.3390/f12060757 - 08 Jun 2021
Cited by 1 | Viewed by 632

Abstract Numerous countries across the globe have witnessed the recent decades' trend of multi-storey timber buildings on the rise, owing to advances in engineering sciences and timber construction technologies. Despite the growth and numerous advantages of timber construction, the global scale of multi-storey timber [...] Read more.
(This article belongs to the Special Issue Timber and Construction Structure)

► Show Figures

Open Access Review

Structural Vulnerability Assessment of Heritage Timber Buildings: A Methodological Proposal

by Amirhosein Shabani, Mahdi Kioumarsi, Vagelis Plevris and Haris Stamatopoulos
Forests 2020, *11*(8), 881; https://doi.org/10.3390/f11080881 - 13 Aug 2020
Cited by 4 | Viewed by 1347

Abstract The conservation of heritage structures is pivotal not only due to their cultural or historical importance for nations, but also for understanding their construction techniques as a lesson that can be applied to contemporary structures. Timber is considered to be the oldest organic [...] Read more.
(This article belongs to the Special Issue Timber and Construction Structure)

► Show Figures

Show export options

Displaying articles 1-8

MDPI

Subscribe to receive issue release notifications and newsletters from MDPI journals

Select options

Enter your email address...

Subscribe

Further Information
Article Processing Charges
Pay an Invoice
Open Access Policy
Contact MDPI
Jobs at MDPI

Guidelines
For Authors
For Reviewers
For Editors
For Librarians
For Publishers
For Societies

MDPI Initiatives
Sciforum
MDPI Books
Preprints
Scilit
SciProfiles
Encyclopedia
JAMS
Proceedings Series

Follow MDPI
LinkedIn
Facebook
Twitter

IMPACT FACTOR 2.221

forests

Submit to Forests

Review for Forests

Journal Menu

- Forests Home
- Aims & Scope
- Editorial Board
- Reviewer Board
- Topics Board
- Instructions for Authors
- Special Issues
- Sections & Collections
- Article Processing Charge
- Indexing & Archiving
- Editor's Choice Articles
- Most Cited & Viewed
- Journal Statistics
- Journal History
- Journal Awards
- Editorial Office

Journal Browser

volume

issue

Go

Forthcoming issue

Current issue

Vol. 12 (2021) Vol. 6 (2015)
Vol. 11 (2020) Vol. 5 (2014)
Vol. 10 (2019) Vol. 4 (2013)
Vol. 9 (2018) Vol. 3 (2012)
Vol. 8 (2017) Vol. 2 (2011)
Vol. 7 (2016) Vol. 1 (2010)

Forests, Volume 11, Issue 12 (December 2020) – 140 articles

Cover Story (view full-size image): In Northeast India, and many other parts of the world, shifting cultivation is an important land-use sustaining the livelihoods of large numbers of rural people. Despite this, there are concerns regarding shortened fallow length and forest recovery following cultivation. In this paper, we determine the important, but often ignored, below-ground components of ecosystem recovery focusing on roots and their interactions with soil nitrogen availability. We also show how there are strong seasonal patterns of root biomass, production, and nitrogen cycling in these montane forests that are on the very edge of the tropics at 23 degrees north. The picture here shows our natural forest reference site, the Reiek Community Forest. View this paper

- Issues are regarded as officially published after their release is announced to the table of contents alert mailing list.
- You may sign up for e-mail alerts to receive table of contents of newly released issues.
- PDF is the official format for papers published in both, html and pdf forms. To view the papers in pdf format, click on the "PDF Full-text" link, and use the free Adobe Reader to open them.

Order results: Publication Date

Result details: Normal

Show export options

Open Access Article

Urban Green Corridors Analysis for a Rapid Urbanization City Exemplified in Gaoyou City, Jiangsu

by Helot Wang and Zongping Pei

Forests 2020, *11*(12), 1374; https://doi.org/10.3390/f11121374 - 21 Dec 2020

Viewed by 456

Abstract The undergoing trend and development towards urbanization and the consequences of socio-ecological and climate change are increasing the pressure on cities worldwide. The planning of urban green and blue spaces is essential for sustainable urban development, especially for the conservation of urban ecosystems [...] Read more.

(This article belongs to the Section Forest Ecology and Management)

► Show Figures

Open Access Article

Effect of Weathering on Surface Functional Groups of Charred Norway Spruce Cladding Panels

by Maija Kymäläinen, Hannu Turunen and Lauri Rautkari

Forests 2020, *11*(12), 1373; https://doi.org/10.3390/f11121373 - 21 Dec 2020

Viewed by 501

Abstract Norway spruce cladding panels were surface charred with a prototype device utilizing a hot plate method. The panels were used to construct a test wall that was exposed to natural weathering for a period of two years. The changes in functional groups were [...] Read more.

(This article belongs to the Special Issue Wood Modification: Physical Properties and Biological Efficacy)

► Show Figures

Open Access Article

Molecular Cloning and Expression Analysis of the Endogenous Cellulase Gene *MaCel1* in *Monochamus alternatus*

by Yachao Li, Hao Chen, Xu Chu, Qiuyu Ma, Guanghong Liang, Songqing Wu, Rong Wang, Mulualem Tigabu, Feiping Zhang and Xia Hu

Forests 2020, *11*(12), 1372; https://doi.org/10.3390/f11121372 - 21 Dec 2020

Viewed by 326

Abstract The purpose of this study was to characterize the endogenous cellulase gene *MaCel1* of *Monochamus alternatus*, which is an important vector of *Bursaphelenchus xylophilus*, a pine wood nematode, which causes pine wilt disease (PWD). In this study, *MaCel1* was cloned by [...] Read more.

(This article belongs to the Section Forest Ecophysiology and Biology)

► Show Figures

Open Access Article

Phenotypic Plasticity of Drought Tolerance Traits in a Widespread Eucalypt (*Eucalyptus obliqua*)

by Carola Pritzkow, Christopher Szota, Virginia G. Williamson and Stefan K. Arndt

Forests 2020, *11*(12), 1371; https://doi.org/10.3390/f11121371 - 21 Dec 2020

Viewed by 425

Abstract Long-term studies of tree responses to drought stress help us to understand the capacity of species to adapt to their environment. In this study, we investigated how *Eucalyptus obliqua* adjusts physiological and morphological traits in response to seasonal and multi-year droughts. We monitored [...] Read more.

(This article belongs to the Special Issue The Physiology of Tree Response to Drought)

► Show Figures

Open Access Article

Evaluating the Economic Incentives of Biomass Removal on Site Preparation for Different Harvesting Systems in Australia

by Michael Berry and John Sessions

Forests 2020, *11*(12), 1370; https://doi.org/10.3390/f11121370 - 21 Dec 2020

Viewed by 464

Abstract *Research Highlights*: This study evaluated the impacts of biomass recovery on site preparation costs while proposing a mathematical model and framework to catalogue the benefits depending on harvesting system. *Background and Objectives*: Biomass as a viable product depends on the requisite costs of [...] Read more.

(This article belongs to the Section Forest Economics, Policy, and Social Science)

► Show Figures

Open Access Article

Parameter Optimization of the 3PG Model Based on Sensitivity Analysis and a Bayesian Method

by Chenjian Liu, Xiaoman Zheng and Yin Ren

Forests 2020, *11*(12), 1369; https://doi.org/10.3390/f11121369 - 21 Dec 2020

Viewed by 297

Abstract Sensitivity analysis and parameter optimization of stand models can improve their efficiency and accuracy, and increase their applicability. In this study, the sensitivity analysis, screening, and optimization of 63 model parameters of the Physiological Principles in Predicting Growth (3PG) model were performed by [...] Read more.

(This article belongs to the Section Forest Inventory, Modeling and Remote Sensing)

► Show Figures

Open Access Article

Suitability Evaluation and Dominant Function Model for Multifunctional Forest Management

by Zhiqiang Min, Baoguo Wu, Xiaohui Su, Yuting Chen and Yingze Tian
Forests 2020, *11*(12), 1368; https://doi.org/10.3390/f11121368 - 21 Dec 2020
Viewed by 471

Abstract Multifunctional forest management is a common topic and hotspot of forestry research in recent years. Evaluating the suitability of forest land for multifunctional management is the first and most important step for realizing sustainable and multifunctional forest management. This research aims to explore [...] Read more.
(This article belongs to the Special Issue Forest Management and Economics: Integrating Objectives Using Harvest Scheduling and Operations Research)

► Show Figures

Open Access Article

Metabolome and Transcriptome Association Analysis Reveals Regulation of Flavonoid Biosynthesis by Overexpression of *LaMIR166a* in *Larix kaempferi* (Lamb.) Carr

by Yanru Fan, Zhexin Li, Lifang Zhang, Suying Han and Liwang Qi
Forests 2020, *11*(12), 1387; https://doi.org/10.3390/f11121387 - 21 Dec 2020
Viewed by 390

Abstract Somatic embryogenesis is an ideal model process for studying early plant development. Embryonic cell lines of *Larix kaempferi* (Lamb.) Carr overexpressing *LaMIR166a* were obtained in our previous study. Here, a combination of de novo transcriptomics and extensively targeted metabolomics was used to study [...] Read more.
(This article belongs to the Section Forest Ecophysiology and Biology)

► Show Figures

Open Access Article

A New Method for Forest Canopy Hemispherical Photography Segmentation Based on Deep Learning

by Kexin Li, Xinwang Huang, Jingzhe Zhang, Zhihu Sun, Jianping Huang, Chunxue Sun, Qianchong Xie and Wenlong Song
Forests 2020, *11*(12), 1386; https://doi.org/10.3390/f11121386 - 19 Dec 2020
Viewed by 526

Abstract *Research Highlights:* This paper proposes a new method for hemispherical forest canopy image segmentation. The method is based on a deep learning methodology and provides a robust and fully automatic technique for the segmentation of forest canopy hemispherical photography (CHP) and gap fraction [...] Read more.
(This article belongs to the Special Issue Monitoring and Assessing Forest Attributes Based on Remote Sensing Technology)

► Show Figures

Open Access Article

Photosynthetic and Morphological Acclimation to High and Low Light Environments in *Petasites japonicus* subsp. *giganteus*

by Ray Deguchi and Kohei Koyama
Forests 2020, *11*(12), 1385; https://doi.org/10.3390/f11121385 - 19 Dec 2020
Cited by 2 | Viewed by 568

Abstract Within each species, leaf traits such as light-saturated photosynthetic rate or dark respiration rate acclimate to local light environment. Comparing only static physiological traits, however, may not be sufficient to evaluate the effects of such acclimation in the shade because the light environment [...] Read more.
(This article belongs to the Special Issue Relationship between Forest Ecophysiology and Environment)

► Show Figures

Open Access Review

Use of Remote Sensing Data to Improve the Efficiency of National Forest Inventories: A Case Study from the United States National Forest Inventory

by Andrew J. Lister, Hans Andersen, Tracey Frescino, Demetrios Gatziolis, Sean Healey, Linda S. Heath, Greg C. Liknes, Ronald McRoberts, Gretchen G. Moisen, Mark Nelson, Rachel Riemann, Karen Schleewels, Todd A. Schroeder, James Westfall and B. Tyler Wilson
Forests 2020, *11*(12), 1364; https://doi.org/10.3390/f11121364 - 19 Dec 2020
Viewed by 675

Abstract Globally, forests are a crucial natural resource, and their sound management is critical for human and ecosystem health and well-being. Efforts to manage forests depend upon reliable data on the status of and trends in forest resources. When these data come from well-designed [...] Read more.
(This article belongs to the Special Issue Mapping and Monitoring Forest Cover)

► Show Figures

Open Access Article

Molecular Cloning and Functional Characterization of the *DELLA* Gene Family in *Liriodendron* Hybrids

by Yang Liu, Pengkai Wang, Shan Yan, Xin Liu, Lu Lu, Xinying Chen, Ye Lu, Zhaodong Hao, Jisen Shi and Jinhui Chen
Forests 2020, *11*(12), 1363; https://doi.org/10.3390/f11121363 - 18 Dec 2020
Viewed by 344

Abstract DELLA proteins are key components of the gibberellins signal transduction pathway that play negative roles on promoting cell elongation and plant stature. However, the mechanisms underlying DELLA mediated growth inhibition in woody plant species are poorly understood. Here, we identified two *LhDELLA* genes [...] Read more.
(This article belongs to the Section Forest Ecophysiology and Biology)

► Show Figures

Open Access Communication

Changes in Proline Levels during Seed Development of Orthodox and Recalcitrant Seeds of Genus *Acer* in a Climate Change Scenario

by Joanna Kijowska-Oberc, Aleksandra M. Staszak, Mikołaj K. Wawrzyniak and Ewelina Ratajczak
Forests 2020, *11*(12), 1362; https://doi.org/10.3390/f11121362 - 18 Dec 2020
Viewed by 553

Abstract In the present study, we examined the utility of proline usage as a biochemical indicator of metabolic changes caused by climate change (mean temperature and precipitation) during seed development of two *Acer* species differing in desiccation tolerance: Norway maple (*Acer platanoides* L.—desiccation [...] Read more.
(This article belongs to the Special Issue Forest Tree Stress Biology: From Fundamental Research to Emerging Opportunities)

► Show Figures

Open Access Article

Structure and Composition of Terra Firme and Seasonally Flooded Várzea Forests in the Western Brazilian Amazon

by Yennie K. Brudin, Joseph E. Hawes, Carlos A. Peres and Torbjørn Haugaasen
Forests 2020, *11*(12), 1361; https://doi.org/10.3390/f11121361 - 18 Dec 2020
Viewed by 551

Abstract *Research Highlights:* Rare, or sparsely distributed, species drive the floristic diversity of upland, terra firme and seasonally flooded forests in the central Juruá—a remote and hitherto floristically poorly known area in the Brazilian Amazon. *Background and Objectives:* Floristic inventories are critical [...] Read more.
(This article belongs to the Special Issue Structure, Function, and Dynamics of Tropical Floodplain Forests)

► Show Figures

Open Access Commentary

Comparing the Environmental Integrity of Emission Reductions from REDD Programs with Renewable Energy Projects

by Andres B. Espejo, Maria Catalina Becerra-Leal and Naikoa Aguilar-Amuchastegui
Forests 2020, *11*(12), 1360; https://doi.org/10.3390/f11121360 - 18 Dec 2020
Viewed by 770

Abstract Reducing deforestation and forest degradation presents a climate-change mitigation opportunity that is critical to meeting the Paris Agreement goals, and to achieving reductions in the atmospheric concentrations of greenhouse gases (GHGs). Reducing Emissions from Deforestation and Forest Degradation (REDD) provides developing countries with [...] Read more.
(This article belongs to the Special Issue REDD+: Protecting Climate, Forests and Livelihoods)

► Show Figures

Open Access Article

Stomatal and Leaf Morphology Response of European Beech (*Fagus sylvatica* L.) Provenances Transferred to Contrasting Climatic Conditions

by Peter Petrik, Anja Petek, Alena Konôpková, Michal Bosela, Peter Fleischer, Josef Frýdl and Daniel Kurjak
Forests 2020, *11*(12), 1359; https://doi.org/10.3390/f11121359 - 18 Dec 2020
Viewed by 416

Abstract Climate change-induced elevated temperatures and drought are considered to be serious threats to forest ecosystems worldwide, negatively affecting tree growth and viability. We studied nine European beech (*Fagus sylvatica* L.) provenances located in two provenance trial plots with contrasting climates in Central [...] Read more.
(This article belongs to the Special Issue Impacts of Climate Change on Tree Physiology and Responses of Forest Ecosystems)

► Show Figures

Open Access Article

Changes in Community Composition of Tropical Evergreen Forests during Succession in Ta Dung National Park, Central Highlands of Vietnam

by Nguyen Hong Hai, Nguyen Thanh Tan, Tran Quang Bao, Any Mary Petritan, Trinh Hien Mai, Cao Thi Thu Hien, Pham The Anh, Vu Tien Hung and Ion Catalin Petritan
Forests 2020, *11*(12), 1358; https://doi.org/10.3390/f11121358 - 18 Dec 2020
Viewed by 414

Abstract Degradation of tropical forests is a major driver of the global extinction crisis. A key question is understanding the role of evolution history during forest succession in the context of forest restoration for maintaining ecosystem function and stability. This study was conducted in [...] Read more.
(This article belongs to the Special Issue Modelling of Forests Structure and Biomass Distribution)

► Show Figures

Open Access Article

Feature-Level Fusion between Gaofen-5 and Sentinel-1A Data for Tea Plantation Mapping

by Yuja Chen and Shufang Tian
Forests 2020, *11*(12), 1357; https://doi.org/10.3390/f11121357 - 18 Dec 2020
Viewed by 310

Abstract The accurate mapping of tea plantations is significant for government decision-making and environmental protection of tea-producing regions. Hyperspectral and Synthetic Aperture Radar (SAR) data have recently been widely used in land cover classification, but effective integration of these data for tea plantation mapping [...] Read more.
(This article belongs to the Special Issue Remote Sensing Applications in Forests Inventory and Management)

► Show Figures

Open Access Article

Quantitative Genetic Variation in Bark Stripping of *Pinus radiata*

by Judith S. Nantongo, Brad M. Potts, Hugh Fitzgerald, Jessica Newman, Stephen Elms, Don Aurik, Heidi Dungey and Julianne M. O'Reilly-Wapstra
Forests 2020, *11*(12), 1356; https://doi.org/10.3390/f11121356 - 18 Dec 2020
Viewed by 627

Abstract Bark stripping by mammals is a major problem for conifer forestry worldwide. In Australia, bark stripping in the exotic plantations of *Pinus radiata* is mainly caused by native marsupials. As a sustainable management option, we explored the extent to which natural variation in [...] Read more.
(This article belongs to the Special Issue Forest-Mammalian Herbivore Interactions and Contemporary Forest Management)

► Show Figures

Open Access Erratum

Erratum: Perry, K.I., et al. Responses of Ground-Dwelling Invertebrates to Gap Formation and Accumulation of Woody Debris from Invasive Species, Wind, and Salvage Logging Running Title: Perry and Herms: Responses of Ground-Dwelling Invertebrates. *Forests* 2017, *8*, 174

by Kayla I. Perry and Daniel A. Herms
Forests 2020, *11*(12), 1355; https://doi.org/10.3390/f11121355 - 18 Dec 2020
Viewed by 330

Abstract
There is an error in the title of this paper [...] Full article

Open Access Article

Low Population Differentiation but High Phenotypic Plasticity of European Beech in Germany

by Markus Müller, Tanja Kempen, Reiner Finkeldey and Oliver Gailing
Forests 2020, *11*(12), 1354; https://doi.org/10.3390/f11121354 - 18 Dec 2020
Viewed by 459

Abstract Drought is increasingly impairing the vitality of European beech (*Fagus sylvatica* L.) in several regions of its distribution range. In times of climate change, adaptive traits such as plant phenology and frost tolerance are also becoming more important. Adaptive patterns of European [...] Read more.
(This article belongs to the Special Issue Forest and Sustainable Development (9th International Symposium on Forest and Sustainable Development))

► Show Figures

Open Access Correction

Correction: Branca, G., et al. Forest Protection Unifies, Silviculture Divides: A Sociological Analysis of Local Stakeholders' Voices after Coppicing in the Marganai Forest (Sardinia, Italy). *Forests* 2020, *11*, 708

by Giampiero Branca, Irene Piredda, Roberto Scotti, Laura Chessa, Benìa Murgia, Antonio Ganga, Sergio Francesco Campus, Raffaella Lovreglio, Enrico Guastini, Massimiliano Schwarz and Filippo Gladrossich
Forests 2020, *11*(12), 1353; https://doi.org/10.3390/f11121353 - 17 Dec 2020
Viewed by 344

Abstract
We have recently been made aware by the *Forests* Editorial Offices of some errors and omissions in the Introduction Section 1 [...] Full article

Open Access Review

Poplar Short Rotation Coppice Plantations under Mediterranean Conditions: The Case of Spain

by Nerea Oliveira, César Pérez-Cruzado, Isabel Cañellas, Roque Rodríguez-Soalleiro and Hortensia Sixto
Forests 2020, *11*(12), 1352; https://doi.org/10.3390/f11121352 - 17 Dec 2020
Viewed by 452

Abstract Developing a circular bioeconomy based on the sustainable use of biological resources, such as biomass, seems to be the best way of responding to the challenges associated with global change. Among the many sources, short rotation forest crops are an essential instrument for [...] Read more.
(This article belongs to the Special Issue Growth and Development of Short Rotation Woody Crops for Rural and Urban Applications)

► Show Figures

Open Access Article

Uranium Vertical and Lateral Distribution in a German Forested Catchment

by Yajie Sun, Bei Wu, Ingo Wiekenkamp, Annemieke M. Kooijman and Roland Bol
Forests 2020, *11*(12), 1351; https://doi.org/10.3390/f11121351 - 17 Dec 2020
Viewed by 323

Abstract The natural measurements of uranium (U) are important for establishing natural baseline levels of U in soil. The relations between U and other elements are important to determine the extent of geological origin of soil U. The present study was aimed at providing [...] Read more.
(This article belongs to the Section Forest Ecology and Management)

► Show Figures

Open Access Review

Results Based Payments for REDD+ under the Green Climate Fund: Lessons Learned on Social, Environmental and Governance Safeguards

by Daniela Roy Christian, Maria García Espinosa, Andreas Roumann and Jyotsna Puri
Forests 2020, *11*(12), 1350; https://doi.org/10.3390/f11121350 - 17 Dec 2020
Viewed by 516

(This article belongs to the Special Issue Mapping and Monitoring Forest Cover)

► Show Figures

Open Access Article

Implications of Temperate Agroforestry on Sheep and Cattle Productivity, Environmental Impacts and Enterprise Economics. A Systematic Evidence Map

by Matthew W. Jordon, Kathy J. Willis, William J. Harvey, Leo Petrokofsky and Gillian Petrokofsky

Forests 2020, *11*(12), 1321; https://doi.org/10.3390/f11121321 - 11 Dec 2020

Viewed by 748

Abstract The environmental impacts of ruminant livestock farming need to be mitigated to improve the sustainability of food production. These negative impacts have been compounded by the increased spatial and cultural separation of farming and forestry across multiple temperate landscapes and contexts over recent [...] Read more.

(This article belongs to the Special Issue Systematic Methods and Techniques Applied to Forestry and Land Use Management)

► Show Figures

Open Access Article

Management Intensity and Forest Successional Stages as Significant Determinants of Small Mammal Communities in a Lowland Floodplain Forest

by Josef Suchomel, Jan Šipoš and Ondřej Košulič

Forests 2020, *11*(12), 1320; https://doi.org/10.3390/f11121320 - 11 Dec 2020

Viewed by 345

Abstract The conversion of forests from complex natural ecosystems to simplified commercial woodlands is one of the major causes of biodiversity loss. To maintain biodiversity, we need to understand how current management practices influence forest ecosystems. We studied the effects of forest successional stage [...] Read more.

(This article belongs to the Section Forest Ecology and Management)

► Show Figures

Open Access Article

Variation and Genetic Parameters of Leaf Morphological Traits of Eight Families from *Populus simonii* × *P. nigra*

by Jingshan Ren, Xinyue Ji, Changhai Wang, Jianjun Hu, Giuseppe Nervo and Jiahua Li

Forests 2020, *11*(12), 1319; https://doi.org/10.3390/f11121319 - 11 Dec 2020

Cited by 1 | Viewed by 407

Abstract Leaf morphology in *Populus* L. varies extensively among sections, species and clones under strong genetic control. *P. nigra* L. (section *Aigeiros*), with large and triangular leaves, is a commercial forest tree of economic importance for fast growth and high yield in Europe. [...] Read more.

(This article belongs to the Section Forest Ecophysiology and Biology)

► Show Figures

Open Access Article

Assessing the Carbon Storage of Soil and Litter from National Forest Inventory Data in South Korea

by Sunjeoung Lee, Seunghyun Lee, Joonghoon Shin, Jongsu Yim and Jinseok Kang

Forests 2020, *11*(12), 1318; https://doi.org/10.3390/f11121318 - 10 Dec 2020

Viewed by 448

Abstract Research Highlights: The estimation of soil and litter carbon stocks by the Land Use, Land-Use Changes, and Forestry (LULUCF) sectors has the potential to improve reports on national greenhouse gas (GHG) inventories. Background and Objectives: Forests are carbon sinks in the LULUCF sectors [...] Read more.

(This article belongs to the Special Issue Forest Soil Carbon and Climate Changes)

► Show Figures

Open Access Article

How Are Green Spaces Distributed among Different Social Groups in Urban China? A National Level Study

by Longfeng Wu and Seung Kyum Kim

Forests 2020, *11*(12), 1317; https://doi.org/10.3390/f11121317 - 10 Dec 2020

Viewed by 448

Abstract The study analyzes the distributional equity of urban green space (UGS) among different social groups across all urban areas in China. Urban green space is measured in two ways. Park area per capita and vegetation coverage ratio within 1.5 km and 3.2 km [...] Read more.

(This article belongs to the Section Forest Ecology and Management)

► Show Figures

Open Access Article

The Effect of Crown Social Class on Bark Thickness and Sapwood Moisture Content in Norway Spruce

by Luka Krajnc and Jožica Gričar

Forests 2020, *11*(12), 1316; https://doi.org/10.3390/f11121316 - 10 Dec 2020

Viewed by 405

Abstract The research study examined the effect of tree properties (crown social class, diameter at breast height (DBH), and tree height) on bark thickness (BT) and sapwood moisture content (SMC) in Norway spruce (*Picea abies* (L.) H. Karst.). Both examined variables were shown [...] Read more.

(This article belongs to the Special Issue Natural Disturbances under Climate Change: Challenges, Trends, and Management Implications)

► Show Figures

Open Access Article

Moderate- to High-Severity Disturbances Shaped the Structure of Primary *Picea Abies* (L.) Karst. Forest in the Southern Carpathians

by Andreea Petronela Splinu, Ion Cătălin Petrițan, Martin Mikoláš, Pavel Janda, Ondřej Vostarek, Vojtěch Čada and Miroslav Svoboda

Forests 2020, *11*(12), 1315; https://doi.org/10.3390/f11121315 - 10 Dec 2020

Viewed by 468

Abstract Research Highlights: Past disturbances occurred naturally in primary forests in the Southern Carpathians. High- and moderate-severity disturbances shaped the present structure of these ecosystems, which regenerated successfully without forestry interventions. Background and Objectives: Windstorms and bark beetle outbreaks have recently affected large forest [...] Read more.

(This article belongs to the Special Issue Natural Disturbances under Climate Change: Challenges, Trends, and Management Implications)

► Show Figures

Open Access Article

History Lessons from the Late Joseon Dynasty Period of Korea: Human Technology (*Ondol*), Its Impacts on Forests and People, and the Role of the Government

by Jae Soo Bae and Yeon-Su Kim

Forests 2020, *11*(12), 1314; https://doi.org/10.3390/f11121314 - 10 Dec 2020

Viewed by 398

Abstract Historical analogies can help us contextualize new technical developments with social, cultural, and political forces at work. The late Joseon Dynasty period of Korea (1639–1910), a closed economy with detailed written records, provides a rare opportunity to examine a social-ecological system (SES) responding [...] Read more.

(This article belongs to the Section Forest Economics, Policy, and Social Science)

► Show Figures

Open Access Article

The Prediction of Stiffness Reduction Non-Linear Phase in Bamboo Reinforced Concrete Beam Using the Finite Element Method (FEM) and Artificial Neural Networks (ANNs)

by Muhtar

Forests 2020, *11*(12), 1313; https://doi.org/10.3390/f11121313 - 10 Dec 2020

Viewed by 297

Abstract This paper discusses the reduction of the stiffness of bamboo reinforced concrete (BRC) beams to support the use of bamboo as an environmentally friendly building material. Calculation of cross-section stiffness in numerical analysis is very important, especially in the non-linear phase. After the [...] Read more.

(This article belongs to the Special Issue Timber and Construction Structure)

Abstract The current study presents the results of the first dendrochronological survey performed over the East Aegean island of Symi. Research Highlights: Dendrochronological research of the East Aegean region is of paramount importance since dendrochronological data from the region, and especially the islands, are [...] Read more.
(This article belongs to the Special Issue Dendrochronology: An Interdisciplinary Approach to Assess Wooden Cultural Heritage Worldwide)

► Show Figures

Open Access Perspective

Comprehensive Accounting for REDD+ Programs: A Pragmatic Approach as Exemplified in Guyana

by Katherine M. Goslee, Timothy R. H. Pearson, Blanca Bernal, Sophie L. Simon and Hansraje Sukhdeo
Forests 2020, *11*(12), 1285; https://doi.org/10.3390/f11121285 - 27 Nov 2020
Cited by 1 | Viewed by 472

Abstract Completeness is an important element for Reducing Emissions from Deforestation and forest Degradation (REDD+) accounting to ensure transparency and accountability. However, including a full accounting for all emission sources in a REDD+ program is often resource-intensive and cost-prohibitive, especially considering that some emission [...] Read more.
(This article belongs to the Special Issue REDD+: Protecting Climate, Forests and Livelihoods)

► Show Figures

Open Access Article

Exploring the Relationship between Forest Structure and Health

by Jinki Kim, Duk-Byeong Park and Jung Il Seo
Forests 2020, *11*(12), 1284; https://doi.org/10.3390/f11121284 - 27 Nov 2020
Viewed by 474

Abstract There is abundant evidence that green space in urban neighborhood is associated with physical activity and it is well known that physical activity contributes to human health. Physical activity fosters normal growth and development, can reduce the risk of chronic diseases, and can [...] Read more.
(This article belongs to the Special Issue Selected Papers from the 1st International Electronic Conference on Forests (IECF2020))

► Show Figures

Open Access Article

Differences in Forest Use Strategies for Cash Income between Households Living outside and inside Selectively Logged Production Forests in Myanmar

by Thein Saung, Nobuya Mizoue, Tetsuji Ota and Tsuyoshi Kajisa
Forests 2020, *11*(12), 1283; https://doi.org/10.3390/f11121283 - 27 Nov 2020
Cited by 1 | Viewed by 437

Abstract In many tropical regions, rural households often depend on forests for cash income, but there is still little knowledge on how forest use strategies differ among people living in different locations. This study aimed to detect differences in forest use strategies and forest [...] Read more.
(This article belongs to the Section Forest Economics, Policy, and Social Science)

► Show Figures

Open Access Article

Fast Spectrophotometric Method as Alternative for CuO Oxidation to Assess Lignin in Soils with Different Tree Cover

by Tiziana Danise, Michele Innangi, Elena Curcio, Antonietta Fioretto and Georg Guggenberger
Forests 2020, *11*(12), 1282; https://doi.org/10.3390/f11121282 - 27 Nov 2020
Viewed by 291

Abstract Given the ongoing climate change, estimating the amount of less degradable plant compounds that can be stored in the soil, such as lignin, is a topic of primary importance. There are few methods applicable to soils for the determination of lignin, such as [...] Read more.
(This article belongs to the Special Issue Forest Litter Decomposition: An Integrative Approach)

► Show Figures

Open Access Article

The Influence of Urban Conditions on the Phenology of *Aesculus hippocastanum* L. Using the Example of Wroclaw (Poland)

by Iwona Dominika Orzechowska-Szajda, Robert Krzysztof Sobolewski, Joanna Lewandowska, Paulina Kowalska and Robert Kalbarczyk
Forests 2020, *11*(12), 1281; https://doi.org/10.3390/f11121281 - 26 Nov 2020
Viewed by 711

Abstract The differences in plant phenology between rural and urban areas are the subject of research conducted all over the world. There are few studies aimed at assessing the impact of the urban heat island on plant vegetation only in urban areas. The aim [...] Read more.
(This article belongs to the Special Issue Urban Forestry and Green Infrastructures)

► Show Figures

Open Access Article

Genetically Determined Differences in Annual Shoot Elongation of Young Norway Spruce

by Baiba Jansone, Una Neimane, Silva Šēnhofa, Roberts Matisons and Āris Jansons
Forests 2020, *11*(12), 1280; https://doi.org/10.3390/f11121280 - 26 Nov 2020
Viewed by 257

Abstract The annual shoot elongation could be described by a non-linear growth model to characterize differences in its dynamics among spruce genotypes, the effect of each shoot elongation phase on the total shoot length, and the genetic differences for a particular growth phase. The [...] Read more.
(This article belongs to the Section Forest Ecology and Management)

► Show Figures

Open Access Article

Evaluation of Abiotic Controls on Windthrow Disturbance Using a Generalized Additive Model: A Case Study of the Tatra National Park, Slovakia

by Vladimír Fleischer, Stanislav Katina, Jozef Minár, Norbert Polčák, Martin Bánovský, Martin Marotta, Stanislav Zámečník and František Petrovič
Forests 2020, *11*(12), 1259; https://doi.org/10.3390/f11121259 - 26 Nov 2020
Viewed by 410

Abstract Windthrows are the most important type of disturbance occurring in the forests of Central Europe. On 19 November 2004, the strong northeastern katabatic winds caused significant damage and land cover change to more than 126 km^2 of spruce forests in the Tatra [...] Read more.
(This article belongs to the Special Issue Biodiversity and Management of Temperate Floodplain Forests)

► Show Figures

Open Access Article

Discriminant Analysis of the Damage Degree Caused by Pine Shoot Beetle to Yunnan Pine Using UAV-Based Hyperspectral Images

by Mengying Liu, Zhonghui Zhang, Xuelian Liu, Jun Yao, Ting Du, Yunqiang Ma and Lei Shi
Forests 2020, *11*(12), 1258; https://doi.org/10.3390/f11121258 - 26 Nov 2020
Viewed by 313

Abstract Due to the increased frequency and intensity of forest damage caused by diseases and pests, effective methods are needed to accurately monitor the damage degree. Unmanned aerial vehicle (UAV)-based hyperspectral imaging is an effective technique for forest health surveying and monitoring. In this [...] Read more.
(This article belongs to the Special Issue Forestry Applications of Unmanned Aerial Vehicles (UAVs) 2020)

► Show Figures

Open Access Article

The Influence of Scots Pine Log Type (*Pinus sylvestris* L.) on the Mechanical Properties of Lumber

by Sławomir Krzosek, Izabela Burawska-Kupniewska and Piotr Mańkowski
Forests 2020, *11*(12), 1257; https://doi.org/10.3390/f11121257 - 26 Nov 2020
Viewed by 266

Abstract The paper presents an analysis of the influence of geographical origin and Scots pine log type on the mechanical properties of the timber sawn from them. The tested timber was sawn from logs obtained from three different forestry regions in Poland, located in [...] Read more.
(This article belongs to the Special Issue Forest Sustainability: Wood Harvest, Supply and Procurement Chain, and Wood Raw Material Properties)

► Show Figures

Open Access Article

Adaptive Model Building Framework for Production Planning in the Primary Wood Industry

by Matthias Kaltenbrunner, Maria Anna Huka and Manfred Gronalt
Forests 2020, *11*(12), 1256; https://doi.org/10.3390/f11121256 - 26 Nov 2020
Viewed by 294

Abstract Production planning models for the primary wood industry have been proposed for several decades. However, the majority of the research to date is concentrated on individual cases. This paper presents an integrated adaptive modelling framework that combines the proposed approaches and identifies evolving [...] Read more.
(This article belongs to the Section Wood Science and Forest Products)

► Show Figures

Open Access Article

Effects of *Bt-Cry1Ah1* Transgenic Poplar on Target and Non-Target Pests and Their Parasitic Natural Enemy in Field and Laboratory Trials

by Pu Wang, Hui Wei, Weibo Sun, Lingling Li, Peijun Zhou, Dawei Li and Zhuge Qiang
Forests 2020, *11*(12), 1255; https://doi.org/10.3390/f11121255 - 26 Nov 2020
Viewed by 356

Abstract Increasing areas of artificial afforestation and poplar monoculture in China have led to serious problems with insect pests. The development of genetic engineering technology, such as transgenic modification with *Bacillus thuringiensis* (*Bt*) genes, provides novel solutions to the pest problem. We [...] Read more.
(This article belongs to the Section Forest Ecophysiology and Biology)

► Show Figures

Open Access Article

Dimensional Stability of Waterlogged Scots Pine Wood Treated with PEG and Dried Using an Alternative Approach

by Mariusz Fejfer, Jerzy Majka and Magdalena Zborowska
Forests 2020, *11*(12), 1254; https://doi.org/10.3390/f11121254 - 26 Nov 2020
Cited by 1 | Viewed by 305

Abstract Low-intensity drying is widely believed to protect waterlogged archeological wood against the adverse effects of dimensional alteration and cracking. However, slow drying generates substantial costs for the conservation process. This study compares the effects on conservation of highly-degraded sapwood (SW) and slightly-degraded heartwood [...] Read more.
(This article belongs to the Section Wood Science and Forest Products)

► Show Figures

Open Access Article

Monitoring and Management of the Pine Processionary Moth in the North-Western Italian Alps

by Chiara Ferracini, Valerio Saitta, Cristina Pogolotti, Ivan Rollet, Flavio Ventui and Luca Dovigo
Forests 2020, *11*(12), 1253; https://doi.org/10.3390/f11121253 - 26 Nov 2020
Viewed by 505

Abstract The pine processionary moth (PPM), *Thaumetopoea pityocampa* (Denis and Schiffermüller, 1775) (Lepidoptera, Notodontidae), is considered one of the main insect defoliators of conifers in Southern Europe and North Africa. The species is oligophagous on pines and cedars in Mediterranean countries. This 6-year investigation [...] Read more.
(This article belongs to the Special Issue Forest Pathology and Entomology)

► Show Figures

Open Access Article

Estimation of Tree Height by Combining Low Density Airborne LiDAR Data and Images Using the 3D Tree Model: A Case Study in a Subtropical Forest in China

by Xiaocheng Zhou, Wenjun Wang, Liping Di, Lin Lu and Liying Guo
Forests 2020, *11*(12), 1252; https://doi.org/10.3390/f11121252 - 26 Nov 2020
Viewed by 368

Abstract In general, low density airborne LiDAR (Light Detection and Ranging) data are typically used to obtain the average height of forest trees. If the data could be used to obtain the tree height at the single tree level, it would greatly extend the [...] Read more.
(This article belongs to the Section Forest Inventory, Modelling and Remote Sensing)

► Show Figures

Open Access Article

Buds, Bugs and Bienniality: The Floral Biology of *Eschweilera tenuifolia* (O. Berg) Miers in a Black-Water Flooded Forest, Central Amazonia

by Adrian A. Barnett, Sarah A. Boyle, Natalia M. Kinap, Tereza Cristina dos Santos-Barnett, Thiago Turna Camilo, Pia Perolin, Maria Teresa Fernandez Piedade and Bruna M. Bezerra
Forests 2020, *11*(12), 1251; https://doi.org/10.3390/f11121251 - 25 Nov 2020
Viewed by 408

Abstract *Research Highlights:* Our study establishes the biennial nature of flowering intensity as a life-time energy-conserving strategy; we show unexpectedly high flower:fruit rates despite extensive predation of buds and flowers by insect larvae; 'selective' bud abortion may be a key annual energy-saving strategy. [...] Read more.
(This article belongs to the Special Issue Structure, Function, and Dynamics of Tropical Floodplain Forests)

► Show Figures

Open Access Article

Relating Climate, Drought and Radial Growth in Broadleaf Mediterranean Tree and Shrub Species: A New Approach to Quantify Climate-Growth Relationships

by J. Julio Camarero and Álvaro Rubio-Cuadrado
Forests 2020, *11*(12), 1250; https://doi.org/10.3390/f11121250 - 25 Nov 2020
Viewed by 489

Abstract The quantification of climate–growth relationships is a fundamental step in tree-ring sciences. This allows the assessment of functional responses to climate warming, particularly in biodiversity and climate-change hotspots including the Mediterranean Basin. In this region, broadleaf tree and shrub species of pre-Mediterranean, subtropical [...] Read more.
(This article belongs to the Special Issue Dendrochronology and Dendroclimatology in the Mediterranean)

► Show Figures

Open Access Article

The Application of Oak Bark Powder as a Filler for Melamine-Urea-Formaldehyde Adhesive in Plywood Manufacturing

by Radosław Mirski, Jakub Kawalerczyk, Dorota Dziurka, Joanna Siuda and Marek Wieruszewski
Forests 2020, *11*(12), 1249; https://doi.org/10.3390/f11121249 - 25 Nov 2020
Cited by 3 | Viewed by 306

Abstract The woodworking industry generates a great amount of bark which has not yet found a wider industrial application. None of the previously conducted research has considered oak bark application (which is one of the most often processed wood species in Poland) as a [...] Read more.
(This article belongs to the Section Wood Science and Forest Products)

► Show Figures

Open Access Article

Does Shrub Encroachment Indicate Ecosystem Degradation? A Perspective Based on the Spatial Patterns of Woody Plants in a Temperate Savanna-Like Ecosystem of Inner Mongolia, China

by Xiao Wang, Lina Jiang, Xiaohui Yang, Zhongjie Shi and Pengtao Yu
Forests 2020, *11*(12), 1248; https://doi.org/10.3390/f11121248 - 25 Nov 2020
Viewed by 356

Abstract Shrub encroachment, i.e., shrub emergence or an increase in woody plant cover, has been widely observed in arid and semiarid grasslands and savannas worldwide since the 2000s. However, until now, there has been a clear division of opinion regarding its ecological implications. One [...] Read more.
(This article belongs to the Special Issue Spatial Heterogeneity of Forest-Steppes)

► Show Figures

Open Access Article

Effect of Thermal Modification on the Nano-Mechanical Properties of the Wood Cell Wall

and Waterborne Polyacrylic Coating

by Yan Wu, Xinyu Wu, Feng Yang, Haiqiao Zhang, Xinhao Feng and Jilei Zhang
Forests 2020, *11*(12), 1247; https://doi.org/10.3390/f11121247 - 25 Nov 2020
Viewed by 305

Abstract Masson pine (*Pinus massoniana* Lamb.) samples were heat-treated at different treatment temperatures (150, 170, and 190 °C), and the nano-mechanical properties of the wood cell wall, which was coated with a waterborne polyacrylic (WPA) lacquer product, were compared. The elastic modulus ([...] Read more.
(This article belongs to the Special Issue Wood Modification: Physical Properties and Biological Efficacy)

► Show Figures

Open Access Article

Towards a Standard Framework to Identify Green Infrastructure Key Elements in Dense Mediterranean Cities

by Manuel Delgado-Capel and Paloma Cariñanos
Forests 2020, *11*(12), 1246; https://doi.org/10.3390/f11121246 - 25 Nov 2020
Viewed by 475

Abstract Present-day dense cities are increasingly affected by the impacts associated with climate change. The recurrence of extreme climate events is projected to be intensified in cities in the next decades, especially in the most vulnerable areas of the world, such as the Mediterranean [...] Read more.
(This article belongs to the Special Issue Landscape and Urban Planning-Sustainable Forest Development)

► Show Figures

Open Access Article

Simulating Combined Self-Loading Truck and Semitrailer Truck Transport in the Wood Supply Chain

by Christoph Kogler, Alexander Stenitzer and Peter Rauch
Forests 2020, *11*(12), 1245; https://doi.org/10.3390/f11121245 - 25 Nov 2020
Viewed by 551

Abstract Forestry faces frequent and severe natural calamities causing high amounts of salvage wood. Especially under mountainous conditions, regional available self-loading truck capacity is often the main limiting factor causing transport capacity bottlenecks. Therefore, innovative logistics strategies are needed to ensure quick transport of [...] Read more.
(This article belongs to the Special Issue Forest Sustainability: Wood Harvest, Supply and Procurement Chain, and Wood Raw Material Properties)

► Show Figures

Open Access Editorial

Protection and Management of Species, Habitats, Ecosystems and Landscapes: Current Trends and Global Needs

by Panayotis Dimopoulos and Ioannis P. Kokkoris
Forests 2020, *11*(12), 1244; https://doi.org/10.3390/f11121244 - 25 Nov 2020
Viewed by 375

Abstract Human well-being and the prerequisite sustainable environmental management are currently at stake, reaching a bottleneck when trying to cope with (i) the ever-growing world population, (ii) the constantly increasing need for natural resources (and the subsequent overexploitation of species, habitats, ecosystems, and landscapes) [...] Read more.
(This article belongs to the Special Issue Protection and Management of Species, Habitats, Ecosystems and Landscapes)

Open Access Article

Hydrophobization and Photo-Stabilization of *Radiata Pine*wood: The Effect of the Esterification on Thermal and Mechanical Properties

by René Herrera Díaz, Olhana Gordobil, Pedro L. de Hoyos-Martínez, Asne Sandak and Jalel Labidi
Forests 2020, *11*(12), 1243; https://doi.org/10.3390/f11121243 - 24 Nov 2020
Viewed by 501

Abstract Wood protection through chemical modification has received increasing interest over the last decades due to the environmental issues related to conventional biocides or protecting products. Consequently, a wide range of new treatments are developed in laboratories, which are later scaled up in the [...] Read more.
(This article belongs to the Special Issue Methods and New Technologies for Wood Modification)

► Show Figures

Open Access Article

Perceived Loudness Sensitivity Influenced by Brightness in Urban Forests: A Comparison When Eyes Were Opened and Closed

by Xin-Chen Hong, Guang-Yu Wang, Jiang Liu and Emily Dang
Forests 2020, *11*(12), 1242; https://doi.org/10.3390/f11121242 - 24 Nov 2020
Cited by 1 | Viewed by 376

Abstract Soundscape plays a positive, health-related role in urban forests, and there is a competitive allocation of cognitive resources between soundscapes and lightscapes. This study aimed to explore the relationship between perceived loudness sensitivity and brightness in urban forests through eye opening and closure. [...] Read more.

► Show Figures

Open Access Article

Multiple Factors Influence Seasonal and Interannual Litterfall Production in a Tropical Dry Forest in Mexico

by Hernán Morffi-Mestre, Gregorio Ángeles-Pérez, Jennifer S. Powers, José Luis Andrade, Astrid Helena Huechacona Ruiz, Filogonio May-Pat, Francisco Chi-May and Juan Manuel Dupuy
Forests 2020, *11*(12), 1241; https://doi.org/10.3390/f11121241 - 24 Nov 2020
Viewed by 411

Abstract Litterfall production plays a fundamental role in the dynamics and function of tropical forest ecosystems, as it supplies 70–80% of nutrients entering the soil. This process varies annually and seasonally, depending on multiple environmental factors. However, few studies spanning several years have addressed [...] Read more.
(This article belongs to the Section Forest Ecology and Management)

► Show Figures

Open Access Article

Risk Assessment of Potential Food Chain Threats from Edible Wild Mushrooms Collected in Forest Ecosystems with Heavy Metal Pollution in Upper Silesia, Poland

by Marek Pająk, Michał Gąsiorek, Michał Jasik, Wiktor Halecki, Krzysztof Otremba and Marcin Pietrzykowski
Forests 2020, *11*(12), 1240; https://doi.org/10.3390/f11121240 - 24 Nov 2020
Viewed by 346

Abstract In this study, the contents of selected heavy metals (Zn, Cu, Cd, Pb, Cr, and Ni) and macroelements (C, N, K, P, S, Mg, Na, and Ca) were measured in wild mushrooms growing in a heavily polluted forest ecosystem in the northeastern part [...] Read more.
(This article belongs to the Section Forest Ecology and Management)

► Show Figures

Open Access Article

A Deep Learning Approach for Calamity Assessment Using Sentinel-2 Data

by Daniel Schoevogel, Melanie Brandmeier and Manuel Weis
Forests 2020, *11*(12), 1239; https://doi.org/10.3390/f11121239 - 24 Nov 2020
Viewed by 834

Abstract The number of severe storm events has increased in recent decades due to climate change. These storms are one of the main causes for timber loss in European forests and damaged areas are prone to further degradation by, for example, bark beetle infestations. [...] Read more.
(This article belongs to the Section Forest Inventory, Modeling and Remote Sensing)

► Show Figures

Open Access Article

An Assessment of the Spatial Variability of Tropical Swamp Forest along a 300 km Long Transect in the Usumacinta River Basin, Mexico

by Rubén Martínez-Camilo, José Alberto Gallardo-Cruz, Jonathan V. Solórzano, Candelario Peralta-Carreta, Delio Antonio Jiménez-López, Ofelia Castillo-Acosta, Miguelina Sánchez-González and Jorge A. Meave
Forests 2020, *11*(12), 1238; https://doi.org/10.3390/f11121238 - 24 Nov 2020
Viewed by 516

Abstract The provision of valuable ecosystem services by tropical swamp forests (mainly carbon sequestration and storage in

biomass and soil) explains their ecological importance. Current efforts toward the conservation of these ecosystems, however, face strong limitations as their spatial variation is largely unknown, particularly [...] Read more.
(This article belongs to the Section Forest Ecology and Management)

► Show Figures

Open Access Article

Species, Climatypes, Climate Change, and Forest Health: A Conversion of Science to Practice for Inland Northwest (USA) Forests

by Gerald E. Rehfeldt, Marcus V. Warwell and Robert A. Monserud
Forests 2020, *11*(12), 1237; https://doi.org/10.3390/f11121237 - 24 Nov 2020
Cited by 2 | Viewed by 551

Abstract *Research Highlights*: This paper integrates disparate research results pertaining to climate change impacts to 12 co-occurring forest tree species and their climatypes such that management options for the ecosystem as a whole become discernible. *Background and Objectives*: The ecosystem under analysis [...] Read more.
(This article belongs to the Special Issue Genetic Resources and Adaptive Management of Conifers in a Changing World)

► Show Figures

Open Access Article

Fine Root and Soil Nitrogen Dynamics during Stand Development Following Shifting Agriculture in Northeast India

by Dipendra Singha, Francis Q. Brearley and Shri Kant Tripathi
Forests 2020, *11*(12), 1236; https://doi.org/10.3390/f11121236 - 24 Nov 2020
Viewed by 396

Abstract Nitrogen (N) dynamics during changes in land use patterns in tropical forests may profoundly affect fine root dynamics and nutrient cycling processes. Variations in fine root biomass and soil N dynamics were assessed in developing stands of increasing ages following shifting agriculture in [...] Read more.
(This article belongs to the Section Forest Ecology and Management)

► Show Figures

Open Access Review

Reforestation and Sustainable Management of *Pinus merkusii* Forest Plantation in Indonesia: A Review

by Rinaldi Imanuddin, Asep Hidayat, Henti Hendalastuti Rachmat, Marnan Turjaman, Pratiwi, Fitri Nurfatriani, Yonky Indrajaya and Arida Susilowati
Forests 2020, *11*(12), 1235; https://doi.org/10.3390/f11121235 - 24 Nov 2020
Viewed by 677

Abstract *Pinus merkusii* Jungh et de Vriese, known as Tusam or Sumatran pine, is the only pine that grows naturally in the south of the Equator with its natural distribution found in Indonesia, the Philippines, Myanmar, Thailand, Laos, Cambodia, and Vietnam. The Sumatran pine [...] Read more.
(This article belongs to the Special Issue Application of Innovative Silvicultural Treatments on Pine Forests)

► Show Figures

Show export options

Displaying articles 1-140

MDPI

Subscribe to receive issue release notifications and newsletters from MDPI journals

Select options

Enter your email address...

Subscribe

Further Information
Article Processing Charges
Pay an Invoice
Open Access Policy
Contact MDPI
Jobs at MDPI

Guidelines
For Authors
For Reviewers
For Editors
For Librarians
For Publishers
For Societies

MDPI Initiatives
Institutional Open Access Program (IOAP)
Sciforum
Preprints
Scilit
SciProfiles
MDPI Books
Encyclopedia
JAMS
Proceedings
MDPI Blog

Follow MDPI
LinkedIn
Facebook
Twitter

© 1996-2021 MDPI (Basel, Switzerland) unless otherwise stated

Disclaimer Terms and Conditions Privacy Policy

Back to Top

Ads by Google
Send feedback Why this ad? ⓘ

Forests

COUNTRY	SUBJECT AREA AND CATEGORY	PUBLISHER	H-INDEX
Switzerland Universities and research institutions in Switzerland	Agricultural and Biological Sciences └ Forestry	MDPI AG	44

PUBLICATION TYPE	ISSN	COVERAGE	INFORMATION
Journals	19994907	2010-2020	Homepage How to publish in this journal tamartin@ufl.edu

Temenos Multifonds
Temenos Learn More ›

Ads by Google
Send feedback Why this ad? ⓘ

SCOPE

Forests (ISSN 1999-4907) is an international and cross-disciplinary scholarly journal of forestry and forest ecology. It publishes research papers, short communications and review papers. There is no restriction on the length of the papers. Our aim is to encourage scientists to publish their experimental and theoretical research in as much detail as possible. Full experimental and/or methodical details must be provided for research articles. There are, in addition, unique features of this journal: computed data or files regarding the full details of the experimental procedure, if unable to be published in a normal way, can be deposited as supplementary material we also accept manuscripts communicating to a broader audience with regard to research projects financed with public funds manuscripts regarding research proposals and research ideas are welcomed Subject Areas: - forest ecology, management, and restoration- forest economics, natural resource policy and planning- silvicultural systems- forest entomology, forest pathology- forest ecophysiology and biology- forest genetics, tree breeding and biotechnology- climate change impacts, adaptation and mitigation in forests- forest biomass, bioenergy, and carbon sequestration- forest engineering- tropical forests and management- forest inventory, quantitative methods, and remote sensing- forest soil management- forest simulation modeling- forest and nature based recreation- wildland fire science and management- wood properties- human dimensions- urban forests.

Join the conversation about this journal

Ads by Google
Send feedback Why this ad? ⓘ

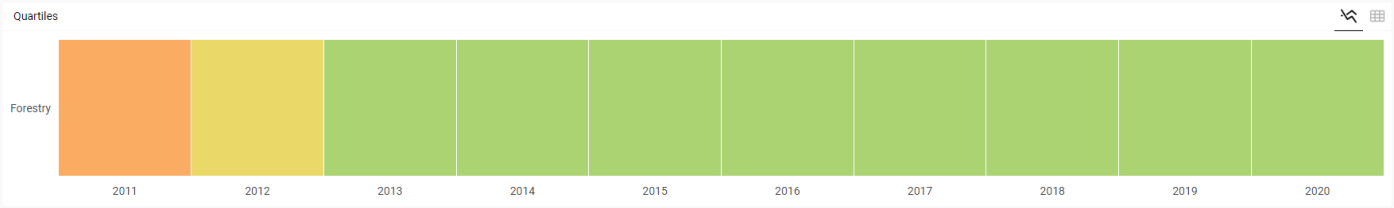

FIND SIMILAR JOURNALS options

1	2	3	4	5
Journal of Forestry Research	IForest	Annals of Forest Science	Forest Ecosystems	Forest Systems
CHN	ITA	USA	DEU	ESP
85% similarity	83% similarity	81% similarity	80% similarity	77% similarity

Ads by Google
Send feedback | Why this ad?

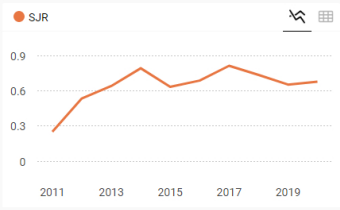

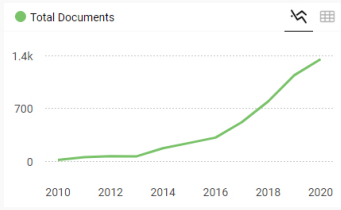

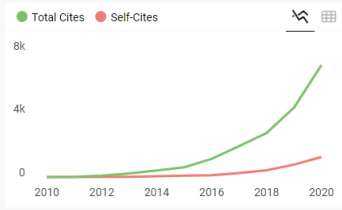

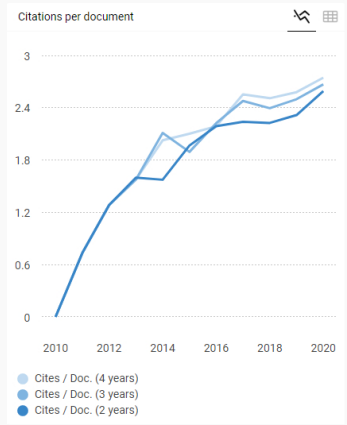

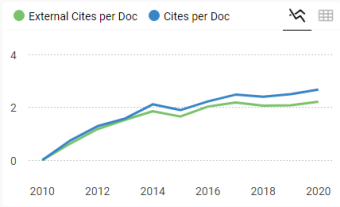

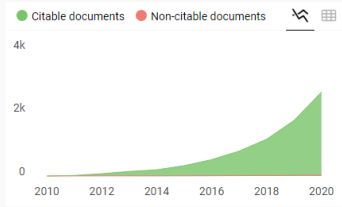

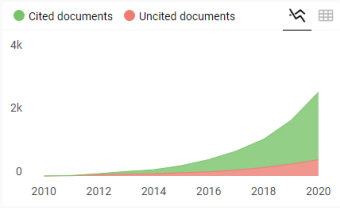

Metrics based on Scopus® data as of April 2021

Grammar and Spelling Checker
Check your grammar, spelling, and punctuation instantly with Grammarly Grammarly
Learn More

Mahmoud 1 year ago

I published my article in Forest. it was great experience.
The Be

reply

SCImago Team

Melanie Ortiz 1 year ago

Dear Mahmoud, thanks for your participation! Best Regards, SCImago Team

M **Mahmoud** 1 year ago

Hi.
I read your comments and i agree with some of them.
I published a article in Remote Sensing From MDPI publisher.

now, I will ready to submit a new article to Forest.

After it i will tell you about my experience. Hope this is a good experience.
The Best Mahmoud

reply

SCImago Team

Melanie Ortiz 1 year ago

Dear Mahmoud, thanks for your participation! Best Regards, SCImago Team

S **sara** 3 years ago

Based on my personal experience and the colleague of mine, this journal is really among the worst journals to publish a paper. They are quite fast in finding reviewers and so on, BUT:

In my case, after 3 rounds of review and a lot of not logical tight deadline, the editor rejected my paper and said your paper was not fit with the scope of the journal, while I satisfied three of four reviewers.

This has happened to my colleague. His paper finally was accepted, but he had difficulties as his paper at first was rejected and he had to convince them that it is not an appropriate decision.
He also had problems by, for example, receiving 100 comments and major revision with 10 days time! [I had the same problem].

I personally recommend the "logical process of review" and "professional editors" of Elsevier and Springer journals than MDPI.
Hope you find this comments useful.

P.S: my publication is going to accept in one of Elsevier journals with impact factor around 5 with a minor revision!

reply

Leave a comment

Name

Email
(will not be published)

I'm not a robot reCAPTCHA Privacy - Terms

Submit

The users of Scimago Journal & Country Rank have the possibility to dialogue through comments linked to a specific journal. The purpose is to have a forum in which general doubts about the processes of publication in the journal, experiences and other issues derived from the publication of papers are resolved. For topics on particular articles, maintain the dialogue through the usual channels with your editor.

Developed by: SCImago Powered by: Scopus

Follow us on @ScimagoJR

Scimago Lab, Copyright 2007-2020. Data Source: Scopus®

forests

an Open Access Journal by MDPI

Indexed in: Ei Compendex | CITESCORE 2.7 SCOPUS | IMPACT FACTOR 2.221

CERTIFICATE OF ACCEPTANCE

Certificate of acceptance for the manuscript (**forests-994547**) titled:

The Prediction of Stiffness Reduction Non-linear Phase in Bamboo Reinforced Concrete Beam Using The Finite Element Method (FEM) and Artificial Neural Networks (ANNs)

Authored by:

Muhtar Muhtar

has been accepted in *Forests* (ISSN 1999-4907) on 25 November 2020

MDPI Academic Open Access Publishing since 1996

Basel, November 2020

forests

MDPI

Article

The Prediction of Stiffness Reduction Non-Linear Phase in Bamboo Reinforced Concrete Beam Using the Finite Element Method (FEM) and Artificial Neural Networks (ANNs)

Muhtar

Faculty of Engineering, University of Muhammadiyah Jember, Jember 68121, Indonesia; muhtar@unmuhjember.ac.id

Received: 25 October 2020; Accepted: 25 November 2020; Published: 10 December 2020

Abstract: This paper discusses the reduction of the stiffness of bamboo reinforced concrete (BRC) beams to support the use of bamboo as an environmentally friendly building material. Calculation of cross-section stiffness in numerical analysis is very important, especially in the non-linear phase. After the initial crack occurs, the stiffness of the cross-section will decrease with increasing load and crack propagation. The calculation of the stiffness in the cross-section of the concrete beam in the non-linear phase is usually approximated by giving a reduction in stiffness. ACI 318-14 provides an alternative, reducing the stiffness of the plastic post-linear beam section through the moment of inertia (I) of the beam section for elastic analysis between $0.50I_g$–$0.25I_g$. This study aims to predict the value of the reduction in the stiffness of the BRC beam section in the non-linear phase through the load-displacement relationship of experimental results validated by the Finite Element Method (FEM) and the Artificial Neural Networks (ANN) method. The experiment used 8 BRC beams and one steel-reinforced concrete (SRC) beam of singly reinforced with a size of 75 mm × 150 mm × 1100 mm. The beams were tested using a four-point loading method. The analysis results showed that the value of the stiffness reduction in the beam cross-sectional in the non-linear phase ranged from $0.5I_g$–$0.05I_g$ for BRC beams, and $0.75I_g$–$0.40I_g$ for SRC beams.

Keywords: stiffness reduction; bamboo reinforced concrete (BRC); finite element method (FEM); artificial neural networks (ANN)

1. Introduction

The impact of increasing industrial development is that it can cause pollution of air, water, soil, and noise. The use of industrial building materials such as ceramics, steel, concrete, and other materials has led to an increase in environmental pollution. The procurement of wood forests or bamboo forests must be done as a counterweight to environmental pollution. Pandey et al. (2017) [1] and Mostafa et al. (2020) [2] revealed that an average tree absorbs one ton of CO_2 and produces 0.7 tons of O_2 for every cubic meter of growth. The use of environmentally friendly building materials such as wood and bamboo must be done. Bamboo is a forest product that provides high economic and ecological value to the community. Bamboo also has enormous potential with promising prospects [3]. Bamboo is one of the commodities produced by Community Forests. However, research on the behavior of bamboo as a building material is mandatory, such as research on the stiffness of bamboo reinforced concrete (BRC) beams.

The stiffness reduction factor is a multiplier to reduce the moment of inertia in gross cross-sectional, and the gross cross-sectional area remains constant. These factors are conservatively enforced by various concrete standards to account for the loss of stiffness in the concrete cross-section due to the

cracking of the concrete. The stiffness of the beam cross-section in the elastic phase or linear phase indicates the full section flexural stiffness, E_cI_g, whereas in the non-linear phase or after the initial crack, the gross cross-section bending stiffness is reduced to the effective flexural stiffness, E_cI_{eff}. The stiffness reduction factor is significantly influenced by the amount of moment or the applied load, while the stiffness reduction factor does not differ from the amount of reinforcement [4]. ACI 318M-14 [5] shows that the gross section flexural stiffness, E_cI_g, is reduced to obtain the effective flexural stiffness, E_cI_e, which causes cracking and other softening effects. As the moment in the concrete section increases, the flexural stiffness will be reduced due to the cracks that continue to propagate and spread. ACI 318M-14 [5] provides stiffness reduction limits for elastic analysis with a moment of inertia limits between $0.25I_g$–$0.5I_g$ for concrete beams. The equation for the moment of inertia effective (I_e) is determined in ACI 318-05 [5] Section 9.5.2.3, as shown in Equation (1).

$$I_e = \left(\frac{M_{cr}}{M_a}\right)^3 I_g + \left[1 - \left(\frac{M_{cr}}{M_a}\right)^3\right] I_{cr} \quad (1)$$

where I_g = moment of inertia of the gross concrete section and I_{cr} = moment of inertia of the crack section including the reinforcement. The moment of inertial effective (I_e) as shown in Equation (1) will decrease as the moment that occurs, M_a. Calculation of the moment of inertia of the crack cross-section, I_{cr} at Equation (1) must pay attention to the number of reinforcement installed. However, the amount of reinforcement is not determined at the initial design stage.

The process of stiffness reduction in the beam section starts from the "*no crack*" and "*cracked*" conditions in the section. In the service load condition or the elastic condition, the stiffness of the beam section is in full condition, even though the moment due to the load continues to increase. In the elastic condition, the moment that occurs (M_a) is still below the moment of cracking (M_{cr}), or the tensile stress of the concrete is still below the modulus of rupture of the concrete beam cross-section, f_r. In the elastic conditions, the difference in stiffness between two different types of beams usually occurs not due to reduced inertia of the cross-section, but due to the properties of the materials used. For example, the stiffness of bamboo reinforced concrete beams is different from the stiffness of steel-reinforced concrete (SRC) beams. In the elastic conditions, the stiffness of BRC beams is lower than the stiffness of SRC beams [6–8]. This is because BRC beams use bamboo reinforcing materials which have elastic properties and high resilience properties. BRC beams with bamboo reinforcement will be able to accept high impact loads without causing stress over the elastic limit, even though displacement has occurred. This indicates that the energy absorbed during loading is stored and released if the material is not loaded.

Meanwhile, the SRC beam uses steel material that has high stiffness and toughness, so that the SRC beam in the service load range or elastic condition does not experience displacement or excessive deformation. Beams that use materials with high stiffness and toughness will be able to withstand high impact loads or shock loads. If the SRC beam gets an impact load, then some of the energy is absorbed and some of the energy is transferred.

Research on modeling and stiffness reduction has been carried out by many researchers. Kai Zhang et al. (2020) [9] investigated the effect of electrochemical rehabilitation (ER) techniques on the fatigue stiffness of RC beams. The results of his research indicated that electrochemical rehabilitation (ER) exacerbated bond breakage, thereby reducing the flexural stiffness of RC beams. Salam Al-Sabah et al. [10] discuss the use of negative stiffness in the failure analysis of concrete beams. In his research, Salman Al-Sabah et al. concluded that the effective and simple one-dimensional stress-strain behavior of concrete was used to study concrete blocks with proportional loading, the only source of non-linearity to consider cracks in concrete. Hong-Song Hu et al. (2016) [11] investigated the effectiveness of square Concrete filled steel tubular (CFST) rod stiffness, and the results proposed an equation for the effective stiffness of square CFST rods. Muhtar et al. [7] tested the flexural of BRC beams and SRC beams, the results showed that the stiffness decreased after the initial cracking. The average stiffness of the BRC beam decreased from 26,324.76 MPa before cracking to 6581.20 MPa

after collapse [7], while the average value of SRC beam stiffness decreased from 30,334.11 MPa before cracking to 16,873.35 MPa after the collapse.

K.A. Patela et al. (2014) [12], in their paper, provide an explicit expression for the effective moment of inertia by considering cracks for reinforced concrete beams (RC) with uniformly distributed loads. The proposed explicit expressions can be used to predict short-run displacement in-service load. The sensitivity analysis shows a substantial dependence of the effective moment of inertia on the selected input parameter. Displacement is an important parameter for examining the serviceability criteria of structures. The short-term displacement is generally calculated using the effective moment of inertia across the span at the service load [12]. Chunyu Fu (2018) [13] presents a method of estimating the stiffness of cracked beams based on the stress distribution. In his conclusion, he said that the presence of cracks causes a nonlinear stress distribution along the beam section, which changes the neutral axis of the cross-section and further affects the stiffness of the beam. J.R. Pique (2008) [14] concluded that when the design is controlled by the minimum reinforcement, especially in the beam, special attention should be paid to the calculation of the real period and maximum distortion. The effective stiffness of the beam with the minimum steel ratio is much lower than that obtained by the proposed reduction factor. As a result, the actual period and actual maximum distortion can be greater. Akmaluddin et al. (2012) [15] concluded that the moment of crack and the value of the moment of inertia of the crack was significantly affected by the presence of bamboo reinforcement in the beam. The experimental results show that the crack moment varies from 0.3 to 0.7 from the ultimate moment. The experimental and theoretical crack moment ratio varies from 0.90 to 1.42. İlker Kalkan (2013) and [16] concluded that the effective moment of inertia and load-displacement curve analysis is highly dependent on the crack moment used in the expression analysis of the effective moment of inertia. Therefore, the experimental cracking moment of the beam should be used in the calculation of the effective moment of inertia for a more accurate comparison of the different analytical methods. Chunyu Fu et al. (2020) [17] concluded that cracking of concrete causes a gradual change in the distribution of strain along with the cross-sectional height of reinforced concrete beams, which in turn affects the instantaneous stiffness. The instantaneous stiffness proved to be highly dependent on the number and depth of cracks. This dependence can be accurately reflected by the method proposed by simulating a gradual change in the concrete strain distribution. Xiuling Feng et al. (2013) [18] examines the reduction factor of flexural stiffness in reinforced concrete columns with an equiaxial cross-section and suggests that the reduction factor is proposed by considering the nonlinear characteristics of the material and its geometric nonlinearity.

The difference in the nonlinear characteristics of the material used in the BRC beam and the SRC beam greatly determines the flexural behavior of the beam. Bamboo reinforced concrete beams have low stiffness and tend to be large displacement. The solution to increasing the stiffness of BRC beams is to use shear reinforcement and the principle of confined concrete [7,19]. In the linear elastic condition, the BRC beam has shown a large displacement, but when the ultimate load is reached and the loading is released gradually, the displacement tends to return to zero. In this study, the reduction of stiffness in the non-linear phase was analyzed through the load vs. displacements that were validated using the finite element method (FEM) and the Artificial Neural Networks (ANN) method. It is suspected that the reduction of the cross-sectional stiffness of the BRC beam is different from the reduction in the stiffness of the SRC beam section. The parameter of the moment of inertia of the cross-section becomes a benchmark in determining the reduction of stiffness according to ACI-318M-14 [5].

2. Materials and Methods

2.1. Treatment of Materials

In this study, the treatment of bamboo material as concrete reinforcement is an important thing to do. The bamboo used is the bamboo "petung" (*Dendrocalamus asper*) which is between three and five years old [20–22]. The part of bamboo that is used as reinforcing of concrete is 6–7 m long from the

base of the bamboo stem [23]. Bamboo is cut according to the size of the bamboo reinforcement to be used, which is 15 × 15 mm^2. Then, bamboo is soaked for ±20–30 days [21]. After soaking, bamboo is dried in free air until it has an absorption level of ±12%.

Application of adhesive or waterproof coating [24,25] is done after the bamboo reinforcement is cleaned and trimmed according to the planned size. The application of a waterproof layer is carried out to prevent the hydrolysis process between bamboo and concrete. Sand sprinkling on bamboo reinforcement is done when the adhesive is half dry to make it stronger [21,26]. The application of sand aims to increase the adhesion strength of bamboo reinforcement to concrete.

An installation of a hose-clamp at both ends of the bamboo reinforcement is done to match the concept of hooks or bends in steel reinforcement. An installation of the hose-clamp only on tensile reinforcement is done to increase bond-stress between bamboo reinforcement and concrete [27,28]. The tensile force on the bamboo reinforcement will be distributed to the concrete through the hose-clamp, which functions as a shear connector. Bamboo treatment is shown in Figure 1.

Figure 1. The materials and treatments of bamboo reinforcement.

2.2. Materials

The concrete mixture used in this study is a normal concrete mixture consisting of Portland Pozzolana Cement (PPC), sand, coarse aggregate, and water with a proportion of 1:1.8:2.82:0.52. Sand and gravel come from the Jember area of Indonesia. The cylindrical specimen measures 150 mm in diameter and 300 mm in height. The cylindrical specimens were press-tested using a Universal Testing Machine (UTM) with a capacity of 2000 kN after the concrete was 28 days old. The procedure for the cylinder specimen compressive test follows ASTM C 39 [29]. The average compressive strength of cylindrical concrete is 31.31 MPa with an average weight of 125.21 N. The properties and characteristics of the concrete are shown in Table 1.

Table 1. Material properties of reinforcing and concrete.

Bar Type and Concrete	Diameter, d (mm)	Modulus of Elasticity (E), (MPa)	Poisson's Ratio (ν)	Tensile Strength, f_y (MPa)	Compressive Strength, f'_c (MPa)
Bamboo	□ 15 × 15	17,235.74	0.20	126.68	-
Steel	ϕ 8	207,735.92	0.25	392.28	-
Concrete	-	26,324.79	0.30	-	31.31

□: a sign of the rectangular cross-sectional shape of bamboo reinforcement.

The tensile test of bamboo reinforcement produces the average tensile stress of 126.68 N/mm^2 with an average strain of 0.0074. The modulus of elasticity of bamboo reinforcement was calculated using the formula $E = \sigma/\varepsilon$ and obtained 17,235.74 MPa. The modulus of elasticity of steel is obtained by 207,735.92 MPa. The properties and characteristics of bamboo and steel reinforcement are shown in Table 1.

The adhesive layer or waterproof coating used was Sikadur®-752 produced by PT. SIKA Indonesia [30]. The specifications for the adhesive sikadur®-752 are shown in Table 2. Installation of hose-clamp on bamboo reinforcement is done when the waterproof layer is half dry [21]. The diameter of the hose-clamp used is $\frac{3}{4}$" made in Taiwan.

Table 2. The specification of Sikadur®-752 [30].

Components	Properties
Color	Yellowish
Density	Approx. 1.08 kg/L
Mix comparison (weight/volume)	2:1
Pot life at +30 °C	35 min
Compressive strength	62 MPa at 7 days (ASTM D-695) 64 MPa at 28 days
Tensile strength	40 MPa at 28 days (ASTM D-790)
Tensile Adhesion Strength	2 MPa (Concrete failure, over mechanically prepared concrete surface)
Coefficient of Thermal Expansion	−20 °C to + 40 °C 89×10^{-6} per °C
Modulus of elasticity	1060 MPa

2.3. Experimental Procedure

The test object consisted of 9 beams with a size of 75 mm × 150 mm × 1100 mm, consisting of 8 bamboo reinforced concrete beams (BRC) and one steel-reinforced concrete beam (SRC). Bamboo reinforcement is installed as tensile reinforcement with a reinforcement area of 450 mm^2. The steel reinforcement used has a diameter of 8 mm with an area of A_s = 100.48 mm^2. The beam geometry and reinforcement detail of the BRC and SRC beams are shown in Figure 2.

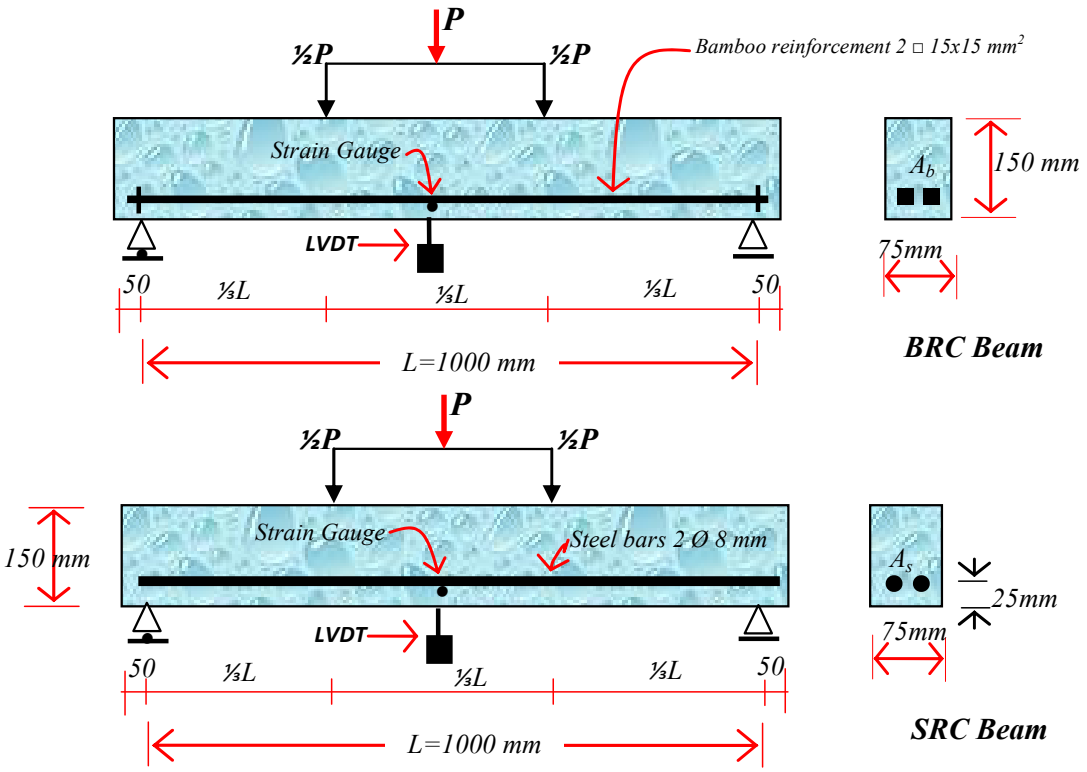

Figure 2. Reinforcement details and beam test settings.

The beam flexural test method was carried out using the four-point method [31]. The test arrangement and load position are shown in Figure 2. Strain gauges are installed on the bamboo

reinforcement at a distance of $\frac{1}{2}$L from the support of the beam. Beam displacement measures use Linear Variable Displacement Transducers (LVDT) with a distance of $\frac{1}{2}$L from the beam support.

The loading stages from zero to the collapse of the beam are used as a hydraulic jack and a load cell connected to a load indicator tool. The load reading on the load indicator is used as a hydraulic jack pump controller, displacement reading, and strain reading according to the planned loading stage. However, when the test object reaches its ultimate load, the displacement reading controls the strain and load reading, while the pumping of the hydraulic jack continues slowly according to the command of the displacement reader. The failure pattern was observed and identified by the cracks that occurred, from the time of the initial crack until the beam collapsed.

2.4. Validation of Numerical Methods

Validation of experimental data using the Finite Element Method (FEM) and Artificial Neural Networks (ANN). The relationship between load vs. displacement experiment results was validated by using the finite element method. The procedure used is inputting material data and loading stages to determine the behavior of the load vs. displacement of BRC beams and SRC beams. The data input for the loading stages is carried out following the loading stages from laboratory experimental data. The numerical method used is the finite element method, using the Fortran PowerStation 4.0 program [32]. The theoretical analysis is used to calculate the load causing the initial crack is the elastic theory (linear analysis) with cross-section transformation. For linear analysis, the input material data is the modulus of elasticity (E) and Poisson's ratio (υ). The calculation of the modulus of elasticity of the composites (E_{comp}) is shown in Tables 3 and 4. The non-linear phase is approximated by decreasing the concrete strength from 0.25 to 0.5 for the calculation of the effective stiffness in the plastic plane [5]. In the analysis of the finite element constitutive relationship, the problem-solving method uses the plane-stress theory. Triangular elements are used to model plane-stress elements with a bidirectional primary displacement at each point so that the element has six degrees of freedom. The discretization of the beam plane is carried out using the triangular elements shown in Figure 3 for BRC beams and Figure 4 for SRC beams.

Table 3. Elasticity Modulus of Composite of BRC beam.

Layer Number	Compressive Strength of Concrete, f'_c	Dimensions of per Layer		Modulus of Elasticity of the Material (E)		Elasticity Modulus of Composite (E_{comp})
	Mpa	b (mm)	h (mm)	Concrete, E_c (MPa)	Bamboo, E_b (MPa)	MPa
4th mesh layer	31.31	75	50	26,851.29	0	26,851.29
3rd mesh layer	31.31	75	60	26,851.29	0	26,851.29
2nd mesh layer	31.31	75	15	26,851.29	1723.57	23,140.89
1st mesh layer	31.31	75	25	26,851.29	0	26,851.29

Table 4. Elasticity Modulus of Composite of SRC beam.

Layer Number	Compressive Strength of Concrete, f'_c	Dimensions of per Layer		Modulus of Elasticity of the Material (E)		Elasticity Modulus of Composite (E_{comp})
	Mpa	b (mm)	h (mm)	Concrete, E_c (MPa)	Steel, E_s (MPa)	MPa
4th mesh layer	31.31	5	50	26,851.29	0	26,851.29
3rd mesh layer	31.31	75	67	26,851.29	0	26,851.29
2nd mesh layer	31.31	75	8	26,851.29	207,735.92	43,209.32
1st mesh layer	31.31	75	25	26,851.29	0	26,851.29

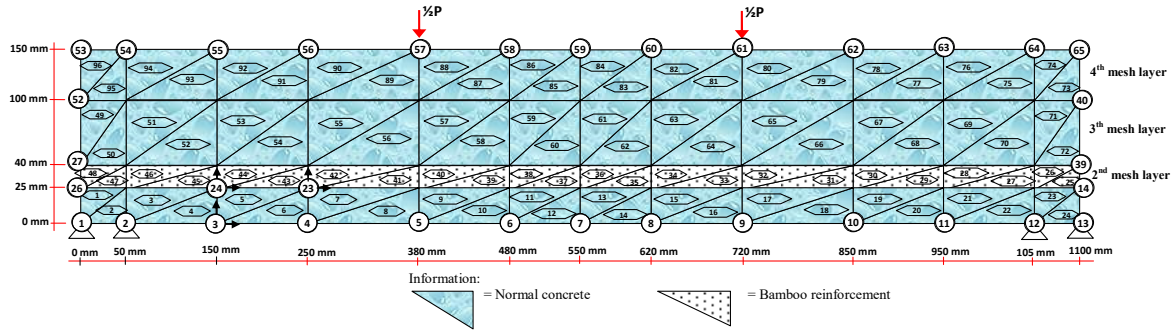

Figure 3. Discretization of the triangular element on the bamboo reinforced concrete (BRC) beam.

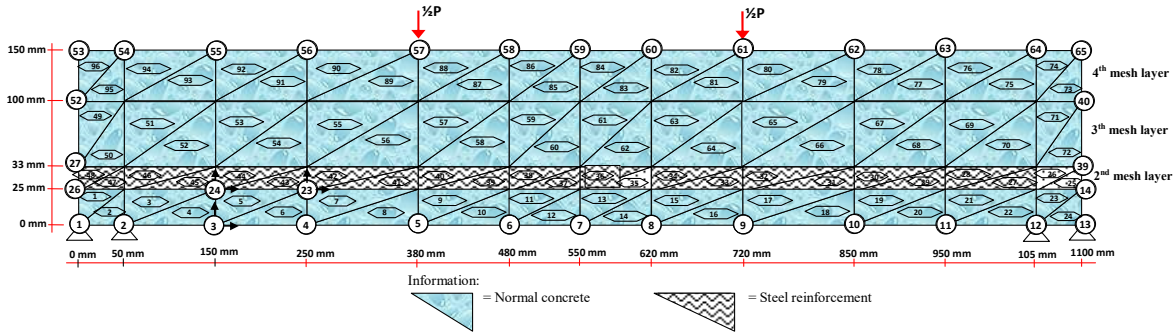

Figure 4. Discretization of the triangular element on the steel-reinforced concrete (SRC) beam.

The modulus of elasticity (E) for each layer is calculated according to the condition of the material. Layers of concrete and bamboo reinforcement are calculated using the following Equation (2) [33].

$$E_e = E_b \cdot V_b + E_c \cdot V_c \tag{2}$$

where E_e = the equivalent elasticity modulus of BRC beam, E_b = elastic modulus of bamboo reinforcement, E_c = modulus of elasticity of concrete, V_b = relative volume of bamboo reinforcement in calculated layers, and V_c = relative volume of concrete in calculated layers. The stress-strain relationship for plane-stress problems has the shape of an equation such as Equation (3).

$$\begin{Bmatrix} \sigma_x \\ \sigma_y \\ \tau_{xy} \end{Bmatrix} = \frac{E}{(1+\nu^2)} \begin{bmatrix} 1 & \nu & 0 \\ \nu & 1 & 0 \\ 0 & 0 & \frac{1-\nu}{2} \end{bmatrix} \begin{Bmatrix} \varepsilon_x \\ \varepsilon_y \\ \gamma_{xy} \end{Bmatrix} \tag{3}$$

where E is the modulus of elasticity and ν is the Poisson's ratio. And the principal stresses in two dimensions are calculated by Equation (4).

$$\sigma_{1,2} = \frac{\sigma_x + \sigma_y}{2} \pm \sqrt{\left(\frac{\sigma_x - \sigma_y}{2}\right)^2 + {\tau_{xy}}^2} = \sigma_{\max} \tag{4}$$

The simulation and steps for preparing a FEM analysis with the Fortran PowerStation 4.0 program [32] are summarized as follows:

Step 1: Discretization of BRC and SRC beam planes with the discretization of triangular elements, the numbering of triangular elements, and the numbering of nodal points as shown in Figures 3 and 4.

Step 2: Calculation and collection of geometry and material data, such as the modulus of elasticity of the material (E), Poisson's ratio (ν), etc.

Step 3: Writing a programming language for triangular elements using the Fortran PowerStation 4.0 program according to the constitutive relationships and FEM modeling as shown in the following link: http://bit.ly/2F17w8F.

Step 4: Open the Fortran PowerStation 4.0 program. An example is shown at the following link: http://bit.ly/2MTh22j.

Step 5: Write programming language data (Step 3) in the Fortran PowerStation 4.0 program. Examples can be seen at the following link: http://bit.ly/2ZvZWMU.

Step 6: Input DATA.DAT of BRC beam and SRC beam in the Fortran PowerStation 4.0 program. Input data is displayed at the following links: http://bit.ly/351FPqU and http://bit.ly/2MBqas9. An example of displaying input data is shown on the following link: http://bit.ly/2u2K2xR.

Step 7: Analyze the program until there are no warnings and errors. If there are warnings and errors, check and correct program data and input data.

Step 8: Download stress data. The stress data are shown at the following link: http://bit.ly/2rDPeaI for the stress of BRC beam, and http://bit.ly/2Q4Ihc1 for the stress of the SRC beam. An example of displaying stress data from the Fortran PowerStation 4.0 program is shown at the following link: http://bit.ly/2ZybLCd.

Step 9: Download displacement data. An example of displaying data displacement from the Fortran PowerStation 4.0 program is shown on the following link: http://bit.ly/2Q7j2Wp.

Step 10: Enter stress and displacement data into the Surfer program to obtain contour image data of stress and displacement. Stress and displacement contour image data.

2.5. Validation of Artificial Neural Networks (ANN)

Artificial Neural Networks (ANN) is a computational system for solving complex problems in civil engineering. In this study, the validation carried out by the Artificial Neural Networks (ANN) method is the validation of the load vs. displacements from laboratory experimental results. The data on the loading and displacement stages of the experimental results were used as input data and target data in this analysis. Previous researchers concluded that Artificial Neural Networks (ANN) can be an alternative in calculating displacement in reinforced concrete beams. Several researchers have used the ANN method for many structural engineering studies, such as predicting the compressive strength of concrete [34], axial strength of composite columns [35], and determination of RC building displacement [36]. Kaczmarek and Szymańska (2016) [37] concluded that the results of calculating displacement in reinforced concrete using ANN proved to be very effective. Abd et al. (2015) [38] concluded that the ANN method is also very good for predicting displacement in concrete beams with a very strong correlation level of 97.27% to the test data. Tuan Ya et al. (2019) [39] used the ANN method to predict displacement in cantilever beams and concluded that the output was very accurate.

The ANN method is currently very popular with researchers in predicting and evaluating the behavior of structures in the field of civil engineering. This is because the ANN method has an advantage in the nonlinear correlation between the input variables presented. Khademi et al. (2017) [40] predicts the compressive strength of concrete at 28 days of age by considering the experimental results, three different models of multiple linear regression (MLR), artificial neural networks (ANN), and adaptive neuro-fuzzy inference system (ANFIS). The results of his research concluded that the ANN and ANFIS models can predict the 28-day concrete compressive strength more accurately and the ANN model can perform better than the ANFIS model in terms of R^2. The ANN and ANFIS models are preferred because the nonlinear correlation between the input variables presented is better. The ANN and ANFIS models have higher accuracy requirements than the multiple linear regression (MLR) model. The accuracy of the prediction is very much dependent on the number of input variables. The greater the number of input parameters, the more accurate the results of the predictor model will be.

Xuan Li et al. (2019) [41] predict the service life of corroded concrete sewer pipes using three data-driven models, namely multiple linear regression (MLR), artificial neural networks (ANN), and adaptive neuro-fuzzy inference system (ANFIS). The one conclusion suggests that the ANN

and ANFIS models perform better than the MLR models for corrosion prediction, with or without considering the interactions between environmental factors.

The ANN data is divided into three different subsets [40], namely (1) Training: at this stage, the subset is trained and studied as occurs in the human brain, where the number of epochs is repeated until an acceptable model accuracy is obtained; (2) Validation: at this stage, the subset shows how well the model is trained, and estimates model properties such as misclassification, mean error for numerical predictors; and (3) Test: at this stage, the subset verifies the performance of the training subset built into the ANN model.

This paper uses even load input data, while the target data is the displacement of the laboratory test results. The distribution of the ANN model data composition consists of training 70%, validation 15%, and testing 15%. ANN architecture on a rectangular beam is shown in Figure 5. The process of implementing input data in the ANN model architecture consists of (1) Input layer, consisting of 1 neuron, namely displacement data variable of experimental results; (2) Hidden layer, consisting of 10 neurons. At this stage, the input layer will forward the data to the hidden layer or the output layer through a set of weights. This weight is a link from each neuron to other neurons in the next layer which will help adjust the ANN structure to the given displacement data pattern using learning. In the learning process, the weights will be updated continuously until one of the numbers of iterations, errors, and processing time has been reached. This is done to adjust the ANN structure to the desired pattern based on certain problems that will be solved using ANN. Weight is known as the independent parameter. During the training process, the weights will be modified to improve the accuracy of the results. The third layer is (3) Output layer, consisting of 1 neuron which is the expected output target, error, and weight. Error is the error rate of the displacement data node of the process carried out, while weight is the weight of the displacement data node with a value ranging between −1 and 1. Then the displacement data resulting from the training process is processed into a graphic image of the load vs. displacement relationship.

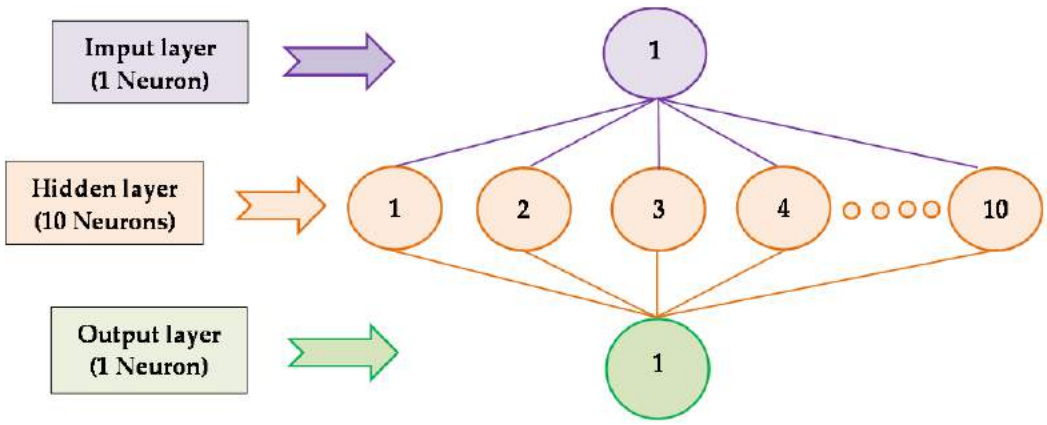

Figure 5. Schematic of Artificial Neural Networks (ANN) model architecture for BRC beam and SRC beam.

3. Results

3.1. Experimental

Table 5 shows the results of theoretical calculations and experiments for BRC and SRC beams. From the theoretical calculation, the BRC beam has an initial crack load of 6.87 kN and an SRC beam of 6.51 kN. The laboratory test results of the BRC beam experienced an initial crack at a load of 7.69 kN and an SRC beam had an initial crack at a load of 10 kN. The average ultimate load of the BRC beam occurs at a load of 31.31 kN or 97.27% of the theoretical collapse load of 32.19 kN. This shows that with the correct treatment of bamboo reinforcement, the BRC beam can reach load capacity according to

the results of the theoretical calculations. As is known, the researchers concluded that the ultimate load of BRC beams is very low when compared to the theoretical calculations. Dewi et al. (2017) [42] concluded that the bending capacity of bamboo reinforced concrete beams only reaches 56% of its capacity if the tensile strength of bamboo is full. Nathan (2014) [43] concluded that the flexural capacity of reinforced concrete beams only reaches 29% to 39% of the beam capacity steel-reinforced concrete with the same width and reinforcement dimensions. Khare (2005) [44] concluded that the flexural capacity of reinforced concrete beams is only 35% of steel-reinforced concrete beams at the same strength level.

Table 5. Results of theoretical calculations and experimental for the load capacity of BRC beams and SRC beams.

Specimens	Sample No	Theoretical Calculations		Flexural Test Results			
		First Crack Load (kN)	Ultimate Load (kN)	First Crack Load, P_{cr} (kN)	Failure Load, P_{ult} (kN)	Displacement at Failure (mm)	P_{cr}/P_{ult} (%)
(a) BRC-1	1	6.90	32.20	8.50	31.50	10.92	26.98
	2			8.00	29.00	11.90	27.59
(b) BRC-2	3			7.00	31.00	13.02	22.58
	4			7.50	33.00	12.18	22.73
(c) BRC-3	5			8.00	33.50	14.69	23.88
	6			7.50	33.00	9.32	22.73
(d) BRC-4	7			7.50	29.50	7.61	25.42
	8			7.50	30.00	10.69	25.00
	Average:			7.69	31.31		24.61
(e) SRC	9	6.50	24.20	10.00	24.00	6.33	41.57

SRC beams reach a collapse load of 24 kN or almost approaching the theoretical collapse load of 24.12 kN. This shows that the adhesion strength of steel-reinforcement with concrete is higher. Figures 6 and 7 show that the relationship of the load vs. displacement of the BRC beam and the SRC beam is different. The SRC beam shows the regions of the elastic limit, elastoplastic limit, and plastic limit. Meanwhile, the BRC beam only shows the plastic limit point or the ultimate load point. This shows that the behavior of reinforced concrete beams is very much determined by the properties and characteristics of the materials used.

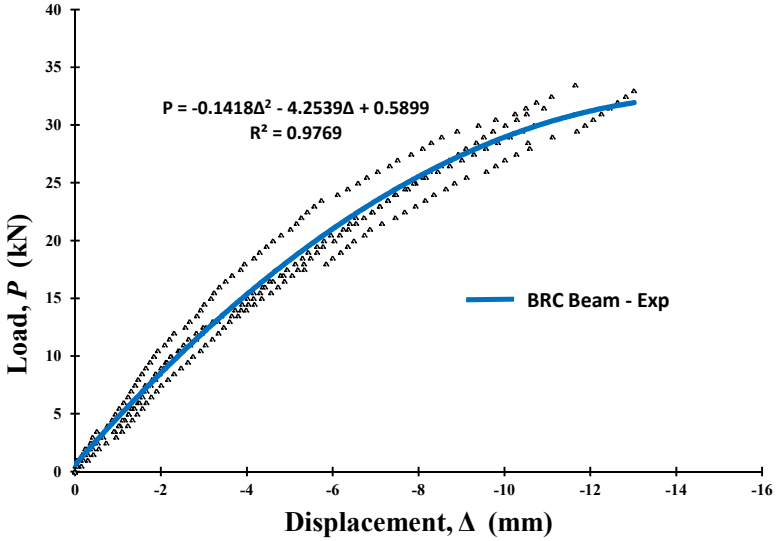

Figure 6. The relationship of load vs. displacement of BRC beam of experimental results.

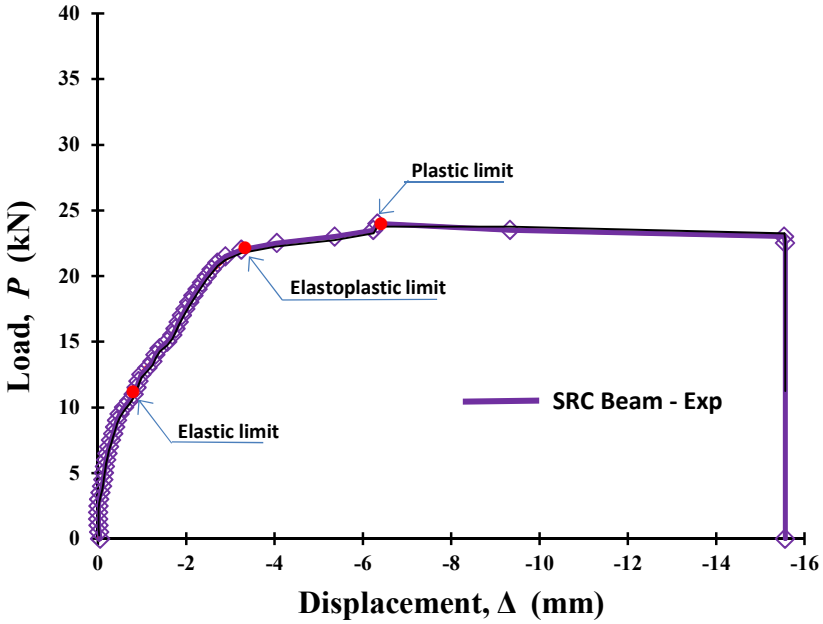

Figure 7. The relationship of load vs. displacement of SRC beam of experimental results.

Mechanical properties and characteristics of steel and bamboo materials are the dominant factors in the behavior model of the load and displacement relationship [6]. The difference between the stress and strain relationship patterns of bamboo and steel is in the position of the melting point and the fracture stress. Steel material shows a clear melting point, while bamboo reinforcement does not show a clear melting point. However, after the fracture stress, the relationship pattern of the stress-strain relationship tends to return to zero. This shows that bamboo has good elastic properties [7].

3.2. *Validation with the ANN Method*

The load vs. displacement relationship data from the experimental results is the basis used for the train and the network. Neural networks are designed by determining their structure experimentally. The data that trains the artificial neural network is the input, and the ability to reproduce the training pattern is tested. Convergence analysis was carried out to determine the optimal number of neurons in the hidden layer of ANN. Excessive neurons reduce the computational performance of ANN, whereas a lack of neurons causes difficulties in characterizing the input-output relationship. As suggested by Caudill and Mishra et al. (2019) [45], the upper limit of the number of neurons in the hidden layer is twice the number of inputs plus 1. After the number of neurons in the hidden layer is reached, the MSE, RMSE, and R^2 observations are stopped and no increase is assumed significant. The artificial neural network architecture used in this paper: IHO: 1-10-1 [Input-Hidden-Output] means that this artificial neural network consists of 1 input neuron, one hidden layer with 10 neurons, and 1 output neuron (predictive values of the load vs. displacement relationship).

Table 6 presents the performance results of ANN architecture for ten simulations. The process which has the lowest MSE is selected for comparison with experimental data. Figures 8–12 illustrate the prediction of the load vs. displacement of the BRC and SRC beams obtained when using the ANN model after training and when using the data obtained experimentally for training data, validation data, test data, and all data. Figures 8–12 shows the correlation between the value of the BRC beam and the SRC beam relationship obtained in the laboratory and the load vs. displacement values obtained using ANN analysis. The convergence of the position of the point with the line y = x indicates the identification of values with very high accuracy. The correlation value of laboratory data using ANN shows an average value of *R* Square of 0.999. This indicates that the two results are consistent. The prediction results of the ANN method show that the percentage of errors is very small, with a maximum error of 0.26%. Overall, the comparison of experimental data with the predicted results

of the ANN method shows an error of not more than 1%. From the data from the two analyses and the load vs. displacement relationship pattern, it can be concluded that the stiffness of the BRC beam has similarities.

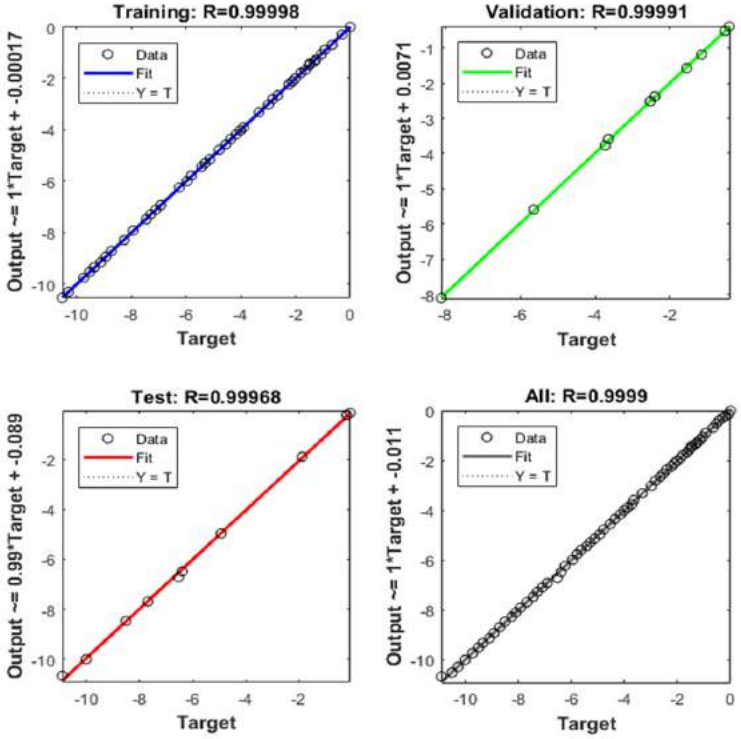

Figure 8. Prediction of the load vs. displacement relationship using ANN and using experimental observation for the training, validation, testing, and all datasets (BRC-1).

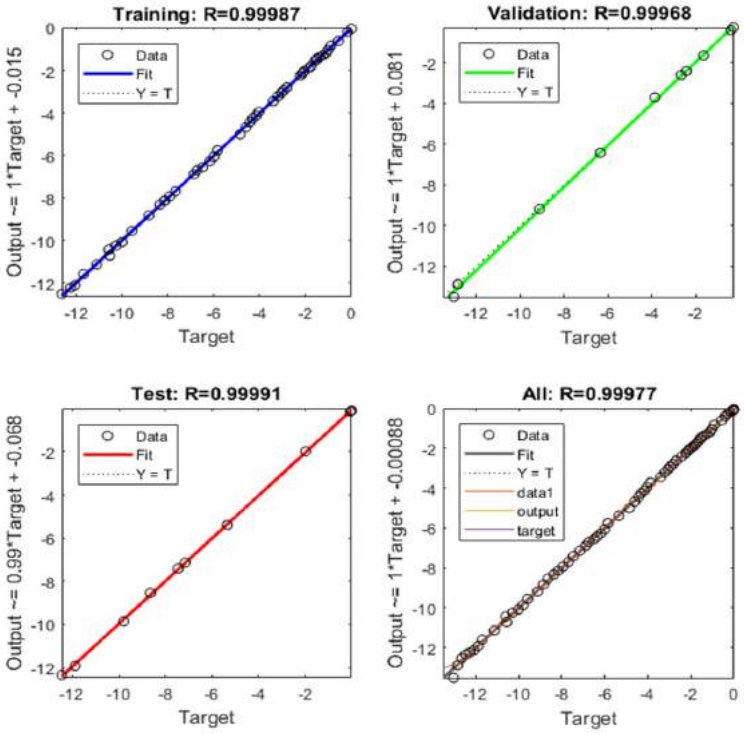

Figure 9. Prediction of the load vs. displacement relationship using ANN and using experimental observation for the training, validation, testing, and all datasets (BRC-2).

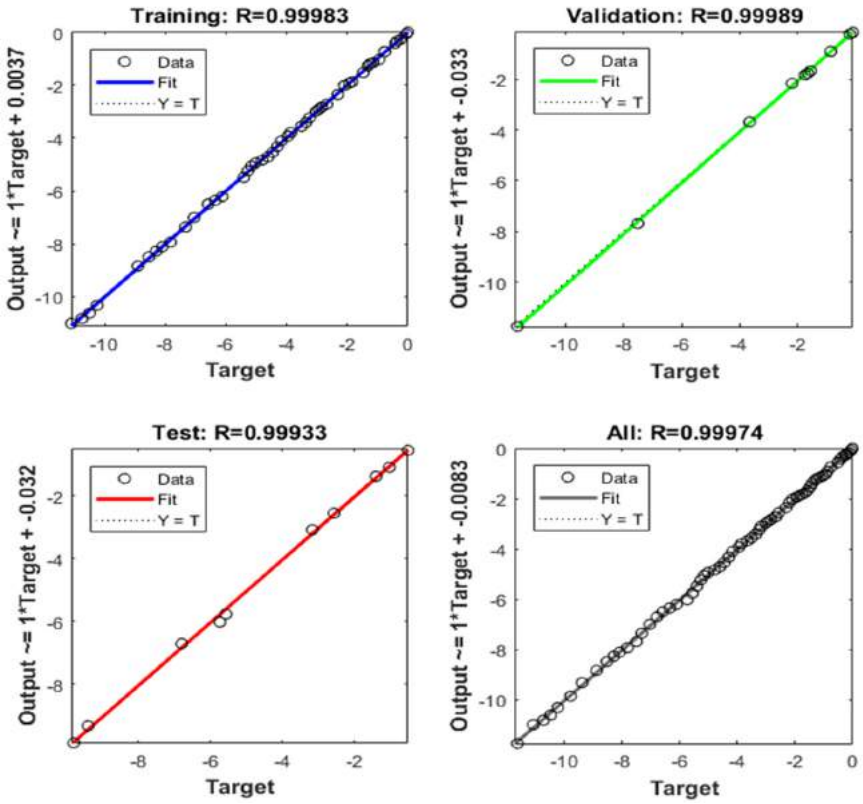

Figure 10. Prediction of the load vs. displacement relationship using ANN and using experimental observation for the training, validation, testing, and all datasets (BRC-3).

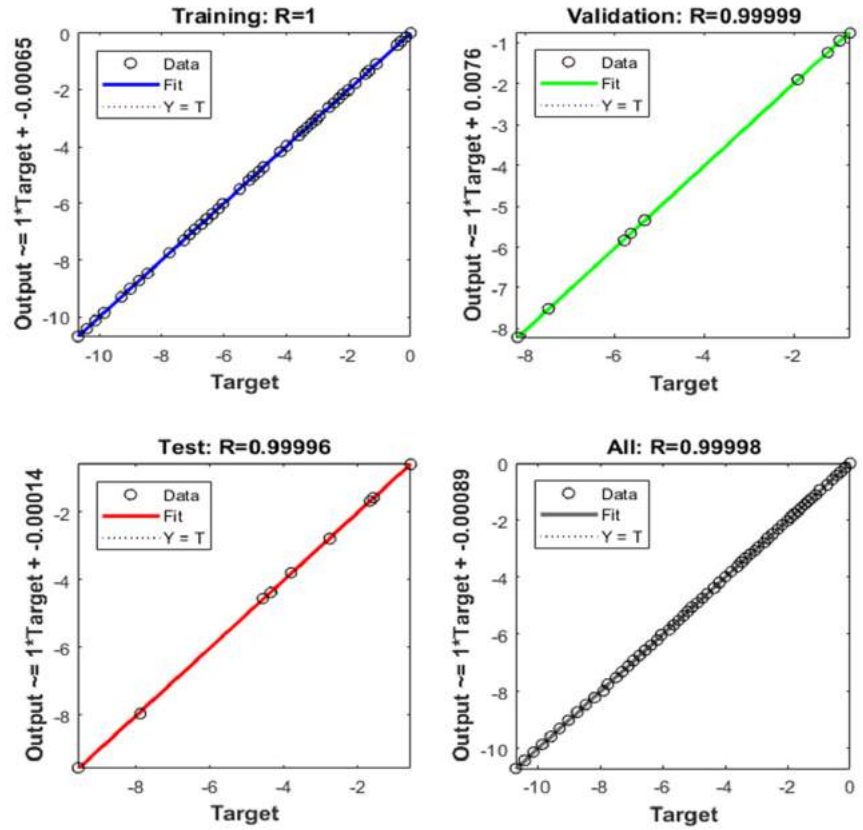

Figure 11. Prediction of the load vs. displacement relationship using ANN and using experimental observation for the training, validation, testing, and all datasets (BRC-4).

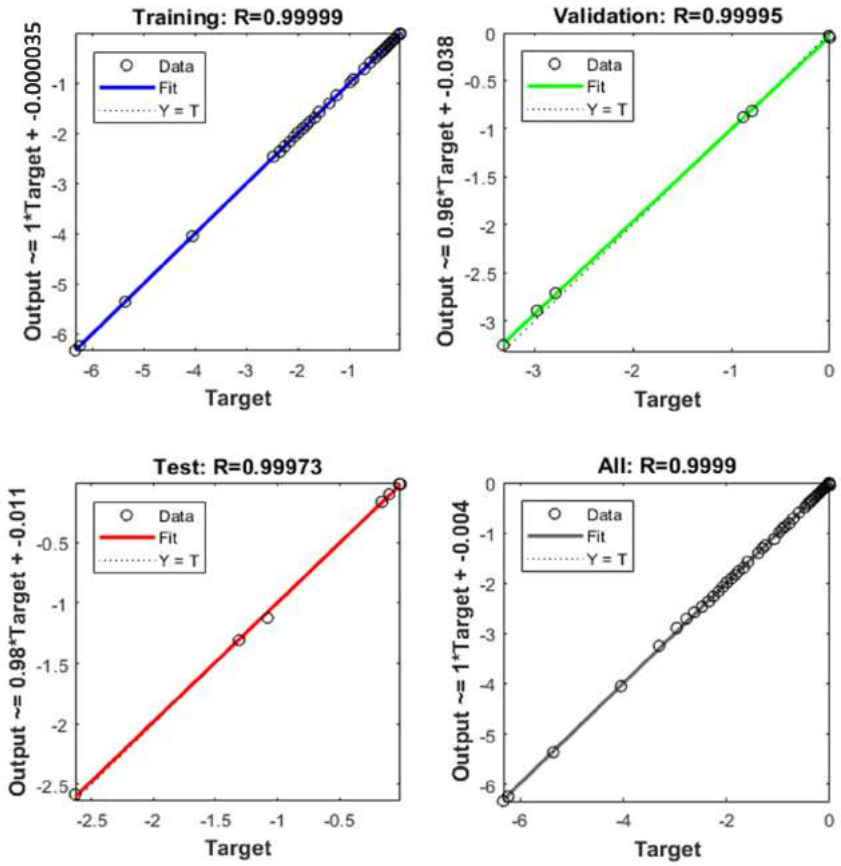

Figure 12. Prediction of the load vs. displacement relationship using ANN and using experimental observation for the training, validation, testing, and all datasets (SRC).

Table 6. The validation results of the relationship load vs. displacement using the ANN method.

Specimens	The Correlation Coefficient (*R*)			Mean Square Error (MSE)		
	Training	Validation	Testing	Training	Validation	Testing
BRC-1	1.0000	0.9999	0.9997	0.0004	0.0011	0.0110
BRC-2	0.9999	0.9997	0.9999	0.0038	0.0276	0.0048
BRC-3	0.9998	0.9999	0.9993	0.0034	0.0075	0.0152
BRC-4	1.0000	1.0000	1.0000	0.0001	0.0009	0.0010
SRC	1.0000	1.0000	0.9997	0.0001	0.0027	0.0006

The data merger of ANN analysis results from each BRC beam specimen into a load vs. displacement relationship. The merger is done to determine the suitability of the load vs. displacement relationship model through the R^2 parameter. From the results of the regression analysis, it is found that R^2 = 0.9771, or almost close to 1. This shows that the model has high suitability, as shown in Figure 13. Figure 13 illustrates the load vs. displacement relationship for all BRC beam typologies from ANN analysis.

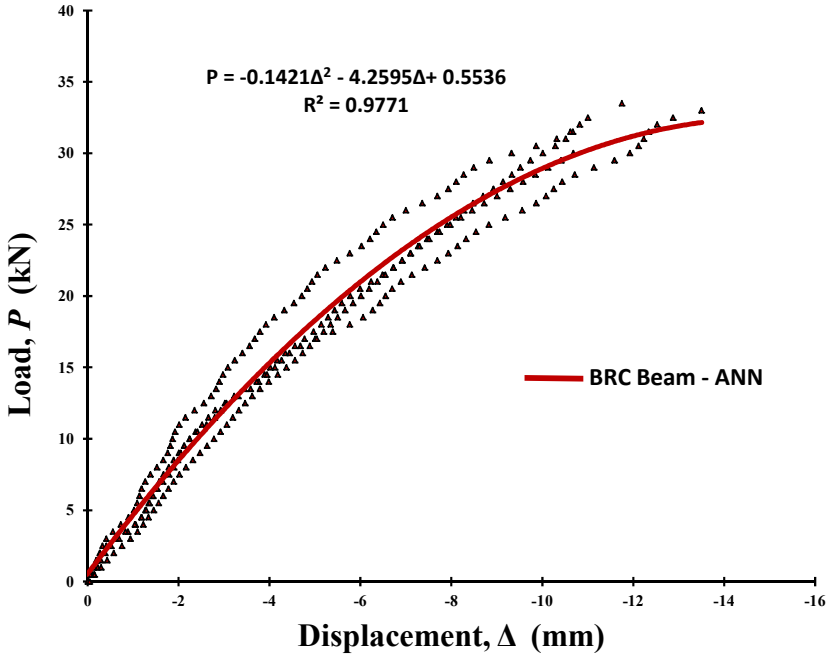

Figure 13. The relationship of load vs. displacement of BRC beam of ANN results.

3.3. Validation with the Finite Element Method

Validation of the relationship of load vs. displacement with the finite element method is done by inputting the geometry of the cross-section, load data, modulus of elasticity (E) per layer, and Poisson's ratio (υ). The load vs. displacement relationship diagram of the experimental results as shown in Figures 6 and 7 is used as a guide for the stages of the analysis process using the finite element method. And the cross-sectional stiffness input via the per-layer modulus of elasticity (E) is shown in Tables 7 and 8. The analysis execution using the finite element method uses the Fortran PowerStation 4.0 program. The process of calculating displacement and stress with the Fortran PowerStation 4.0 program is carried out in stages according to the loading and stiffness stages per layer from the beam's elastic condition, initial crack, elastoplastic, and plastic conditions until the beam collapses. The displacement data resulting from the finite element method is processed into a load vs. displacement relationship as shown in Figure 14. The displacement contours when the ultimate load are shown in Figure 15 for BRC beams and Figure 16 for SRC beams. The stress contours at the time of the load collapse are shown in Figure 17 for BRC beams and Figure 18 for SRC beams.

Table 7. The modulus of elasticity for each layer of the BRC beam in the non-linear phase.

Layer Number	Modulus of Elasticity (*E*) of the BRC Beam													
	Elastic Condition	Plastic Conditions with Gradual Loads												
	0–8.5 kN	9 kN	11 kN	13 kN	15 kN	17 kN	19 kN	21 kN	23 kN	25 kN	27 kN	29 kN	31 kN	33 kN
4th mesh layer	26,851.29	16,110.77	16,110.77	16,110.77	16,110.77	16,110.77	16,110.77	16,110.77	16,110.77	16,110.77	12,083.08	11,277.54	11,277.54	8592.41
3th mesh layer	26,851.29	16,110.77	16,110.77	16,110.77	16,110.77	16,110.77	16,110.77	16,110.77	16,110.77	1208.31	10,740.52	9397.95	9397.95	7518.36
2nd mesh layer	23,140.89	13,884.53	11,570.44	11,570.44	11,570.44	11,570.44	10,413.40	10,413.40	10,413.40	10,413.40	6942.27	6942.27	6942.27	5553.81
1st mesh layer	26,851.29	13,425.65	11,814.57	10,203.49	8323.90	6712.82	5101.75	5101.75	5101.75	3759.18	3222.16	2685.13	1611.08	1329.14

Table 8. The modulus of elasticity for each layer of the SRC beam in the non-linear phase.

Layer Number	Modulus of Elasticity (*E*) of the SRC Beam										
	Elastic Condition	Plastic Conditions with Gradual Loads									
	0–9 kN	10 kN	11 kN	12 kN	13 kN	15 kN	17 kN	19 KN	21 KN	23 kN	24 kN
4th mesh layer	26,851.29	26,851.29	20,138.47	20,138.47	20,138.47	20,138.47	20,138.47	18,795.90	18,795.90	13,425.65	11,411.80
3th mesh layer	26,851.29	26,851.29	20,138.47	20,138.47	18,795.90	18,795.90	18,795.90	17,453.34	17,453.34	13,425.65	11,411.80
2nd mesh layer	43,209.32	43,209.32	30,586.93	30,586.93	28,547.80	28,547.80	26,508.67	26,508.67	24,469.54	20,391,29	17,332.60
1st mesh layer	26,851.29	26,851.29	20,138.47	20,138.47	18,795.90	18,795.90	17,453.34	16,110.77	14,768.21	13,425.65	12,083.08

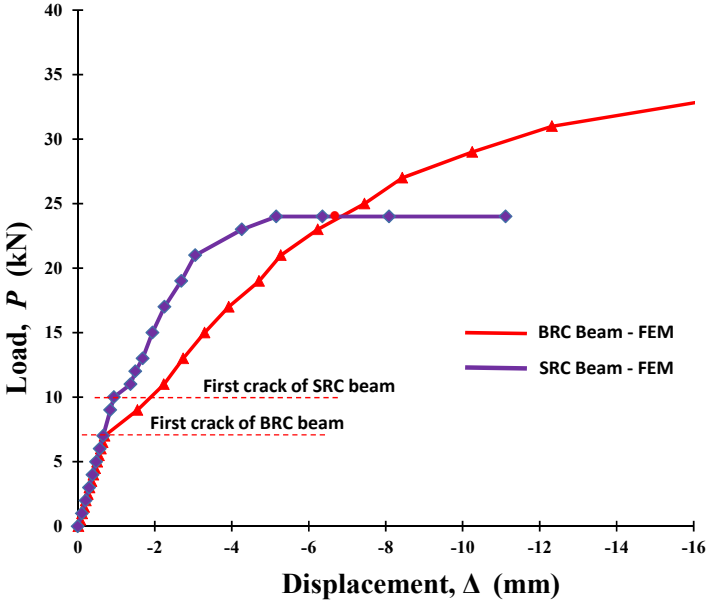

Figure 14. The relationship of load vs. displacement of BRC beam of finite element method (FEM) results.

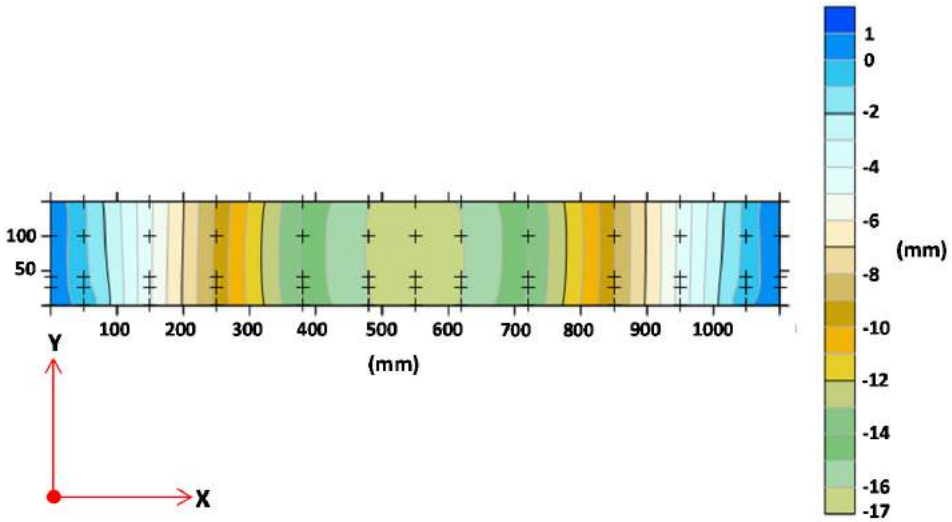

Figure 15. The displacement contour of Y-direction of BRC beam.

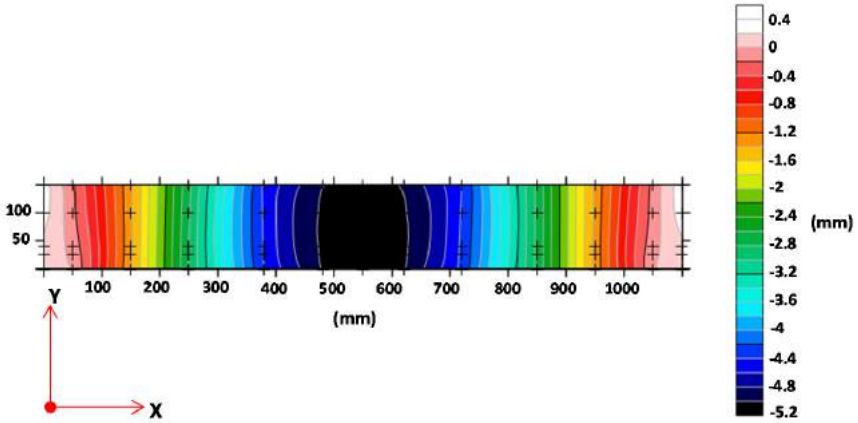

Figure 16. The displacement contour of Y-direction of SRC beam.

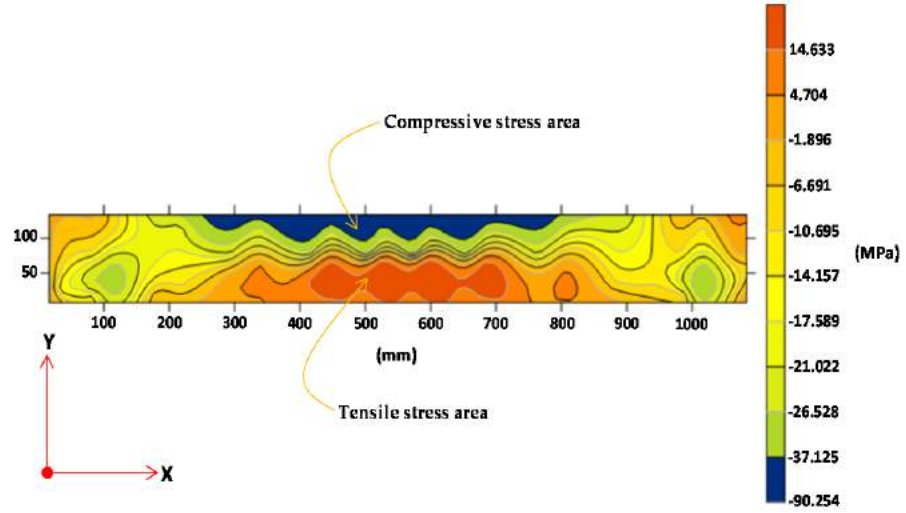

Figure 17. The stress contour of X-direction of BRC beam.

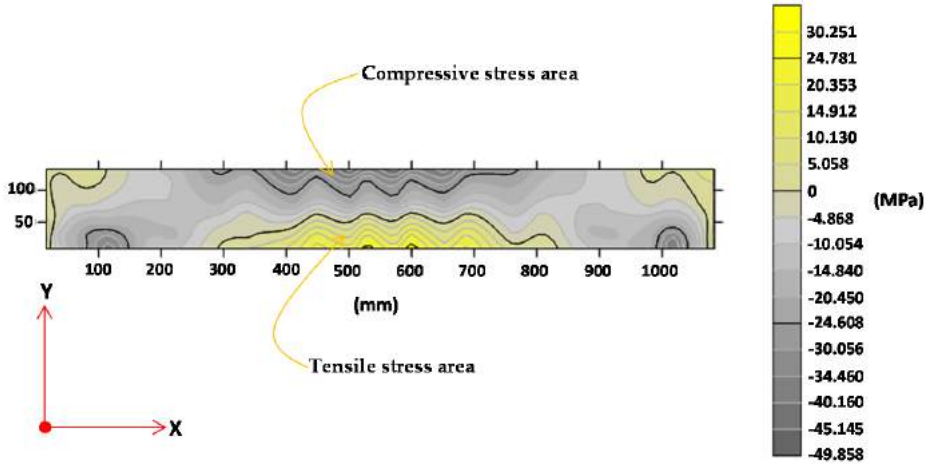

Figure 18. The stress contour of X-direction of SRC beam.

4. Discussion

Merging is carried out on the load vs. displacement relationship diagram from the experimental results, ANN analysis, and finite element method (FEM) analysis. Figure 19 shows the combined load vs. displacement diagram of the ANN analysis results with the experimental results. Figure 19 shows that the load vs. displacement relationship diagram the two analyses results are very coincided or show high suitability. However, at a load of approximately 90% of the collapse load, the load vs. displacement relationship diagram shows different behavior. Figure 20 shows the combined load vs. displacement diagram of the experimental results, ANN analysis, and the results of the finite element method analysis. Figure 19 shows that the artificial neural networks (ANN) model has a higher R^2 value when compared to the R^2 value of the multiple linear regression model (MLR). ANN analysis has better predictive accuracy. This is the same as the conclusion of 2 researchers, namely Khademi et al. (2017) [40], who concluded that the ANN model has higher accuracy than the multiple linear regression (MLR) model, and Xuan Li et al. (2019) [41], who concluded that the ANN model performs better than the MLR models with or without considering the interactions between factors. The accuracy of the prediction is very much dependent on the number of input variables. The greater the number of input parameters, the more accurate the results of the predicted model.

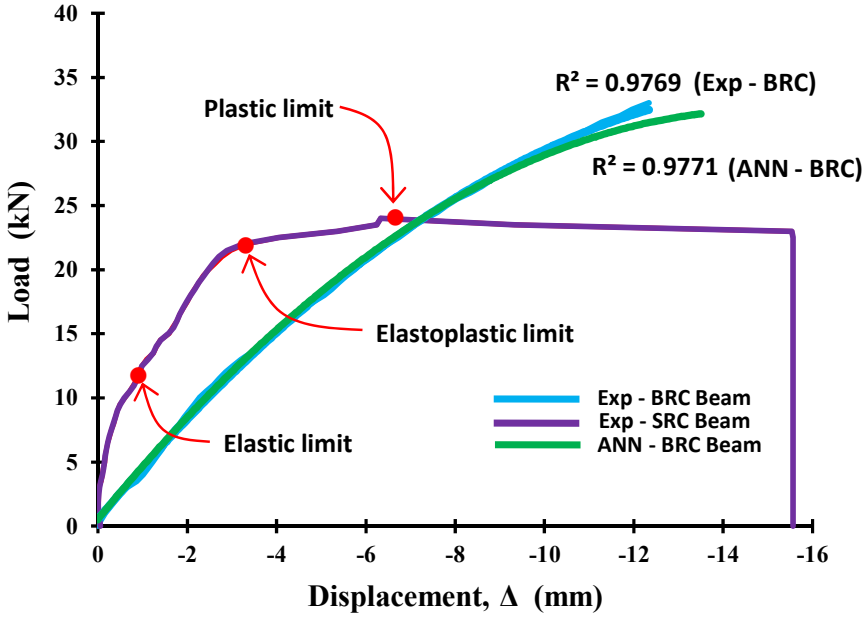

Figure 19. The combined of the load vs. displacement relationship of BRC beam of the experimental results and ANN analysis.

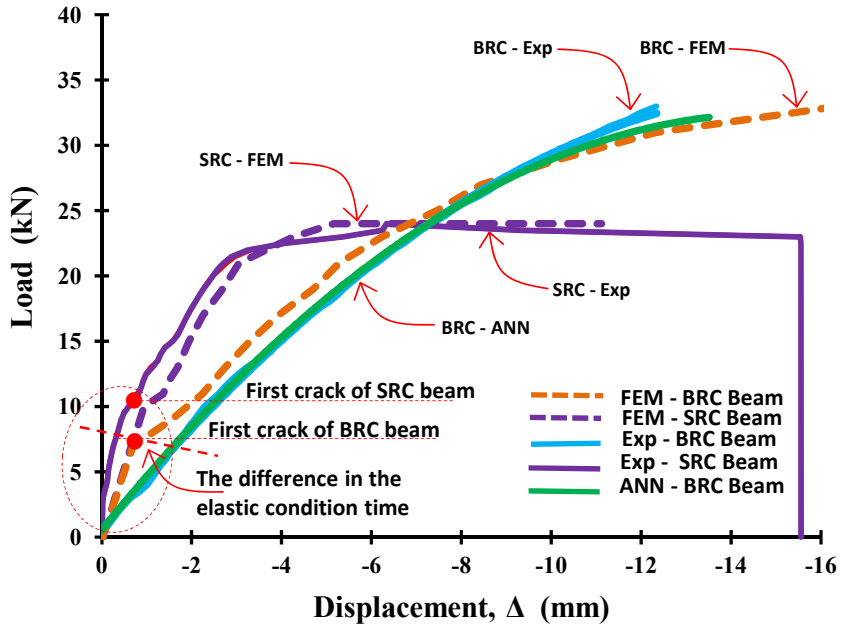

Figure 20. The combined of the load vs. displacement relationship of BRC beam and SRC beam of the experimental results, ANN analysis, and FEM.

The diagram of the relationship between load and displacement of the BRC beam from FEM analysis and experimental results shows the difference in elastic conditions or until the initial crack occurs. The experimental results showed negative differences with the results of the FEM analysis. This shows the influence of the nature and characteristics of bamboo. The parts of bamboo stems have a non-uniform or uncertain modulus of elasticity. Tensile strength and modulus of elasticity of bamboo tested in the laboratory are sometimes different from bamboo which is used as beam reinforcement. As is known, bamboo trees from base to tip have different tensile strength and fiber density. Meanwhile, the relationship diagram of load vs. displacement of the SRC beam experiment results is positively different from the results of the FEM analysis when the elastic condition or until the initial crack occurs. Positive differences can be ignored, in the sense that the quality of the steel used is better than the

quality of steel tested in the laboratory. However, in this study, the analysis of stiffness reduction in BRC and SRC beams was focused after the beam experienced an initial crack or non-linear phase.

Figure 20 shows that inelastic conditions there is a difference in stiffness between the two types of beams. The stiffness of bamboo reinforced concrete beams (BRC) is lower than the stiffness of steel-reinforced concrete beams (SRC). This difference occurs not due to reduced cross-section inertia or I_g of cross-sectional reduction, but due to the nature of the material used. This is because the BRC beam uses bamboo reinforcing material, which has high elastic and resilience properties. BRC beams with bamboo reinforcement will be able to accept high impact loads without causing over stress at the elastic limit, even though displacement has occurred. This indicates that the energy absorbed during loading is stored and released if the material is not loaded. Meanwhile, the SRC beam uses steel material that has high stiffness and toughness, so that the SRC beam in the service load range or elastic conditions does not experience excessive displacement or deformation. Beams that use materials with high stiffness and toughness will be able to withstand high impact loads or shock loads. If the SRC beam gets an impact load, then some of the energy is absorbed and some of the energy is transferred.

In the non-linear phase or after initial cracking, the beam stiffness changes from the full-sectional flexural stiffness, E_cI_g, to the effective bending stiffness, E_cI_{eff}. In the non-linear phase, the stiffness of the beam section continues to decrease with increasing loads, moments, and cracks. The area of the beam section continues to decrease with increasing cracks and automatically causes the beam section stiffness (E_cI_g) to decrease. As shown in Table 6 and Figure 21, the stiffness of the BRC beam decreases after the initial cracking occurs as the increasing loading stage is applied. The increase in load causes the flexural moment to increase, the displacement increases, and the crack propagation continues to spread towards the compressed block of the beam cross-section. The crack propagation from 1st mesh layer to the 2nd mesh layer onwards runs linearly with reduced cross-sectional stiffness from the lower fiber of the cross-section tensile block to the upper fiber of the compressive block of the beam cross-section. The increase in crack propagation towards the compressive block of cross-section causes the neutral line to change. Chunyu Fu et al. (2018) [13] concluded that the presence of cracks causes a nonlinear stress distribution along the beam cross-section, which changes the neutral axis of the cross-section and further affects the stiffness of the beam. Figure 21 shows that the stiffness of the BRC beam cross-section decreases from the initial crack until the beam collapses. The stiffness of BRC beams is reduced by 50% after initial cracking to 95% at collapse. The stiffness reduction goes step by step according to the moment (M_a) applied to the beam. Sang-Whan Han et al. (2009) [4] revealed that the stiffness reduction factor was significantly affected by the amount of moment or the applied load, while the stiffness reduction factor did not differ from the amount of reinforcement. The decrease in the moment of inertia of the full cross-sectional Ig of the BRC beam ranged from $0.5I_g$–$0.05I_g$ for the elastoplastic and plastic regions. Meanwhile, ACI-318M-14 [5] recommends the stiffness of the beam cross-section for elastic analysis in the non-linear phase of $0.5I_g$–$0.25I_g$. The difference in the value of the reduction in the stiffness of the cross-section at collapse correlates with the differences in the properties and characteristics of the material used as beam reinforcement. Bamboo reinforced concrete beams (BRC) exhibit high displacement behavior, but once the collapse load is reached and gradually released, displacement tends to return to zero. It is linear with its elastic properties and the stress vs. strain relationship behavior of bamboo.

Table 7 and Figure 22 show a decrease in stiffness or a decrease in the moment of inertia of the SRC beam cross-section. Stiffness decreases after initial cracking as the applied load increases. Figure 22 shows that the cross-sectional stiffness of the SRC beam decreases from the initial crack until the beam collapses. The stiffness of the SRC beam was reduced by 25% after initial cracking to 60% at collapse. The decrease in the moment of inertia full cross-section (I_g) for SRC beams ranged from $0.75I_g$–$0.40I_g$ for the elastoplastic and plastic regions. Meanwhile, ACI-318M-14 [5] recommends the cross-sectional stiffness of reinforced concrete beams for elastic analysis in the non-linear phase of $0.5I_g$–$0.25I_g$. The difference in the value of the reduction in the cross-sectional stiffness of the SRC beam with the ACI-318M-14 [5] requirements is due to the beam cross-section reinforcement method,

namely the SRC beam in this study using a single reinforcement method. SRC beam with single reinforcement shows that when the steel reinforcement undergoes second melting and the moment of inertia of the cross-section is still around 40%, the steel reinforcement is not able to withstand the tensile stress that occurs so that the neutral line of the cross-section continues to shift upwards towards the upper fiber of the compression block of the cross-section. Meanwhile, BRC beams with bamboo reinforcement have good elastic properties, where after the ultimate load is reached, the large displacement shrinks back to near-zero or the beam returns flat [7], as shown in the video at the following link: https://goo.gl/6AVWmP. Although the stiffness or inertia of the BRC beam cross-section is still around 5%, bamboo reinforcement is still able to withstand the tensile stress that occurs, as stated by Ghavami (2005) [24] that bamboo has high tensile strength. If we control with the crack pattern, the crack lines on the BRC beam majority stop below the cross-section neutral line, while the crack lines on the SRC beam tend to continue to propagate upwards towards the upper fibers of the compressive block of the beam cross-section, as shown in Figures 23 and 24. And if we look at Figures 17 and 18, the tensile stress contour of the BRC beam has a wider zone and spreads to the side when compared to the SRC beam.

Figures 25 and 26 show the relationship between the stiffness reduction factor (ϕ_K) and the M_a/M_{cr} of the BRC beam and the SRC beam. The stiffness reduction factor (ϕ_K) is the ratio of the moment of inertia of the effective section (I_e) divided by the moment of inertia of the cross-section (I_g). The stiffness reduction factor (ϕ_K) is significantly influenced by the applied moment level. The equation of the beam stiffness reduction factor is related to the ratio between the applied moment and an initial crack moment or M_a/M_{cr}. The equation for the stiffness reduction factor is shown in Equation (5) or Equation (6) for a BRC beam. The stiffness reduction factor equation for the SRC beam is shown in Equation (7) or Equation (8). Figure 27 shows a comparison of the relationship between the stiffness reduction factor and the M_a/M_{cr} of the BRC beam and SRC beam. The diagram of the relationship between the stiffness reduction factor and M_a/M_{cr} shows that the SRC beam has a smaller stiffness reduction factor than the BRC beam in the non-linear phase. However, the SRC beam shows a collapse at the moment of inertia of the effective cross-section (I_e), which is relatively still large when compared to BRC beams. BRC beams collapse at the effective cross-section inertia of about 5%, and SRC beams collapse at the effective section inertia of about 40%. The alternative of moments of inertia from various sources is shown in Table 9.

$$\phi_K = 0.646 - 0.1023\left(\frac{M_a}{M_{cr}}\right) \tag{5}$$

$$\frac{I_e}{I_g} = 0.646 - 0.1023\left(\frac{M_a}{M_{cr}}\right) \tag{6}$$

$$\phi_K = 0.697 - 0.1472\left(\frac{M_a}{M_{cr}}\right) \tag{7}$$

$$\frac{I_e}{I_g} = 0.697 - 0.1472\left(\frac{M_a}{M_{cr}}\right) \tag{8}$$

Table 9. The alternative value of I for elastic analysis from various sources.

Source and Information	Alternative Value of I for Elastic Analysis
ACI-318M-14 [5]	$0.25I_g$–$0.5I_g$
FEMA 356-2000 [46]	0.5 EI_g–$0.8EI_g$
New Zealand Code [47]	$0.35I_g$
Paulay and Priestley, 1992 [48]	$0.30I_g$–$0.50I_g$
In this research (singly reinforced beam)	
-BRC Beam	$0.05I_g$–$0.5I_g$
-SRC Beam	$0.4I_g$–$0.75I_g$

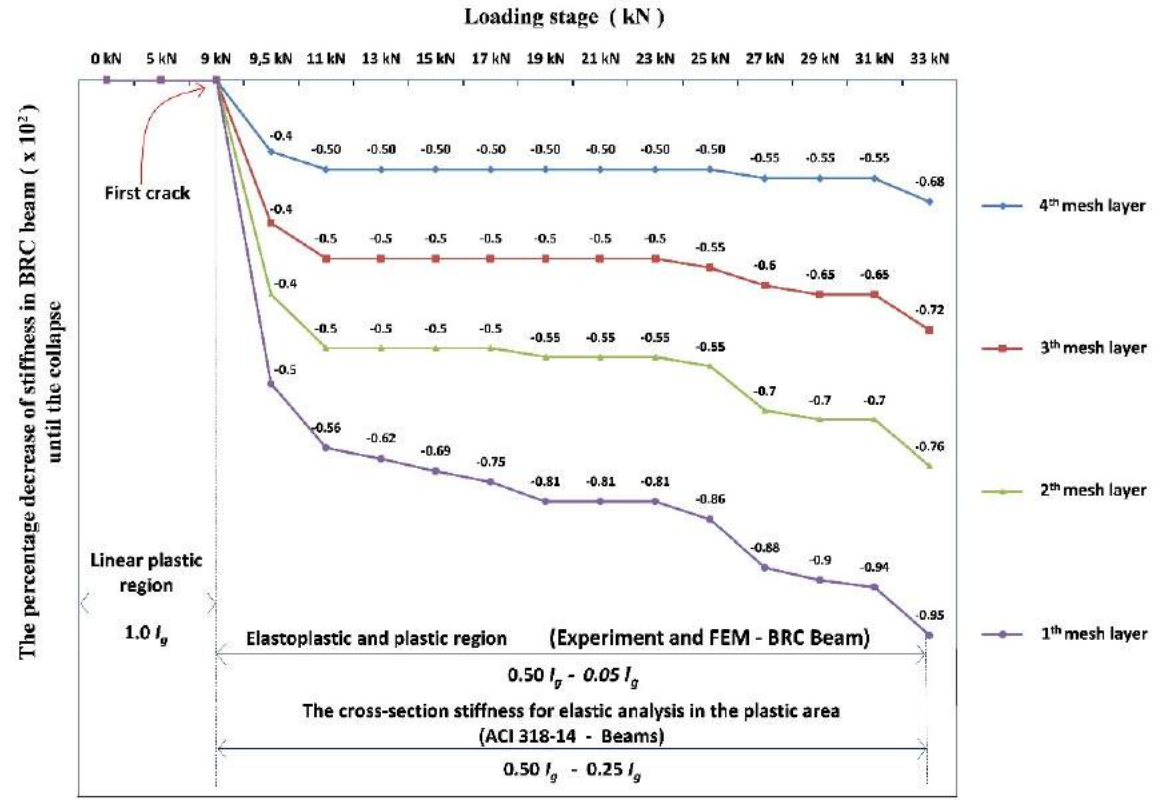

Figure 21. Decreased stiffness of BRC beam cross-section in the span middle.

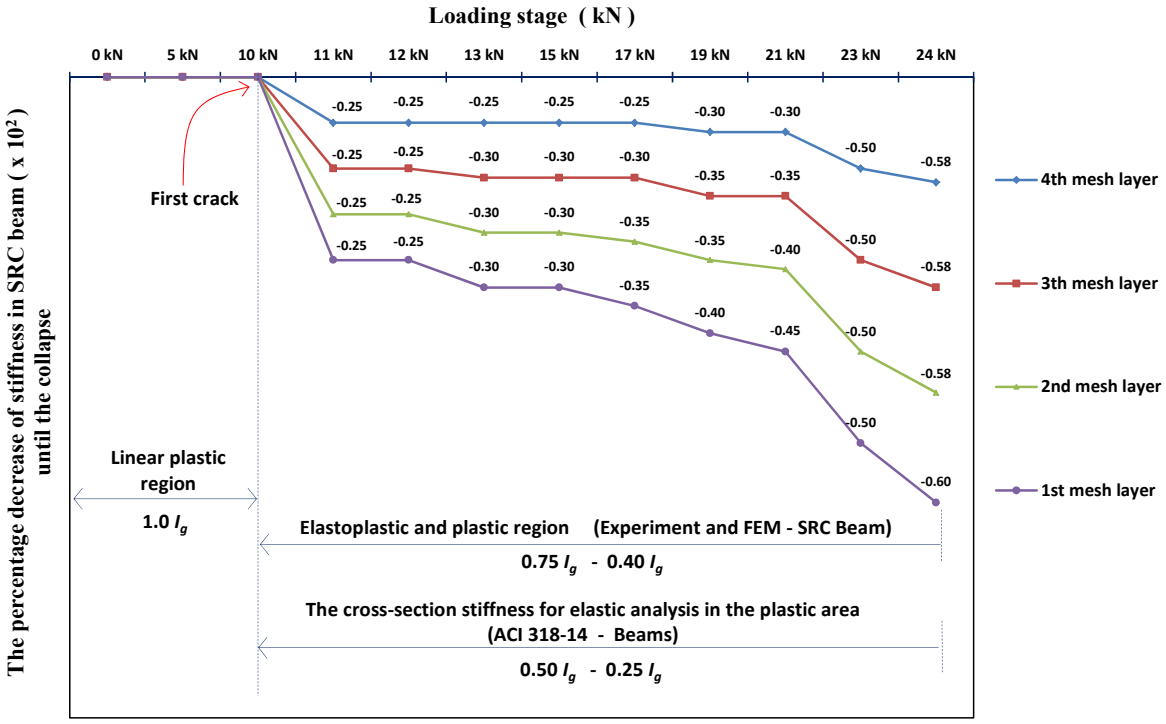

Figure 22. Decreased stiffness of SRC beam cross-section in the span middle.

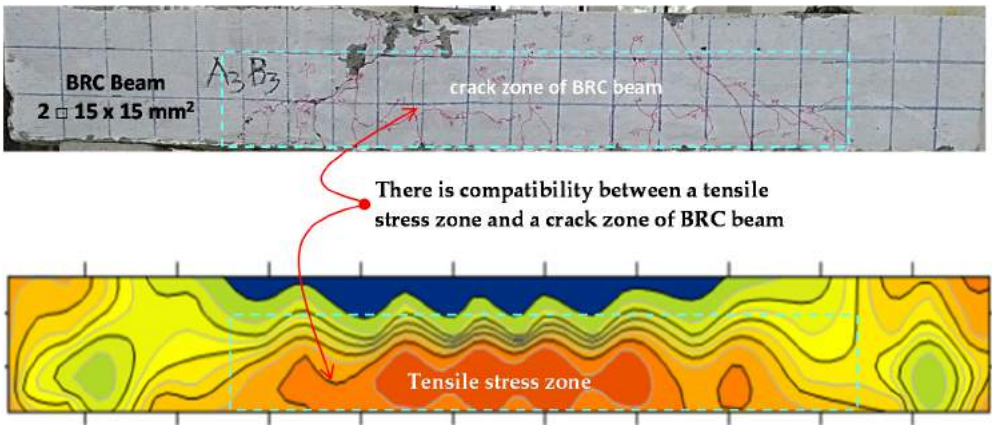

Figure 23. The crack pattern and tensile stress zone of BRC beam.

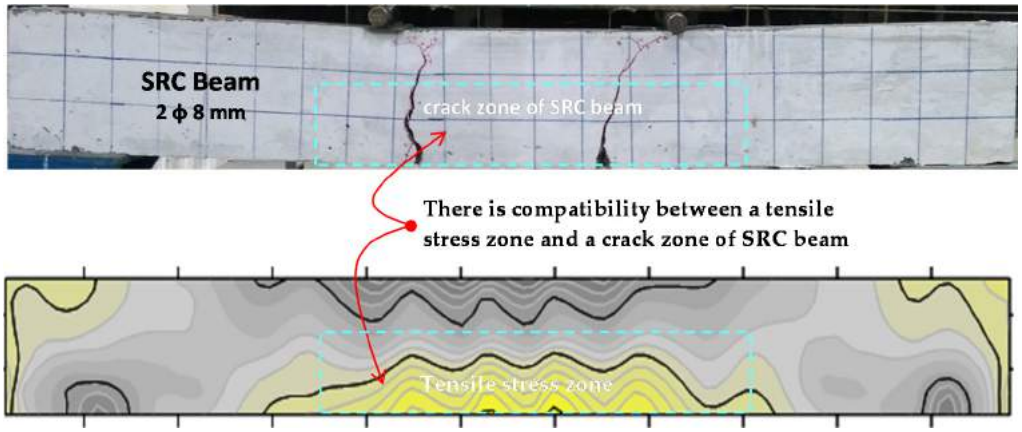

Figure 24. The crack pattern and tensile stress zone of SRC beam.

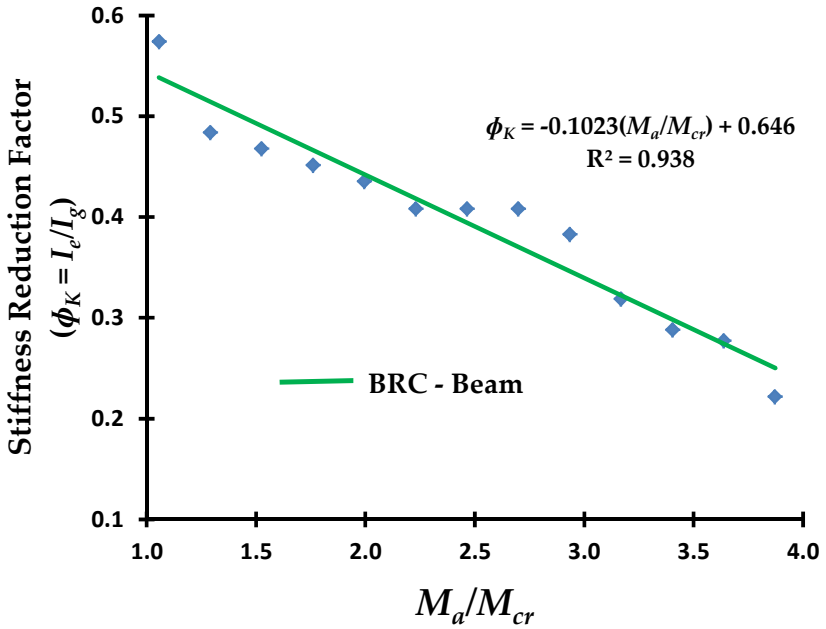

Figure 25. The relationship of the stiffness reduction factor (ϕ_K) and the M_a/M_{cr} of the BRC beam.

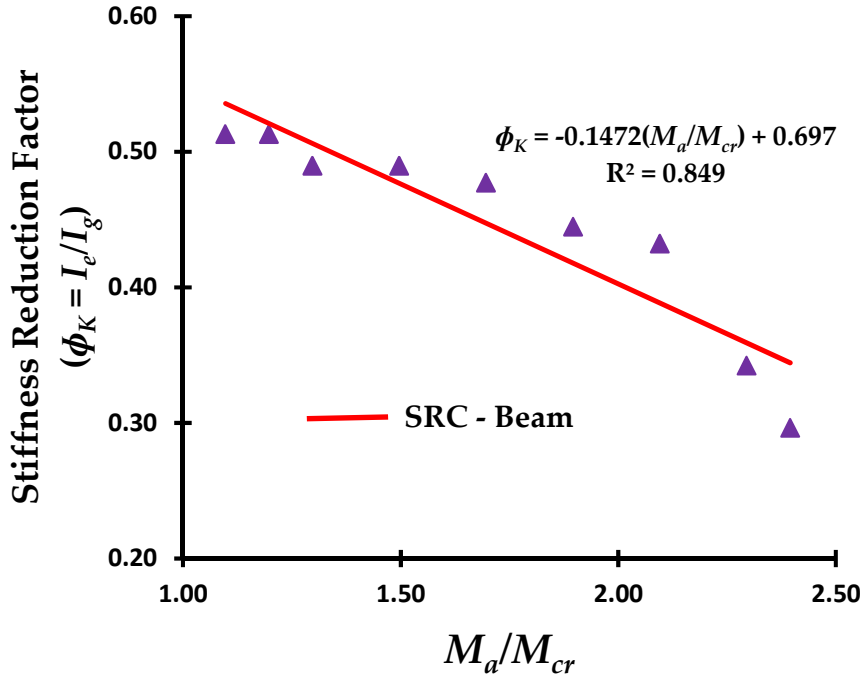

Figure 26. The relationship of the stiffness reduction factor (ϕ_K) and the M_a/M_{cr} of the SRC beam.

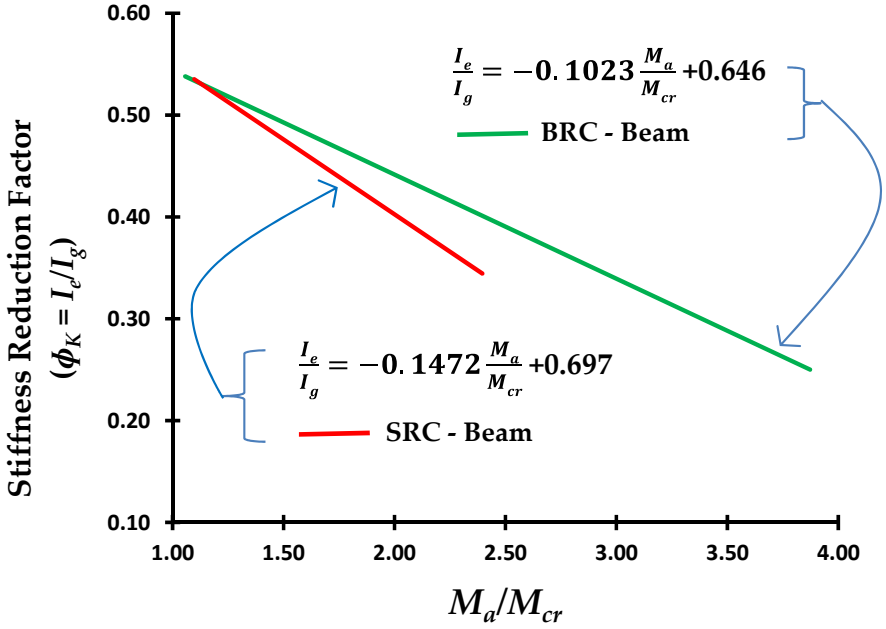

Figure 27. Comparison of the relationship of the stiffness reduction factor (ϕ_K) and the M_a/M_{cr} of the BRC beam and SRC beam.

5. Conclusions

The relationship pattern of load vs. displacement reflects the stiffness pattern of structural elements. The properties and characteristics of the material in the reinforcing concrete elements have a dominant influence on the relationship pattern of the load vs. displacement of reinforced concrete elements. Bamboo reinforced concrete beams (BRC) have a different load vs. displacement relationship pattern when compared to steel reinforced concrete beams (SRC). BRC beams have elastic properties and high resilience properties that can accept high impact loads without causing over stress at the elastic limit, even though displacement has occurred. While SRC beams have high stiffness and

toughness so that SRC beams are not subject to excessive displacement or deformation at service load ranges or elastic conditions.

Results of the validation of the relationship pattern of the load vs. displacement of the BRC beams shows that the ANN model has a higher R^2 value when compared to the R^2 value of the MLR model. ANN analysis has a higher prediction accuracy. The accuracy of the prediction depends very much on the number of input variables. The greater the number of input parameters, the more accurate the prediction model results.

The cross-sectional stiffness of BRC beams is reduced by 50% after initial cracking and reduced by 95% at collapse. The cross-sectional stiffness of the SRC beam was reduced by 25% after initial cracking and reduced by 60% at collapse. The reduction in stiffness is significantly affected by the amount of applied moment (M_a) or the load applied that caused cracks and a reduction in the moment of inertia of the cross-section.

The initial decrease in cross-sectional stiffness of BRC beams occurs at a load of about 24% of the ultimate load and BRC beams occur at loads of about 40% ultimate load. BRC beam collapse occurs when the moment of inertia of the effective cross-section (I_e) is 5%, while the SRC beam collapse occurs when the moment of inertia of the effective cross-section (I_e) is 40%. The reduction in stiffness in the cross-section of the beam in the non-linear phase ranged from $0.5I_g$–$0.05I_g$ for BRC beams, and $0.75I_g$–$0.40I_g$ for SRC beams. ACI-318M-14 standard recommends the cross-sectional stiffness of reinforced concrete beams for elastic analysis in the non-linear phase of $0.5I_g$–$0.25I_g$.

The SRC beams have a smaller stiffness reduction factor (ϕ_K) than BRC beams in the non-linear phase. However, the SRC beam shows a collapse at the moment of inertia of the effective cross-section (I_e), which is relatively large when compared to BRC beams.

Funding: APC financing entirely by the DPRM Republic of Indonesia and LPPM of the University of Muhammadiyah Jember, Indonesia.

Acknowledgments: My gratitude goes to the LPPM of the Muhammadiyah University of Jember, Indonesia, and DPRM of the Republic of Indonesia as the funder of this research and APC.

Conflicts of Interest: The author declares no conflict of interest.

References

1. Pandey, K.K.; Ramakantha, V.; Chauhan, S.S.; Kumar, A.A. *Wood is Good*; Springer: Singapore, 2017.
2. Mohammadabadi, M.; Jarvis, J.; Yadama, V.; Cofer, W. Predictive Models for Elastic Bending Behavior of a Wood Composite Sandwich Panel. *Forests* **2020**, *11*, 624. [CrossRef]
3. Ministry of Environment and Forestry of the Republic of Indonesia. Memanfaatkan Bambu Sebagai Salah Satu Potensi Hutan Rakyat. 18 October 2018. Available online: https://www.menlhk.go.id/site/single_post/1444 (accessed on 24 October 2020).
4. Han, S.W.; Park, Y.M.; Kee, S.H. Stiffness Reduction Factor for Flat Slab Structures under Lateral Loads. *J. Struct. Eng.* **2009**, *135*, 743. [CrossRef]
5. ACI Committee 318 Standard. *Building Code Requirements for Structural Concrete*; American Concrete Institute: Farmington Hills, MI, USA, 2014.
6. Gunasti, A.; Dewi, I.C.; Dasuki, M.; Ariyani, S.; Mahmudi, I.; Abadi, T.; Rahman, M.; Hidayatullah, S.; Nilogiri, A.; Galuh, S.D.; et al. The Prediction of Stiffness of Bamboo-Reinforced Concrete Beams Using Experiment Data and Artificial Neural Networks (ANNs). *Crystals* **2020**, *10*, 757.
7. Muhtar; Dewi, S.M.; Wisnumurti; Munawir, A. Enhancing bamboo reinforcement using a hose-clamp to increase bond-stress and slip resistance. *J. Build. Eng.* **2019**, *26*, 100896. [CrossRef]
8. Muhtar; Dewi, S.M.; Wisnumurti; Munawir, A. The flexural behavior model of bamboo reinforced concrete beams using a hose clamp. *Proc. Mater. Sci. Eng. Chem.* **2019**, *276*, 1033. [CrossRef]
9. Zhang, K.; Zhang, J.; Jin, W.; Mao, J.; Long, J. Stiffness degradation for the fatigue of reinforced concrete beams after electrochemical rehabilitation. *Constr. Build. Mater.* **2020**, *260*, 120455. [CrossRef]
10. Salam, A.S.A.; Debra, L.F. Use of negative stiffness in failure analysis of concrete beams. *Eng. Struct.* **2016**, *126*, 187–199.

11. Hu, H.S.; Nie, J.G.; Wang, Y.H. Effective stiffness of rectangular concrete-filled steel tubular members Hong-Song. *J. Constr. Steel Res.* **2016**, *116*, 233–246. [CrossRef]
12. Patel, K.A.; Bhardwaj, A.; Chaudhary, S.; Nagpal, A. Explicit expression for effective moment of inertia of RC beams. *Lat. Am. J. Solids Struct.* **2015**, *12*, 542–560. [CrossRef]
13. Fu, C.; Wang, Y.; Tong, D. Stiffness Estimation of Cracked Beams Based on Nonlinear Stress Distributions Near the Crack. *Math. Probl. Eng.* **2018**, *2018*, 5987973. [CrossRef]
14. Pique, J.R.; Burgos, M. Effective rigidity of reinforced concrete elements in seismic analysis and design. In Proceedings of the 14 World Conference on Earthquake Engineering, Beijing, China, 12–17 October 2008.
15. Akmaluddin, A.; Pathurahman. Effective Moment of Inertia Approach for Predicting Displacement of Concrete Beams Reinforced with Twisted Bamboo Cables. *Int. J. Civ. Environ. Eng. IJCEE-IJENS* **2012**, *12*, 6–13.
16. Kalkan, İ. Displacement Prediction for Reinforced Concrete Beams through Different Effective Moment of Inertia Expressions. *Int. J. Eng. Res. Dev.* **2013**, *5*, 1.
17. Fu, C.; Tong, D.; Wang, Y. Assessing the Instantaneous Stiffness of Cracked Reinforced Concrete Beams Based on a Gradual Change in Strain Distributions. *Adv. Mater. Sci. Eng.* **2020**, *2020*, 7453619. [CrossRef]
18. Feng, X.; Shen, M.; Sun, C.; Chen, J.; Luo, P. Research on flexural stiffness reduction factor of the reinforced concrete column with equiaxial shaped section. In Proceedings of the 13th COTA International Conference of Transportation Professionals (CICTP 2013), Shenzhen, China, 13–16 August 2013; pp. 168–174.
19. Muhtar; Dewi, S.M.; Wisnumurti; Munawir, A. The stiffness and cracked pattern of bamboo reinforced concrete beams using a hose clamp. *Int. J. Civ. Eng. Technol.* **2018**, *9*, 273–284.
20. Agarwal, A.; Nanda, B.; Maity, D. Experimental investigation on chemically treated bamboo reinforced concrete beams and columns. *Constr. Build. Mater.* **2014**, *71*, 610–617. [CrossRef]
21. Muhtar. Experimental data from strengthening bamboo reinforcement using adhesives and hose-clamps. *Data Brief* **2019**, *27*, 104827. [CrossRef]
22. Rahman, M.M.; Rashid, M.H.; Hossain, M.A.; Hasan, M.T.; Hasan, M.K. Performance evaluation of bamboo reinforced concrete beam. *Int. J. Eng. Technol. IJET-IJENS* **2011**, *11*, 113–118.
23. Muhtar. Precast Bridges of Bamboo Reinforced Concrete in Disadvantaged Village Areas in Indonesia. *Appl. Sci.* **2020**, *10*, 7158. [CrossRef]
24. Ghavami, K. Bamboo as reinforcement in structural concrete elements. *Cem. Concr. Compos.* **2005**, *27*, 637–649. [CrossRef]
25. Javadian, A.; Wielopolski, M.; Smith, I.F.C.; Hebel, D.E. Bond-behavior study of newly developed bamboo-composite reinforcement in concrete. *Constr. Build. Mater.* **2016**, *122*, 110–117. [CrossRef]
26. Muhtar, M.; Dewi, S.; Wisnumurti; Munawir, A. Bond-slip improvement of bamboo reinforcement in the concrete beam using hose clamps. In Proceedings of the 2nd International Multidisciplinary Conference, Jakarta, Indonesia, 15 November 2016; pp. 385–393.
27. Gunasti, A.; Manggala, A.S.; Nusant, A.F.P.; Nilogiri, A. Effect of Reinforcement Details on Precast Bridge Frames of Bamboo Reinforced Concrete to Load Capacity and Crack Patterns. *Int. J. Eng. Res. Technol.* **2020**, *13*, 631–636.
28. Muhtar. Cracked Pattern of Bamboo Reinforced Concrete Beams Using Double Reinforcement with the Strengthening on Tensile Reinforcement. *Int. J. Eng. Res. Technol.* **2020**, *13*, 608–612.
29. ASTM C 39 Standard. *Standard Test Method for Compressive Strength of Cylindrical Concrete Specimens*; ASTM International: West Conshohocken, PA, USA, 2003.
30. PT SIKA Indonesia. Sikadur®-752. 02, 2-3. 2016. Available online: https://www.scribd.com/document/374071630/Sikadur-752 (accessed on 24 October 2020).
31. ASTM C 09 Standard. *Standard Test Method for Flexural Strength of Concrete (Using Simple Beam with Third-Point Loading)*; ASTM International: West Conshohocken, PA, USA, 2002.
32. Muhtar. Numerical validation data of tensile stress zones and crack zones in bamboo reinforced concrete beams using the Fortran PowerStation 4.0 program. *Data Brief* **2020**, *29*, 105332. [CrossRef]
33. Avram, C.; Facaoaru, I.; Filimon, I.; Mirsu, O.; Tertea, I. Concrete Strength and Strain. In *Developments in Civil Engineering 3*; Elsvier S.P. Company: New York, NY, USA, 1981.
34. Naderpour, H.; Kheyroddin, A.; Amiri, G.G. Prediction of FRP-confined compressive strength of concrete using artificial neural networks. *Compos. Struct.* **2010**, *92*, 2817–2829. [CrossRef]

35. Ahmadi, M.; Naderpour, H.; Kheyroddin, A. Utilization of artificial neural networks to prediction of the capacity of CCFT short columns subject to short term axial load. *Arch. Civ. Mech. Eng.* **2014**, *14*, 510–517. [CrossRef]
36. Khademi, F.; Akbari, M.; Nikoo, M. Displacement determination of concrete reinforcement building using data-driven models. *Int. J. Sustain. Built Environ.* **2017**, *6*, 400–411. [CrossRef]
37. Kaczmarek, M.; Szymanska, A. Application of Artificial Neural Networks to Predict the Displacements of Reinforced Concrete Beams. *Studia Geotech. Mech.* **2016**, *38*, 37–46. [CrossRef]
38. Abd, A.M.; Salman, W.D.; Ahmed, Q.W. ANN, and Statistical Modelling to Predict the Displacement of Continuous Reinforced Concrete. *Diyala J. Eng. Sci.* **2015**, *08*, 134–143.
39. Ya Tuan, T.M.Y.S.; Alebrahim, R.; Fitri, N.; Alebrahim, M. Analysis of Cantilever Beam Displacement under Uniformly Distributed Load using Artificial Neural Networks. In Proceedings of the MATEC Web of Conferences, Los Angeles, CA, USA, 3–4 February 2018.
40. Khademi, F.; Akbari, M.; Mohammadmehdi, S.; Nikoo, M. Multiple linear regression, artificial neural network, and fuzzy logic prediction of 28 days compressive strength of concrete. *Front. Struct. Civ. Eng.* **2017**, *11*, 90–99. [CrossRef]
41. Li, X.; Khademi, F.; Liu, Y.; Akbari, M.; Wang, C.; Bond, P.L.; Keller, J.; Jiang, G. Evaluation of data-driven models for predicting the service life of concrete sewer pipes subjected to corrosion. *J. Environ. Manag.* **2019**, *234*, 431–439. [CrossRef]
42. Dewi, S.M.; Nuralinah, D. The Recent Research on Bamboo Reinforced Concrete. *MATEC Web Conf.* **2017**, *103*, 2001. [CrossRef]
43. Nathan, S. *Application of Bamboo for Flexural and Shear Reinforcement in Concrete Beams*; Clemson University: Clemson, SC, USA, 2014.
44. Khare, L. *Performance Evaluation of Bamboo Reinforced Concrete Beams*; UT Arlington: Arlington, TX, USA, 2005.
45. Mishra, M.; Agarwal, A.; Maity, D. Neural-network-based approach to predict the displacement of plain, steel-reinforced, and bamboo-reinforced concrete beams from experimental data. *SN Appl. Sci.* **2019**, *1*, 584. [CrossRef]
46. FEMA 356 Standard. *Prestandard and Commentary for the Seismic Rehabilitation of Buildings*; American Society of Civil Engineers: Reston, VA, USA, 2000.
47. New Zealand Standard. *Code of Practice for the Design of Concrete Structures*; Part 1; Standards New Zealand: Wellington, New Zealand, 1995.
48. Paulay, T.; Priestley, M.J.N. *Seismic Design of Reinforced Concrete and Masonry Buildings*; Wiley Interscience: New York, NY, USA, 1992.

Publisher's Note: MDPI stays neutral with regard to jurisdictional claims in published maps and institutional affiliations.

© 2020 by the author. Licensee MDPI, Basel, Switzerland. This article is an open access article distributed under the terms and conditions of the Creative Commons Attribution (CC BY) license (http://creativecommons.org/licenses/by/4.0/).

forests

Submit to this Journal

Review for this Journal

Edit a Special Issue

Article Menu

Article Overview

- Abstract
- Open Access and Permissions
- Share and Cite
- Article Metrics
- Related Articles
- Order Article Reprints

Article Versions

Related Info Links

More by Authors Links

Abstract Views 292

Full-Text Views 275

Open Access Article

The Prediction of Stiffness Reduction Non-Linear Phase in Bamboo Reinforced Concrete Beam Using the Finite Element Method (FEM) and Artificial Neural Networks (ANNs)

by Muhtar

Faculty of Engineering, University of Muhammadiyah Jember, Jember 68121, Indonesia

Forests **2020**, *11*(12), 1313; https://doi.org/10.3390/f11121313

Received: 25 October 2020 / **Revised:** 25 November 2020 / **Accepted:** 25 November 2020 / **Published:** 10 December 2020

(This article belongs to the Special Issue Timber and Construction Structure)

View Full-Text Download PDF Browse Figures Citation Export

Abstract

This paper discusses the reduction of the stiffness of bamboo reinforced concrete (BRC) beams to support the use of bamboo as an environmentally friendly building material. Calculation of cross-section stiffness in numerical analysis is very important, especially in the non-linear phase. After the initial crack occurs, the stiffness of the cross-section will decrease with increasing load and crack propagation. The calculation of the stiffness in the cross-section of the concrete beam in the non-linear phase is usually approximated by giving a reduction in stiffness. ACI 318-14 provides an alternative, reducing the stiffness of the plastic post-linear beam section through the moment of inertia (I) of the beam section for elastic analysis between $0.50I_g$–$0.25I_g$. This study aims to predict the value of the reduction in the stiffness of the BRC beam section in the non-linear phase through the load-displacement relationship of experimental results validated by the Finite Element Method (FEM) and the Artificial Neural Networks (ANN) method. The experiment used 8 BRC beams and one steel-reinforced concrete (SRC) beam of singly reinforced with a size of 75 mm × 150 mm × 1100 mm. The beams were tested using a four-point loading method. The analysis results showed that the value of the stiffness reduction in the beam cross-sectional in the non-linear phase ranged from $0.5I_g$–$0.05I_g$ for BRC beams, and $0.75I_g$–$0.40I_g$ for SRC beams. View Full-Text

Keywords: stiffness reduction; bamboo reinforced concrete (BRC); finite element method (FEM); artificial neural networks (ANN)

▼ Show Figures

Figure 1

© This is an open access article distributed under the Creative Commons Attribution License which permits unrestricted use, distribution, and reproduction in any medium, provided the original work is properly cited.

scifeed
Never Miss Any Articles Matching Your Research from Any Publisher
• Get alerts for new papers matching your research
• Find out the new papers from selected authors
• Updated daily for 49'000+ journals and 6000+ publishers

Share and Cite

MDPI and ACS Style
Muhtar. The Prediction of Stiffness Reduction Non-Linear Phase in Bamboo Reinforced Concrete Beam Using the Finite Element Method (FEM) and Artificial Neural Networks (ANNs). *Forests* **2020**, *11*, 1313. https://doi.org/10.3390/f11121313

AMA Style
Muhtar. The Prediction of Stiffness Reduction Non-Linear Phase in Bamboo Reinforced Concrete Beam Using the Finite Element Method (FEM) and Artificial Neural Networks (ANNs). *Forests*. 2020; 11(12):1313. https://doi.org/10.3390/f11121313

Chicago/Turabian Style
Muhtar. 2020. "The Prediction of Stiffness Reduction Non-Linear Phase in Bamboo Reinforced Concrete Beam Using the Finite Element Method (FEM) and Artificial Neural Networks (ANNs)." *Forests* 11, no. 12: 1313. https://doi.org/10.3390/f11121313

Find Other Styles

Type a publisher, journal or format name

ⓘ Note that from the first issue of 2016, MDPI journals use article numbers instead of page numbers. See further details here.

Article Metrics

Citations

Crossref Google Scholar

0 [click to view]

Article Access Statistics

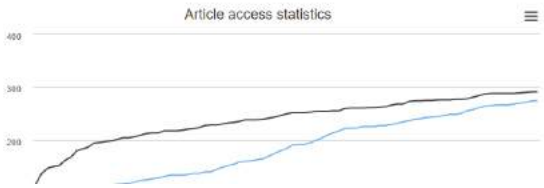

For more information on the journal statistics, click here.

Multiple requests from the same IP address are counted as one view.

Related Articles

The Prediction of Stiffness of Bamboo-Reinforced Concrete Beams Using Experiment Data and Artificial Neural Networks (ANNs)
Mukhtar et al., Crystals

Efficient Structural Design of a Prefab Concrete Connection by Using Artificial Neural Networks
Jorge Navarro-Rubio et al., Sustainability

Material Analysis of Steel Fibre Reinforced High-Strength Concrete in Terms of Flexural Behaviour: Experimental and Numerical Investigation
Byukusenge et al., Materials, 2020

Numerical Simulation of Steel Reinforced Concrete (SRC) Joints
Mentese, Isaac et al., Metals, 2016

Experimental verification of detection and prediction of multiple cracks by vibrations: FEM and ANN
Prasad Ramchandra Bavaskar et al., Multidiscipline Modeling in Materials and Structures, 2014

Analysis of loss in flexural stiffness of in-service prestressed hollow plate beam
Guanhua Zhang et al., International Journal of Structural Integrity, 2019

Decay Analysis of Cross-Section Stiffness of Corroded Reinforced Concrete Structure
ZHOU Jiaxing et al., Journal of Chongqing Jiaotong University (Natural Science), 2018

Hear from the leaders in digital health at Reuters Events' Digital Health
Thomson Reuters

Powered by TREND MD

Search more from Scilit

stiffness reduction; bamboo reinforced concrete (BRC); finite element method (FEM); artificial neural net

Search

© 1996-2021 MDPI (Basel, Switzerland) unless otherwise stated

forests

MDPI

Article

The Prediction of Stiffness Reduction Non-linear Phase in Bamboo Reinforced Concrete Beam Using The Finite Element Method (FEM) and Artificial Neural Networks (ANNs)

Muhtar

Faculty of Engineering, University of Muhammadiyah Jember, Jember 68121, Indonesia; muhtar@unmuhjember.ac.id

Received: date; Accepted: date; Published: date

Abstract: This paper discusses the reduction of the stiffness of bamboo reinforced concrete (BRC) beams to support the use of bamboo as an environmentally friendly building material. Calculation of cross-section stiffness in numerical analysis is very important, especially in the non-linear phase. After the initial crack occurs, the stiffness of the cross-section will decrease with increasing load and crack propagation. The calculation of the stiffness in the cross-section of the concrete beam in the non-linear phase is usually approximated by giving a reduction in stiffness. ACI 318-14 provides an alternative, reducing the stiffness of the plastic post-linear beam section through the moment of inertia (I) of the beam section for elastic analysis between $0.50I_g$–$0.25I_g$. This study aims to predict the value of the reduction in the stiffness of the BRC beam section in the non-linear phase through the load-displacement relationship of experimental results validated by the Finite Element Method (FEM) and the Artificial Neural Networks (ANN) method. The experiment used 8 BRC beams and one steel-reinforced concrete (SRC) beam of singly reinforced with a size of 75 mm × 150 mm × 1100 mm. The beams were tested using a four-point loading method. The analysis results showed that the value of the stiffness reduction in the beam cross-sectional in the non-linear phase ranged from $0.5I_g$—$0.05I_g$ for BRC beams, and $0.75I_g$—$0.40I_g$ for SRC beams.

Keywords: stiffness reduction; bamboo reinforced concrete (BRC); finite element method (FEM); artificial neural networks (ANN)

1. Introduction

The impact of increasing industrial development is that it can cause pollution of air, water, soil, and noise. The use of industrial building materials such as ceramics, steel, concrete, and other materials has led to an increase in environmental pollution. The procurement of wood forests or bamboo forests must be done as a counterweight to environmental pollution. Pandey et al. (2017) [1] and Mostafa et al. (2020) [2] revealed that an average tree absorbs one ton of CO_2 and produces 0.7 tons of O_2 for every cubic meter of growth. The use of environmentally friendly building materials such as wood and bamboo must be done. Bamboo is a forest product that provides high economic and ecological value to the community. Bamboo also has enormous potential with promising prospects [3]. Bamboo is one of the commodities produced by Community Forests. However, research on the behavior of bamboo as a building material is mandatory, such as research on the stiffness of bamboo reinforced concrete (BRC) beams.

The stiffness reduction factor is a multiplier to reduce the moment of inertia in gross cross-sectional, and the gross cross-sectional area remains constant. These factors are conservatively

Commented [CH1]: Attention AE/ME. The following layout issues have not been checked by the English Editing Department and must be carefully verified by the AE/Layout Department: All callout issues, bold usage of callouts, and references to callouts in the text. Correct callout usage in figures. Figure and Table layout issues. Footnote formatting and Glossaries have not been checked. En dash usage for negative values, en dash usage to indicate relationships, en dash usage to indicate bonds (especially in chemistry). The English Editing Department is not responsible for correct italic usage for genes, proteins and technical terminology. This responsibility belongs to the authors. The following are also not checked: spacing between numbers and units of measurement, ratios, en dashes for ranges, date and time formats, punctuation in equation lines, and less than/more than spacing (< >). Finally, capitalization and layout of titles/headings must be properly checked as well as ensuring 'Eq.' and 'Fig.' are properly spelled out, as these are layout issues.

Commented [M2]: This author is different from Redmine. Please confirm.

Commented [M3]: Is this necessary? Can this be deleted.?

Commented [M4]: Please carefully check the accuracy of names and affiliations.

Commented [M5]: Please check if this should be en dash.

Commented [M6]: We changed it to multiplication sign, please confirm.

Commented [M7]: Is the italics necessary?

enforced by various concrete standards to account for the loss of stiffness in the concrete cross-section due to the cracking of the concrete. The stiffness of the beam cross-section in the elastic phase or linear phase indicates the full section flexural stiffness, E_cI_g, whereas in the non-linear phase or after the initial crack, the gross cross-section bending stiffness is reduced to the effective flexural stiffness, E_cI_{eff}. The stiffness reduction factor is significantly influenced by the amount of moment or the applied load, while the stiffness reduction factor does not differ from the amount of reinforcement [4]. ACI 318M-14 [5] shows that the gross section flexural stiffness, E_cI_g, is reduced to obtain the effective flexural stiffness, E_cI_e, which causes cracking and other softening effects. As the moment in the concrete section increases, the flexural stiffness will be reduced due to the cracks that continue to propagate and spread. ACI 318M-14 [5] provides stiffness reduction limits for elastic analysis with a moment of inertia limits between $0.25I_g$—$0.5I_g$ for concrete beams. The equation for the moment of inertia effective (I_e) is determined in ACI 318-05 [5] Section 9.5.2.3, as shown in Equation (1).

Commented [M8]: There is no Section 9.5.2.3, please confirm if it refers to this article.

$$I_e = \left(\frac{M_{cr}}{M_a}\right)^3 I_g + \left[1 - \left(\frac{M_{cr}}{M_a}\right)^3\right] I_{cr} \quad (1)$$

where I_g = moment of inertia of the gross concrete section and I_{cr} = moment of inertia of the crack section including the reinforcement. The moment of inertial effective (I_e) as shown in Equation (1) will decrease as the moment that occurs, M_a. Calculation of the moment of inertia of the crack cross-section, I_{cr} at Equation (1) must pay attention to the number of reinforcement installed. However, the amount of reinforcement is not determined at the initial design stage.

The process of stiffness reduction in the beam section starts from the "*no crack*" and "*cracked*" conditions in the section. In the service load condition or the elastic condition, the stiffness of the beam section is in full condition, even though the moment due to the load continues to increase. In the elastic condition, the moment that occurs (M_a) is still below the moment of cracking (M_{cr}), or the tensile stress of the concrete is still below the modulus of rupture of the concrete beam cross-section, f_r. In the elastic conditions, the difference in stiffness between two different types of beams usually occurs not due to reduced inertia of the cross-section, but due to the properties of the materials used. For example, the stiffness of bamboo reinforced concrete beams is different from the stiffness of steel-reinforced concrete (SRC) beams. In the elastic conditions, the stiffness of ~~bamboo reinforced concrete beams (~~BRC~~)~~ beams is lower than the stiffness of ~~steel-reinforced concrete beams (~~SRC~~)~~ beams [6–8]. ~~T~~This is because BRC beams use bamboo reinforcing materials which have elastic properties and high resilience properties. BRC beams with bamboo reinforcement will be able to accept high impact loads without causing stress over the elastic limit, even though displacement has occurred. This indicates that the energy absorbed during loading is stored and released if the material is not loaded.

Meanwhile, the SRC beam uses steel material that has high stiffness and toughness, so that the SRC beam in the service load range or elastic condition~~, the beam~~ does not experience displacement or excessive deformation ~~excessive~~. Beams that use materials with high stiffness and toughness will be able to withstand high impact loads or shock loads. If the SRC beam gets an impact load, then some of the energy is absorbed and some of the energy is transferred.

Research on modeling and stiffness reduction has been carried out by many researchers. Kai Zhang et al. (2020) [9] investigated the effect of electrochemical rehabilitation (ER) techniques on the fatigue stiffness of RC beams. The results of his research indicated that electrochemical rehabilitation (ER) exacerbated bond breakage, thereby reducing the flexural stiffness of RC beams. Salam Al-Sabah et al. [10] discuss the use of negative stiffness in the failure analysis of concrete beams. In his research, Salman Al-Sabah et al. concluded that the effective and simple one-dimensional stress-strain behavior of concrete was used to study concrete blocks with proportional loading, t~~.~~ ~~T~~he only source of non-linearity to consider cracks in concrete. Hong-Song Hu et al. (2016) [11] investigated the effectiveness of square CFST rod stiffness, and the results proposed an equation for the effective stiffness of square CFST rods. Muhtar et al. [7] tested the flexural of BRC beams and SRC beams, the results showed that the stiffness decreased after the initial cracking. The average stiffness of the BRC beam decreased from 26,324.76 MPa before cracking to 6581.20 MPa after collapse [7], while the average value of SRC beam stiffness decreased from 30,334.11 MPa before cracking to 16873.35 MPa after the collapse.

Commented [CH9]: Please define, if appropriate.

K.A. Patela et al. (2014) [12], in their paper, provide an explicit expression for the effective moment of inertia by considering cracks for reinforced concrete beams (RC) with uniformly distributed loads. The proposed explicit expressions can be used to predict short-run displacement in-service load. The sensitivity analysis shows a substantial dependence of the effective moment of inertia on the selected input parameter. Displacement is an important parameter for examining the serviceability criteria of structures. The short-term displacement is generally calculated using the effective moment of inertia across the span at the service load [12]. Chunyu Fu (2018) [13] presents a method of estimating the stiffness of cracked beams based on the stress distribution. In his conclusion, he said that the presence of cracks causes a nonlinear stress distribution along the beam section, which changes the neutral axis of the cross-section and further affects the stiffness of the beam. J.R. Pique (2008) [14] concluded that when the design is controlled by the minimum reinforcement, especially in the beam, special attention should be paid to the calculation of the real period and maximum distortion. The effective stiffness of the beam with the minimum steel ratio is much lower than that obtained by the proposed reduction factor. As a result, the actual period and actual maximum distortion can be greater. Akmaluddin et al. (2012) [15] concluded that the moment of crack and the value of the moment of inertia of the crack was significantly affected by the presence of bamboo reinforcement in the beam. The experimental results show that the crack moment varies from 0.3 to 0.7 from the ultimate moment. The experimental and theoretical crack moment ratio varies from 0.90 to 1.42. İlker Kalkan (2013) and [16] concluded that the effective moment of inertia and load-displacement curve analysis is highly dependent on the crack moment used in the expression analysis of the effective moment of inertia. Therefore, the experimental cracking moment of the beam should be used in the calculation of the effective moment of inertia for a more accurate comparison of the different analytical methods. Chunyu Fu et al. (2020) [17] concluded that cracking of concrete causes a gradual change in the distribution of strain along with the cross-sectional height of reinforced concrete beams, which in turn affects the instantaneous stiffness. The instantaneous stiffness proved to be highly dependent on the number and depth of cracks. This dependence can be accurately reflected by the method proposed by simulating a gradual change in the concrete strain distribution. Xiuling Feng et al. (2013) [18] examines the reduction factor of flexural stiffness in reinforced concrete columns with an equiaxial cross-section and suggests that the reduction factor is proposed by considering the nonlinear characteristics of the material and its geometric nonlinearity.

The difference in the nonlinear characteristics of the material used in the BRC beam and the SRC beam greatly determines the flexural behavior of the beam. Bamboo reinforced concrete beams have low stiffness and tend to be large displacement. The solution to increasing the stiffness of BRC beams is to use shear reinforcement and the principle of confined concrete [7,19]. In the linear elastic condition, the BRC beam has shown a large displacement, but when the ultimate load is reached and the loading is released gradually, the displacement tends to return to zero. In this study, the reduction of stiffness in the non-linear phase was analyzed through the load vs. displacements that were validated using the finite element method (FEM) and the Artificial Neural Networks (ANN) method. It is suspected that the reduction of the cross-sectional stiffness of the BRC beam is different from the reduction in the stiffness of the SRC beam section. The parameter of the moment of inertia of the cross-section becomes a benchmark in determining the reduction of stiffness according to ACI-318M-14 [5].

2. Materials and Methods

2.1. Treatment of Materials

In this study, the treatment of bamboo material as concrete reinforcement is an important thing to do. The bamboo used is the bamboo "petung" (*Dendrocalamus asper*) which is between three and five years old [20–22]. The part of bamboo that is used as reinforcing of concrete is 6–7 m long from the base of the bamboo stem [23]. Bamboo is cut according to the size of the bamboo reinforcement to be used, which is 15 x 15 mm^2. Then, bamboo is soaked for ±20–30 days [21]. After soaking, bamboo is dried in free air until it has an absorption level of ± 12%.

Application of adhesive or waterproof coating [24,25] is done after the bamboo reinforcement is cleaned and trimmed according to the planned size. The application of a waterproof layer is carried out to prevent the hydrolysis process between bamboo and concrete. Sand sprinkling on bamboo reinforcement is done when the adhesive is half dry to make it stronger [21,26]. The application of sand aims to increase the adhesion strength of bamboo reinforcement to concrete.

An ~~i~~Installation of a hose-clamp at both ends of the bamboo reinforcement is done to match the concept of hooks or bends in steel reinforcement. An ~~i~~Installation of the hose-clamp only on tensile reinforcement is done to increase bond-stress between bamboo reinforcement and concrete [27,28]. The tensile force on the bamboo reinforcement will be distributed to the concrete through the hose-clamp, which functions as a shear connector. Bamboo treatment is shown in Figure 1.

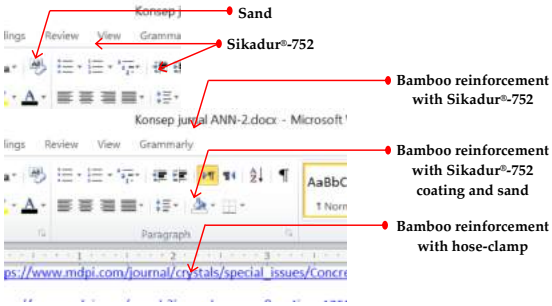

Figure 1. The materials and treatments of bamboo reinforcement.

2.2. *Materials*

The concrete mixture used in this study is a normal concrete mixture consisting of Portland Pozzolana Cement (PPC), sand, coarse aggregate, and water with a proportion of 1:1.8:2.82:0.52. Sand and gravel come from the Jember area of Indonesia. The cylindrical specimen measures 150 mm in diameter and 300 mm in height. The cylindrical specimens were press-tested using a Universal Testing Machine (UTM) with a capacity of 2000 kN after the concrete was 28 days old. The procedure for the cylinder specimen compressive test follows ASTM C 39 [29]. The average compressive strength of cylindrical concrete is 31.31 MPa with an average weight of 125.21 N. The properties and characteristics of the concrete are shown in Table 1.

Table 1. Material properties of reinforcing and concrete.

Bar Type and Concrete	Diameter, d (mm)	Modulus of Elasticity (E), (MPa)	Poisson's Ratio (ν)	Tensile Strength, f_y (MPa)	Compressive Strength, f'_c (MPa)
Bamboo	□ 15 × 15	17,235.74	0.20	126.68	-
Steel	ϕ 8	207,735.92	0.25	392.28	-
Concrete	-	26,324.79	0.30	-	31.31

The tensile test of bamboo reinforcement produces the average tensile stress of 126.68 N/mm^2 with an average strain of 0.0074. The modulus of elasticity of bamboo reinforcement was calculated using the formula $E = \sigma/\varepsilon$ and obtained 17,235.74 MPa. The modulus of elasticity of steel is obtained by 207,735.92 MPa. The properties and characteristics of bamboo and steel reinforcement are shown in Table 1.

Formatted: Font: Not Bold

Commented [M10]: Please check it.

The adhesive layer or waterproof coating used was Sikadur®-752 produced by PT. SIKA Indonesia [30]. The specifications for the adhesive sikadur®-752 are shown in Table 2. Installation of hose-clamp on bamboo reinforcement is done when the waterproof layer is half dry [21]. The diameter of the hose-clamp used is ¾" made in Taiwan.

Table 2. The specification of Sikadur®-752 [30].

Components	Properties
Colour	Yellowish
Density	Approx. 1.08 kg/L
Mix comparison (weight/volume)	2:1
Pot life at +30 °C	35 min
Compressive strength	62 MPa at 7 days (ASTM D-695) 64 MPa at 28 days
Tensile strength	40 MPa at 28 days (ASTM D-790)
Tensile Adhesion Strength	2 MPa (Concrete failure, over mechanically prepared concrete surface)
Coefficient of Thermal Expansion	−20 °C to + 40 °C 89 × 10^{-6} per °C
Modulus of elasticity	1060 MPa

Commented [M11]: We changed to it, please confirm if it is correct.

2.3 Experimental Procedure

The test object consisted of 9 beams with a size of 75 mm × 150 mm × 1100 mm, consisting of 8 bamboo reinforced concrete beams (BRC), and one steel-reinforced concrete beam (SRC). Bamboo reinforcement is installed as tensile reinforcement with a reinforcement area of 450 mm². The steel reinforcement used has a diameter of 8 mm with an area of A_s = 100.48 mm². The beam geometry and reinforcement detail of the BRC and SRC beams are shown in Figure 2.

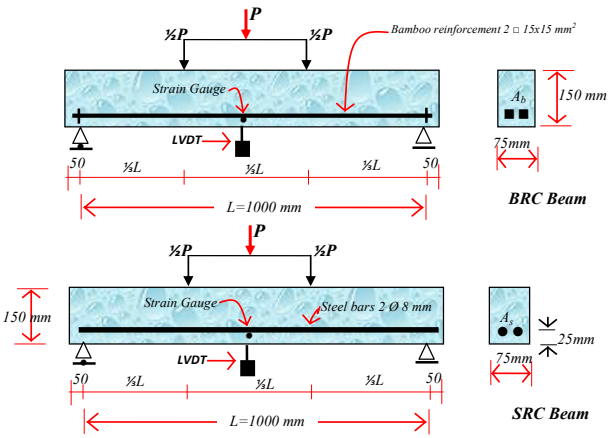

Figure 2. Reinforcement details and beam test settings.

The beam flexural test method was carried out using the four-point method [31]. The test arrangement and load position are shown in Figure 2. Strain gauges are installed on the bamboo reinforcement at a distance of ½L from the support of the beam. Beam displacement measures using

Linear Variable Displacement Transducers (LVDT) ~~*(Linear Variable Displacement Transducers)*~~ with a distance of ½L from the beam support.

The loading stages from zero to the collapse of the beam are used as a hydraulic jack and a load cell connected to a load indicator tool. The load reading on the load indicator is used as a hydraulic jack pump controller, displacement reading, and strain reading according to the planned loading stage. However, when the test object reaches its ultimate load, the displacement reading controls the strain and load reading, while the pumping of the hydraulic jack continues slowly according to the command of the displacement reader. The failure pattern was observed and identified by the cracks that occurred, from the time of the initial crack until the beam collapsed.

2.4. Validation of Numerical Methods

Validation of experimental data was found by using the Finite Element Method (FEM) and Artificial Neural Networks (ANN). The relationship between load vs. displacement experiment results was validated by using the finite element method. The procedure used is inputting material data and loading stages to determine the behavior of the load vs. displacement of BRC beams and SRC beams. The data input for the loading stages is carried out following the loading stages from laboratory experimental data. The numerical method used is the finite element method, using the Fortran PowerStation 4.0 program [32]. The theoretical analysis is used to calculate the load causing the initial crack using elastic theory (*linear analysis*) with cross-section transformation. For linear analysis, the input material data is the modulus of elasticity (E) and Poisson's ratio (υ). The calculation of the modulus of elasticity of the composites (E_{comp}) is shown in Tables 3 and 4. The non-linear phase is approximated by decreasing the concrete strength from 0.25 to 0.5 for the calculation of the effective stiffness in the plastic plane [5]. In the analysis of the finite element constitutive relationship, the problem-solving method uses the plane-stress theory. Triangular elements are used to model plane-stress elements with a bidirectional primary displacement at each point so that the element has six degrees of freedom. The discretization of the beam plane is carried out using the triangular elements shown in Figure 3 for BRC beams and Figure 4 for SRC beams.

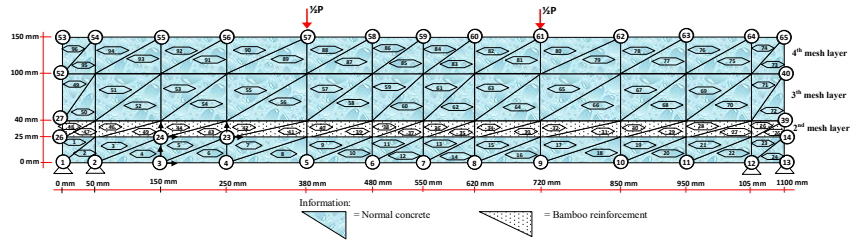

Figure 3. Discretization of the triangular element on the bamboo reinforced concrete (BRC) beam.

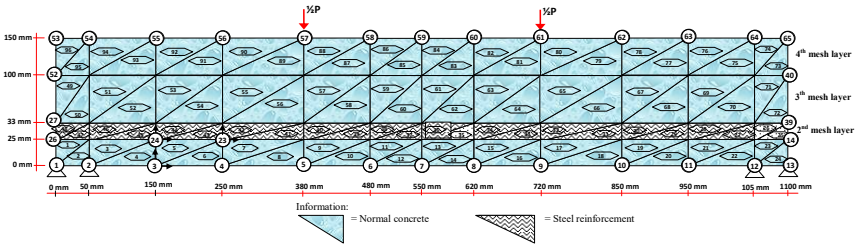

Figure 4. Discretization of the triangular element on the steel-reinforced concrete (SRC) beam.

Formatted: Font: Not Italic

Commented [CH12]: Please check that intended meaning is retained.

Commented [CH13]: Please check that intended meaning is retained.

Table 3. Elasticity Modulus of Composite of BRC beam.

Layer Number	Compressive Strength of Concrete, f'_c	Dimensions of per Layer		Modulus of Elasticity of the Material (E)		Elasticity Modulus of Composite (E_{comp})
	Mpa	b (mm)	h (mm)	Concrete, E_c (MPa)	Bamboo, E_b (MPa)	MPa
4th mesh layer	31.31	75	50	26,851.29	0	26,851.29
3rd mesh layer	31.31	75	60	26,851.29	0	26,851.29
2nd mesh layer	31.31	75	15	26,851.29	1723.57	23,140.89
1st mesh layer	31.31	75	25	26,851.29	0	26,851.29

Table 4. Elasticity Modulus of Composite of SRC beam

Layer Number	Compressive Strength of Concrete, f'_c	Dimensions of per Layer		Modulus of Elasticity of the Material (E)		Elasticity Modulus of Composite (E_{comp})
	Mpa	b (mm)	h (mm)	Concrete, E_c (MPa)	Steel, E_s (MPa)	MPa
4th mesh layer	31.31	5	50	26,851.29	0	26,851.29
3rd mesh layer	31.31	75	67	26,851.29	0	26,851.29
2nd mesh layer	31.31	75	8	26,851.29	207,735.92	43,209.32
1st mesh layer	31.31	75	25	26,851.29	0	26,851.29

The modulus of elasticity (E) for each layer is calculated according to the condition of the material. Layers of concrete and bamboo reinforcement are calculated using the following Equation. (2) [33].

$$E_e = E_b.V_b + E_c.V_c \quad (2)$$

where E_e = the equivalent elasticity modulus of BRC beam, E_b = elastic modulus of bamboo reinforcement, E_c = modulus of elasticity of concrete, V_b = relative volume of bamboo reinforcement in calculated layers, and V_c = relative volume of concrete in calculated layers. The stress-strain relationship for plane-stress problems has the shape of an equation such as Equation (3).

$$\begin{Bmatrix} \sigma_x \\ \sigma_y \\ \tau_{xy} \end{Bmatrix} = \frac{E}{(1+\nu^2)} \begin{bmatrix} 1 & \nu & 0 \\ \nu & 1 & 0 \\ 0 & 0 & \frac{1-\nu}{2} \end{bmatrix} \begin{Bmatrix} \varepsilon_x \\ \varepsilon_y \\ \gamma_{xy} \end{Bmatrix} \quad (3)$$

where E is the modulus of elasticity and ν is the Poisson's ratio. And the principal stresses in two dimensions are calculated by Equation (4).

$$\sigma_{1,2} = \frac{\sigma_x + \sigma_y}{2} \pm \sqrt{\left(\frac{\sigma_x - \sigma_y}{2}\right)^2 + \tau_{xy}{}^2} = \sigma_{\max} \quad (4)$$

The simulation and steps for preparing a FEM analysis with the Fortran PowerStation 4.0 program [32] are summarized as follows:

Step 1: Discretization of BRC and SRC beam planes with the discretization of triangular elements, the numbering of triangular elements, and the numbering of nodal points as shown in Figures 3(d) and Figure 4.

Step 2: Calculation and collection of geometry and material data, such as the modulus of elasticity of the material (E), Poisson's ratio (ν), etc.
Step 3: Writing a programming language for triangular elements using the Fortran PowerStation 4.0 program according to the constitutive relationships and FEM modeling as shown in the following link: http://bit.ly/2F17w8F.
Step 4: Open the Fortran PowerStation 4.0 program. An example is shown at the following link: http://bit.ly/2MTh22j.
Step 5: Write programming language data (Step 3) in the Fortran PowerStation 4.0 program. Examples can be seen at the following link: http://bit.ly/2ZvZWMU.
Step 6: Input DATA.DAT of BRC beam and SRC beam in the Fortran PowerStation 4.0 program. Input data is displayed at the following links: http://bit.ly/351FPqU and http://bit.ly/2MBqas9. An example of displaying input data is shown on the following link: http://bit.ly/2u2K2xR.
Step 7: Analyze the program until there are no warnings and errors. If there are warnings and errors, check and correct program data and input data.
Step 8: Download stress data. The stress data are shown at the following link: http://bit.ly/2rDPeaI for the stress of BRC beam, and http://bit.ly/2Q4Ihc1: for the stress of the SRC beam. An example of displaying stress data from the Fortran PowerStation 4.0 program is shown at the following link: http://bit.ly/2ZybLCd.
Step 9: Download displacement data. An example of displaying data displacement from the Fortran PowerStation 4.0 program is shown on the following link: http://bit.ly/2Q7j2Wp.
Step 10: Enter stress and displacement data into the Surfer program to obtain contour image data of stress and displacement. Stress and displacement contour image data are shown in Figures 15–18.

Commented [M14]: Figures should be cited in numerical order.

2.4. Validation of Artificial Neural Networks (ANN)

Artificial Neural Networks (ANN) is a computational system for solving complex problems in civil engineering. In this study, the validation carried out by the Artificial Neural Networks (ANN) method is the validation of the load vs. displacements from laboratory experimental results. The data on the loading and displacement stages of the experimental results were used as input data and target data in this analysis. Previous researchers concluded that Artificial Neural Networks (ANN) can be an alternative in calculating displacement in reinforced concrete beams. Several researchers have used the ANN method for many structural engineering studies, such as predicting the compressive strength of concrete [34], axial strength of composite columns [35], and determination of RC building displacement [36]. Kaczmarek and Szymańska (2016) [37] concluded that the results of calculating displacement in reinforced concrete using ANN proved to be very effective. Abd et al. (2015) [38] concluded that the ANN method is also very good for predicting displacement in concrete beams with a very strong correlation level of 97.27% to the test data. Tuan Ya et al. (2019) [39] used the ANN method to predict displacement in cantilever beams and concluded that the output was very accurate.

The ANN method is currently very popular with researchers in predicting and evaluating the behavior of structures in the field of civil engineering. This is because the ANN method has an advantage in the nonlinear correlation between the input variables presented ~~is better~~. Khademi et al. (2017) [40] predicts the compressive strength of concrete at 28 days of age by considering the experimental results, three different models of multiple linear regression (MLR), artificial neural networks (ANN), and adaptive neuro-fuzzy inference system (ANFIS). The results of his research concluded that the ANN and ANFIS models can predict the 28-day concrete compressive strength more accurately and the ANN model can perform better than the ANFIS model in terms of R^2. The ANN and ANFIS models are preferred because the nonlinear correlation between the input variables presented is better. The ANN and ANFIS models have higher accuracy requirements than the multiple linear regression (MLR) model. The accuracy of the prediction is very much dependent on the number of input variables. The greater the number of input parameters, the more accurate the results of the predictor model will be.

Xuan Li et al. (2019) [41] predict the service life of corroded concrete sewer pipes using three data-driven models, namely multiple linear regression (MLR), artificial neural networks (ANN), and

adaptive neuro-fuzzy inference system (ANFIS). The one conclusion suggests that the ANN and ANFIS models perform better than the MLR models for corrosion prediction, with or without considering the interactions between environmental factors.

The ANN data is divided into three different subsets [40], namely: (1) Training, at this stage, the subset is trained and studied as occurs in the human brain, where the number of epochs is repeated until an acceptable model accuracy is obtained; (2) Validation, at this stage, the subset shows how well the model is trained, and estimates model properties such as misclassification, mean error for numerical predictors; and (3) Test, at this stage, the subset verifies the performance of the training subset built into the ANN model.

This paper uses even load input data, while the target data is the displacement of the laboratory test results. The distribution of the ANN model data composition consists of training 70%, validation 15%, and testing 15%. ANN architecture on a rectangular beam is shown in Figure 5. The process of implementing input data in the ANN model architecture consists of (1) Input layer, consisting of 1 neuron, namely displacement data variable of experimental results; (2) Hidden layer, consisting of 10 neurons. At this stage, the input layer will forward the data to the hidden layer or the output layer through a set of weights. This weight is a link from each neuron to other neurons in the next layer which will help adjust the ANN structure to the given displacement data pattern using learning. In the learning process, the weights will be updated continuously until one of the numbers of iterations, errors, and processing time has been reached. This is done to adjust the ANN structure to the desired pattern based on certain problems that will be solved using ANN. Weight ~~or what~~ is known as the independent parameter. During the training process, the weights will be modified to improve the accuracy of the results, ~~and~~ The third layer is (3) Output layer, consisting of 1 neuron which is the expected output target, error, and weight. Error is the error rate of the displacement data node of the process carried out, while weight is the weight of the displacement data node with a value ranging between –1 and 1. Then the displacement data resulting from the training process is processed into a graphic image of the load vs. displacement relationship.

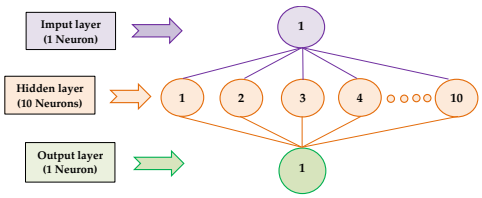

Figure 5. Schematic of Artificial Neural Networks (ANN) model architecture for BRC beam and SRC beam.

3. Results

3.1. Experimental

Table 5 shows the results of theoretical calculations and experiments for BRC and SRC beams. From the theoretical calculation, the BRC beam has an initial crack load of 6.87 kN and an SRC beam of 6.51 kN. The laboratory test results of the BRC beam experienced an initial crack at a load of 7.69 kN and an SRC beam had an initial crack at a load of 10 kN. The average ultimate load of the BRC beam occurs at a load of 31.31 kN or 97.27% of the theoretical collapse load of 32.19 kN, This shows that with the correct treatment of bamboo reinforcement, the BRC beam can reach load capacity according to the results of the theoretical calculations. As is known, the researchers concluded that the ultimate load of BRC beams is very low when compared to the theoretical calculations, ~~including (1)~~ Dewi et al. (2017) [42] concluded that the bending capacity of bamboo reinforced concrete beams only reaches 56% of its capacity if the tensile strength of bamboo is full, ~~(2)~~ Nathan (2014) [43] concluded that the flexural capacity of reinforced concrete beams only reaches 29% to 39% of the beam capacity steel-reinforced concrete with the same width and reinforcement dimensions, ~~(3) and~~

Khare (2005) [44] concluded that the flexural capacity of reinforced concrete beams is only 35% of steel-reinforced concrete beams at the same strength level.

SRC beams reach a collapse load of 24 kN or almost approaching the theoretical collapse load of 24.12 kN, This shows that the adhesion strength of steel-reinforcement with concrete is higher. Figures 6 and 7 show that the relationship of the load vs. displacement of the BRC beam and the SRC beam is different. The SRC beam shows the regions of the elastic limit, elastoplastic limit, and plastic limit. Meanwhile, the BRC beam only shows the plastic limit point or the ultimate load point. This shows that the behavior of reinforced concrete beams is very much determined by the properties and characteristics of the materials used.

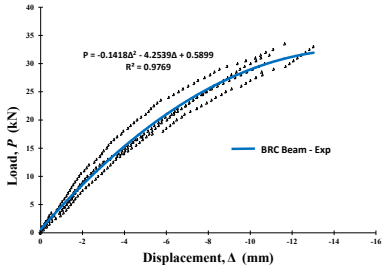

Figure 6. The relationship of load vs. displacement of BRC beam of experimental results.

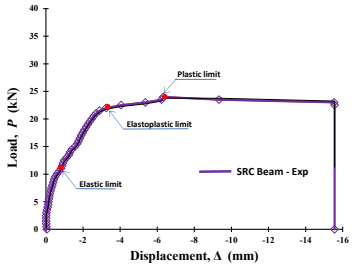

Figure 7. The relationship of load vs. displacement of SRC beam of experimental results.

Mechanical properties and characteristics of steel and bamboo materials are the dominant factors in the behavior model of the load and displacement relationship [6]. The difference between the stress and strain relationship patterns of bamboo and steel is in the position of the melting point and the fracture stress. Steel material shows a clear melting point, while bamboo reinforcement does not show a clear melting point. However, after the fracture stress, the relationship pattern of the stress-strain relationship tends to return to zero, This shows that bamboo has good elastic properties [7].

Table 5. Results of theoretical calculations and experimental for the load capacity of BRC beams and SRC beams.

Specimens	Sample no	Theoretical Calculations		Flexural Test Results			
		First Crack Load (kN)	Ultimate Load (kN)	First Crack Load, P_{cr} (kN)	Failure Load, P_{ult} (kN)	Displacement at Failure (mm)	P_{cr}/P_{ult} (%)
(a) BRC-1	1	6.90	32.20	8.50	31.50	10.92	26.98
	2			8.00	29.00	11.90	27.59

(b) BRC-2	3			7.00	31.00	13.02	22.58
	4			7.50	33.00	12.18	22.73
(c) BRC-3	5			8.00	33.50	14.69	23.88
	6			7.50	33.00	9.32	22.73
(d) BRC-4	7			7.50	29.50	7.61	25.42
	8			7.50	30.00	10.69	25.00
Average:				7.69	31.31		24.61
(e) SRC	9	6.50	24.20	10.00	24.00	6.33	41.57

3.2. Validation with the ANN Method

The load vs. displacement relationship data from the experimental results is the basis used for the train and the network. Neural networks are designed by determining their structure experimentally. The data that trains the artificial neural network is the input, and the ability to reproduce the training pattern is tested. Convergence analysis was carried out to determine the optimal number of neurons in the hidden layer of ANN. Excessive neurons reduce the computational performance of ANN, whereas a lack of neurons causes difficulties in characterizing the input-output relationship. As suggested by Caudill and Mishra et al. (2019) [45], the upper limit of the number of neurons in the hidden layer is twice the number of inputs plus 1. After the number of neurons in the hidden layer is reached, the MSE, RMSE, and R^2 observations are stopped and no increase is assumed significant. The artificial neural network architecture used in this paper: IHO: 1-10-1 [Input-Hidden-Output] means that this artificial neural network consists of 1 input neuron, one hidden layer with 10 neurons, and 1 output neuron (predictive values of the load vs. displacement relationship).

Table 6 presents the performance results of ANN architecture for ten simulations. The process which has the lowest MSE is selected for comparison with experimental data. Figures 8–12 illustrate the prediction of the load vs. displacement of the BRC and SRC beams obtained when using the ANN model after training and when using the data obtained experimentally for training data, validation data, test data, and all data. Figures 8–12 shows the correlation between the value of the BRC beam and the SRC beam relationship obtained in the laboratory and the load vs. displacement values obtained using ANN analysis. The convergence of the position of the point with the line y = x indicates the identification of values with very high accuracy. The correlation value of laboratory data using ANN shows an average value of *R* Square of 0.999., This indicates that the two results are consistent. The prediction results of the ANN method show that the percentage of errors is very small, with a maximum error of 0.26%. Overall, the comparison of experimental data with the predicted results of the ANN method shows an error of not more than 1%. From the data from the two analyszes and the load vs. displacement relationship pattern, it can be concluded that the stiffness of the BRC beam has similarities.

Table 6. The validation results of the relationship load vs. displacement using the ANN method.

Specimens	The Correlation Coefficient (*R*)			Mean Square Error (MSE)		
	Training	Validation	Testing	Training	Validation	Testing
BRC-1	1.0000	0.9999	0.9997	0.0004	0.0011	0.0110
BRC-2	0.9999	0.9997	0.9999	0.0038	0.0276	0.0048
BRC-3	0.9998	0.9999	0.9993	0.0034	0.0075	0.0152
BRC-4	1.0000	1.0000	1.0000	0.0001	0.0009	0.0010
SRC	1.0000	1.0000	0.9997	0.0001	0.0027	0.0006

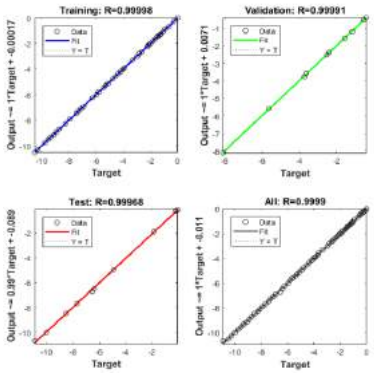

Figure 8. Prediction of the load vs. displacement relationship using ANN and using experimental observation for the training, validation, testing, and all datasets (BRC-1).

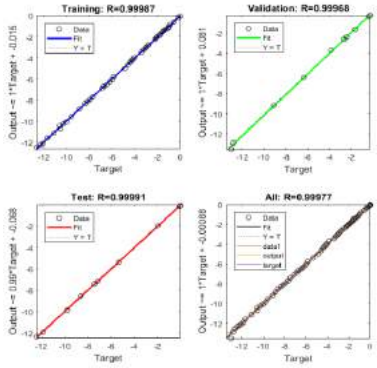

Figure 9. Prediction of the load vs. displacement relationship using ANN and using experimental observation for the training, validation, testing, and all datasets (BRC-2).

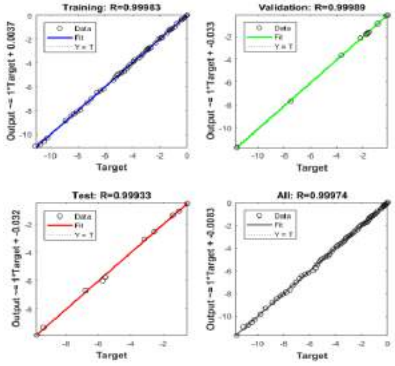

Figure 10. Prediction of the load vs. displacement relationship using ANN and using experimental observation for the training, validation, testing, and all datasets (BRC-3).

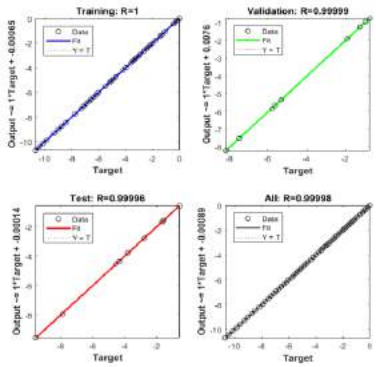

Figure 11. Prediction of the load vs. displacement relationship using ANN and using experimental observation for the training, validation, testing, and all datasets (BRC-4).

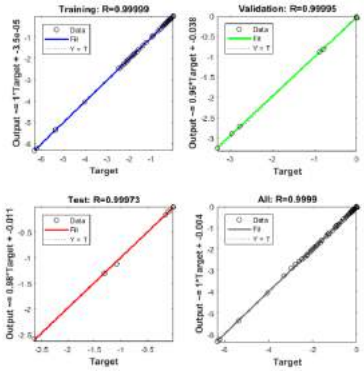

Figure 12. Prediction of the load vs. displacement relationship using ANN and using experimental observation for the training, validation, testing, and all datasets (SRC).

The data merger of ANN analysis results from each BRC beam specimen into a load vs. displacement relationship. The merger is done to determine the suitability of the load vs. displacement relationship model through the R^2 parameter. From the results of the regression analysis, it is found that R^2 = 0.9771, or almost close to 1, This shows that the model has high suitability, as shown in Figure 13. Figure 13 illustrates the load vs. displacement relationship for all BRC beam typologies from ANN analysis.

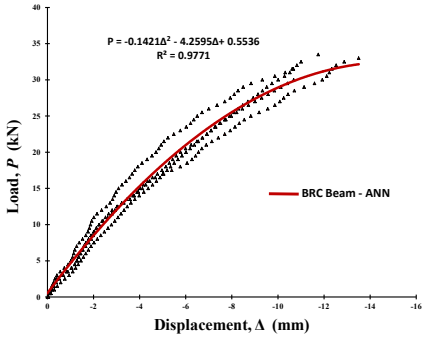

Figure 13. The relationship of load vs. displacement of BRC beam of ANN results.

3.3. Validation with the Finite Element Method

Validation of the relationship of load vs. displacement with the finite element method is done by inputting the geometry of the cross-section, load data, modulus of elasticity (E) per layer, and Poisson's ratio (υ). The load vs. displacement relationship diagram of the experimental results as shown in Figures 6 and 7 is used as a guide for the stages of the analysis process using the finite element method. And the cross-sectional stiffness input via the per-layer modulus of elasticity (E) is shown in Tables 7 and 8. The analysis execution using the finite element method uses the Fortran PowerStation 4.0 program. The process of calculating displacement and stress with the Fortran PowerStation 4.0 program is carried out in stages according to the loading and stiffness stages per layer from the beam's elastic condition, initial crack, elastoplastic, and plastic conditions until the beam collapses. The displacement data resulting from the finite element method is processed into a load vs. displacement relationship as shown in Figure 14. The displacement ~~when~~ of the load ultimate is shown in Figure 15 for BRC beams and Figure 16 for SRC beams. The stress contours at the time of the load collapse are shown in Figure 17 for BRC beams and Figure 18 for SRC beams.

Commented [CH15]: Please check that intended meaning is retained.

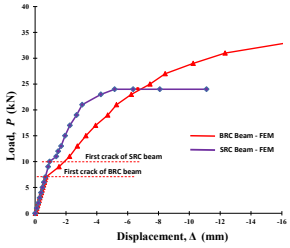

Figure 14. The relationship of load vs. displacement of BRC beam of finite element method (FEM) results.

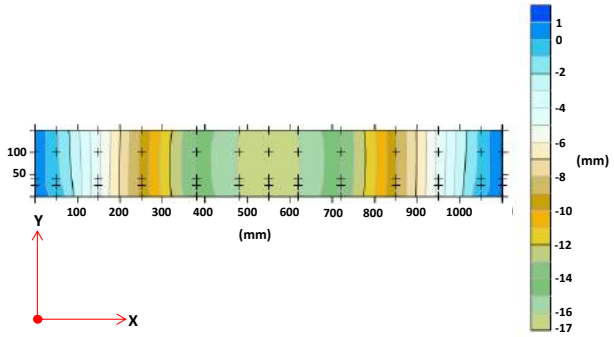

Figure 15. The displacement contour of Y-direction of BRC beam.

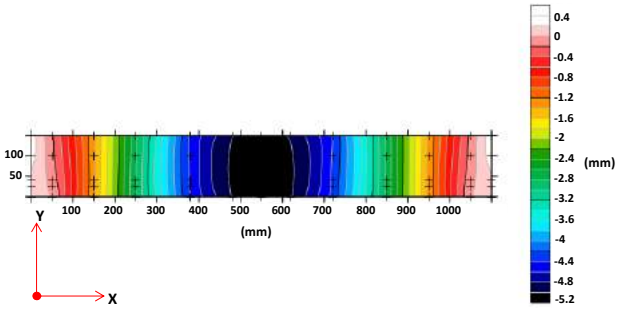

Figure 16. The displacement contour of Y-direction of SRC beam.

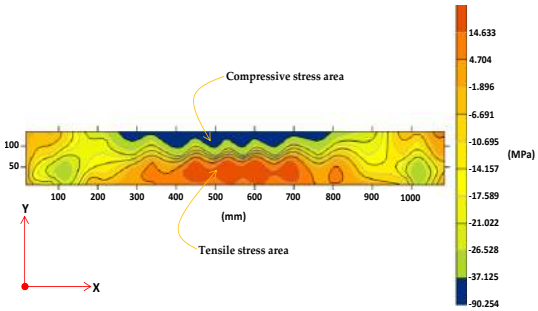

Figure 17. The stress contour of X-direction of BRC beam.

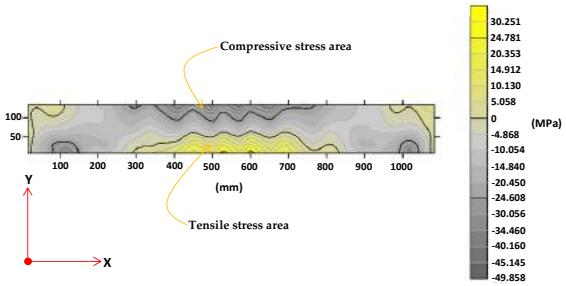

Figure 18. The stress contour of X-direction of SRC beam.

Table 7. The modulus of elasticity for each layer of the BRC beam in the non-linear phase.

Layer Number	Modulus of Elasticity (*E*) of the BRC Beam													
	Elastic Condition	Plastic Conditions with Gradual Loads												
	0–8.5 kN	9 kN	11 kN	13 kN	15 kN	17 kN	19 kN	21 kN	23 kN	25 kN	27 kN	29 kN	31 kN	33 k
4th mesh layer	26851.29	16,110.77	16,110.77	16,110.77	16,110.77	16,110.77	16,110.77	16,110.77	16,110.77	16,110.77	12,083.08	11,277.54	11,277.54	8592
3th mesh layer	26851.29	16,110.77	16,110.77	16,110.77	16,110.77	16,110.77	16,110.77	16,110.77	16,110.77	1208.31	10,740.52	9397.95	9397.95	7518
2nd mesh layer	23140.89	13,884.53	11,570.44	11,570.44	11,570.44	11,570.44	10,413.40	10,413.40	10,413.40	10,413.40	6942.27	6942.27	6942.27	5553
1st mesh layer	26851.29	13,425.65	11,814.57	10,203.49	8323.90	6712.82	5101.75	5101.75	5101.75	3759.18	3222.16	2685.13	1611.08	1329

Table 8. The modulus of elasticity for each layer of the SRC beam in the non-linear phase.

Layer Number	Modulus of Elasticity (*E*) of the SRC Beam										
	Elastic Condition	Plastic Conditions with Gradual Loads									
	0–9 kN	10 kN	11 kN	12 kN	13 kN	15 kN	17 kN	19 KN	21 KN	23 kN	24 kN
4th mesh layer	26,851.29	26,851.29	20,138.47	20,138.47	20,138.47	20,138.47	20,138.47	18,795.90	18,795.90	13,425.65	11,411.80
3th mesh layer	26,851.29	26,851.29	20,138.47	20,138.47	18,795.90	18,795.90	18,795.90	17,453.34	17,453.34	13,425.65	11,411.80
2nd mesh layer	43,209.32	43,209.32	30,586.93	30,586.93	28,547.80	28,547.80	26,508.67	26,508.67	24,469.54	20,391,29	17,332.60
1st mesh layer	26,851.29	26,851.29	20,138.47	20,138.47	18,795.90	18,795.90	17,453.34	16,110.77	14,768.21	13,425.65	12,083.08

4. Discussion

Merging is carried out on the load vs. displacement relationship diagram from the experimental results, ANN analysis, and finite element method (FEM) analysis. Figure 19 shows the combined load vs. displacement diagram of the ANN analysis results with the experimental results. Figure 19 shows that the load vs. displacement relationship diagram the two analyszes results are very coincided or show high suitability. However, at a load of approximately 90% of the collapse load, the load vs. displacement relationship diagram shows different behavior. Figure 20 shows the combined load vs. displacement diagram of the experimental results, ANN analysis, and the results of the finite element method analysis. Figure 19 shows that the artificial neural networks (ANN) model has a higher R^2 value when compared to the R^2 value of the multiple linear regression model (MLR). ANN analysis has better predictive accuracy. This is the same as the conclusion of 2 researchers, namely Khademi et al. (2017) [40], whoich concluded that tThe ANN model has higher accuracy than the multiple linear regression (MLR) model, and Xuan Li et al. (2019) [41], who concluded that the ANN model performs better than the MLR models with or without considering the interactions between factors. The accuracy of the prediction is very much dependent on the number of input variables.; Tthe greater the number of input parameters, the more accurate the results of the predicted model.

The diagram of the relationship between load and displacement of the BRC beam from FEM analysis and experimental results shows the difference in elastic conditions or until the initial crack occurs. The experimental results showed negative differences with the results of the FEM analysis. This shows the influence of the nature and characteristics of bamboo. The parts of bamboo stems have a non-uniform or uncertain modulus of elasticity. Tensile strength and modulus of elasticity of bamboo tested in the laboratory are sometimes different from bamboo which is used as beam reinforcement. As is known, bamboo trees from base to tip have different tensile strength and fiber density. Meanwhile, the load vs. displacement diagram of the SRC beam experiment results has a positive difference with the results of the FEM analysis when the elastic condition occurs or until the initial crack occurs. Positive differences can be ignored, in the sense that the quality of the steel used is better than the quality of steel tested in the laboratory. However, in this study, the analysis of stiffness reduction in BRC and SRC beams was focused after the beam experienced an initial crack or non-linear phase.

Commented [CH16]: Please check that intended meaning is retained.

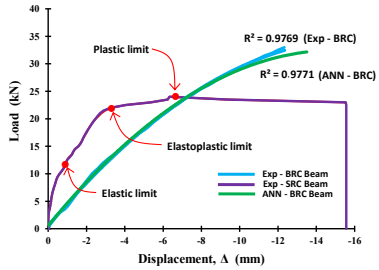

Figure 19. The combined of the load vs. displacement relationship of BRC beam of the experimental results and ANN analysis.

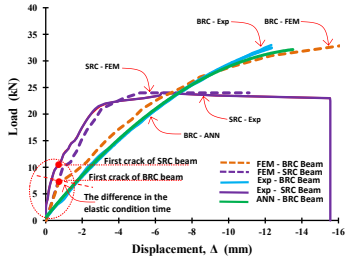

Figure 20. The combined of the load vs. displacement relationship of BRC beam and SRC beam of the experimental results, ANN analysis, and FEM.

Figure 20 shows that inelastic conditions there is a difference in stiffness between the two types of beams. The stiffness of bamboo reinforced concrete beams (BRC) is lower than the stiffness of steel-reinforced concrete beams (SRC). This difference occurs not due to reduced cross-section inertia or I_g of cross-sectional reduction, but due to the nature of the material used. This is because the BRC beam uses bamboo reinforcing material, which has high elastic and resilience properties. BRC beams with bamboo reinforcement will be able to accept high impact loads without causing over stress at the elastic limit, even though displacement has occurred. This indicates that the energy absorbed during loading is stored and released if the material is not loaded. Meanwhile, the SRC beam uses steel material that has high stiffness and toughness, so that the SRC beam in the service load range or elastic conditions~~, the beam~~ does not experience excessive displacement or deformation. Beams that use materials with high stiffness and toughness will be able to withstand high impact loads or shock loads. If the SRC beam gets an impact load, then some of the energy is absorbed and some of the energy is transferred.

In the non-linear phase or after initial cracking, the beam stiffness changes from the full-sectional flexural stiffness, E_cI_g, to the effective bending stiffness, E_cI_{eff}. In the non-linear phase, the stiffness of the beam section continues to decrease with increasing loads, moments, and cracks. The area of the beam section continues to decrease with increasing cracks and automatically causes the beam section stiffness (E_cI_g) to decrease. As shown in Table 6 and Figure 21, the stiffness of the BRC beam decreases after the initial cracking occurs as the increasing loading stage is applied. The increase in load causes the flexural moment to increase, the displacement increases, and the crack propagation continues to spread towards the compressed block of the beam cross-section. The crack propagation from 1st mesh layer to the 2nd mesh layer onwards runs linearly with reduced cross-sectional stiffness from the lower fiber of the cross-section tensile block to the upper fiber of the compressive block of the beam cross-section. The increase in crack propagation towards the compressive block of cross-section causes the neutral line to change. Chunyu Fu et al. (2018) [13] concluded that the presence of cracks causes a nonlinear stress distribution along the beam cross-section, which changes the neutral axis of the cross-section and further affects the stiffness of the beam. Figure 21 shows that the stiffness of the BRC beam cross-section decreases from the initial crack until the beam collapses. The stiffness of BRC beams is reduced by 50% after initial cracking to 95% at collapse. The stiffness reduction goes step by step according to the moment (M_a) applied to the beam. Sang-Whan Han et al. (2009) [4] revealed that the stiffness reduction factor was significantly affected by the amount of moment or the applied load, while the stiffness reduction factor did not differ from the amount of reinforcement. The decrease in the moment of inertia of the full cross-sectional Ig of the BRC beam ranged from $0.5I_g$—$0.05I_g$ for the elastoplastic and plastic regions. Meanwhile, ACI-318M-14 [5] recommends the stiffness of the beam cross-section for elastic analysis in the non-linear phase of $0.5I_g$—$0.25I_g$. The difference in the value of the reduction in the stiffness of the cross-section at collapse correlates with the differences in the properties and characteristics of the material used as beam reinforcement. Bamboo reinforced concrete beams (BRC) exhibit high displacement behavior, but once the collapse load is reached and

gradually released, displacement tends to return to zero. It is linear with its elastic properties and the stress vs. strain relationship behavior of bamboo.

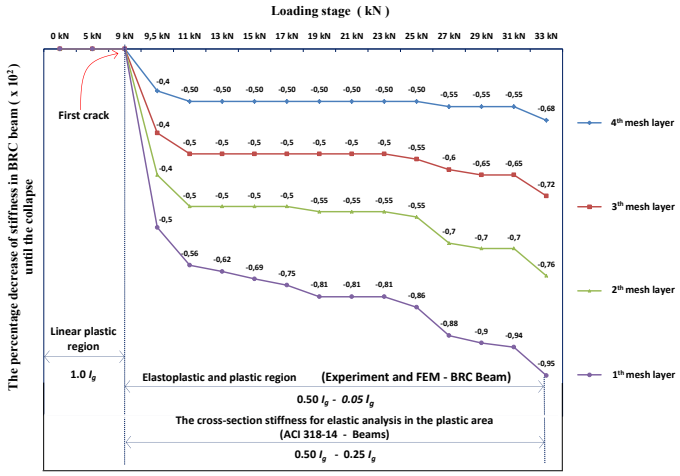

Figure 21. Decreased stiffness of BRC beam cross-section in the span middle.

Table 7 and Figure 22 show a decrease in stiffness or a decrease in the moment of inertia of the SRC beam cross-section. Stiffness decreases after initial cracking as the applied load increases. Figure 22 shows that the cross-sectional stiffness of the SRC beam decreases from the initial crack until the beam collapses. The stiffness of the SRC beam was reduced by 25% after initial cracking to 60% at collapse. The decrease in the moment of inertia full cross-section (I_g) for SRC beams ranged from $0.75I_g$—$0.40I_g$ for the elastoplastic and plastic regions. Meanwhile, ACI-318M-14 [5] recommends the cross-sectional stiffness of reinforced concrete beams for elastic analysis in the non-linear phase of $0.5I_g$—$0.25I_g$. The difference in the value of the reduction in the cross-sectional stiffness of the SRC beam with the ACI-318M-14 [5] requirements is due to the beam cross-section reinforcement method, namely the SRC beam in this study using a single reinforcement method. SRC beam with single reinforcement shows that when the steel reinforcement undergoes second melting and the moment of inertia of the cross-section is still around 40%, the steel reinforcement is not able to withstand the tensile stress that occurs so that the neutral line of the cross-section continues to shift upwards towards the upper fiber of the compression block of the cross-section. Meanwhile, BRC beams with bamboo reinforcement have good elastic properties, where after the ultimate load is reached, the large displacement shrinks back to near-zero or the beam returns flat [7], as shown in the video at the following link: https://goo.gl/6AVWmP. Although the stiffness or inertia of the BRC beam cross-section is still around 5%, bamboo reinforcement is still able to withstand the tensile stress that occurs, as stated by Ghavami (2005) [24] that bamboo has high tensile strength. If we control with the crack pattern, the crack lines on the BRC beam majority stop below the cross-section neutral line, while the crack lines on the SRC beam tend to continue to propagate upwards towards the upper fibers of the compressive block of the beam cross-section, as shown in Figures 23 and 24. And if we look at Figures 17 and 18, the tensile stress contour of the BRC beam has a wider zone and spreads to the side when compared to the SRC beam.

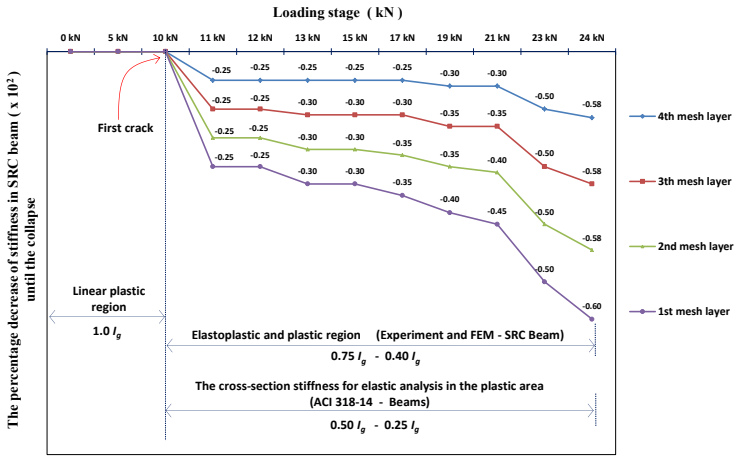

Figure 22. Decreased stiffness of SRC beam cross-section in the span middle.

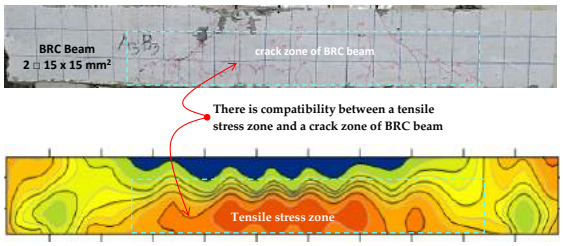

Figure 23. The crack pattern and tensile stress zone of BRC beam.

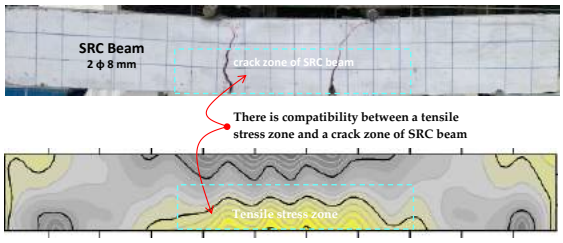

Figure 24. The crack pattern and tensile stress zone of SRC beam.

Figures 25 and 26 show the relationship between the stiffness reduction factor (ϕ_K) and the M_a/M_{cr} of the BRC beam and the SRC beam. The stiffness reduction factor (ϕ_K) is the ratio of the moment of inertia of the effective section (I_e) divided by the moment of inertia of the cross-section (I_g). The stiffness reduction factor (ϕ_K) is significantly influenced by the applied moment level. The equation of the beam stiffness reduction factor is related to the ratio between the applied moment and an initial crack moment or M_a/M_{cr}. The equation for the stiffness reduction factor is shown in Eequation (5) or Eequation (6) for a BRC beam. TAnd the stiffness reduction factor equation for the SRC beam is shown in Eequation (7) or Eequation (8). Figure 27 shows a comparison of the relationship between the stiffness reduction factor and the M_a/M_{cr} of the BRC beam and SRC beam. The diagram of the relationship between the stiffness reduction factor and M_a/M_{cr} shows that the SRC beam has a smaller

stiffness reduction factor than the BRC beam in the non-linear phase. However, the SRC beam shows a collapse at the moment of inertia of the effective cross-section $(I_e)_c$ which is relatively still large when compared to BRC beams. BRC beams collapse at the effective cross-section inertia of about 5%, and SRC beams collapse at the effective section inertia of about 40%. The alternative of moments of inertia from various sources is shown in Table 9.

$$\phi_K = 0.646 - 0.1023\left(\frac{M_a}{M_{cr}}\right) \quad (5)$$

$$\frac{I_e}{I_g} = 0.646 - 0.1023\left(\frac{M_a}{M_{cr}}\right) \quad (6)$$

$$\phi_K = 0.697 - 0.1472\left(\frac{M_a}{M_{cr}}\right) \quad (7)$$

$$\frac{I_e}{I_g} = 0.697 - 0.1472\left(\frac{M_a}{M_{cr}}\right) \quad (8)$$

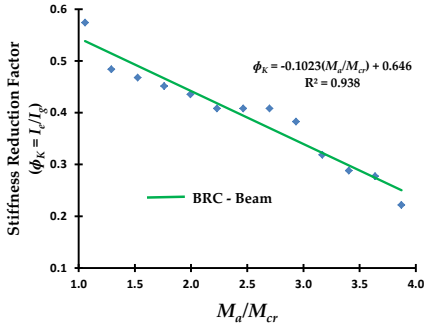

Figure 25. The relationship of the stiffness reduction factor (ϕ_K) and the M_a/M_{cr} of the BRC beam.

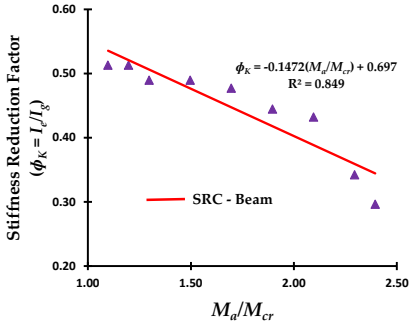

Figure 26. The relationship of the stiffness reduction factor (ϕ_K) and the M_a/M_{cr} of the SRC beam.

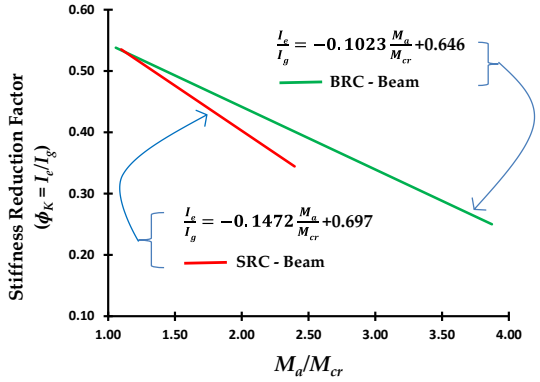

Figure 27. Comparison of the relationship of the stiffness reduction factor (ϕ_K) and the M_a/M_{cr} of the BRC beam and SRC beam.

Table 9. The alternative value of *I* for elastic analysis from various sources.

Source and Information	Alternative value of *I* for elastic analysis
ACI-318M-14 [5]	$0.25I_g$—$0.5I_g$
FEMA 356-2000 [46]	$0.5\ EI_g$—$0.8EI_g$
New Zealand Code [47]	$0.35I_g$
Paulay and Priestley, 1992 [48]	$0.30I_g$—$0.50I_g$
In this research (singly reinforced beam)	
- BRC Beam	$0.05I_g$—$0.5I_g$
- SRC Beam	$0.4I_g$—$0.75I_g$

5. Conclusions

The relationship pattern of load vs. displacement reflects the stiffness pattern of structural elements. The properties and characteristics of the material in the reinforcing concrete elements have a dominant influence on the relationship pattern of the load vs. displacement of reinforced concrete elements. Bamboo reinforced concrete beams (BRC) have a different load vs. displacement relationship pattern when compared to steel reinforced concrete beams (SRC). BRC beams have elastic properties and high resilience properties that can accept high impact loads without causing over stress at the elastic limit, even though displacement has occurred. While SRC beams have high stiffness and toughness so that SRC beams are not subject to excessive displacement or deformation at service load ranges or elastic conditions.

Results of the validation of the relationship pattern of the load vs. displacement of the BRC beams shows that the ANN model has a higher R^2 value when compared to the R^2 value of the MLR model. ANN analysis has a higher prediction accuracy. The accuracy of the prediction depends very much on the number of input variables, The greater the number of input parameters, the more accurate the prediction model results.

The cross-sectional stiffness of BRC beams is reduced by 50% after initial cracking and reduced by 95% at collapse. The cross-sectional stiffness of the SRC beam was reduced by 25% after initial cracking and reduced by 60% at collapse. The reduction in stiffness is significantly affected by the amount of applied moment (M_a) or the load applied that causeding cracks and a reduction in the moment of inertia of the cross-section.

The initial decrease in cross-sectional stiffness of BRC beams occurs at a load of about 24% of the ultimate load and BRC beams occur at loads of about 40% ultimate load. BRC beam collapse occurs when the moment of inertia of the effective cross-section (I_e) is 5%, while the SRC beam collapse

occurs when the moment of inertia of the effective cross-section (I_e) is 40%. The reduction in stiffness in the cross-section of the beam in the non-linear phase ranged from $0.5I_g$—$0.05I_g$ for BRC beams, and $0.75I_g$—$0.40I_g$ for SRC beams. ACI-318M-14 standard recommends the cross-sectional stiffness of reinforced concrete beams for elastic analysis in the non-linear phase of $0.5I_g$—$0.25I_g$.

The SRC beams have a smaller stiffness reduction factor (ϕ_K) than BRC beams in the non-linear phase. However, the SRC beam shows a collapse at the moment of inertia of the effective cross-section (I_e), which is relatively large when compared to BRC beams.

Author Contributions:

Funding: APC financing entirely by the DPRM Republic of Indonesia and LPPM of the University of Muhammadiyah Jember, Indonesia.

Acknowledgments: My gratitude goes to the LPPM of the Muhammadiyah University of Jember, Indonesia, and DPRM of the Republic of Indonesia as the funder of this research and APC.

Conflicts of Interest: The authors declare no conflicts of interest.

Commented [M17]: For research articles with several authors, a short paragraph specifying their individual contributions must be provided. The following statements should be used "Conceptualization, X.X. and Y.Y.; methodology, X.X.; software, X.X.; validation, X.X., Y.Y. and Z.Z.; formal analysis, X.X.; investigation, X.X.; resources, X.X.; data curation, X.X.; writing—original draft preparation, X.X.; writing—review and editing, X.X.; visualization, X.X.; supervision, X.X.; project administration, X.X.; funding acquisition, Y.Y. All authors have read and agreed to the published version of the manuscript.", please turn to the CRediT taxonomy for the term explanation. Authorship must be limited to those who have contributed substantially to the work reported.

References

1. Pandey, K.K.; Ramakantha, V.; Chauhan, S.S.; Kumar, A.A. Wood is Good; Springer: Singapore, **2017**
2. Mohammadabadi, M.; Jarvis, J.; Yadama, V.; Cofer, W. Predictive Models for Elastic Bending Behavior of a Wood Composite Sandwich Panel. *Forests*. **2020**, 11, 624.
3. Ministry of Environment and Forestry of the Republic of Indonesia. Memanfaatkan Bambu sebagai Salah Satu Potensi Hutan Rakyat. 18 October **2018.**

Available online: https://www.menlhk.go.id/site/single_post/1444 (accessed on 24 October 2020).

4. Han, S. W.; Park, Y. M.; Kee, S. H. Stiffness Reduction Factor for Flat Slab Structures under Lateral Loads. *Journal Of Structural Engineering*. **2009**, 135, 6, 743.
5. ACI Committee 318 Standard. Building Code Requirements for Structural Concrete. **2014**.
6. Muhtar; Gunasti, A.; Dewi, I.C.; *et al*. The Prediction of Stiffness of Bamboo-Reinforced Concrete Beams Using Experiment Data and Artificial Neural Networks (ANNs). *Crystals*. ***2020***, 10, 757.
7. Muhtar, S. M. Dewi, Wisnumurti, and A. Munawir. Enhancing bamboo reinforcement using a hose-clamp to increase bond-stress and slip resistance. *Journal of Building Engineering*. **2019**, 26, 100896.
8. Muhtar; Dewi, S.M.; Wisnumurti; Munawir, A. The flexural behavior model of bamboo reinforced concrete beams using a hose clamp. *Proc. Mater. Sci. Eng. Chem*. **2019**, 1033.
9. Zhang, K.; Zhang, J.; et al. Stiffness degradation for the fatigue of reinforced concrete beams after electrochemical rehabilitation. *Construction and Building Materials*. 2020, 260, 120455.
10. Salam, A. S. A.; Debra, L. F. Use of negative stiffness in failure analysis of concrete beams. *Engineering Structures*. 2016, 126, 187–199.
11. Hu, H.S.; Nie, J. G.; and Wang, Y.H. Effective stiffness of rectangular concrete-filled steel tubular members Hong-Song. *Journal of Constructional Steel Research*. 2016, 116, 233–246.
12. Patel, K. A.; Bhardwaj, A.; Chaudhary, S.; Nagpal, A. Explicit expression for effective moment of inertia of RC beams. *Latin American Journal of Solids and Structures*. 2015, 12, 542–560.
13. Fu, C.; Wang, Y.; Tong, D. Stiffness Estimation of Cracked Beams Based on Nonlinear Stress Distributions Near the Crack. *Mathematical Problems in Engineering*. **2018**, 2018, 12 pages.
14. Pique, J. R.; Burgos, M. Effective Rigidity of Reinforced Concrete Elements in Seismic Analysis and Design. *The 14 World Conference on Earthquake Engineering*, Beijing, China, October 12-17, **2008**.
15. Akmaluddin; Pathurahman. Effective Moment of Inertia Approach for Predicting Displacement of Concrete Beams Reinforced with Twisted Bamboo Cables. *International Journal of Civil & Environmental Engineering IJCEE-IJENS*. **2012**, 12, 6–13.

16. Kalkan, İ. Displacement Prediction for Reinforced Concrete Beams Through Different Effective Moment of Inertia Expressions. *International Journal of Engineering Research and Development*. **2013**, 5, 1.
17. Fu, C.; Tong, D.; Wang, Y. Assessing the Instantaneous Stiffness of Cracked Reinforced Concrete Beams Based on a Gradual Change in Strain Distributions. *Advances in Materials Science and Engineering*. 2020, 2020, 10 pages.
18. Feng, X.; Shen, M.; Sun, C.; Chen, J.; Luo, P. Research on flexural stiffness reduction factor of the reinforced concrete column with equiaxial shaped section," in *13th COTA International Conference of Transportation Professionals (CICTP 2013)*, **2013**, 168–174.
19. Muhtar, S. M. Dewi, Wisnumurti, and A. Munawir. The stiffness and cracked pattern of bamboo reinforced concrete beams using a hose clamp. *International Journal of Civil Engineering and Technology*. **2018**, 9, 273–284.
20. Agarwal, A.; Nanda, B.; Maity, D. Experimental investigation on chemically treated bamboo reinforced concrete beams and columns. *Construction and Building Materials*. **2014**, 71, 610–617.
21. Muhtar. Experimental data from strengthening bamboo reinforcement using adhesives and hose-clamps. *Data in brief*. **2019**, 27, 104827.
22. Rahman, M. M.; Rashid, M. H.; Hossain, M. A.; Hasan, M. T.; Hasan, M. K. Performance evaluation of bamboo reinforced concrete beam. *International Journal of Engineering & Technology IJET-IJENS*. **2011**, 11, 113–118.
23. Muhtar. Precast Bridges of Bamboo Reinforced Concrete in Disadvantaged Village Areas in Indonesia. *Applied Sciences*. **2020**, 10, 7158.
24. Ghavami, K. Bamboo as reinforcement in structural concrete elements. *Cement and Concrete Composites*. **2005**, 27, 637–649.
25. Javadian, A.; Wielopolski, M.; Smith, I. F. C.; Hebel, D. E. Bond-behavior study of newly developed bamboo-composite reinforcement in concrete. *Construction and Building Materials*. **2016**, 122, 110–117.
26. Muhtar, Dewi, S. M.; Wisnumurti; Munawir, A. Bond-slip improvement of bamboo reinforcement in the concrete beam using hose clamps. *Proceedings The 2nd International Multidisciplinary Conference.* Jakarta, Indonesia, 15 November **2016**, 385–393.
27. Muhtar, Gunasti, A.; Manggala, A. S.; Nusant, A. F. P.; Hanafi; Nilogiri, A. Effect of Reinforcement Details on Precast Bridge Frames of Bamboo Reinforced Concrete to Load Capacity and Crack Patterns. *International Journal of Engineering Research and Technology*. **2020**, 13, 631–636.
28. Muhtar. Cracked Pattern of Bamboo Reinforced Concrete Beams Using Double Reinforcement with the Strengthening on Tensile Reinforcement. *International Journal of Engineering Research and Technology*. 2020, 13, 608–612.
29. ASTM C 39 Standard. *Standard Test Method for Compressive Strength of Cylindrical Concrete Specimens*. 2003. West Conshohocken.
30. PT SIKA Indonesia. Sikadur®-752. 02, 2-3. **2016**. Available online: https://www.scribd.com/document/374071630/Sikadur-752 (accessed on 24 October 2020).
31. ASTM C 09 Standard, *Standard Test Method for Flexural Strength of Concrete (Using Simple Beam with Third-Point Loading)*. **2002**. West Conshohocken.
32. Muhtar. Numerical validation data of tensile stress zones and crack zones in bamboo reinforced concrete beams using the Fortran PowerStation 4.0 program. *Data in Brief*. **2020**, 29, 105332.
33. Avram, C.; Facaoaru, I.; Filimon, I.; Mirsu, O.; Tertea, I. *Concrete strength and strain*. Developments in Civil Engineering 3, **1981**.

34. Naderpour, H.; Kheyroddin, A.; Amiri, G. G. Prediction of FRP-confined compressive strength of concrete using artificial neural networks. *Composite Structures*. **2010**, 92, 2817–2829.
35. Ahmadi, M.; Naderpour, H.; Kheyroddin, A. Utilization of artificial neural networks to prediction of the capacity of CCFT short columns subject to short term axial load. *Archives of Civil and Mechanical Engineering*. **2014**, 14, 510–517.
36. Khademi, F.; Akbari, M.; Nikoo, M. Displacement determination of concrete reinforcement building using data-driven models. *International Journal of Sustainable Built Environment*. **2017**, 6, 400–411.
37. Kaczmarek, M.; Szymanska, A. Application of Artificial Neural Networks to Predict The Displacements of Reinforced Concrete Beams. *Studia Geotechnica et Mechanica*. **2016**, 38, 37–46.
38. Abd, A. M.; Salman, W. D.; Ahmed, Q. W. ANN, and Statistical Modelling to Predict The Displacement of Continuous Reinforced Concrete. *Diyala Journal of Engineering Sciences*. **2015**, 134–143.
39. Ya Tuan, T. M. Y. S.; Alebrahim, R.; Fitri, N.; Alebrahim. M. Analysis of Cantilever Beam Displacement under Uniformly Distributed Load using Artificial Neural Networks. *MATEC Web of Conferences*, Louisiana, USA. February 3-4, **2018**.
40. Khademi, F.; Akbari, M.; Mohammadmehdi, S.; Nikoo, M. Multiple linear regression, artificial neural network, and fuzzy logic prediction of 28 days compressive strength of concrete. *Frontiers of Structural and Civil Engineering*. **2017**, 1190–99.
41. Li, X.; Liu, Y.; Akbari, M.; Wang, C.; Bond, P. L.; et al. Evaluation of data-driven models for predicting the service life of concrete sewer pipes subjected to corrosion. *Journal of Environmental Management*. **2019**, 234, 431–439.
42. Dewi, S. M.; Nuralinah, D. The Recent Research on Bamboo Reinforced Concrete. in *MATEC Web of Conferences*, **2017**, 103, 2001.
43. Nathan, S. Application of Bamboo for Flexural and Shear Reinforcement in Concrete Beams. Clemson University, **2014.**
44. Khare, L. Performance Evaluation of Bamboo Reinforced Concrete Beams. **2005.**
45. Mishra, M.; Agarwal, A.; Maity, D. Neural-network-based approach to predict the displacement of plain, steel-reinforced, and bamboo-reinforced concrete beams from experimental data. *SN Applied Sciences*. **2019**, 1, 584.
46. FEMA 356 Standard. Prestandard and commentary for the seismic rehabilitation of buildings. November **2000**.
47. New Zealand Standard. *Code of practice for the design of concrete structures*, Part 1, Wellington, New Zealand, **1995**.
48. Paulay, T.; Priestley, M. J. N. Seismic Design of Reinforced Concrete and Masonry Buildings. Wiley Interscience. **1992**.

Publisher's Note: MDPI stays neutral with regard to jurisdictional claims in published maps and institutional affiliations.

© 2020 by the authors. Submitted for possible open access publication under the terms and conditions of the Creative Commons Attribution (CC BY) license (http://creativecommons.org/licenses/by/4.0/).

forests

MDPI

Article

The Prediction of Stiffness Reduction Non-linear Phase in Bamboo Reinforced Concrete Beam Using The Finite Element Method (FEM) and Artificial Neural Networks (ANNs)

Muhtar

Faculty of Engineering, University of Muhammadiyah Jember, Jember 68121, Indonesia; muhtar@unmuhjember.ac.id

Received: date; Accepted: date; Published: date

Abstract: This paper discusses the reduction of the stiffness of bamboo reinforced concrete (BRC) beams to support the use of bamboo as an environmentally friendly building material. Calculation of cross-section stiffness in numerical analysis is very important, especially in the non-linear phase. After the initial crack occurs, the stiffness of the cross-section will decrease with increasing load and crack propagation. The calculation of the stiffness in the cross-section of the concrete beam in the non-linear phase is usually approximated by giving a reduction in stiffness. ACI 318-14 provides an alternative, reducing the stiffness of the plastic post-linear beam section through the moment of inertia (I) of the beam section for elastic analysis between $0.50I_g$–$0.25I_g$. This study aims to predict the value of the reduction in the stiffness of the BRC beam section in the non-linear phase through the load-displacement relationship of experimental results validated by the Finite Element Method (FEM) and the Artificial Neural Networks (ANN) method. The experiment used 8 BRC beams and one steel-reinforced concrete (SRC) beam of singly reinforced with a size of 75 mm × 150 mm × 1100 mm. The beams were tested using a four-point loading method. The analysis results showed that the value of the stiffness reduction in the beam cross-sectional in the non-linear phase ranged from $0.5I_g$–$0.05I_g$ for BRC beams, and $0.75I_g$–$0.40I_g$ for SRC beams.

Keywords: stiffness reduction; bamboo reinforced concrete (BRC); finite element method (FEM); artificial neural networks (ANN)

1. Introduction

The impact of increasing industrial development is that it can cause pollution of air, water, soil, and noise. The use of industrial building materials such as ceramics, steel, concrete, and other materials has led to an increase in environmental pollution. The procurement of wood forests or bamboo forests must be done as a counterweight to environmental pollution. Pandey et al. (2017) [1] and Mostafa et al. (2020) [2] revealed that an average tree absorbs one ton of CO_2 and produces 0.7 tons of O_2 for every cubic meter of growth. The use of environmentally friendly building materials such as wood and bamboo must be done. Bamboo is a forest product that provides high economic and ecological value to the community. Bamboo also has enormous potential with promising prospects [3]. Bamboo is one of the commodities produced by Community Forests. However, research on the behavior of bamboo as a building material is mandatory, such as research on the stiffness of bamboo reinforced concrete (BRC) beams.

The stiffness reduction factor is a multiplier to reduce the moment of inertia in gross cross-sectional, and the gross cross-sectional area remains constant. These factors are conservatively

Comment [M1]: This author is different from you register in our system. Shall we change to Muhtar Muhtar? Please confirm.

Comment [M2]: Is this necessary? Can this be deleted? (We will add the link later)

Comment [M3]: Please carefully check the accuracy of names, emails and affiliations.

Comment [M4]: Please check if this should be en dash. We changed all the hyphen to en-dash. Please confirm.

Comment [M5]: We changed it to multiplication sign, please confirm.

Comment [M6]: Is the italics necessary?

enforced by various concrete standards to account for the loss of stiffness in the concrete cross-section due to the cracking of the concrete. The stiffness of the beam cross-section in the elastic phase or linear phase indicates the full section flexural stiffness, E_cI_g, whereas in the non-linear phase or after the initial crack, the gross cross-section bending stiffness is reduced to the effective flexural stiffness, E_cI_{eff}. The stiffness reduction factor is significantly influenced by the amount of moment or the applied load, while the stiffness reduction factor does not differ from the amount of reinforcement [4]. ACI 318M-14 [5] shows that the gross section flexural stiffness, E_cI_g, is reduced to obtain the effective flexural stiffness, E_cI_e, which causes cracking and other softening effects. As the moment in the concrete section increases, the flexural stiffness will be reduced due to the cracks that continue to propagate and spread. ACI 318M-14 [5] provides stiffness reduction limits for elastic analysis with a moment of inertia limits between $0.25I_g$–$0.5I_g$ for concrete beams. The equation for the moment of inertia effective (I_e) is determined in ACI 318-05 [5] Section 9.5.2.3, as shown in Equation (1).

Comment [M7]: There is no Section 9.5.2.3, please confirm if it refers to this article.

$$I_e = \left(\frac{M_{cr}}{M_a}\right)^3 I_g + \left[1 - \left(\frac{M_{cr}}{M_a}\right)^3\right] I_{cr} \quad (1)$$

where I_g = moment of inertia of the gross concrete section and I_{cr} = moment of inertia of the crack section including the reinforcement. The moment of inertial effective (I_e) as shown in Equation (1) will decrease as the moment that occurs, M_a. Calculation of the moment of inertia of the crack cross-section, I_{cr} at Equation (1) must pay attention to the number of reinforcement installed. However, the amount of reinforcement is not determined at the initial design stage.

The process of stiffness reduction in the beam section starts from the "*no crack*" and "*cracked*" conditions in the section. In the service load condition or the elastic condition, the stiffness of the beam section is in full condition, even though the moment due to the load continues to increase. In the elastic condition, the moment that occurs (M_a) is still below the moment of cracking (M_{cr}), or the tensile stress of the concrete is still below the modulus of rupture of the concrete beam cross-section, f_r. In the elastic conditions, the difference in stiffness between two different types of beams usually occurs not due to reduced inertia of the cross-section, but due to the properties of the materials used. For example, the stiffness of bamboo reinforced concrete beams is different from the stiffness of steel-reinforced concrete (SRC) beams. In the elastic conditions, the stiffness of BRC beams is lower than the stiffness of SRC beams [6–8]. This is because BRC beams use bamboo reinforcing materials which have elastic properties and high resilience properties. BRC beams with bamboo reinforcement will be able to accept high impact loads without causing stress over the elastic limit, even though displacement has occurred. This indicates that the energy absorbed during loading is stored and released if the material is not loaded.

Meanwhile, the SRC beam uses steel material that has high stiffness and toughness, so that the SRC beam in the service load range or elastic condition does not experience displacement or excessive deformation. Beams that use materials with high stiffness and toughness will be able to withstand high impact loads or shock loads. If the SRC beam gets an impact load, then some of the energy is absorbed and some of the energy is transferred.

Research on modeling and stiffness reduction has been carried out by many researchers. Kai Zhang et al. (2020) [9] investigated the effect of electrochemical rehabilitation (ER) techniques on the fatigue stiffness of RC beams. The results of his research indicated that electrochemical rehabilitation (ER) exacerbated bond breakage, thereby reducing the flexural stiffness of RC beams. Salam Al-Sabah et al. [10] discuss the use of negative stiffness in the failure analysis of concrete beams. In his research, Salman Al-Sabah et al. concluded that the effective and simple one-dimensional stress-strain behavior of concrete was used to study concrete blocks with proportional loading, the only source of non-linearity to consider cracks in concrete. Hong-Song Hu et al. (2016) [11] investigated the effectiveness of square CFST rod stiffness, and the results proposed an equation for the effective stiffness of square CFST rods. Muhtar et al. [7] tested the flexural of BRC beams and SRC beams, the results showed that the stiffness decreased after the initial cracking. The average stiffness of the BRC beam decreased from 26,324.76 MPa before cracking to 6581.20 MPa after

Comment [CH8]: Please define, if appropriate.

collapse [7], while the average value of SRC beam stiffness decreased from 30,334.11 MPa before cracking to 16873.35 MPa after the collapse.

K.A. Patela et al. (2014) [12], in their paper, provide an explicit expression for the effective moment of inertia by considering cracks for reinforced concrete beams (RC) with uniformly distributed loads. The proposed explicit expressions can be used to predict short-run displacement in-service load. The sensitivity analysis shows a substantial dependence of the effective moment of inertia on the selected input parameter. Displacement is an important parameter for examining the serviceability criteria of structures. The short-term displacement is generally calculated using the effective moment of inertia across the span at the service load [12]. Chunyu Fu (2018) [13] presents a method of estimating the stiffness of cracked beams based on the stress distribution. In his conclusion, he said that the presence of cracks causes a nonlinear stress distribution along the beam section, which changes the neutral axis of the cross-section and further affects the stiffness of the beam. J.R. Pique (2008) [14] concluded that when the design is controlled by the minimum reinforcement, especially in the beam, special attention should be paid to the calculation of the real period and maximum distortion. The effective stiffness of the beam with the minimum steel ratio is much lower than that obtained by the proposed reduction factor. As a result, the actual period and actual maximum distortion can be greater. Akmaluddin et al. (2012) [15] concluded that the moment of crack and the value of the moment of inertia of the crack was significantly affected by the presence of bamboo reinforcement in the beam. The experimental results show that the crack moment varies from 0.3 to 0.7 from the ultimate moment. The experimental and theoretical crack moment ratio varies from 0.90 to 1.42. İlker Kalkan (2013) and [16] concluded that the effective moment of inertia and load-displacement curve analysis is highly dependent on the crack moment used in the expression analysis of the effective moment of inertia. Therefore, the experimental cracking moment of the beam should be used in the calculation of the effective moment of inertia for a more accurate comparison of the different analytical methods. Chunyu Fu et al. (2020) [17] concluded that cracking of concrete causes a gradual change in the distribution of strain along with the cross-sectional height of reinforced concrete beams, which in turn affects the instantaneous stiffness. The instantaneous stiffness proved to be highly dependent on the number and depth of cracks. This dependence can be accurately reflected by the method proposed by simulating a gradual change in the concrete strain distribution. Xiuling Feng et al. (2013) [18] examines the reduction factor of flexural stiffness in reinforced concrete columns with an equiaxial cross-section and suggests that the reduction factor is proposed by considering the nonlinear characteristics of the material and its geometric nonlinearity.

The difference in the nonlinear characteristics of the material used in the BRC beam and the SRC beam greatly determines the flexural behavior of the beam. Bamboo reinforced concrete beams have low stiffness and tend to be large displacement. The solution to increasing the stiffness of BRC beams is to use shear reinforcement and the principle of confined concrete [7,19]. In the linear elastic condition, the BRC beam has shown a large displacement, but when the ultimate load is reached and the loading is released gradually, the displacement tends to return to zero. In this study, the reduction of stiffness in the non-linear phase was analyzed through the load vs. displacements that were validated using the finite element method (FEM) and the Artificial Neural Networks (ANN) method. It is suspected that the reduction of the cross-sectional stiffness of the BRC beam is different from the reduction in the stiffness of the SRC beam section. The parameter of the moment of inertia of the cross-section becomes a benchmark in determining the reduction of stiffness according to ACI-318M-14 [5].

2. Materials and Methods

2.1. Treatment of Materials

In this study, the treatment of bamboo material as concrete reinforcement is an important thing to do. The bamboo used is the bamboo "petung" (*Dendrocalamus asper*) which is between three and five years old [20–22]. The part of bamboo that is used as reinforcing of concrete is 6–7 m long from the base of the bamboo stem [23]. Bamboo is cut according to the size of the bamboo reinforcement to

be used, which is 15 x 15 mm². Then, bamboo is soaked for ±20–30 days [21]. After soaking, bamboo is dried in free air until it has an absorption level of ± 12%.

Application of adhesive or waterproof coating [24,25] is done after the bamboo reinforcement is cleaned and trimmed according to the planned size. The application of a waterproof layer is carried out to prevent the hydrolysis process between bamboo and concrete. Sand sprinkling on bamboo reinforcement is done when the adhesive is half dry to make it stronger [21,26]. The application of sand aims to increase the adhesion strength of bamboo reinforcement to concrete.

An installation of a hose-clamp at both ends of the bamboo reinforcement is done to match the concept of hooks or bends in steel reinforcement. An installation of the hose-clamp only on tensile reinforcement is done to increase bond-stress between bamboo reinforcement and concrete [27,28]. The tensile force on the bamboo reinforcement will be distributed to the concrete through the hose-clamp, which functions as a shear connector. Bamboo treatment is shown in Figure 1.

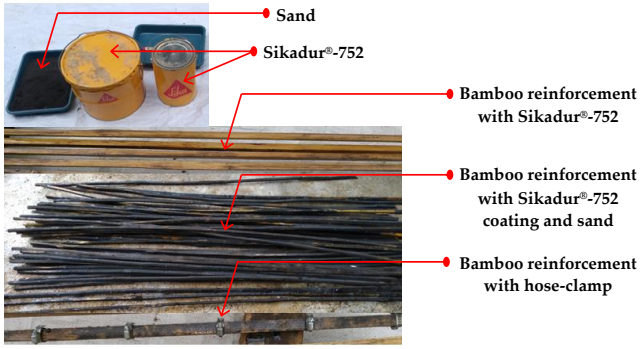

Figure 1. The materials and treatments of bamboo reinforcement.

2.2. Materials

The concrete mixture used in this study is a normal concrete mixture consisting of Portland Pozzolana Cement (PPC), sand, coarse aggregate, and water with a proportion of 1:1.8:2.82:0.52. Sand and gravel come from the Jember area of Indonesia. The cylindrical specimen measures 150 mm in diameter and 300 mm in height. The cylindrical specimens were press-tested using a Universal Testing Machine (UTM) with a capacity of 2000 kN after the concrete was 28 days old. The procedure for the cylinder specimen compressive test follows ASTM C 39 [29]. The average compressive strength of cylindrical concrete is 31.31 MPa with an average weight of 125.21 N. The properties and characteristics of the concrete are shown in Table 1.

Table 1. Material properties of reinforcing and concrete.

Bar Type and Concrete	Diameter, d (mm)	Modulus of Elasticity (*E*), (MPa)	Poisson's Ratio (ν)	Tensile Strength, f_y (MPa)	Compressive Strength, f'_c (MPa)
Bamboo	□ 15 × 15	17,235.74	0.20	126.68	-
Steel	ϕ 8	207,735.92	0.25	392.28	-
Concrete	-	26,324.79	0.30	-	31.31

Comment [M9]: Please check it. Can we delete it?

The tensile test of bamboo reinforcement produces the average tensile stress of 126.68 N/mm² with an average strain of 0.0074. The modulus of elasticity of bamboo reinforcement was calculated using the formula $E = \sigma/\varepsilon$ and obtained 17,235.74 MPa. The modulus of elasticity of steel is obtained

by 207,735.92 MPa. The properties and characteristics of bamboo and steel reinforcement are shown in Table 1.

The adhesive layer or waterproof coating used was Sikadur®-752 produced by PT. SIKA Indonesia [30]. The specifications for the adhesive sikadur®-752 are shown in Table 2. Installation of hose-clamp on bamboo reinforcement is done when the waterproof layer is half dry [21]. The diameter of the hose-clamp used is ¾″ made in Taiwan.

Table 2. The specification of Sikadur®-752 [30].

Components	Properties
Color	Yellowish
Density	Approx. 1.08 kg/L
Mix comparison (weight/volume)	2:1
Pot life at +30 °C	35 min
Compressive strength	62 MPa at 7 days (ASTM D-695) 64 MPa at 28 days
Tensile strength	40 MPa at 28 days (ASTM D-790)
Tensile Adhesion Strength	2 MPa (Concrete failure, over mechanically prepared concrete surface)
Coefficient of Thermal Expansion	−20 °C to + 40 °C 89 × 10^{-6} per °C
Modulus of elasticity	1060 MPa

Comment [M10]: We changed to it, please confirm if it is correct.

2.3 Experimental Procedure

The test object consisted of 9 beams with a size of 75 mm × 150 mm × 1100 mm, consisting of 8 bamboo reinforced concrete beams (BRC) and one steel-reinforced concrete beam (SRC). Bamboo reinforcement is installed as tensile reinforcement with a reinforcement area of 450 mm². The steel reinforcement used has a diameter of 8 mm with an area of A_s = 100.48 mm². The beam geometry and reinforcement detail of the BRC and SRC beams are shown in Figure 2.

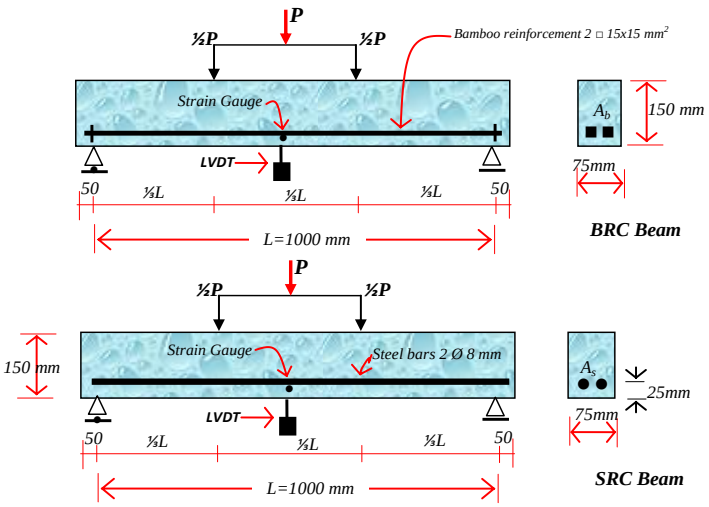

Figure 2. Reinforcement details and beam test settings.

The beam flexural test method was carried out using the four-point method [31]. The test arrangement and load position are shown in Figure 2. Strain gauges are installed on the bamboo

reinforcement at a distance of ½L from the support of the beam. Beam displacement measures use Linear Variable Displacement Transducers (LVDT) with a distance of ½L from the beam support.

The loading stages from zero to the collapse of the beam are used as a hydraulic jack and a load cell connected to a load indicator tool. The load reading on the load indicator is used as a hydraulic jack pump controller, displacement reading, and strain reading according to the planned loading stage. However, when the test object reaches its ultimate load, the displacement reading controls the strain and load reading, while the pumping of the hydraulic jack continues slowly according to the command of the displacement reader. The failure pattern was observed and identified by the cracks that occurred, from the time of the initial crack until the beam collapsed.

2.4. Validation of Numerical Methods

Validation of experimental data was found by using the Finite Element Method (FEM) and Artificial Neural Networks (ANN). The relationship between load vs. displacement experiment results was validated by using the finite element method. The procedure used is inputting material data and loading stages to determine the behavior of the load vs. displacement of BRC beams and SRC beams. The data input for the loading stages is carried out following the loading stages from laboratory experimental data. The numerical method used is the finite element method, using the Fortran PowerStation 4.0 program [32]. The theoretical analysis is used to calculate the load causing the initial crack using elastic theory (*linear analysis*) with cross-section transformation. For linear analysis, the input material data is the modulus of elasticity (E) and Poisson's ratio (υ). The calculation of the modulus of elasticity of the composites (E_{comp}) is shown in Tables 3 and 4. The non-linear phase is approximated by decreasing the concrete strength from 0.25 to 0.5 for the calculation of the effective stiffness in the plastic plane [5]. In the analysis of the finite element constitutive relationship, the problem-solving method uses the plane-stress theory. Triangular elements are used to model plane-stress elements with a bidirectional primary displacement at each point so that the element has six degrees of freedom. The discretization of the beam plane is carried out using the triangular elements shown in Figure 3 for BRC beams and Figure 4 for SRC beams.

Comment [CH11]: Please check that intended meaning is retained.

Comment [CH12]: Please check that intended meaning is retained.

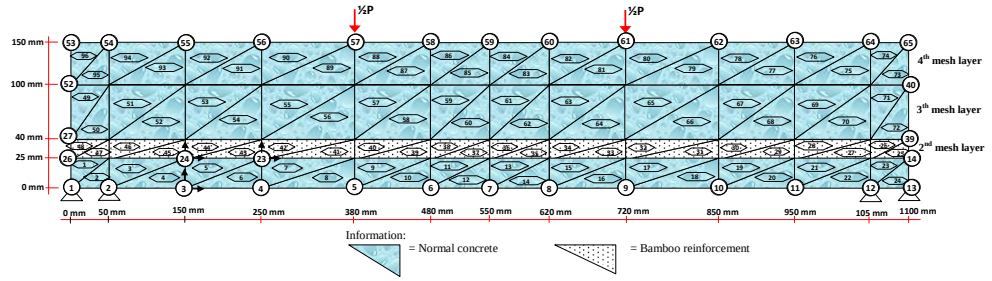

Figure 3. Discretization of the triangular element on the bamboo reinforced concrete (BRC) beam.

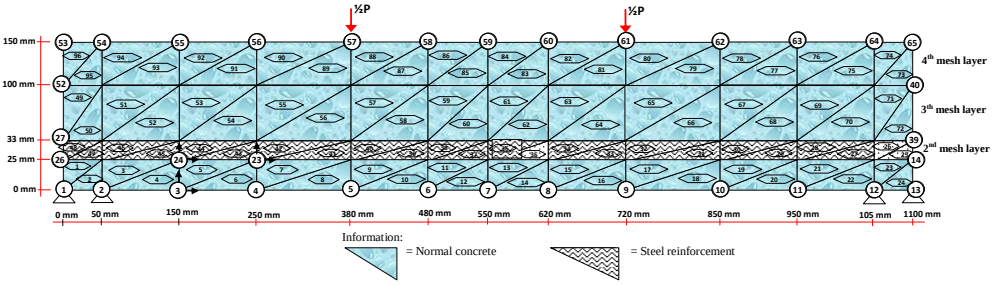

Figure 4. Discretization of the triangular element on the steel-reinforced concrete (SRC) beam.

Table 3. Elasticity Modulus of Composite of BRC beam.

Layer Number	Compressive Strength of Concrete, f'_c	Dimensions of per Layer		Modulus of Elasticity of the Material (E)		Elasticity Modulus of Composite (E_{comp})
	Mpa	b (mm)	h (mm)	Concrete, E_c (MPa)	Bamboo, E_b (MPa)	MPa
4th mesh layer	31.31	75	50	26,851.29	0	26,851.29
3rd mesh layer	31.31	75	60	26,851.29	0	26,851.29
2nd mesh layer	31.31	75	15	26,851.29	1723.57	23,140.89
1st mesh layer	31.31	75	25	26,851.29	0	26,851.29

Table 4. Elasticity Modulus of Composite of SRC beam

Layer Number	Compressive Strength of Concrete, f'_c	Dimensions of per Layer		Modulus of Elasticity of the Material (E)		Elasticity Modulus of Composite (E_{comp})
	Mpa	b (mm)	h (mm)	Concrete, E_c (MPa)	Steel, E_s (MPa)	MPa
4th mesh layer	31.31	5	50	26,851.29	0	26,851.29
3rd mesh layer	31.31	75	67	26,851.29	0	26,851.29
2nd mesh layer	31.31	75	8	26,851.29	207,735.92	43,209.32
1st mesh layer	31.31	75	25	26,851.29	0	26,851.29

The modulus of elasticity (E) for each layer is calculated according to the condition of the material. Layers of concrete and bamboo reinforcement are calculated using the following Equation. (2) [33].

$$E_e = E_b.V_b + E_c.V_c \quad (2)$$

where E_e = the equivalent elasticity modulus of BRC beam, E_b = elastic modulus of bamboo reinforcement, E_c = modulus of elasticity of concrete, V_b = relative volume of bamboo reinforcement in calculated layers, and V_c = relative volume of concrete in calculated layers. The stress-strain relationship for plane-stress problems has the shape of an equation such as Equation (3).

$$\begin{Bmatrix} \sigma_x \\ \sigma_y \\ \tau_{xy} \end{Bmatrix} = \frac{E}{(1+\nu^2)} \begin{bmatrix} 1 & \nu & 0 \\ \nu & 1 & 0 \\ 0 & 0 & \frac{1-\nu}{2} \end{bmatrix} \begin{Bmatrix} \varepsilon_x \\ \varepsilon_y \\ \gamma_{xy} \end{Bmatrix} \quad (3)$$

where E is the modulus of elasticity and ν is the Poisson's ratio. And the principal stresses in two dimensions are calculated by Equation (4).

$$\sigma_{1,2} = \frac{\sigma_x + \sigma_y}{2} \pm \sqrt{\left(\frac{\sigma_x - \sigma_y}{2}\right)^2 + {\tau_{xy}}^2} = \sigma_{\max} \quad (4)$$

The simulation and steps for preparing a FEM analysis with the Fortran PowerStation 4.0 program [32] are summarized as follows:

Step 1: Discretization of BRC and SRC beam planes with the discretization of triangular elements, the numbering of triangular elements, and the numbering of nodal points as shown in Figures 3(d) and Figure 4.

Step 2: Calculation and collection of geometry and material data, such as the modulus of elasticity of the material (E), Poisson's ratio (ν), etc.

Step 3: Writing a programming language for triangular elements using the Fortran PowerStation 4.0 program according to the constitutive relationships and FEM modeling as shown in the following link: http://bit.ly/2F17w8F.
Step 4: Open the Fortran PowerStation 4.0 program. An example is shown at the following link: http://bit.ly/2MTh22j.
Step 5: Write programming language data (Step 3) in the Fortran PowerStation 4.0 program. Examples can be seen at the following link: http://bit.ly/2ZvZWMU.
Step 6: Input DATA.DAT of BRC beam and SRC beam in the Fortran PowerStation 4.0 program. Input data is displayed at the following links: http://bit.ly/351FPqU and http://bit.ly/2MBqas9. An example of displaying input data is shown on the following link: http://bit.ly/2u2K2xR.
Step 7: Analyze the program until there are no warnings and errors. If there are warnings and errors, check and correct program data and input data.
Step 8: Download stress data. The stress data are shown at the following link: http://bit.ly/2rDPeaI for the stress of BRC beam, and http://bit.ly/2Q4Ihc1 for the stress of the SRC beam. An example of displaying stress data from the Fortran PowerStation 4.0 program is shown at the following link: http://bit.ly/2ZybLCd.
Step 9: Download displacement data. An example of displaying data displacement from the Fortran PowerStation 4.0 program is shown on the following link: http://bit.ly/2Q7j2Wp.
Step 10: Enter stress and displacement data into the Surfer program to obtain contour image data of stress and displacement. Stress and displacement contour image data are shown in Figures 15–18.

Comment [M13]: Figures should be cited in numerical order.

2.4. Validation of Artificial Neural Networks (ANN)

Artificial Neural Networks (ANN) is a computational system for solving complex problems in civil engineering. In this study, the validation carried out by the Artificial Neural Networks (ANN) method is the validation of the load vs. displacements from laboratory experimental results. The data on the loading and displacement stages of the experimental results were used as input data and target data in this analysis. Previous researchers concluded that Artificial Neural Networks (ANN) can be an alternative in calculating displacement in reinforced concrete beams. Several researchers have used the ANN method for many structural engineering studies, such as predicting the compressive strength of concrete [34], axial strength of composite columns [35], and determination of RC building displacement [36]. Kaczmarek and Szymańska (2016) [37] concluded that the results of calculating displacement in reinforced concrete using ANN proved to be very effective. Abd et al. (2015) [38] concluded that the ANN method is also very good for predicting displacement in concrete beams with a very strong correlation level of 97.27% to the test data. Tuan Ya et al. (2019) [39] used the ANN method to predict displacement in cantilever beams and concluded that the output was very accurate.

The ANN method is currently very popular with researchers in predicting and evaluating the behavior of structures in the field of civil engineering. This is because the ANN method has an advantage in the nonlinear correlation between the input variables presented. Khademi et al. (2017) [40] predicts the compressive strength of concrete at 28 days of age by considering the experimental results, three different models of multiple linear regression (MLR), artificial neural networks (ANN), and adaptive neuro-fuzzy inference system (ANFIS). The results of his research concluded that the ANN and ANFIS models can predict the 28-day concrete compressive strength more accurately and the ANN model can perform better than the ANFIS model in terms of R^2. The ANN and ANFIS models are preferred because the nonlinear correlation between the input variables presented is better. The ANN and ANFIS models have higher accuracy requirements than the multiple linear regression (MLR) model. The accuracy of the prediction is very much dependent on the number of input variables. The greater the number of input parameters, the more accurate the results of the predictor model will be.

Xuan Li et al. (2019) [41] predict the service life of corroded concrete sewer pipes using three data-driven models, namely multiple linear regression (MLR), artificial neural networks (ANN), and adaptive neuro-fuzzy inference system (ANFIS). The one conclusion suggests that the ANN and

ANFIS models perform better than the MLR models for corrosion prediction, with or without considering the interactions between environmental factors.

The ANN data is divided into three different subsets [40], namely (1) Training: at this stage, the subset is trained and studied as occurs in the human brain, where the number of epochs is repeated until an acceptable model accuracy is obtained; (2) Validation: at this stage, the subset shows how well the model is trained, and estimates model properties such as misclassification, mean error for numerical predictors; and (3) Test: at this stage, the subset verifies the performance of the training subset built into the ANN model.

This paper uses even load input data, while the target data is the displacement of the laboratory test results. The distribution of the ANN model data composition consists of training 70%, validation 15%, and testing 15%. ANN architecture on a rectangular beam is shown in Figure 5. The process of implementing input data in the ANN model architecture consists of (1) Input layer, consisting of 1 neuron, namely displacement data variable of experimental results; (2) Hidden layer, consisting of 10 neurons. At this stage, the input layer will forward the data to the hidden layer or the output layer through a set of weights. This weight is a link from each neuron to other neurons in the next layer which will help adjust the ANN structure to the given displacement data pattern using learning. In the learning process, the weights will be updated continuously until one of the numbers of iterations, errors, and processing time has been reached. This is done to adjust the ANN structure to the desired pattern based on certain problems that will be solved using ANN. Weight is known as the independent parameter. During the training process, the weights will be modified to improve the accuracy of the results. The third layer is (3) Output layer, consisting of 1 neuron which is the expected output target, error, and weight. Error is the error rate of the displacement data node of the process carried out, while weight is the weight of the displacement data node with a value ranging between –1 and 1. Then the displacement data resulting from the training process is processed into a graphic image of the load vs. displacement relationship.

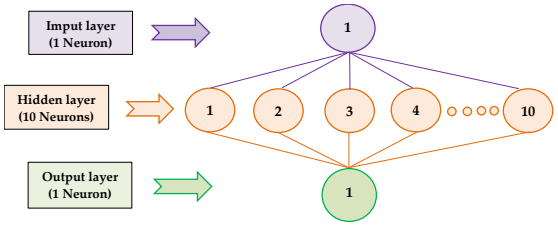

Figure 5. Schematic of Artificial Neural Networks (ANN) model architecture for BRC beam and SRC beam.

3. Results

3.1. Experimental

Table 5 shows the results of theoretical calculations and experiments for BRC and SRC beams. From the theoretical calculation, the BRC beam has an initial crack load of 6.87 kN and an SRC beam of 6.51 kN. The laboratory test results of the BRC beam experienced an initial crack at a load of 7.69 kN and an SRC beam had an initial crack at a load of 10 kN. The average ultimate load of the BRC beam occurs at a load of 31.31 kN or 97.27% of the theoretical collapse load of 32.19 kN. This shows that with the correct treatment of bamboo reinforcement, the BRC beam can reach load capacity according to the results of the theoretical calculations. As is known, the researchers concluded that the ultimate load of BRC beams is very low when compared to the theoretical calculations. Dewi et al. (2017) [42] concluded that the bending capacity of bamboo reinforced concrete beams only reaches 56% of its capacity if the tensile strength of bamboo is full. Nathan (2014) [43] concluded that the flexural capacity of reinforced concrete beams only reaches 29% to 39% of the beam capacity steel-reinforced concrete with the same width and reinforcement dimensions. Khare (2005) [44]

concluded that the flexural capacity of reinforced concrete beams is only 35% of steel-reinforced concrete beams at the same strength level.

SRC beams reach a collapse load of 24 kN or almost approaching the theoretical collapse load of 24.12 kN. This shows that the adhesion strength of steel-reinforcement with concrete is higher. Figures 6 and 7 show that the relationship of the load vs. displacement of the BRC beam and the SRC beam is different. The SRC beam shows the regions of the elastic limit, elastoplastic limit, and plastic limit. Meanwhile, the BRC beam only shows the plastic limit point or the ultimate load point. This shows that the behavior of reinforced concrete beams is very much determined by the properties and characteristics of the materials used.

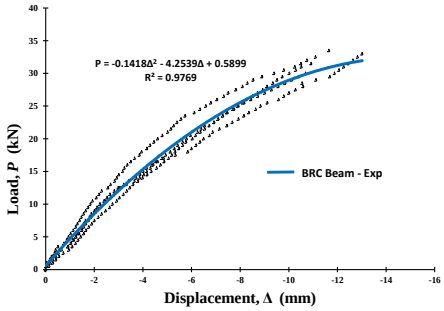

Figure 6. The relationship of load vs. displacement of BRC beam of experimental results.

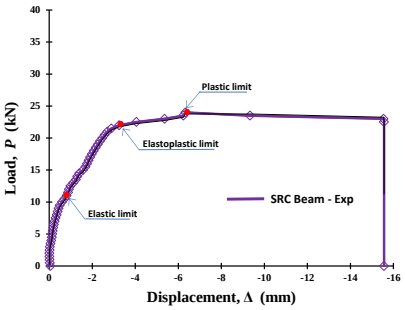

Figure 7. The relationship of load vs. displacement of SRC beam of experimental results.

Mechanical properties and characteristics of steel and bamboo materials are the dominant factors in the behavior model of the load and displacement relationship [6]. The difference between the stress and strain relationship patterns of bamboo and steel is in the position of the melting point and the fracture stress. Steel material shows a clear melting point, while bamboo reinforcement does not show a clear melting point. However, after the fracture stress, the relationship pattern of the stress-strain relationship tends to return to zero. This shows that bamboo has good elastic properties [7].

Table 5. Results of theoretical calculations and experimental for the load capacity of BRC beams and SRC beams.

Specimens	Sample no	Theoretical Calculations		Flexural Test Results			
		First Crack Load (kN)	Ultimate Load (kN)	First Crack Load, P_{cr} (kN)	Failure Load, P_{ult} (kN)	Displacement at Failure (mm)	P_{cr}/P_{ult} (%)
(a) BRC-1	1	6.90	32.20	8.50	31.50	10.92	26.98

	2			8.00	29.00	11.90	27.59
(b) BRC-2	3			7.00	31.00	13.02	22.58
	4			7.50	33.00	12.18	22.73
(c) BRC-3	5			8.00	33.50	14.69	23.88
	6			7.50	33.00	9.32	22.73
(d) BRC-4	7			7.50	29.50	7.61	25.42
	8			7.50	30.00	10.69	25.00
Average:				7.69	31.31		24.61
(e) SRC	9	6.50	24.20	10.00	24.00	6.33	41.57

3.2. Validation with the ANN Method

The load vs. displacement relationship data from the experimental results is the basis used for the train and the network. Neural networks are designed by determining their structure experimentally. The data that trains the artificial neural network is the input, and the ability to reproduce the training pattern is tested. Convergence analysis was carried out to determine the optimal number of neurons in the hidden layer of ANN. Excessive neurons reduce the computational performance of ANN, whereas a lack of neurons causes difficulties in characterizing the input-output relationship. As suggested by Caudill and Mishra et al. (2019) [45], the upper limit of the number of neurons in the hidden layer is twice the number of inputs plus 1. After the number of neurons in the hidden layer is reached, the MSE, RMSE, and R^2 observations are stopped and no increase is assumed significant. The artificial neural network architecture used in this paper: IHO: 1-10-1 [Input-Hidden-Output] means that this artificial neural network consists of 1 input neuron, one hidden layer with 10 neurons, and 1 output neuron (predictive values of the load vs. displacement relationship).

Table 6 presents the performance results of ANN architecture for ten simulations. The process which has the lowest MSE is selected for comparison with experimental data. Figures 8–12 illustrate the prediction of the load vs. displacement of the BRC and SRC beams obtained when using the ANN model after training and when using the data obtained experimentally for training data, validation data, test data, and all data. Figures 8–12 shows the correlation between the value of the BRC beam and the SRC beam relationship obtained in the laboratory and the load vs. displacement values obtained using ANN analysis. The convergence of the position of the point with the line y = x indicates the identification of values with very high accuracy. The correlation value of laboratory data using ANN shows an average value of *R* Square of 0.999. This indicates that the two results are consistent. The prediction results of the ANN method show that the percentage of errors is very small, with a maximum error of 0.26%. Overall, the comparison of experimental data with the predicted results of the ANN method shows an error of not more than 1%. From the data from the two analyses and the load vs. displacement relationship pattern, it can be concluded that the stiffness of the BRC beam has similarities.

Table 6. The validation results of the relationship load vs. displacement using the ANN method.

Specimens	The Correlation Coefficient (*R*)			Mean Square Error (MSE)		
	Training	Validation	Testing	Training	Validation	Testing
BRC-1	1.0000	0.9999	0.9997	0.0004	0.0011	0.0110
BRC-2	0.9999	0.9997	0.9999	0.0038	0.0276	0.0048
BRC-3	0.9998	0.9999	0.9993	0.0034	0.0075	0.0152
BRC-4	1.0000	1.0000	1.0000	0.0001	0.0009	0.0010
SRC	1.0000	1.0000	0.9997	0.0001	0.0027	0.0006

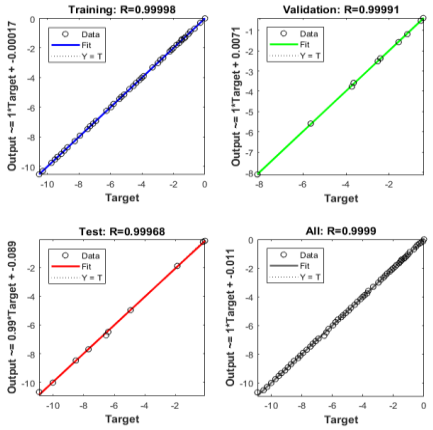

Figure 8. Prediction of the load vs. displacement relationship using ANN and using experimental observation for the training, validation, testing, and all datasets (BRC-1).

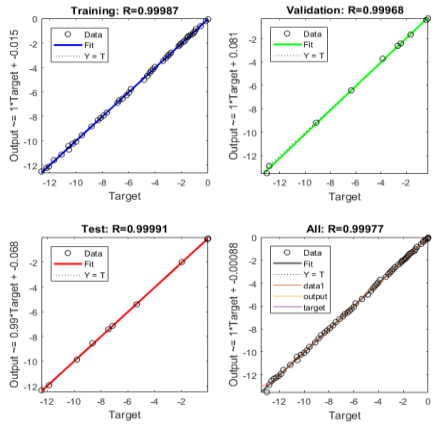

Figure 9. Prediction of the load vs. displacement relationship using ANN and using experimental observation for the training, validation, testing, and all datasets (BRC-2).

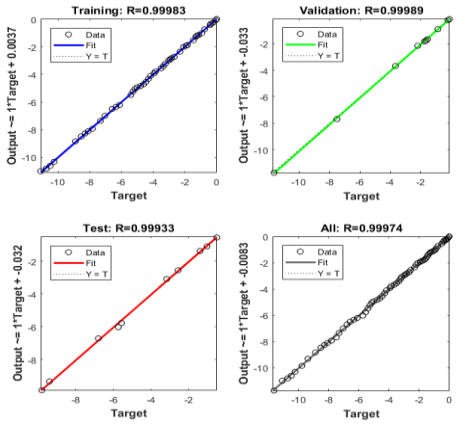

Figure 10. Prediction of the load vs. displacement relationship using ANN and using experimental observation for the training, validation, testing, and all datasets (BRC-3).

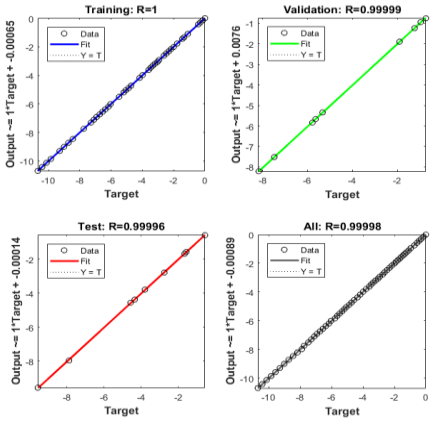

Figure 11. Prediction of the load vs. displacement relationship using ANN and using experimental observation for the training, validation, testing, and all datasets (BRC-4).

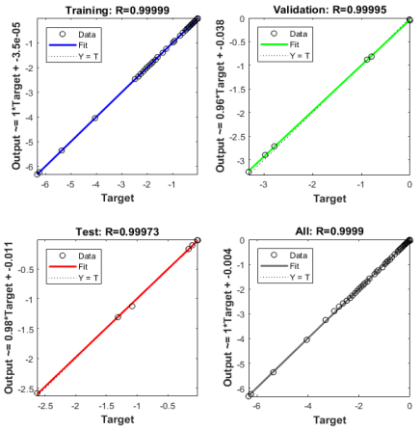

Figure 12. Prediction of the load vs. displacement relationship using ANN and using experimental observation for the training, validation, testing, and all datasets (SRC).

The data merger of ANN analysis results from each BRC beam specimen into a load vs. displacement relationship. The merger is done to determine the suitability of the load vs. displacement relationship model through the R^2 parameter. From the results of the regression analysis, it is found that R^2 = 0.9771, or almost close to 1. This shows that the model has high suitability, as shown in Figure 13. Figure 13 illustrates the load vs. displacement relationship for all BRC beam typologies from ANN analysis.

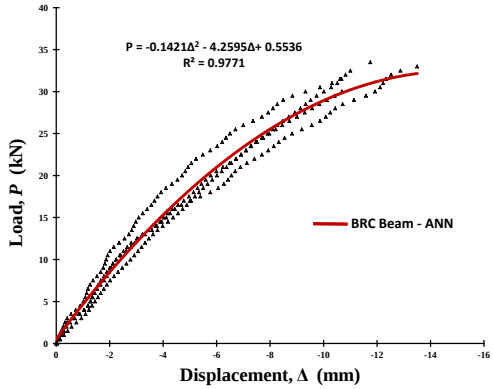

Figure 13. The relationship of load vs. displacement of BRC beam of ANN results.

3.3. Validation with the Finite Element Method

Validation of the relationship of load vs. displacement with the finite element method is done by inputting the geometry of the cross-section, load data, modulus of elasticity (E) per layer, and Poisson's ratio (υ). The load vs. displacement relationship diagram of the experimental results as shown in Figures 6 and 7 is used as a guide for the stages of the analysis process using the finite element method. And the cross-sectional stiffness input via the per-layer modulus of elasticity (E) is shown in Tables 7 and 8. The analysis execution using the finite element method uses the Fortran PowerStation 4.0 program. The process of calculating displacement and stress with the Fortran PowerStation 4.0 program is carried out in stages according to the loading and stiffness stages per layer from the beam's elastic condition, initial crack, elastoplastic, and plastic conditions until the beam collapses. The displacement data resulting from the finite element method is processed into a load vs. displacement relationship as shown in Figure 14. The displacement of the load ultimate is shown in Figure 15 for BRC beams and Figure 16 for SRC beams. The stress contours at the time of the load collapse are shown in Figure 17 for BRC beams and Figure 18 for SRC beams.

Comment [CH14]: Please check that intended meaning is retained.

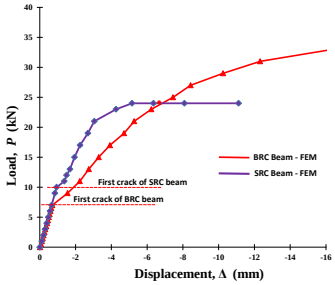

Figure 14. The relationship of load vs. displacement of BRC beam of finite element method (FEM) results.

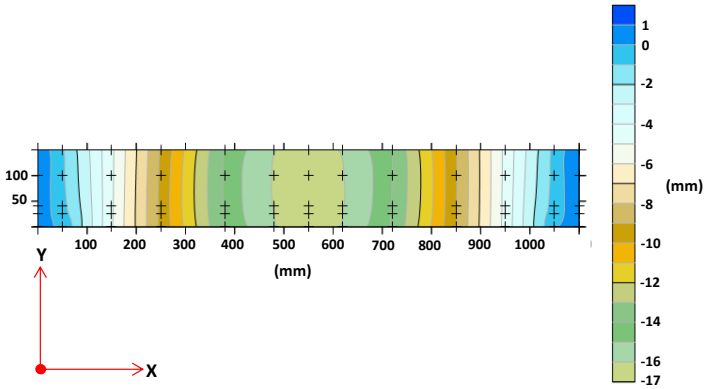

Figure 15. The displacement contour of Y-direction of BRC beam.

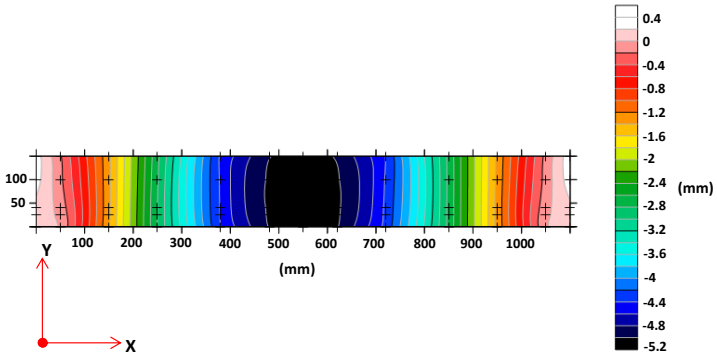

Figure 16. The displacement contour of Y-direction of SRC beam.

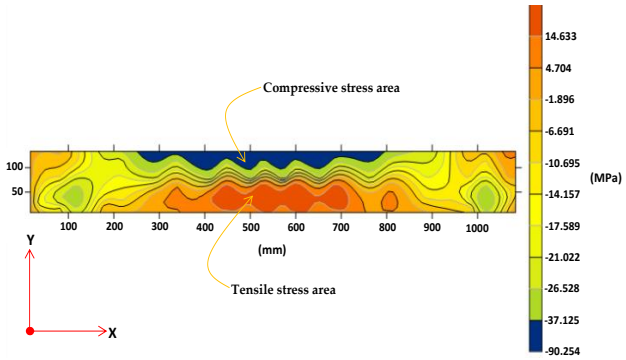

Figure 17. The stress contour of X-direction of BRC beam.

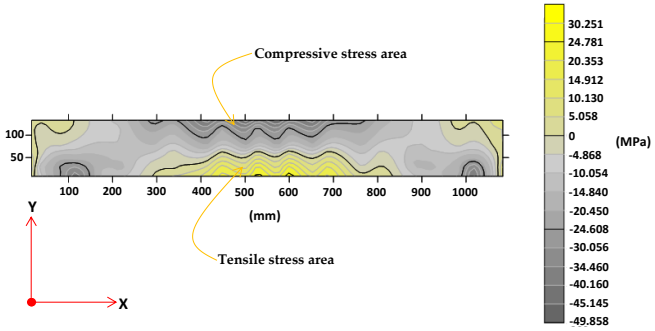

Figure 18. The stress contour of X-direction of SRC beam.

Table 7. The modulus of elasticity for each layer of the BRC beam in the non-linear phase.

Layer Number	Modulus of Elasticity (*E*) of the BRC Beam													
	Elastic Condition	Plastic Conditions with Gradual Loads												
	0–8.5 kN	9 kN	11 kN	13 kN	15 kN	17 kN	19 kN	21 kN	23 kN	25 kN	27 kN	29 kN	31 kN	33 kN
4th mesh layer	26851.29	16,110.77	16,110.77	16,110.77	16,110.77	16,110.77	16,110.77	16,110.77	16,110.77	16,110.77	12,083.08	11,277.54	11,277.54	8592.41
3th mesh layer	26851.29	16,110.77	16,110.77	16,110.77	16,110.77	16,110.77	16,110.77	16,110.77	16,110.77	1208.31	10,740.52	9397.95	9397.95	7518.36
2nd mesh layer	23140.89	13,884.53	11,570.44	11,570.44	11,570.44	11,570.44	10,413.40	10,413.40	10,413.40	10,413.40	6942.27	6942.27	6942.27	5553.81
1st mesh layer	26851.29	13,425.65	11,814.57	10,203.49	8323.90	6712.82	5101.75	5101.75	5101.75	3759.18	3222.16	2685.13	1611.08	1329.14

Table 8. The modulus of elasticity for each layer of the SRC beam in the non-linear phase.

Layer Number	Modulus of Elasticity (*E*) of the SRC Beam										
	Elastic Condition	Plastic Conditions with Gradual Loads									
	0–9 kN	10 kN	11 kN	12 kN	13 kN	15 kN	17 kN	19 KN	21 KN	23 kN	24 kN
4th mesh layer	26,851.29	26,851.29	20,138.47	20,138.47	20,138.47	20,138.47	20,138.47	18,795.90	18,795.90	13,425.65	11,411.80
3th mesh layer	26,851.29	26,851.29	20,138.47	20,138.47	18,795.90	18,795.90	18,795.90	17,453.34	17,453.34	13,425.65	11,411.80
2nd mesh layer	43,209.32	43,209.32	30,586.93	30,586.93	28,547.80	28,547.80	26,508.67	26,508.67	24,469.54	20,391,29	17,332.60
1st mesh layer	26,851.29	26,851.29	20,138.47	20,138.47	18,795.90	18,795.90	17,453.34	16,110.77	14,768.21	13,425.65	12,083.08

4. Discussion

Merging is carried out on the load vs. displacement relationship diagram from the experimental results, ANN analysis, and finite element method (FEM) analysis. Figure 19 shows the combined load vs. displacement diagram of the ANN analysis results with the experimental results. Figure 19 shows that the load vs. displacement relationship diagram the two analyses results are very coincided or show high suitability. However, at a load of approximately 90% of the collapse load, the load vs. displacement relationship diagram shows different behavior. Figure 20 shows the combined load vs. displacement diagram of the experimental results, ANN analysis, and the results of the finite element method analysis. Figure 19 shows that the artificial neural networks (ANN) model has a higher R^2 value when compared to the R^2 value of the multiple linear regression model (MLR). ANN analysis has better predictive accuracy. This is the same as the conclusion of 2 researchers, namely Khademi et al. (2017) [40], who concluded that the ANN model has higher accuracy than the multiple linear regression (MLR) model, and Xuan Li et al. (2019) [41], who concluded that the ANN model performs better than the MLR models with or without considering the interactions between factors. The accuracy of the prediction is very much dependent on the number of input variables. The greater the number of input parameters, the more accurate the results of the predicted model.

The diagram of the relationship between load and displacement of the BRC beam from FEM analysis and experimental results shows the difference in elastic conditions or until the initial crack occurs. The experimental results showed negative differences with the results of the FEM analysis. This shows the influence of the nature and characteristics of bamboo. The parts of bamboo stems have a non-uniform or uncertain modulus of elasticity. Tensile strength and modulus of elasticity of bamboo tested in the laboratory are sometimes different from bamboo which is used as beam reinforcement. As is known, bamboo trees from base to tip have different tensile strength and fiber density. Meanwhile, the load vs. displacement diagram of the SRC beam experiment results has a positive difference with the results of the FEM analysis when the elastic condition occurs or until the initial crack occurs. Positive differences can be ignored, in the sense that the quality of the steel used is better than the quality of steel tested in the laboratory. However, in this study, the analysis of stiffness reduction in BRC and SRC beams was focused after the beam experienced an initial crack or non-linear phase.

Comment [CH15]: Please check that intended meaning is retained.

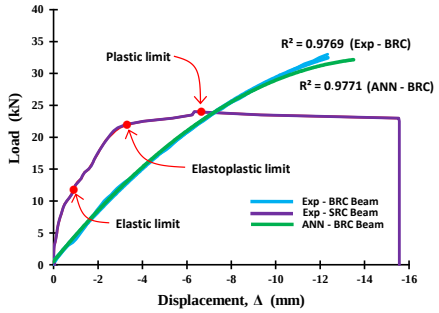

Figure 19. The combined of the load vs. displacement relationship of BRC beam of the experimental results and ANN analysis.

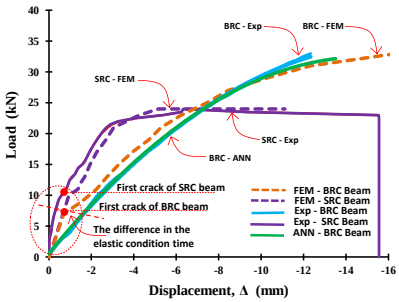

Figure 20. The combined of the load vs. displacement relationship of BRC beam and SRC beam of the experimental results, ANN analysis, and FEM.

Figure 20 shows that inelastic conditions there is a difference in stiffness between the two types of beams. The stiffness of bamboo reinforced concrete beams (BRC) is lower than the stiffness of steel-reinforced concrete beams (SRC). This difference occurs not due to reduced cross-section inertia or I_g of cross-sectional reduction, but due to the nature of the material used. This is because the BRC beam uses bamboo reinforcing material, which has high elastic and resilience properties. BRC beams with bamboo reinforcement will be able to accept high impact loads without causing over stress at the elastic limit, even though displacement has occurred. This indicates that the energy absorbed during loading is stored and released if the material is not loaded. Meanwhile, the SRC beam uses steel material that has high stiffness and toughness, so that the SRC beam in the service load range or elastic conditions does not experience excessive displacement or deformation. Beams that use materials with high stiffness and toughness will be able to withstand high impact loads or shock loads. If the SRC beam gets an impact load, then some of the energy is absorbed and some of the energy is transferred.

In the non-linear phase or after initial cracking, the beam stiffness changes from the full-sectional flexural stiffness, E_cI_g, to the effective bending stiffness, E_cI_{eff}. In the non-linear phase, the stiffness of the beam section continues to decrease with increasing loads, moments, and cracks. The area of the beam section continues to decrease with increasing cracks and automatically causes the beam section stiffness (E_cI_g) to decrease. As shown in Table 6 and Figure 21, the stiffness of the BRC beam decreases after the initial cracking occurs as the increasing loading stage is applied. The increase in load causes the flexural moment to increase, the displacement increases, and the crack propagation continues to spread towards the compressed block of the beam cross-section. The crack propagation from 1st mesh layer to the 2nd mesh layer onwards runs linearly with reduced cross-sectional stiffness from the lower fiber of the cross-section tensile block to the upper fiber of the compressive block of the beam cross-section. The increase in crack propagation towards the compressive block of cross-section causes the neutral line to change. Chunyu Fu et al. (2018) [13] concluded that the presence of cracks causes a nonlinear stress distribution along the beam cross-section, which changes the neutral axis of the cross-section and further affects the stiffness of the beam. Figure 21 shows that the stiffness of the BRC beam cross-section decreases from the initial crack until the beam collapses. The stiffness of BRC beams is reduced by 50% after initial cracking to 95% at collapse. The stiffness reduction goes step by step according to the moment (M_a) applied to the beam. Sang-Whan Han et al. (2009) [4] revealed that the stiffness reduction factor was significantly affected by the amount of moment or the applied load, while the stiffness reduction factor did not differ from the amount of reinforcement. The decrease in the moment of inertia of the full cross-sectional Ig of the BRC beam ranged from $0.5I_g$–$0.05I_g$ for the elastoplastic and plastic regions. Meanwhile, ACI-318M-14 [5] recommends the stiffness of the beam cross-section for elastic analysis in the non-linear phase of $0.5I_g$–$0.25I_g$. The difference in the value of the reduction in the stiffness of the cross-section at collapse correlates with the differences in the properties and characteristics of the material used as beam reinforcement. Bamboo reinforced concrete beams (BRC) exhibit high displacement behavior, but once the collapse load is reached and gradually released,

displacement tends to return to zero. It is linear with its elastic properties and the stress vs. strain relationship behavior of bamboo.

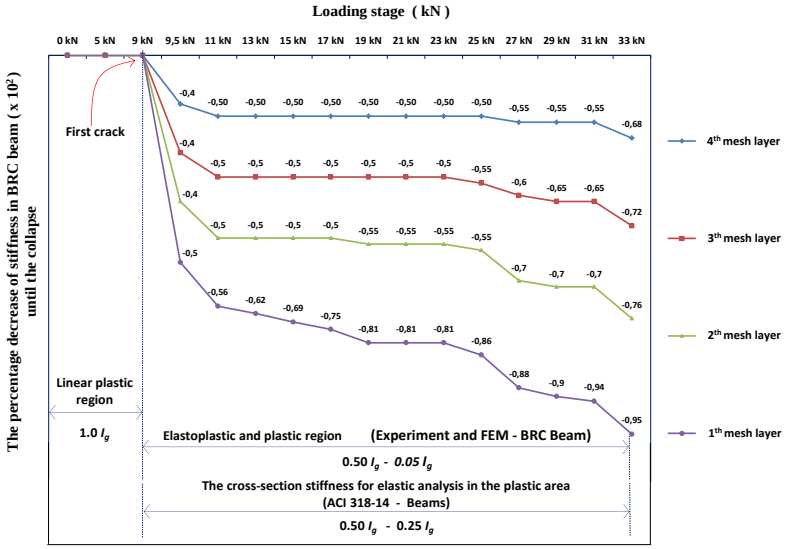

Figure 21. Decreased stiffness of BRC beam cross-section in the span middle.

Table 7 and Figure 22 show a decrease in stiffness or a decrease in the moment of inertia of the SRC beam cross-section. Stiffness decreases after initial cracking as the applied load increases. Figure 22 shows that the cross-sectional stiffness of the SRC beam decreases from the initial crack until the beam collapses. The stiffness of the SRC beam was reduced by 25% after initial cracking to 60% at collapse. The decrease in the moment of inertia full cross-section (I_g) for SRC beams ranged from $0.75I_g$–$0.40I_g$ for the elastoplastic and plastic regions. Meanwhile, ACI-318M-14 [5] recommends the cross-sectional stiffness of reinforced concrete beams for elastic analysis in the non-linear phase of $0.5I_g$–$0.25I_g$. The difference in the value of the reduction in the cross-sectional stiffness of the SRC beam with the ACI-318M-14 [5] requirements is due to the beam cross-section reinforcement method, namely the SRC beam in this study using a single reinforcement method. SRC beam with single reinforcement shows that when the steel reinforcement undergoes second melting and the moment of inertia of the cross-section is still around 40%, the steel reinforcement is not able to withstand the tensile stress that occurs so that the neutral line of the cross-section continues to shift upwards towards the upper fiber of the compression block of the cross-section. Meanwhile, BRC beams with bamboo reinforcement have good elastic properties, where after the ultimate load is reached, the large displacement shrinks back to near-zero or the beam returns flat [7], as shown in the video at the following link: https://goo.gl/6AVWmP. Although the stiffness or inertia of the BRC beam cross-section is still around 5%, bamboo reinforcement is still able to withstand the tensile stress that occurs, as stated by Ghavami (2005) [24] that bamboo has high tensile strength. If we control with the crack pattern, the crack lines on the BRC beam majority stop below the cross-section neutral line, while the crack lines on the SRC beam tend to continue to propagate upwards towards the upper fibers of the compressive block of the beam cross-section, as shown in Figures 23 and 24. And if we look at Figures 17 and 18, the tensile stress contour of the BRC beam has a wider zone and spreads to the side when compared to the SRC beam.

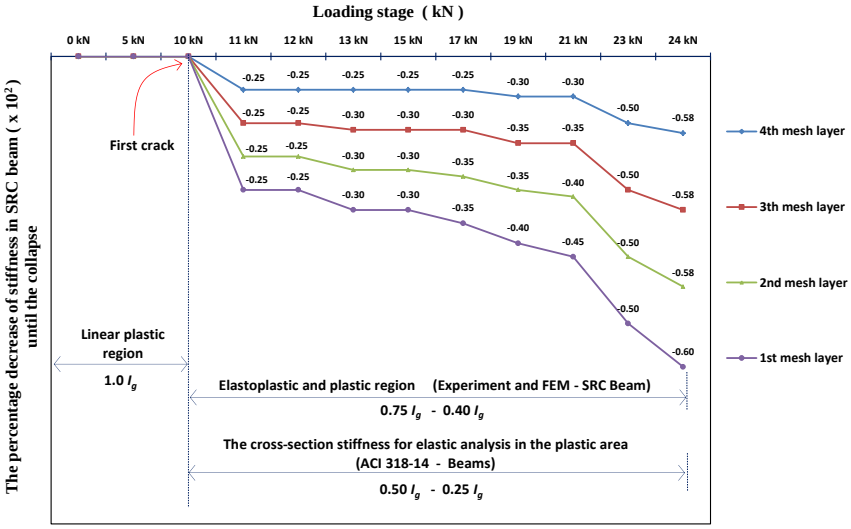

Figure 22. Decreased stiffness of SRC beam cross-section in the span middle.

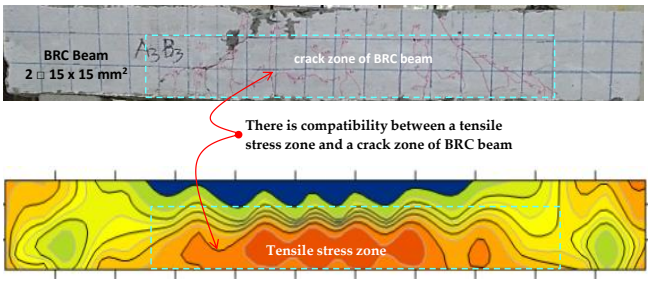

Figure 23. The crack pattern and tensile stress zone of BRC beam.

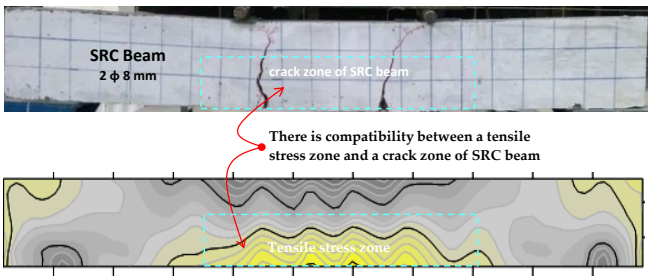

Figure 24. The crack pattern and tensile stress zone of SRC beam.

Figures 25 and 26 show the relationship between the stiffness reduction factor (ϕ_K) and the M_a/M_{cr} of the BRC beam and the SRC beam. The stiffness reduction factor (ϕ_K) is the ratio of the moment of inertia of the effective section (I_e) divided by the moment of inertia of the cross-section (I_g). The stiffness reduction factor (ϕ_K) is significantly influenced by the applied moment level. The equation of the beam stiffness reduction factor is related to the ratio between the applied moment and an initial crack moment or M_a/M_{cr}. The equation for the stiffness reduction factor is shown in Equation (5) or Equation (6) for a BRC beam. The stiffness reduction factor equation for the SRC beam is shown in Equation (7) or Equation (8). Figure 27 shows a comparison of the relationship between the stiffness reduction factor and the M_a/M_{cr} of the BRC beam and SRC beam. The diagram of the relationship between the stiffness reduction factor and M_a/M_{cr} shows that the SRC beam has a

smaller stiffness reduction factor than the BRC beam in the non-linear phase. However, the SRC beam shows a collapse at the moment of inertia of the effective cross-section (I_e), which is relatively still large when compared to BRC beams. BRC beams collapse at the effective cross-section inertia of about 5%, and SRC beams collapse at the effective section inertia of about 40%. The alternative of moments of inertia from various sources is shown in Table 9.

$$\phi_K = 0.646 - 0.1023\left(\frac{M_a}{M_{cr}}\right) \quad (5)$$

$$\frac{I_e}{I_g} = 0.646 - 0.1023\left(\frac{M_a}{M_{cr}}\right) \quad (6)$$

$$\phi_K = 0.697 - 0.1472\left(\frac{M_a}{M_{cr}}\right) \quad (7)$$

$$\frac{I_e}{I_g} = 0.697 - 0.1472\left(\frac{M_a}{M_{cr}}\right) \quad (8)$$

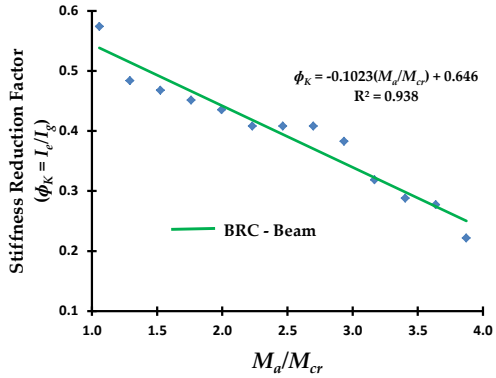

Figure 25. The relationship of the stiffness reduction factor (ϕ_K) and the M_a/M_{cr} of the BRC beam.

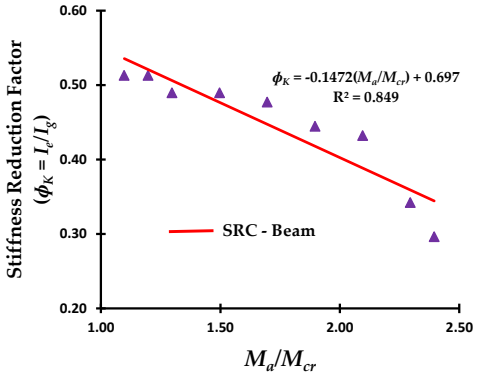

Figure 26. The relationship of the stiffness reduction factor (ϕ_K) and the M_a/M_{cr} of the SRC beam.

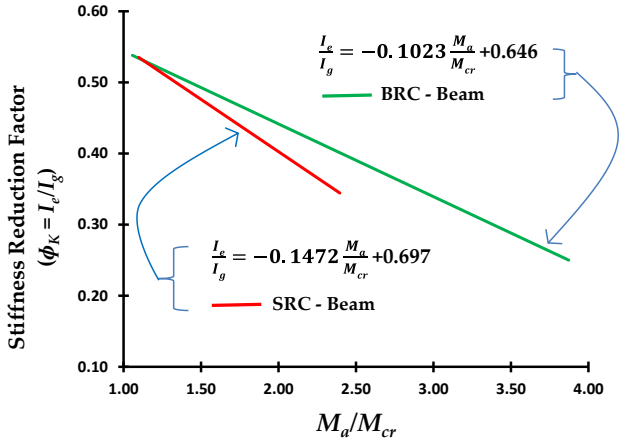

Figure 27. Comparison of the relationship of the stiffness reduction factor (ϕ_K) and the M_a/M_{cr} of the BRC beam and SRC beam.

Table 9. The alternative value of *I* for elastic analysis from various sources.

Source and Information	Alternative value of *I* for elastic analysis
ACI-318M-14 [5]	$0.25I_g$–$0.5I_g$
FEMA 356-2000 [46]	$0.5\ EI_g$–$0.8EI_g$
New Zealand Code [47]	$0.35I_g$
Paulay and Priestley, 1992 [48]	$0.30I_g$–$0.50I_g$
In this research (singly reinforced beam)	
- BRC Beam	$0.05I_g$–$0.5I_g$
- SRC Beam	$0.4I_g$–$0.75I_g$

5. Conclusions

The relationship pattern of load vs. displacement reflects the stiffness pattern of structural elements. The properties and characteristics of the material in the reinforcing concrete elements have a dominant influence on the relationship pattern of the load vs. displacement of reinforced concrete elements. Bamboo reinforced concrete beams (BRC) have a different load vs. displacement relationship pattern when compared to steel reinforced concrete beams (SRC). BRC beams have elastic properties and high resilience properties that can accept high impact loads without causing over stress at the elastic limit, even though displacement has occurred. While SRC beams have high stiffness and toughness so that SRC beams are not subject to excessive displacement or deformation at service load ranges or elastic conditions.

Results of the validation of the relationship pattern of the load vs. displacement of the BRC beams shows that the ANN model has a higher R^2 value when compared to the R^2 value of the MLR model. ANN analysis has a higher prediction accuracy. The accuracy of the prediction depends very much on the number of input variables. The greater the number of input parameters, the more accurate the prediction model results.

The cross-sectional stiffness of BRC beams is reduced by 50% after initial cracking and reduced by 95% at collapse. The cross-sectional stiffness of the SRC beam was reduced by 25% after initial cracking and reduced by 60% at collapse. The reduction in stiffness is significantly affected by the amount of applied moment (M_a) or the load applied that caused cracks and a reduction in the moment of inertia of the cross-section.

The initial decrease in cross-sectional stiffness of BRC beams occurs at a load of about 24% of the ultimate load and BRC beams occur at loads of about 40% ultimate load. BRC beam collapse occurs when the moment of inertia of the effective cross-section (I_e) is 5%, while the SRC beam

collapse occurs when the moment of inertia of the effective cross-section (I_e) is 40%. The reduction in stiffness in the cross-section of the beam in the non-linear phase ranged from $0.5I_g$–$0.05I_g$ for BRC beams, and $0.75I_g$–$0.40I_g$ for SRC beams. ACI-318M-14 standard recommends the cross-sectional stiffness of reinforced concrete beams for elastic analysis in the non-linear phase of $0.5I_g$–$0.25I_g$.

The SRC beams have a smaller stiffness reduction factor ($\phi\kappa$) than BRC beams in the non-linear phase. However, the SRC beam shows a collapse at the moment of inertia of the effective cross-section (I_e), which is relatively large when compared to BRC beams.

Author Contributions:

Funding: APC financing entirely by the DPRM Republic of Indonesia and LPPM of the University of Muhammadiyah Jember, Indonesia.

Acknowledgments: My gratitude goes to the LPPM of the Muhammadiyah University of Jember, Indonesia, and DPRM of the Republic of Indonesia as the funder of this research and APC.

Conflicts of Interest: The authors declare no conflicts of interest.

Comment [M16]: For research articles with several authors, a short paragraph specifying their individual contributions must be provided. The following statements should be used "Conceptualization, X.X. and Y.Y.; methodology, X.X.; software, X.X.; validation, X.X., Y.Y. and Z.Z.; formal analysis, X.X.; investigation, X.X.; resources, X.X.; data curation, X.X.; writing—original draft preparation, X.X.; writing—review and editing, X.X.; visualization, X.X.; supervision, X.X.; project administration, X.X.; funding acquisition, Y.Y. All authors have read and agreed to the published version of the manuscript.", please turn to the CRediT taxonomy for the term explanation. Authorship must be limited to those who have contributed substantially to the work reported.

References

1. Pandey, K.K.; Ramakantha, V.; Chauhan, S.S.; Kumar, A.A. *Wood is Good*; Springer: Singapore, 2017.
2. Mohammadabadi, M.; Jarvis, J.; Yadama, V.; Cofer, W. Predictive Models for Elastic Bending Behavior of a Wood Composite Sandwich Panel. *Forests* **2020**, *11*, 624.
3. Ministry of Environment and Forestry of the Republic of Indonesia. Memanfaatkan Bambu sebagai Salah Satu Potensi Hutan Rakyat. 18 October 2018**.** Available online: https://www.menlhk.go.id/site/single_post/1444 (accessed on 24 October 2020).
4. Han, S.W.; Park, Y.M.; Kee, S.H. Stiffness Reduction Factor for Flat Slab Structures under Lateral Loads. *J. Struct. Eng.* **2009**, *135*, 743.
5. ACI Committee 318 Standard. *Building Code Requirements for Structural Concrete*; 2014.
6. Gunasti, A.; Dewi, I.C.; Dasuki, M.; Ariyani, S.; Mahmudi, I.; Abadi, T.; Rahman, M.; Hidayatullah, S.; Nilogiri, A.; Galuh, S.D.; et al. The Prediction of Stiffness of Bamboo-Reinforced Concrete Beams Using Experiment Data and Artificial Neural Networks (ANNs). *Crystals* **2020**, *10*, 757.
7. Muhtar; Dewi, S.M.; Wisnumurti; Munawir, A. Enhancing bamboo reinforcement using a hose-clamp to increase bond-stress and slip resistance. *J. Build. Eng.* **2019**, *26*, 100896.
8. Muhtar; Dewi, S.M.; Wisnumurti; Munawir, A. The flexural behavior model of bamboo reinforced concrete beams using a hose clamp. *Proc. Mater. Sci. Eng. Chem*. **2019**, *276*, 1033.
9. Zhang, K.; Zhang, J.; Jin, W.; Mao, J.; Long, J. Stiffness degradation for the fatigue of reinforced concrete beams after electrochemical rehabilitation. *Constr. Build. Mater.* **2020**, *260*, 120455.
10. Salam, A.S.A.; Debra, L.F. Use of negative stiffness in failure analysis of concrete beams. *Eng. Struct.* **2016**, *126*, 187–199.
11. Hu, H.S.; Nie, J.G.; Wang, Y.H. Effective stiffness of rectangular concrete-filled steel tubular members Hong-Song. *J. Constr. Steel Res.* **2016**, *116*, 233–246.
12. Patel, K.A.; Bhardwaj, A.; Chaudhary, S.; Nagpal, A. Explicit expression for effective moment of inertia of RC beams. *Lat. Am. J. Solids Struct.* **2015**, *12*, 542–560.
13. Fu, C.; Wang, Y.; Tong, D. Stiffness Estimation of Cracked Beams Based on Nonlinear Stress Distributions Near the Crack. *Math. Probl. Eng.* **2018**, *2018*, 1–12.
14. Pique, J.R.; Burgos, M. Effective rigidity of reinforced concrete elements in seismic analysis and design. In Proceedings of the 14 World Conference on Earthquake Engineering, Beijing, China, 12–17 October 2008.
15. Akmaluddin; Pathurahman. Effective Moment of Inertia Approach for Predicting Displacement of Concrete Beams Reinforced with Twisted Bamboo Cables. *Int. J. Civ. Environ. Eng. IJCEE-IJENS* **2012**, *12*, 6–13.
16. Kalkan, İ. Displacement Prediction for Reinforced Concrete Beams through Different Effective Moment of Inertia Expressions. *Int. J. Eng. Res. Dev.* **2013**, *5*, 1.
17. Fu, C.; Tong, D.; Wang, Y. Assessing the Instantaneous Stiffness of Cracked Reinforced Concrete Beams Based on a Gradual Change in Strain Distributions. *Adv. Mater. Sci. Eng.* **2020**, *2020*, 1–10.

Comment [M17]: Please add the publisher and location.

18. Feng, X.; Shen, M.; Sun, C.; Chen, J.; Luo, P. Research on flexural stiffness reduction factor of the reinforced concrete column with equiaxial shaped section. In Proceedings of the 13th COTA International Conference of Transportation Professionals (CICTP 2013), 2013; pp. 168–174.
19. Muhtar; Dewi, S.M.; Wisnumurti; Munawir, A. The stiffness and cracked pattern of bamboo reinforced concrete beams using a hose clamp. *Int. J. Civ. Eng. Technol.* **2018**, *9*, 273–284.
20. Agarwal, A.; Nanda, B.; Maity, D. Experimental investigation on chemically treated bamboo reinforced concrete beams and columns. *Constr. Build. Mater.* **2014**, *71*, 610–617.
21. Muhtar. Experimental data from strengthening bamboo reinforcement using adhesives and hose-clamps. *Data Brief* **2019**, *27*, 104827.
22. Rahman, M.M.; Rashid, M.H.; Hossain, M.A.; Hasan, M.T.; Hasan, M.K. Performance evaluation of bamboo reinforced concrete beam. *Int. J. Eng. Technol. IJET-IJENS* **2011**, *11*, 113–118.
23. Muhtar. Precast Bridges of Bamboo Reinforced Concrete in Disadvantaged Village Areas in Indonesia. *Appl. Sci.* **2020**, *10*, 7158.
24. Ghavami, K. Bamboo as reinforcement in structural concrete elements. *Cem. Concr. Compos.* **2005**, *27*, 637–649.
25. Javadian, A.; Wielopolski, M.; Smith, I.F.C.; Hebel, D.E. Bond-behavior study of newly developed bamboo-composite reinforcement in concrete. *Constr. Build. Mater.* **2016**, *122*, 110–117.
26. Muhtar, M.; Dewi, S.; Wisnumurti; Munawir, A. Bond-slip improvement of bamboo reinforcement in the concrete beam using hose clamps. In Proceedings of the 2nd International Multidisciplinary Conference, Jakarta, Indonesia, 15 November 2016; pp. 385–393.
27. Gunasti, A.; Manggala, A.S.; Nusant, A.F.P.; Nilogiri, A. Effect of Reinforcement Details on Precast Bridge Frames of Bamboo Reinforced Concrete to Load Capacity and Crack Patterns. *Int. J. Eng. Res. Technol.* **2020**, *13*, 631–636.
28. Muhtar. Cracked Pattern of Bamboo Reinforced Concrete Beams Using Double Reinforcement with the Strengthening on Tensile Reinforcement. *Int. J. Eng. Res. Technol.* **2020**, *13*, 608–612.
29. ASTM C 39 Standard. *Standard Test Method for Compressive Strength of Cylindrical Concrete Specimens*; West Conshohocken, PA, USA, 2003.
30. PT SIKA Indonesia. Sikadur®-752. 02, 2-3. 2016. Available online: https://www.scribd.com/document/374071630/Sikadur-752 (accessed on 24 October 2020).
31. ASTM C 09 Standard. *Standard Test Method for Flexural Strength of Concrete (Using Simple Beam with Third-Point Loading)*; West Conshohocken, PA, USA, 2002.
32. Muhtar. Numerical validation data of tensile stress zones and crack zones in bamboo reinforced concrete beams using the Fortran PowerStation 4.0 program. *Data Brief* **2020**, *29*, 105332.
33. Avram, C.; Facaoaru, I.; Filimon, I.; Mirsu, O.; Tertea, I. *Concrete Strength and Strain*; Developments in Civil Engineering 3; 1981.
34. Naderpour, H.; Kheyroddin, A.; Amiri, G.G. Prediction of FRP-confined compressive strength of concrete using artificial neural networks. *Compos. Struct.* **2010**, *92*, 2817–2829.
35. Ahmadi, M.; Naderpour, H.; Kheyroddin, A. Utilization of artificial neural networks to prediction of the capacity of CCFT short columns subject to short term axial load. *Arch. Civ. Mech. Eng.* **2014**, *14*, 510–517.
36. Khademi, F.; Akbari, M.; Nikoo, M. Displacement determination of concrete reinforcement building using data-driven models. *Int. J. Sustain. Built Environ.* **2017**, *6*, 400–411.
37. Kaczmarek, M.; Szymanska, A. Application of Artificial Neural Networks to Predict the Displacements of Reinforced Concrete Beams. *Studia Geotech. Mech.* **2016**, *38*, 37–46.
38. Abd, A.M.; Salman, W.D.; Ahmed, Q.W. ANN, and Statistical Modelling to Predict the Displacement of Continuous Reinforced Concrete. *Diyala J. Eng. Sci.* **2015**, 134–143.
39. Ya Tuan, T.M.Y.S.; Alebrahim, R.; Fitri, N.; Alebrahim. M. Analysis of Cantilever Beam Displacement under Uniformly Distributed Load using Artificial Neural Networks. In Proceedings of the MATEC Web of Conferences, LA, USA, 3–4 February 2018.
40. Khademi, F.; Akbari, M.; Mohammadmehdi, S.; Nikoo, M. Multiple linear regression, artificial neural network, and fuzzy logic prediction of 28 days compressive strength of concrete. *Front. Struct. Civ. Eng.* **2017**, *11*, 90–99.
41. Li, X.; Khademi, F.; Liu, Y.; Akbari, M.; Wang, C.; Bond, P.L.; Keller, J.; Jiang, G. Evaluation of data-driven models for predicting the service life of concrete sewer pipes subjected to corrosion. *J. Environ. Manag.* **2019**, *234*, 431–439.

Comment [M18]: Please add the location and date of the conference.

Comment [M19]: Please add the publisher.

Comment [M20]: Please add the publisher.

Comment [M21]: Please add the publisher and location.

Comment [M22]: Please add volume number or doi.

Comment [M23]: Please add location.

42. Dewi, S.M.; Nuralinah, D. The Recent Research on Bamboo Reinforced Concrete. In Proceedings of the MATEC Web of Conferences, 2017; Volume 103, p. 2001.
43. Nathan, S. Application of Bamboo for Flexural and Shear Reinforcement in Concrete Beams. Clemson University, 2014**.**
44. Khare, L. *Performance Evaluation of Bamboo Reinforced Concrete Beams*; 2005**.**
45. Mishra, M.; Agarwal, A.; Maity, D. Neural-network-based approach to predict the displacement of plain, steel-reinforced, and bamboo-reinforced concrete beams from experimental data. *SN Appl. Sci.* **2019**, *1*, 584.
46. FEMA 356 Standard. *Prestandard and Commentary for the Seismic Rehabilitation of Buildings*; November 2000.
47. New Zealand Standard. *Code of Practice for the Design of Concrete Structures*; Part 1; Wellington, New Zealand, 1995.
48. Paulay, T.; Priestley, M.J.N. *Seismic Design of Reinforced Concrete and Masonry Buildings*; Wiley Interscience: 1992.

Publisher's Note: MDPI stays neutral with regard to jurisdictional claims in published maps and institutional affiliations.

© 2020 by the authors. Submitted for possible open access publication under the terms and conditions of the Creative Commons Attribution (CC BY) license (http://creativecommons.org/licenses/by/4.0/).

Comment [M24]: Please add location and date.

Comment [M25]: Please add the location.

Comment [M26]: Please add the publisher and location.

Comment [M27]: Please add the publisher and location.

Comment [M28]: Please add the publisher.

Comment [M29]: Please add the location of the publisher.

forests

MDPI

Article

The Prediction of Stiffness Reduction Non-linear Phase in Bamboo Reinforced Concrete Beam Using The Finite Element Method (FEM) and Artificial Neural Networks (ANNs)

Muhtar

Faculty of Engineering, University of Muhammadiyah Jember, Jember 68121, Indonesia; muhtar@unmuhjember.ac.id

Received: date; Accepted: date; Published: date

Abstract: This paper discusses the reduction of the stiffness of bamboo reinforced concrete (BRC) beams to support the use of bamboo as an environmentally friendly building material. Calculation of cross-section stiffness in numerical analysis is very important, especially in the non-linear phase. After the initial crack occurs, the stiffness of the cross-section will decrease with increasing load and crack propagation. The calculation of the stiffness in the cross-section of the concrete beam in the non-linear phase is usually approximated by giving a reduction in stiffness. ACI 318-14 provides an alternative, reducing the stiffness of the plastic post-linear beam section through the moment of inertia (I) of the beam section for elastic analysis between $0.50I_g$–$0.25I_g$. This study aims to predict the value of the reduction in the stiffness of the BRC beam section in the non-linear phase through the load-displacement relationship of experimental results validated by the Finite Element Method (FEM) and the Artificial Neural Networks (ANN) method. The experiment used 8 BRC beams and one steel-reinforced concrete (SRC) beam of singly reinforced with a size of 75 mm × 150 mm × 1100 mm. The beams were tested using a four-point loading method. The analysis results showed that the value of the stiffness reduction in the beam cross-sectional in the non-linear phase ranged from $0.5I_g$–$0.05I_g$ for BRC beams, and $0.75I_g$–$0.40I_g$ for SRC beams.

Keywords: stiffness reduction; bamboo reinforced concrete (BRC); finite element method (FEM); artificial neural networks (ANN)

1. Introduction

The impact of increasing industrial development is that it can cause pollution of air, water, soil, and noise. The use of industrial building materials such as ceramics, steel, concrete, and other materials has led to an increase in environmental pollution. The procurement of wood forests or bamboo forests must be done as a counterweight to environmental pollution. Pandey et al. (2017) [1] and Mostafa et al. (2020) [2] revealed that an average tree absorbs one ton of CO_2 and produces 0.7 tons of O_2 for every cubic meter of growth. The use of environmentally friendly building materials such as wood and bamboo must be done. Bamboo is a forest product that provides high economic and ecological value to the community. Bamboo also has enormous potential with promising prospects [3]. Bamboo is one of the commodities produced by Community Forests. However, research on the behavior of bamboo as a building material is mandatory, such as research on the stiffness of bamboo reinforced concrete (BRC) beams.

The stiffness reduction factor is a multiplier to reduce the moment of inertia in gross cross-sectional, and the gross cross-sectional area remains constant. These factors are conservatively

Comment [M1]: No, It's correct

Comment [M2]: Yes, just delete it

Comment [M3]: It's correct.

Comment [M4]: Ok, No problem (it's a hyphen "between", not a minus sign).

Comment [M5]: Ok, No problem.

Comment [M6]: No. (I've changed it)

enforced by various concrete standards to account for the loss of stiffness in the concrete cross-section due to the cracking of the concrete. The stiffness of the beam cross-section in the elastic phase or linear phase indicates the full section flexural stiffness, E_cI_g, whereas in the non-linear phase or after the initial crack, the gross cross-section bending stiffness is reduced to the effective flexural stiffness, E_cI_{eff}. The stiffness reduction factor is significantly influenced by the amount of moment or the applied load, while the stiffness reduction factor does not differ from the amount of reinforcement [4]. ACI 318M-14 [5] shows that the gross section flexural stiffness, E_cI_g, is reduced to obtain the effective flexural stiffness, E_cI_e, which causes cracking and other softening effects. As the moment in the concrete section increases, the flexural stiffness will be reduced due to the cracks that continue to propagate and spread. ACI 318M-14 [5] provides stiffness reduction limits for elastic analysis with a moment of inertia limits between $0.25I_g$–$0.5I_g$ for concrete beams. The equation for the moment of inertia effective (I_e) is determined in ACI 318-05 [5] Section 9.5.2.3, as shown in Equation (1).

Comment [M7]: Ok, just delete it.

$$I_e = \left(\frac{M_{cr}}{M_a}\right)^3 I_g + \left[1 - \left(\frac{M_{cr}}{M_a}\right)^3\right] I_{cr} \quad (1)$$

where I_g = moment of inertia of the gross concrete section and I_{cr} = moment of inertia of the crack section including the reinforcement. The moment of inertial effective (I_e) as shown in Equation (1) will decrease as the moment that occurs, M_a. Calculation of the moment of inertia of the crack cross-section, I_{cr} at Equation (1) must pay attention to the number of reinforcement installed. However, the amount of reinforcement is not determined at the initial design stage.

The process of stiffness reduction in the beam section starts from the "*no crack*" and "*cracked*" conditions in the section. In the service load condition or the elastic condition, the stiffness of the beam section is in full condition, even though the moment due to the load continues to increase. In the elastic condition, the moment that occurs (M_a) is still below the moment of cracking (M_{cr}), or the tensile stress of the concrete is still below the modulus of rupture of the concrete beam cross-section, f_r. In the elastic conditions, the difference in stiffness between two different types of beams usually occurs not due to reduced inertia of the cross-section, but due to the properties of the materials used. For example, the stiffness of bamboo reinforced concrete beams is different from the stiffness of steel-reinforced concrete (SRC) beams. In the elastic conditions, the stiffness of BRC beams is lower than the stiffness of SRC beams [6–8]. This is because BRC beams use bamboo reinforcing materials which have elastic properties and high resilience properties. BRC beams with bamboo reinforcement will be able to accept high impact loads without causing stress over the elastic limit, even though displacement has occurred. This indicates that the energy absorbed during loading is stored and released if the material is not loaded.

Meanwhile, the SRC beam uses steel material that has high stiffness and toughness, so that the SRC beam in the service load range or elastic condition does not experience displacement or excessive deformation. Beams that use materials with high stiffness and toughness will be able to withstand high impact loads or shock loads. If the SRC beam gets an impact load, then some of the energy is absorbed and some of the energy is transferred.

Research on modeling and stiffness reduction has been carried out by many researchers. Kai Zhang et al. (2020) [9] investigated the effect of electrochemical rehabilitation (ER) techniques on the fatigue stiffness of RC beams. The results of his research indicated that electrochemical rehabilitation (ER) exacerbated bond breakage, thereby reducing the flexural stiffness of RC beams. Salam Al-Sabah et al. [10] discuss the use of negative stiffness in the failure analysis of concrete beams. In his research, Salman Al-Sabah et al. concluded that the effective and simple one-dimensional stress-strain behavior of concrete was used to study concrete blocks with proportional loading, the only source of non-linearity to consider cracks in concrete. Hong-Song Hu et al. (2016) [11] investigated the effectiveness of square CFST rod stiffness, and the results proposed an equation for the effective stiffness of square CFST rods. Muhtar et al. [7] tested the flexural of BRC beams and SRC beams, the results showed that the stiffness decreased after the initial cracking. The average stiffness of the BRC beam decreased from 26,324.76 MPa before cracking to 6581.20 MPa after

Comment [CH8]: CFST (Concrete filled steel tubular)

collapse [7], while the average value of SRC beam stiffness decreased from 30,334.11 MPa before cracking to 16873.35 MPa after the collapse.

K.A. Patela et al. (2014) [12], in their paper, provide an explicit expression for the effective moment of inertia by considering cracks for reinforced concrete beams (RC) with uniformly distributed loads. The proposed explicit expressions can be used to predict short-run displacement in-service load. The sensitivity analysis shows a substantial dependence of the effective moment of inertia on the selected input parameter. Displacement is an important parameter for examining the serviceability criteria of structures. The short-term displacement is generally calculated using the effective moment of inertia across the span at the service load [12]. Chunyu Fu (2018) [13] presents a method of estimating the stiffness of cracked beams based on the stress distribution. In his conclusion, he said that the presence of cracks causes a nonlinear stress distribution along the beam section, which changes the neutral axis of the cross-section and further affects the stiffness of the beam. J.R. Pique (2008) [14] concluded that when the design is controlled by the minimum reinforcement, especially in the beam, special attention should be paid to the calculation of the real period and maximum distortion. The effective stiffness of the beam with the minimum steel ratio is much lower than that obtained by the proposed reduction factor. As a result, the actual period and actual maximum distortion can be greater. Akmaluddin et al. (2012) [15] concluded that the moment of crack and the value of the moment of inertia of the crack was significantly affected by the presence of bamboo reinforcement in the beam. The experimental results show that the crack moment varies from 0.3 to 0.7 from the ultimate moment. The experimental and theoretical crack moment ratio varies from 0.90 to 1.42. İlker Kalkan (2013) and [16] concluded that the effective moment of inertia and load-displacement curve analysis is highly dependent on the crack moment used in the expression analysis of the effective moment of inertia. Therefore, the experimental cracking moment of the beam should be used in the calculation of the effective moment of inertia for a more accurate comparison of the different analytical methods. Chunyu Fu et al. (2020) [17] concluded that cracking of concrete causes a gradual change in the distribution of strain along with the cross-sectional height of reinforced concrete beams, which in turn affects the instantaneous stiffness. The instantaneous stiffness proved to be highly dependent on the number and depth of cracks. This dependence can be accurately reflected by the method proposed by simulating a gradual change in the concrete strain distribution. Xiuling Feng et al. (2013) [18] examines the reduction factor of flexural stiffness in reinforced concrete columns with an equiaxial cross-section and suggests that the reduction factor is proposed by considering the nonlinear characteristics of the material and its geometric nonlinearity.

The difference in the nonlinear characteristics of the material used in the BRC beam and the SRC beam greatly determines the flexural behavior of the beam. Bamboo reinforced concrete beams have low stiffness and tend to be large displacement. The solution to increasing the stiffness of BRC beams is to use shear reinforcement and the principle of confined concrete [7,19]. In the linear elastic condition, the BRC beam has shown a large displacement, but when the ultimate load is reached and the loading is released gradually, the displacement tends to return to zero. In this study, the reduction of stiffness in the non-linear phase was analyzed through the load vs. displacements that were validated using the finite element method (FEM) and the Artificial Neural Networks (ANN) method. It is suspected that the reduction of the cross-sectional stiffness of the BRC beam is different from the reduction in the stiffness of the SRC beam section. The parameter of the moment of inertia of the cross-section becomes a benchmark in determining the reduction of stiffness according to ACI-318M-14 [5].

2. Materials and Methods

2.1. Treatment of Materials

In this study, the treatment of bamboo material as concrete reinforcement is an important thing to do. The bamboo used is the bamboo "petung" (*Dendrocalamus asper*) which is between three and five years old [20–22]. The part of bamboo that is used as reinforcing of concrete is 6–7 m long from the base of the bamboo stem [23]. Bamboo is cut according to the size of the bamboo reinforcement to

be used, which is 15 x 15 mm². Then, bamboo is soaked for ±20–30 days [21]. After soaking, bamboo is dried in free air until it has an absorption level of ± 12%.

Application of adhesive or waterproof coating [24,25] is done after the bamboo reinforcement is cleaned and trimmed according to the planned size. The application of a waterproof layer is carried out to prevent the hydrolysis process between bamboo and concrete. Sand sprinkling on bamboo reinforcement is done when the adhesive is half dry to make it stronger [21,26]. The application of sand aims to increase the adhesion strength of bamboo reinforcement to concrete.

An installation of a hose-clamp at both ends of the bamboo reinforcement is done to match the concept of hooks or bends in steel reinforcement. An installation of the hose-clamp only on tensile reinforcement is done to increase bond-stress between bamboo reinforcement and concrete [27,28]. The tensile force on the bamboo reinforcement will be distributed to the concrete through the hose-clamp, which functions as a shear connector. Bamboo treatment is shown in Figure 1.

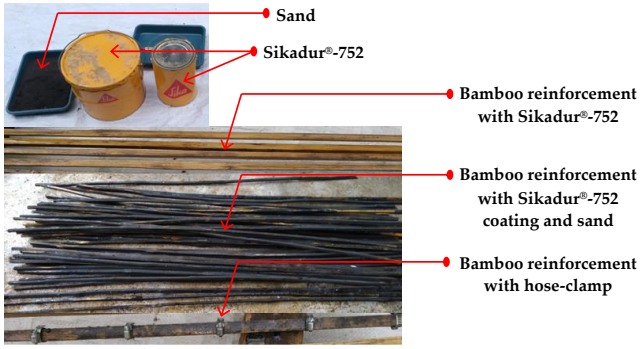

Figure 1. The materials and treatments of bamboo reinforcement.

2.2. Materials

The concrete mixture used in this study is a normal concrete mixture consisting of Portland Pozzolana Cement (PPC), sand, coarse aggregate, and water with a proportion of 1:1.8:2.82:0.52. Sand and gravel come from the Jember area of Indonesia. The cylindrical specimen measures 150 mm in diameter and 300 mm in height. The cylindrical specimens were press-tested using a Universal Testing Machine (UTM) with a capacity of 2000 kN after the concrete was 28 days old. The procedure for the cylinder specimen compressive test follows ASTM C 39 [29]. The average compressive strength of cylindrical concrete is 31.31 MPa with an average weight of 125.21 N. The properties and characteristics of the concrete are shown in Table 1.

Table 1. Material properties of reinforcing and concrete.

Bar Type and Concrete	Diameter, d (mm)	Modulus of Elasticity (*E*), (MPa)	Poisson's Ratio (ν)	Tensile Strength, f_y (MPa)	Compressive Strength, f'_c (MPa)
Bamboo	□ 15 × 15	17,235.74	0.20	126.68	-
Steel	ϕ 8	207,735.92	0.25	392.28	-
Concrete	-	26,324.79	0.30	-	31.31

Comment [M9]: It is a sign of the rectangular cross-sectional shape of bamboo reinforcement.

The tensile test of bamboo reinforcement produces the average tensile stress of 126.68 N/mm² with an average strain of 0.0074. The modulus of elasticity of bamboo reinforcement was calculated using the formula $E = \sigma/\varepsilon$ and obtained 17,235.74 MPa. The modulus of elasticity of steel is obtained

by 207,735.92 MPa. The properties and characteristics of bamboo and steel reinforcement are shown in Table 1.

The adhesive layer or waterproof coating used was Sikadur®-752 produced by PT. SIKA Indonesia [30]. The specifications for the adhesive sikadur®-752 are shown in Table 2. Installation of hose-clamp on bamboo reinforcement is done when the waterproof layer is half dry [21]. The diameter of the hose-clamp used is ¾″ made in Taiwan.

Table 2. The specification of Sikadur®-752 [30].

Components	Properties
Color	Yellowish
Density	Approx. 1.08 kg/L
Mix comparison (weight/volume)	2:1
Pot life at +30 °C	35 min
Compressive strength	62 MPa at 7 days (ASTM D-695) 64 MPa at 28 days
Tensile strength	40 MPa at 28 days (ASTM D-790)
Tensile Adhesion Strength	2 MPa (Concrete failure, over mechanically prepared concrete surface)
Coefficient of Thermal Expansion	−20 °C to + 40 °C 89 × 10^{-6} per °C
Modulus of elasticity	1060 MPa

Comment [M10]: Yes, It's correct.

2.3 Experimental Procedure

The test object consisted of 9 beams with a size of 75 mm × 150 mm × 1100 mm, consisting of 8 bamboo reinforced concrete beams (BRC) and one steel-reinforced concrete beam (SRC). Bamboo reinforcement is installed as tensile reinforcement with a reinforcement area of 450 mm². The steel reinforcement used has a diameter of 8 mm with an area of A_s = 100.48 mm². The beam geometry and reinforcement detail of the BRC and SRC beams are shown in Figure 2.

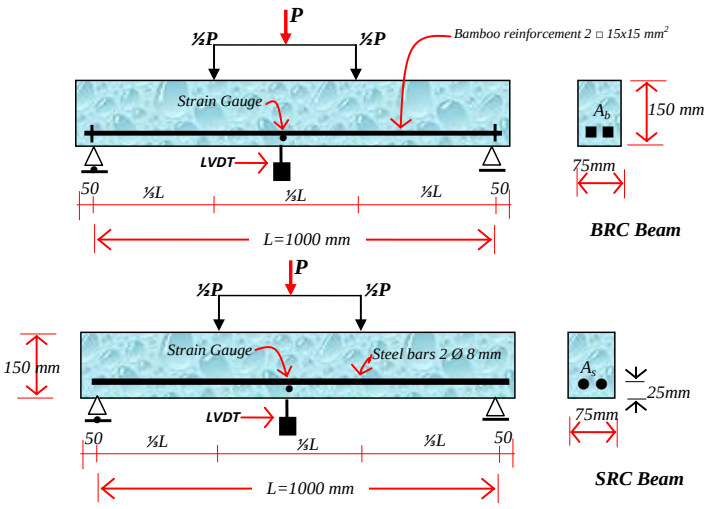

Figure 2. Reinforcement details and beam test settings.

The beam flexural test method was carried out using the four-point method [31]. The test arrangement and load position are shown in Figure 2. Strain gauges are installed on the bamboo

reinforcement at a distance of ½L from the support of the beam. Beam displacement measures use Linear Variable Displacement Transducers (LVDT) with a distance of ½L from the beam support.

The loading stages from zero to the collapse of the beam are used as a hydraulic jack and a load cell connected to a load indicator tool. The load reading on the load indicator is used as a hydraulic jack pump controller, displacement reading, and strain reading according to the planned loading stage. However, when the test object reaches its ultimate load, the displacement reading controls the strain and load reading, while the pumping of the hydraulic jack continues slowly according to the command of the displacement reader. The failure pattern was observed and identified by the cracks that occurred, from the time of the initial crack until the beam collapsed.

2.4. Validation of Numerical Methods

Validation of experimental data was found by using the Finite Element Method (FEM) and Artificial Neural Networks (ANN). The relationship between load vs. displacement experiment results was validated by using the finite element method. The procedure used is inputting material data and loading stages to determine the behavior of the load vs. displacement of BRC beams and SRC beams. The data input for the loading stages is carried out following the loading stages from laboratory experimental data. The numerical method used is the finite element method, using the Fortran PowerStation 4.0 program [32]. The theoretical analysis is used to calculate the load causing the initial crack using elastic theory (*linear analysis*) with cross-section transformation. For linear analysis, the input material data is the modulus of elasticity (E) and Poisson's ratio (υ). The calculation of the modulus of elasticity of the composites (E_{comp}) is shown in Tables 3 and 4. The non-linear phase is approximated by decreasing the concrete strength from 0.25 to 0.5 for the calculation of the effective stiffness in the plastic plane [5]. In the analysis of the finite element constitutive relationship, the problem-solving method uses the plane-stress theory. Triangular elements are used to model plane-stress elements with a bidirectional primary displacement at each point so that the element has six degrees of freedom. The discretization of the beam plane is carried out using the triangular elements shown in Figure 3 for BRC beams and Figure 4 for SRC beams.

Comment [CH11]: Please replace with "**Validation of experimental data using the Finite Element Method (FEM) and Artificial Neural Networks (ANN)**".

Comment [CH12]: Please replace with "**The theoretical analysis is used to calculate the load causing the initial crack is the elastic theory (linear analysis) with cross-section transformation**".

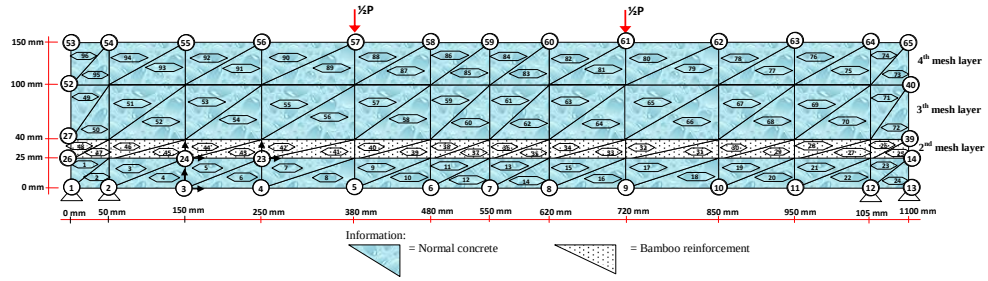

Figure 3. Discretization of the triangular element on the bamboo reinforced concrete (BRC) beam.

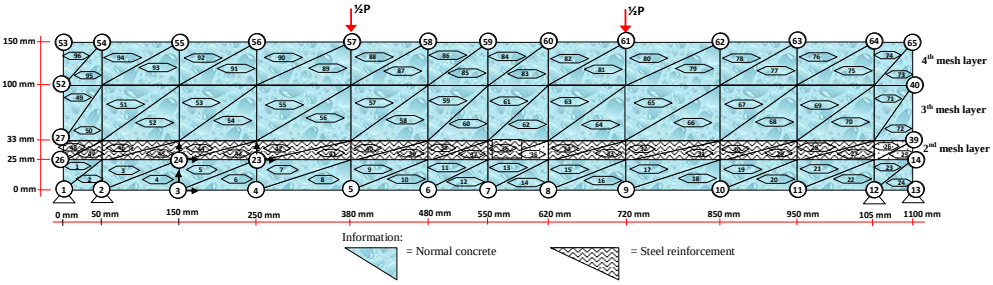

Figure 4. Discretization of the triangular element on the steel-reinforced concrete (SRC) beam.

Table 3. Elasticity Modulus of Composite of BRC beam.

Layer Number	Compressive Strength of Concrete, f'_c	Dimensions of per Layer		Modulus of Elasticity of the Material (E)		Elasticity Modulus of Composite (E_{comp})
	Mpa	b (mm)	h (mm)	Concrete, E_c (MPa)	Bamboo, E_b (MPa)	MPa
4th mesh layer	31.31	75	50	26,851.29	0	26,851.29
3rd mesh layer	31.31	75	60	26,851.29	0	26,851.29
2nd mesh layer	31.31	75	15	26,851.29	1723.57	23,140.89
1st mesh layer	31.31	75	25	26,851.29	0	26,851.29

Table 4. Elasticity Modulus of Composite of SRC beam

Layer Number	Compressive Strength of Concrete, f'_c	Dimensions of per Layer		Modulus of Elasticity of the Material (E)		Elasticity Modulus of Composite (E_{comp})
	Mpa	b (mm)	h (mm)	Concrete, E_c (MPa)	Steel, E_s (MPa)	MPa
4th mesh layer	31.31	5	50	26,851.29	0	26,851.29
3rd mesh layer	31.31	75	67	26,851.29	0	26,851.29
2nd mesh layer	31.31	75	8	26,851.29	207,735.92	43,209.32
1st mesh layer	31.31	75	25	26,851.29	0	26,851.29

The modulus of elasticity (E) for each layer is calculated according to the condition of the material. Layers of concrete and bamboo reinforcement are calculated using the following Equation. (2) [33].

$$E_e = E_b.V_b + E_c.V_c \quad (2)$$

where E_e = the equivalent elasticity modulus of BRC beam, E_b = elastic modulus of bamboo reinforcement, E_c = modulus of elasticity of concrete, V_b = relative volume of bamboo reinforcement in calculated layers, and V_c = relative volume of concrete in calculated layers. The stress-strain relationship for plane-stress problems has the shape of an equation such as Equation (3).

$$\begin{Bmatrix} \sigma_x \\ \sigma_y \\ \tau_{xy} \end{Bmatrix} = \frac{E}{(1+\nu^2)} \begin{bmatrix} 1 & \nu & 0 \\ \nu & 1 & 0 \\ 0 & 0 & \frac{1-\nu}{2} \end{bmatrix} \begin{Bmatrix} \varepsilon_x \\ \varepsilon_y \\ \gamma_{xy} \end{Bmatrix} \quad (3)$$

where E is the modulus of elasticity and ν is the Poisson's ratio. And the principal stresses in two dimensions are calculated by Equation (4).

$$\sigma_{1,2} = \frac{\sigma_x + \sigma_y}{2} \pm \sqrt{\left(\frac{\sigma_x - \sigma_y}{2}\right)^2 + \tau_{xy}{}^2} = \sigma_{\max} \quad (4)$$

The simulation and steps for preparing a FEM analysis with the Fortran PowerStation 4.0 program [32] are summarized as follows:

Step 1: Discretization of BRC and SRC beam planes with the discretization of triangular elements, the numbering of triangular elements, and the numbering of nodal points as shown in Figures 3(d) and Figure 4.

Step 2: Calculation and collection of geometry and material data, such as the modulus of elasticity of the material (E), Poisson's ratio (ν), etc.

Step 3: Writing a programming language for triangular elements using the Fortran PowerStation 4.0 program according to the constitutive relationships and FEM modeling as shown in the following link: http://bit.ly/2F17w8F.
Step 4: Open the Fortran PowerStation 4.0 program. An example is shown at the following link: http://bit.ly/2MTh22j.
Step 5: Write programming language data (Step 3) in the Fortran PowerStation 4.0 program. Examples can be seen at the following link: http://bit.ly/2ZvZWMU.
Step 6: Input DATA.DAT of BRC beam and SRC beam in the Fortran PowerStation 4.0 program. Input data is displayed at the following links: http://bit.ly/351FPqU and http://bit.ly/2MBqas9. An example of displaying input data is shown on the following link: http://bit.ly/2u2K2xR.
Step 7: Analyze the program until there are no warnings and errors. If there are warnings and errors, check and correct program data and input data.
Step 8: Download stress data. The stress data are shown at the following link: http://bit.ly/2rDPeaI for the stress of BRC beam, and http://bit.ly/2Q4Ihc1 for the stress of the SRC beam. An example of displaying stress data from the Fortran PowerStation 4.0 program is shown at the following link: http://bit.ly/2ZybLCd.
Step 9: Download displacement data. An example of displaying data displacement from the Fortran PowerStation 4.0 program is shown on the following link: http://bit.ly/2Q7j2Wp.
Step 10: Enter stress and displacement data into the Surfer program to obtain contour image data of stress and displacement. Stress and displacement contour image data. are shown in Figures 15–18.

Comment [M13]: Please delete from: "are shown in Figures 15–18."

2.4. Validation of Artificial Neural Networks (ANN)

Artificial Neural Networks (ANN) is a computational system for solving complex problems in civil engineering. In this study, the validation carried out by the Artificial Neural Networks (ANN) method is the validation of the load vs. displacements from laboratory experimental results. The data on the loading and displacement stages of the experimental results were used as input data and target data in this analysis. Previous researchers concluded that Artificial Neural Networks (ANN) can be an alternative in calculating displacement in reinforced concrete beams. Several researchers have used the ANN method for many structural engineering studies, such as predicting the compressive strength of concrete [34], axial strength of composite columns [35], and determination of RC building displacement [36]. Kaczmarek and Szymańska (2016) [37] concluded that the results of calculating displacement in reinforced concrete using ANN proved to be very effective. Abd et al. (2015) [38] concluded that the ANN method is also very good for predicting displacement in concrete beams with a very strong correlation level of 97.27% to the test data. Tuan Ya et al. (2019) [39] used the ANN method to predict displacement in cantilever beams and concluded that the output was very accurate.

The ANN method is currently very popular with researchers in predicting and evaluating the behavior of structures in the field of civil engineering. This is because the ANN method has an advantage in the nonlinear correlation between the input variables presented. Khademi et al. (2017) [40] predicts the compressive strength of concrete at 28 days of age by considering the experimental results, three different models of multiple linear regression (MLR), artificial neural networks (ANN), and adaptive neuro-fuzzy inference system (ANFIS). The results of his research concluded that the ANN and ANFIS models can predict the 28-day concrete compressive strength more accurately and the ANN model can perform better than the ANFIS model in terms of R^2. The ANN and ANFIS models are preferred because the nonlinear correlation between the input variables presented is better. The ANN and ANFIS models have higher accuracy requirements than the multiple linear regression (MLR) model. The accuracy of the prediction is very much dependent on the number of input variables. The greater the number of input parameters, the more accurate the results of the predictor model will be.

Xuan Li et al. (2019) [41] predict the service life of corroded concrete sewer pipes using three data-driven models, namely multiple linear regression (MLR), artificial neural networks (ANN), and adaptive neuro-fuzzy inference system (ANFIS). The one conclusion suggests that the ANN and

ANFIS models perform better than the MLR models for corrosion prediction, with or without considering the interactions between environmental factors.

The ANN data is divided into three different subsets [40], namely (1) Training: at this stage, the subset is trained and studied as occurs in the human brain, where the number of epochs is repeated until an acceptable model accuracy is obtained; (2) Validation: at this stage, the subset shows how well the model is trained, and estimates model properties such as misclassification, mean error for numerical predictors; and (3) Test: at this stage, the subset verifies the performance of the training subset built into the ANN model.

This paper uses even load input data, while the target data is the displacement of the laboratory test results. The distribution of the ANN model data composition consists of training 70%, validation 15%, and testing 15%. ANN architecture on a rectangular beam is shown in Figure 5. The process of implementing input data in the ANN model architecture consists of (1) Input layer, consisting of 1 neuron, namely displacement data variable of experimental results; (2) Hidden layer, consisting of 10 neurons. At this stage, the input layer will forward the data to the hidden layer or the output layer through a set of weights. This weight is a link from each neuron to other neurons in the next layer which will help adjust the ANN structure to the given displacement data pattern using learning. In the learning process, the weights will be updated continuously until one of the numbers of iterations, errors, and processing time has been reached. This is done to adjust the ANN structure to the desired pattern based on certain problems that will be solved using ANN. Weight is known as the independent parameter. During the training process, the weights will be modified to improve the accuracy of the results. The third layer is (3) Output layer, consisting of 1 neuron which is the expected output target, error, and weight. Error is the error rate of the displacement data node of the process carried out, while weight is the weight of the displacement data node with a value ranging between –1 and 1. Then the displacement data resulting from the training process is processed into a graphic image of the load vs. displacement relationship.

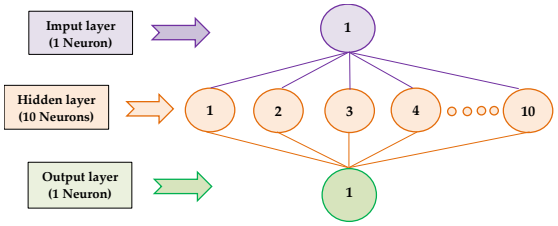

Figure 5. Schematic of Artificial Neural Networks (ANN) model architecture for BRC beam and SRC beam.

3. Results

3.1. Experimental

Table 5 shows the results of theoretical calculations and experiments for BRC and SRC beams. From the theoretical calculation, the BRC beam has an initial crack load of 6.87 kN and an SRC beam of 6.51 kN. The laboratory test results of the BRC beam experienced an initial crack at a load of 7.69 kN and an SRC beam had an initial crack at a load of 10 kN. The average ultimate load of the BRC beam occurs at a load of 31.31 kN or 97.27% of the theoretical collapse load of 32.19 kN. This shows that with the correct treatment of bamboo reinforcement, the BRC beam can reach load capacity according to the results of the theoretical calculations. As is known, the researchers concluded that the ultimate load of BRC beams is very low when compared to the theoretical calculations. Dewi et al. (2017) [42] concluded that the bending capacity of bamboo reinforced concrete beams only reaches 56% of its capacity if the tensile strength of bamboo is full. Nathan (2014) [43] concluded that the flexural capacity of reinforced concrete beams only reaches 29% to 39% of the beam capacity steel-reinforced concrete with the same width and reinforcement dimensions. Khare (2005) [44]

concluded that the flexural capacity of reinforced concrete beams is only 35% of steel-reinforced concrete beams at the same strength level.

SRC beams reach a collapse load of 24 kN or almost approaching the theoretical collapse load of 24.12 kN. This shows that the adhesion strength of steel-reinforcement with concrete is higher. Figures 6 and 7 show that the relationship of the load vs. displacement of the BRC beam and the SRC beam is different. The SRC beam shows the regions of the elastic limit, elastoplastic limit, and plastic limit. Meanwhile, the BRC beam only shows the plastic limit point or the ultimate load point. This shows that the behavior of reinforced concrete beams is very much determined by the properties and characteristics of the materials used.

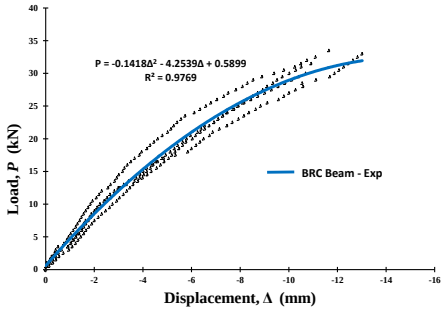

Figure 6. The relationship of load vs. displacement of BRC beam of experimental results.

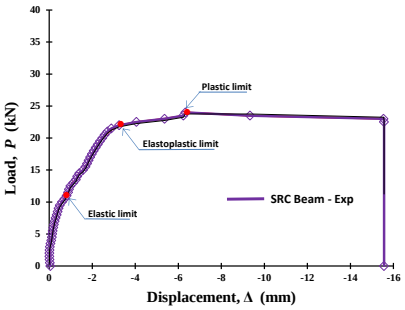

Figure 7. The relationship of load vs. displacement of SRC beam of experimental results.

Mechanical properties and characteristics of steel and bamboo materials are the dominant factors in the behavior model of the load and displacement relationship [6]. The difference between the stress and strain relationship patterns of bamboo and steel is in the position of the melting point and the fracture stress. Steel material shows a clear melting point, while bamboo reinforcement does not show a clear melting point. However, after the fracture stress, the relationship pattern of the stress-strain relationship tends to return to zero. This shows that bamboo has good elastic properties [7].

Table 5. Results of theoretical calculations and experimental for the load capacity of BRC beams and SRC beams.

Specimens	Sample no	Theoretical Calculations		Flexural Test Results			
		First Crack Load (kN)	Ultimate Load (kN)	First Crack Load, P_{cr} (kN)	Failure Load, P_{ult} (kN)	Displacement at Failure (mm)	P_{cr}/P_{ult} (%)
(a) BRC-1	1	6.90	32.20	8.50	31.50	10.92	26.98

	2			8.00	29.00	11.90	27.59
(b) BRC-2	3			7.00	31.00	13.02	22.58
	4			7.50	33.00	12.18	22.73
(c) BRC-3	5			8.00	33.50	14.69	23.88
	6			7.50	33.00	9.32	22.73
(d) BRC-4	7			7.50	29.50	7.61	25.42
	8			7.50	30.00	10.69	25.00
Average:				7.69	31.31		24.61
(e) SRC	9	6.50	24.20	10.00	24.00	6.33	41.57

3.2. Validation with the ANN Method

The load vs. displacement relationship data from the experimental results is the basis used for the train and the network. Neural networks are designed by determining their structure experimentally. The data that trains the artificial neural network is the input, and the ability to reproduce the training pattern is tested. Convergence analysis was carried out to determine the optimal number of neurons in the hidden layer of ANN. Excessive neurons reduce the computational performance of ANN, whereas a lack of neurons causes difficulties in characterizing the input-output relationship. As suggested by Caudill and Mishra et al. (2019) [45], the upper limit of the number of neurons in the hidden layer is twice the number of inputs plus 1. After the number of neurons in the hidden layer is reached, the MSE, RMSE, and R^2 observations are stopped and no increase is assumed significant. The artificial neural network architecture used in this paper: IHO: 1-10-1 [Input-Hidden-Output] means that this artificial neural network consists of 1 input neuron, one hidden layer with 10 neurons, and 1 output neuron (predictive values of the load vs. displacement relationship).

Table 6 presents the performance results of ANN architecture for ten simulations. The process which has the lowest MSE is selected for comparison with experimental data. Figures 8–12 illustrate the prediction of the load vs. displacement of the BRC and SRC beams obtained when using the ANN model after training and when using the data obtained experimentally for training data, validation data, test data, and all data. Figures 8–12 shows the correlation between the value of the BRC beam and the SRC beam relationship obtained in the laboratory and the load vs. displacement values obtained using ANN analysis. The convergence of the position of the point with the line y = x indicates the identification of values with very high accuracy. The correlation value of laboratory data using ANN shows an average value of *R* Square of 0.999. This indicates that the two results are consistent. The prediction results of the ANN method show that the percentage of errors is very small, with a maximum error of 0.26%. Overall, the comparison of experimental data with the predicted results of the ANN method shows an error of not more than 1%. From the data from the two analyses and the load vs. displacement relationship pattern, it can be concluded that the stiffness of the BRC beam has similarities.

Table 6. The validation results of the relationship load vs. displacement using the ANN method.

Specimens	The Correlation Coefficient (*R*)			Mean Square Error (MSE)		
	Training	Validation	Testing	Training	Validation	Testing
BRC-1	1.0000	0.9999	0.9997	0.0004	0.0011	0.0110
BRC-2	0.9999	0.9997	0.9999	0.0038	0.0276	0.0048
BRC-3	0.9998	0.9999	0.9993	0.0034	0.0075	0.0152
BRC-4	1.0000	1.0000	1.0000	0.0001	0.0009	0.0010
SRC	1.0000	1.0000	0.9997	0.0001	0.0027	0.0006

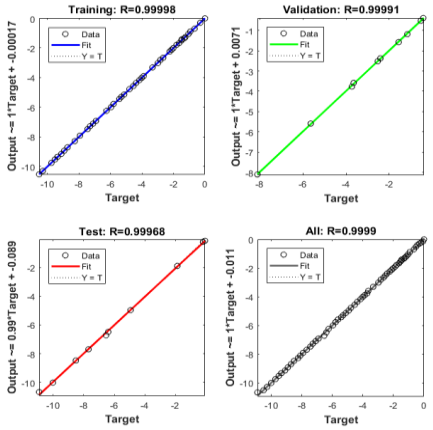

Figure 8. Prediction of the load vs. displacement relationship using ANN and using experimental observation for the training, validation, testing, and all datasets (BRC-1).

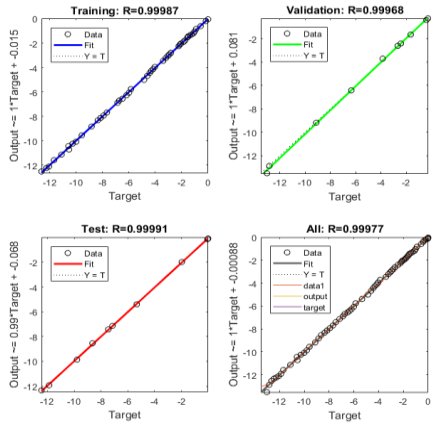

Figure 9. Prediction of the load vs. displacement relationship using ANN and using experimental observation for the training, validation, testing, and all datasets (BRC-2).

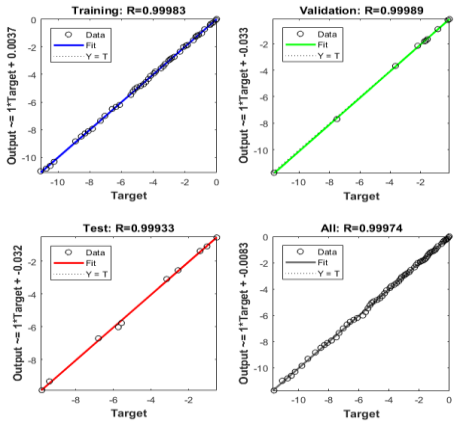

Figure 10. Prediction of the load vs. displacement relationship using ANN and using experimental observation for the training, validation, testing, and all datasets (BRC-3).

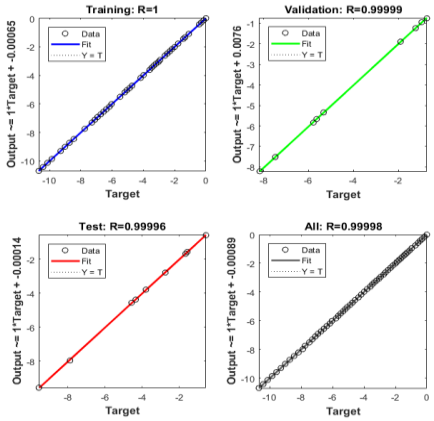

Figure 11. Prediction of the load vs. displacement relationship using ANN and using experimental observation for the training, validation, testing, and all datasets (BRC-4).

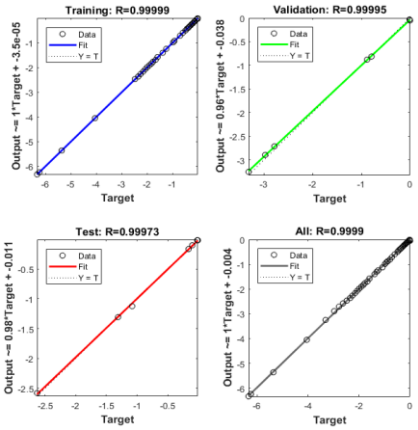

Figure 12. Prediction of the load vs. displacement relationship using ANN and using experimental observation for the training, validation, testing, and all datasets (SRC).

The data merger of ANN analysis results from each BRC beam specimen into a load vs. displacement relationship. The merger is done to determine the suitability of the load vs. displacement relationship model through the R^2 parameter. From the results of the regression analysis, it is found that R^2 = 0.9771, or almost close to 1. This shows that the model has high suitability, as shown in Figure 13. Figure 13 illustrates the load vs. displacement relationship for all BRC beam typologies from ANN analysis.

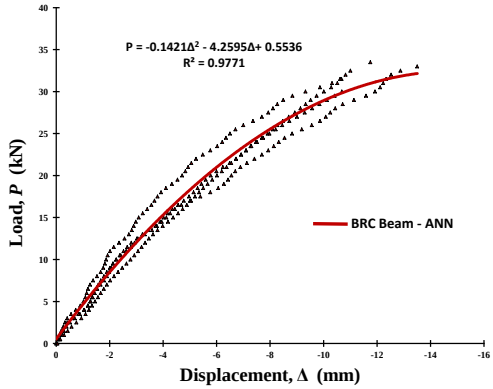

Figure 13. The relationship of load vs. displacement of BRC beam of ANN results.

3.3. Validation with the Finite Element Method

Validation of the relationship of load vs. displacement with the finite element method is done by inputting the geometry of the cross-section, load data, modulus of elasticity (E) per layer, and Poisson's ratio (υ). The load vs. displacement relationship diagram of the experimental results as shown in Figures 6 and 7 is used as a guide for the stages of the analysis process using the finite element method. And the cross-sectional stiffness input via the per-layer modulus of elasticity (E) is shown in Tables 7 and 8. The analysis execution using the finite element method uses the Fortran PowerStation 4.0 program. The process of calculating displacement and stress with the Fortran PowerStation 4.0 program is carried out in stages according to the loading and stiffness stages per layer from the beam's elastic condition, initial crack, elastoplastic, and plastic conditions until the beam collapses. The displacement data resulting from the finite element method is processed into a load vs. displacement relationship as shown in Figure 14. The displacement of the load ultimate is shown in Figure 15 for BRC beams and Figure 16 for SRC beams. The stress contours at the time of the load collapse are shown in Figure 17 for BRC beams and Figure 18 for SRC beams.

Comment [CH14]: Please replace with "**The displacement contours when the ultimate load are shown in Figure 15 for BRC beams and Figure 16 for SRC beams**".

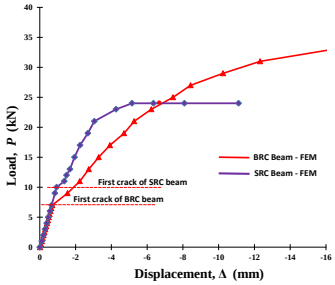

Figure 14. The relationship of load vs. displacement of BRC beam of finite element method (FEM) results.

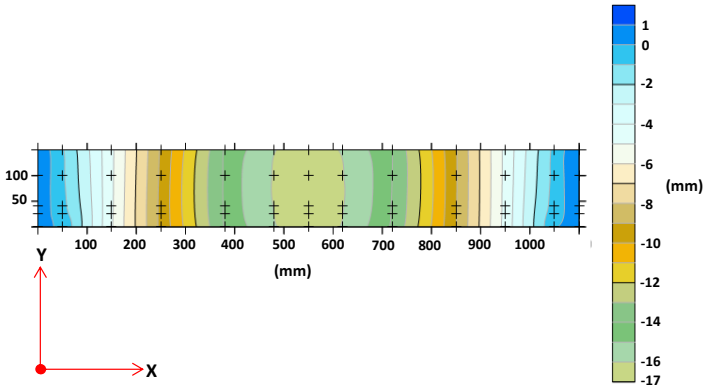

Figure 15. The displacement contour of Y-direction of BRC beam.

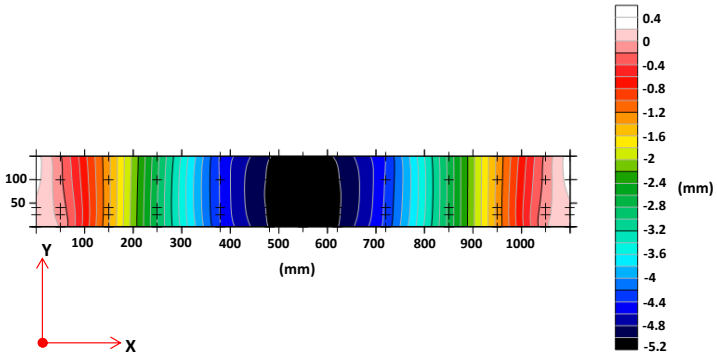

Figure 16. The displacement contour of Y-direction of SRC beam.

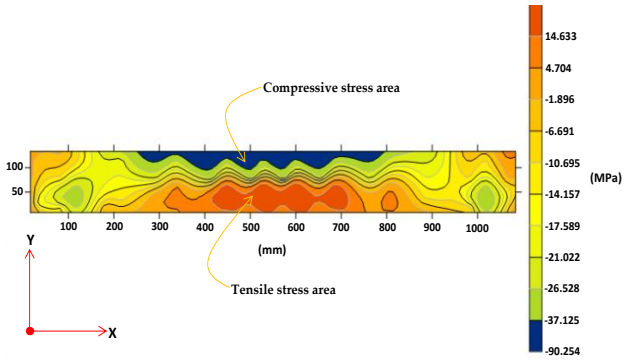

Figure 17. The stress contour of X-direction of BRC beam.

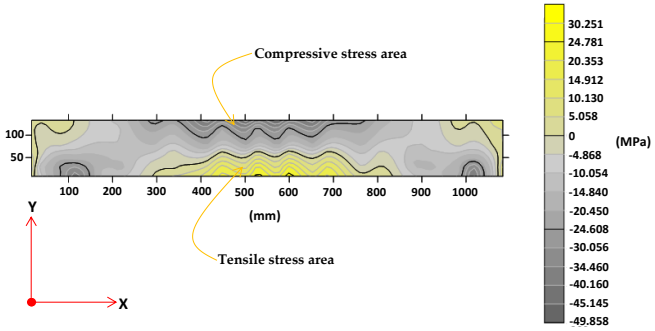

Figure 18. The stress contour of X-direction of SRC beam.

Table 7. The modulus of elasticity for each layer of the BRC beam in the non-linear phase.

Layer Number	Modulus of Elasticity (*E*) of the BRC Beam													
	Elastic Condition	Plastic Conditions with Gradual Loads												
	0–8.5 kN	9 kN	11 kN	13 kN	15 kN	17 kN	19 kN	21 kN	23 kN	25 kN	27 kN	29 kN	31 kN	33 kN
4th mesh layer	26851.29	16,110.77	16,110.77	16,110.77	16,110.77	16,110.77	16,110.77	16,110.77	16,110.77	16,110.77	12,083.08	11,277.54	11,277.54	8592.41
3th mesh layer	26851.29	16,110.77	16,110.77	16,110.77	16,110.77	16,110.77	16,110.77	16,110.77	16,110.77	1208.31	10,740.52	9397.95	9397.95	7518.36
2nd mesh layer	23140.89	13,884.53	11,570.44	11,570.44	11,570.44	11,570.44	10,413.40	10,413.40	10,413.40	10,413.40	6942.27	6942.27	6942.27	5553.81
1st mesh layer	26851.29	13,425.65	11,814.57	10,203.49	8323.90	6712.82	5101.75	5101.75	5101.75	3759.18	3222.16	2685.13	1611.08	1329.14

Table 8. The modulus of elasticity for each layer of the SRC beam in the non-linear phase.

Layer Number	Modulus of Elasticity (*E*) of the SRC Beam										
	Elastic Condition	Plastic Conditions with Gradual Loads									
	0–9 kN	10 kN	11 kN	12 kN	13 kN	15 kN	17 kN	19 KN	21 KN	23 kN	24 kN
4th mesh layer	26,851.29	26,851.29	20,138.47	20,138.47	20,138.47	20,138.47	20,138.47	18,795.90	18,795.90	13,425.65	11,411.80
3th mesh layer	26,851.29	26,851.29	20,138.47	20,138.47	18,795.90	18,795.90	18,795.90	17,453.34	17,453.34	13,425.65	11,411.80
2nd mesh layer	43,209.32	43,209.32	30,586.93	30,586.93	28,547.80	28,547.80	26,508.67	26,508.67	24,469.54	20,391,29	17,332.60
1st mesh layer	26,851.29	26,851.29	20,138.47	20,138.47	18,795.90	18,795.90	17,453.34	16,110.77	14,768.21	13,425.65	12,083.08

4. Discussion

Merging is carried out on the load vs. displacement relationship diagram from the experimental results, ANN analysis, and finite element method (FEM) analysis. Figure 19 shows the combined load vs. displacement diagram of the ANN analysis results with the experimental results. Figure 19 shows that the load vs. displacement relationship diagram the two analyses results are very coincided or show high suitability. However, at a load of approximately 90% of the collapse load, the load vs. displacement relationship diagram shows different behavior. Figure 20 shows the combined load vs. displacement diagram of the experimental results, ANN analysis, and the results of the finite element method analysis. Figure 19 shows that the artificial neural networks (ANN) model has a higher R^2 value when compared to the R^2 value of the multiple linear regression model (MLR). ANN analysis has better predictive accuracy. This is the same as the conclusion of 2 researchers, namely Khademi et al. (2017) [40], who concluded that the ANN model has higher accuracy than the multiple linear regression (MLR) model, and Xuan Li et al. (2019) [41], who concluded that the ANN model performs better than the MLR models with or without considering the interactions between factors. The accuracy of the prediction is very much dependent on the number of input variables. The greater the number of input parameters, the more accurate the results of the predicted model.

The diagram of the relationship between load and displacement of the BRC beam from FEM analysis and experimental results shows the difference in elastic conditions or until the initial crack occurs. The experimental results showed negative differences with the results of the FEM analysis. This shows the influence of the nature and characteristics of bamboo. The parts of bamboo stems have a non-uniform or uncertain modulus of elasticity. Tensile strength and modulus of elasticity of bamboo tested in the laboratory are sometimes different from bamboo which is used as beam reinforcement. As is known, bamboo trees from base to tip have different tensile strength and fiber density. Meanwhile, the load vs. displacement diagram of the SRC beam experiment results has a positive difference with the results of the FEM analysis when the elastic condition occurs or until the initial crack occurs. Positive differences can be ignored, in the sense that the quality of the steel used is better than the quality of steel tested in the laboratory. However, in this study, the analysis of stiffness reduction in BRC and SRC beams was focused after the beam experienced an initial crack or non-linear phase.

Comment [CH15]: Please replace with "**Meanwhile, the relationship diagram of load vs. displacement of the SRC beam experiment results is positively different from the results of the FEM analysis when the elastic condition or until the initial crack occurs**".

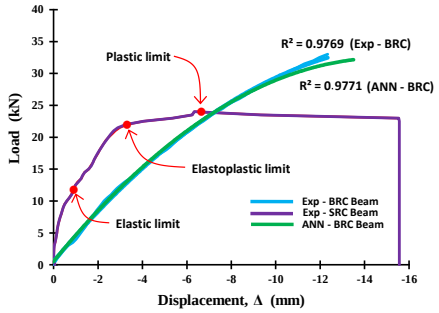

Figure 19. The combined of the load vs. displacement relationship of BRC beam of the experimental results and ANN analysis.

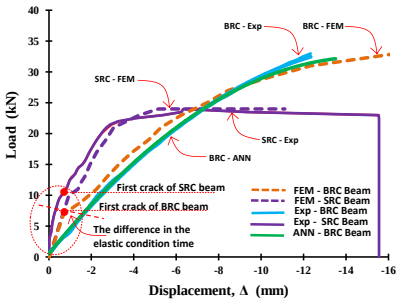

Figure 20. The combined of the load vs. displacement relationship of BRC beam and SRC beam of the experimental results, ANN analysis, and FEM.

Figure 20 shows that inelastic conditions there is a difference in stiffness between the two types of beams. The stiffness of bamboo reinforced concrete beams (BRC) is lower than the stiffness of steel-reinforced concrete beams (SRC). This difference occurs not due to reduced cross-section inertia or I_g of cross-sectional reduction, but due to the nature of the material used. This is because the BRC beam uses bamboo reinforcing material, which has high elastic and resilience properties. BRC beams with bamboo reinforcement will be able to accept high impact loads without causing over stress at the elastic limit, even though displacement has occurred. This indicates that the energy absorbed during loading is stored and released if the material is not loaded. Meanwhile, the SRC beam uses steel material that has high stiffness and toughness, so that the SRC beam in the service load range or elastic conditions does not experience excessive displacement or deformation. Beams that use materials with high stiffness and toughness will be able to withstand high impact loads or shock loads. If the SRC beam gets an impact load, then some of the energy is absorbed and some of the energy is transferred.

In the non-linear phase or after initial cracking, the beam stiffness changes from the full-sectional flexural stiffness, E_cI_g, to the effective bending stiffness, E_cI_{eff}. In the non-linear phase, the stiffness of the beam section continues to decrease with increasing loads, moments, and cracks. The area of the beam section continues to decrease with increasing cracks and automatically causes the beam section stiffness (E_cI_g) to decrease. As shown in Table 6 and Figure 21, the stiffness of the BRC beam decreases after the initial cracking occurs as the increasing loading stage is applied. The increase in load causes the flexural moment to increase, the displacement increases, and the crack propagation continues to spread towards the compressed block of the beam cross-section. The crack propagation from 1st mesh layer to the 2nd mesh layer onwards runs linearly with reduced cross-sectional stiffness from the lower fiber of the cross-section tensile block to the upper fiber of the compressive block of the beam cross-section. The increase in crack propagation towards the compressive block of cross-section causes the neutral line to change. Chunyu Fu et al. (2018) [13] concluded that the presence of cracks causes a nonlinear stress distribution along the beam cross-section, which changes the neutral axis of the cross-section and further affects the stiffness of the beam. Figure 21 shows that the stiffness of the BRC beam cross-section decreases from the initial crack until the beam collapses. The stiffness of BRC beams is reduced by 50% after initial cracking to 95% at collapse. The stiffness reduction goes step by step according to the moment (M_a) applied to the beam. Sang-Whan Han et al. (2009) [4] revealed that the stiffness reduction factor was significantly affected by the amount of moment or the applied load, while the stiffness reduction factor did not differ from the amount of reinforcement. The decrease in the moment of inertia of the full cross-sectional Ig of the BRC beam ranged from $0.5I_g$–$0.05I_g$ for the elastoplastic and plastic regions. Meanwhile, ACI-318M-14 [5] recommends the stiffness of the beam cross-section for elastic analysis in the non-linear phase of $0.5I_g$–$0.25I_g$. The difference in the value of the reduction in the stiffness of the cross-section at collapse correlates with the differences in the properties and characteristics of the material used as beam reinforcement. Bamboo reinforced concrete beams (BRC) exhibit high displacement behavior, but once the collapse load is reached and gradually released,

displacement tends to return to zero. It is linear with its elastic properties and the stress vs. strain relationship behavior of bamboo.

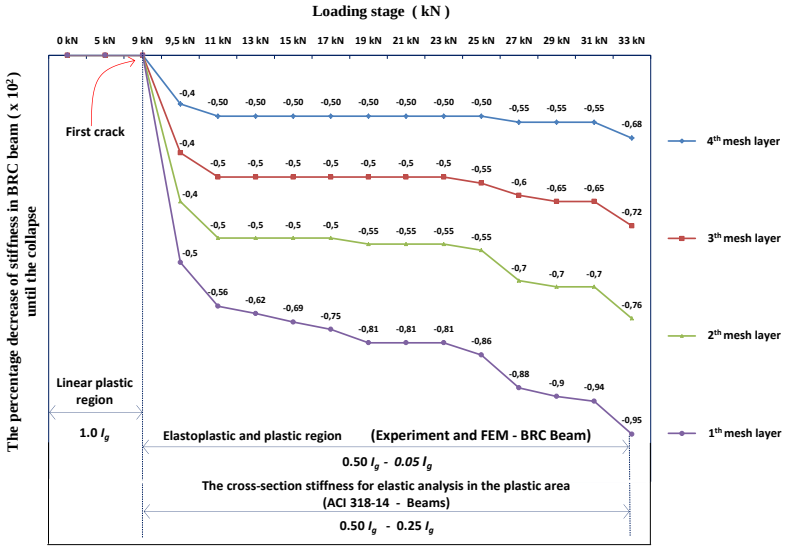

Figure 21. Decreased stiffness of BRC beam cross-section in the span middle.

Table 7 and Figure 22 show a decrease in stiffness or a decrease in the moment of inertia of the SRC beam cross-section. Stiffness decreases after initial cracking as the applied load increases. Figure 22 shows that the cross-sectional stiffness of the SRC beam decreases from the initial crack until the beam collapses. The stiffness of the SRC beam was reduced by 25% after initial cracking to 60% at collapse. The decrease in the moment of inertia full cross-section (I_g) for SRC beams ranged from $0.75I_g$–$0.40I_g$ for the elastoplastic and plastic regions. Meanwhile, ACI-318M-14 [5] recommends the cross-sectional stiffness of reinforced concrete beams for elastic analysis in the non-linear phase of $0.5I_g$–$0.25I_g$. The difference in the value of the reduction in the cross-sectional stiffness of the SRC beam with the ACI-318M-14 [5] requirements is due to the beam cross-section reinforcement method, namely the SRC beam in this study using a single reinforcement method. SRC beam with single reinforcement shows that when the steel reinforcement undergoes second melting and the moment of inertia of the cross-section is still around 40%, the steel reinforcement is not able to withstand the tensile stress that occurs so that the neutral line of the cross-section continues to shift upwards towards the upper fiber of the compression block of the cross-section. Meanwhile, BRC beams with bamboo reinforcement have good elastic properties, where after the ultimate load is reached, the large displacement shrinks back to near-zero or the beam returns flat [7], as shown in the video at the following link: https://goo.gl/6AVWmP. Although the stiffness or inertia of the BRC beam cross-section is still around 5%, bamboo reinforcement is still able to withstand the tensile stress that occurs, as stated by Ghavami (2005) [24] that bamboo has high tensile strength. If we control with the crack pattern, the crack lines on the BRC beam majority stop below the cross-section neutral line, while the crack lines on the SRC beam tend to continue to propagate upwards towards the upper fibers of the compressive block of the beam cross-section, as shown in Figures 23 and 24. And if we look at Figures 17 and 18, the tensile stress contour of the BRC beam has a wider zone and spreads to the side when compared to the SRC beam.

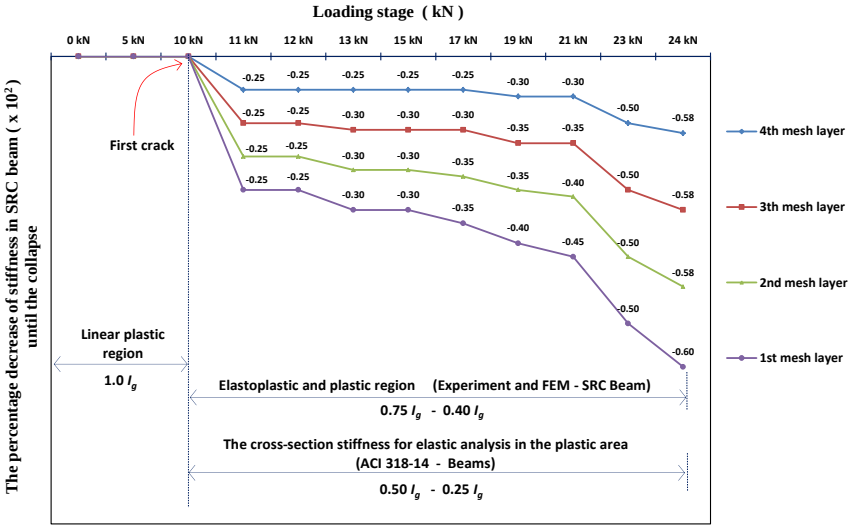

Figure 22. Decreased stiffness of SRC beam cross-section in the span middle.

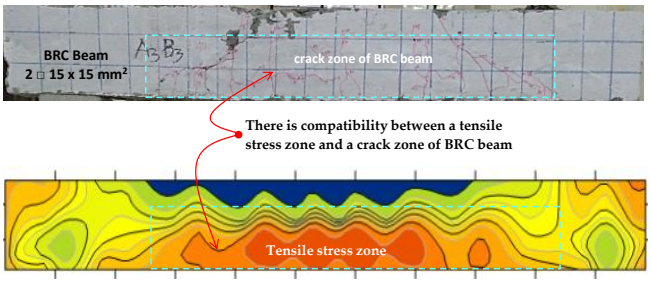

Figure 23. The crack pattern and tensile stress zone of BRC beam.

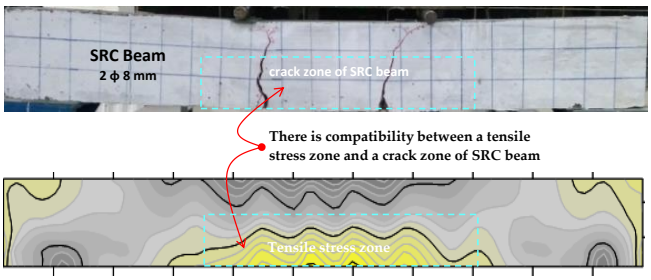

Figure 24. The crack pattern and tensile stress zone of SRC beam.

Figures 25 and 26 show the relationship between the stiffness reduction factor (ϕ_K) and the M_a/M_{cr} of the BRC beam and the SRC beam. The stiffness reduction factor (ϕ_K) is the ratio of the moment of inertia of the effective section (I_e) divided by the moment of inertia of the cross-section (I_g). The stiffness reduction factor (ϕ_K) is significantly influenced by the applied moment level. The equation of the beam stiffness reduction factor is related to the ratio between the applied moment and an initial crack moment or M_a/M_{cr}. The equation for the stiffness reduction factor is shown in Equation (5) or Equation (6) for a BRC beam. The stiffness reduction factor equation for the SRC beam is shown in Equation (7) or Equation (8). Figure 27 shows a comparison of the relationship between the stiffness reduction factor and the M_a/M_{cr} of the BRC beam and SRC beam. The diagram of the relationship between the stiffness reduction factor and M_a/M_{cr} shows that the SRC beam has a

smaller stiffness reduction factor than the BRC beam in the non-linear phase. However, the SRC beam shows a collapse at the moment of inertia of the effective cross-section (I_e), which is relatively still large when compared to BRC beams. BRC beams collapse at the effective cross-section inertia of about 5%, and SRC beams collapse at the effective section inertia of about 40%. The alternative of moments of inertia from various sources is shown in Table 9.

$$\phi_K = 0.646 - 0.1023\left(\frac{M_a}{M_{cr}}\right) \quad (5)$$

$$\frac{I_e}{I_g} = 0.646 - 0.1023\left(\frac{M_a}{M_{cr}}\right) \quad (6)$$

$$\phi_K = 0.697 - 0.1472\left(\frac{M_a}{M_{cr}}\right) \quad (7)$$

$$\frac{I_e}{I_g} = 0.697 - 0.1472\left(\frac{M_a}{M_{cr}}\right) \quad (8)$$

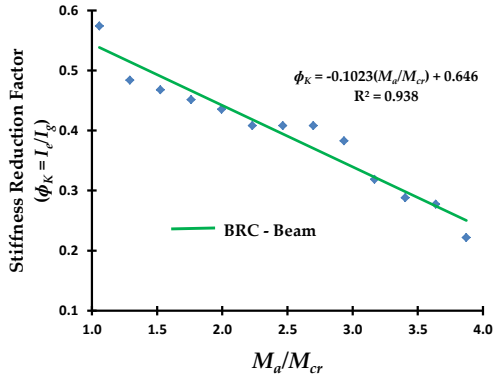

Figure 25. The relationship of the stiffness reduction factor (ϕ_K) and the M_a/M_{cr} of the BRC beam.

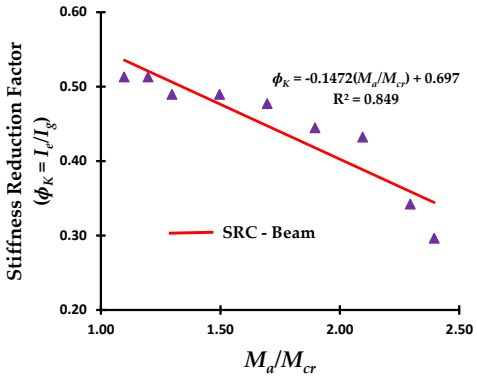

Figure 26. The relationship of the stiffness reduction factor (ϕ_K) and the M_a/M_{cr} of the SRC beam.

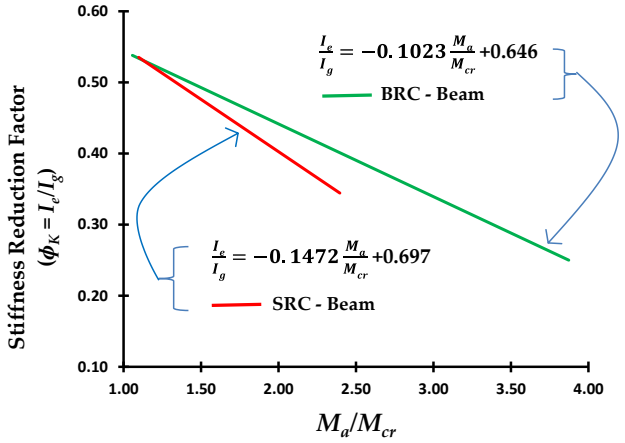

Figure 27. Comparison of the relationship of the stiffness reduction factor (ϕ_K) and the M_a/M_{cr} of the BRC beam and SRC beam.

Table 9. The alternative value of *I* for elastic analysis from various sources.

Source and Information	Alternative value of *I* for elastic analysis
ACI-318M-14 [5]	$0.25I_g$–$0.5I_g$
FEMA 356-2000 [46]	$0.5\ EI_g$–$0.8EI_g$
New Zealand Code [47]	$0.35I_g$
Paulay and Priestley, 1992 [48]	$0.30I_g$–$0.50I_g$
In this research (singly reinforced beam)	
- BRC Beam	$0.05I_g$–$0.5I_g$
- SRC Beam	$0.4I_g$–$0.75I_g$

5. Conclusions

The relationship pattern of load vs. displacement reflects the stiffness pattern of structural elements. The properties and characteristics of the material in the reinforcing concrete elements have a dominant influence on the relationship pattern of the load vs. displacement of reinforced concrete elements. Bamboo reinforced concrete beams (BRC) have a different load vs. displacement relationship pattern when compared to steel reinforced concrete beams (SRC). BRC beams have elastic properties and high resilience properties that can accept high impact loads without causing over stress at the elastic limit, even though displacement has occurred. While SRC beams have high stiffness and toughness so that SRC beams are not subject to excessive displacement or deformation at service load ranges or elastic conditions.

Results of the validation of the relationship pattern of the load vs. displacement of the BRC beams shows that the ANN model has a higher R^2 value when compared to the R^2 value of the MLR model. ANN analysis has a higher prediction accuracy. The accuracy of the prediction depends very much on the number of input variables. The greater the number of input parameters, the more accurate the prediction model results.

The cross-sectional stiffness of BRC beams is reduced by 50% after initial cracking and reduced by 95% at collapse. The cross-sectional stiffness of the SRC beam was reduced by 25% after initial cracking and reduced by 60% at collapse. The reduction in stiffness is significantly affected by the amount of applied moment (M_a) or the load applied that caused cracks and a reduction in the moment of inertia of the cross-section.

The initial decrease in cross-sectional stiffness of BRC beams occurs at a load of about 24% of the ultimate load and BRC beams occur at loads of about 40% ultimate load. BRC beam collapse occurs when the moment of inertia of the effective cross-section (I_e) is 5%, while the SRC beam

collapse occurs when the moment of inertia of the effective cross-section (I_e) is 40%. The reduction in stiffness in the cross-section of the beam in the non-linear phase ranged from $0.5I_g$–$0.05I_g$ for BRC beams, and $0.75I_g$–$0.40I_g$ for SRC beams. ACI-318M-14 standard recommends the cross-sectional stiffness of reinforced concrete beams for elastic analysis in the non-linear phase of $0.5I_g$–$0.25I_g$.

The SRC beams have a smaller stiffness reduction factor (ϕ_K) than BRC beams in the non-linear phase. However, the SRC beam shows a collapse at the moment of inertia of the effective cross-section (I_e), which is relatively large when compared to BRC beams.

Author Contributions:

Comment [M16]: There is no co-author. The author is the first author and the corresponding author. I hope this "Author Contributions" item is removed.

Funding: APC financing entirely by the DPRM Republic of Indonesia and LPPM of the University of Muhammadiyah Jember, Indonesia.

Acknowledgments: My gratitude goes to the LPPM of the Muhammadiyah University of Jember, Indonesia, and DPRM of the Republic of Indonesia as the funder of this research and APC.

Conflicts of Interest: The authors declare no conflicts of interest.

References

1. Pandey, K.K.; Ramakantha, V.; Chauhan, S.S.; Kumar, A.A. *Wood is Good*; Springer: Singapore, 2017.
2. Mohammadabadi, M.; Jarvis, J.; Yadama, V.; Cofer, W. Predictive Models for Elastic Bending Behavior of a Wood Composite Sandwich Panel. *Forests* **2020**, *11*, 624.
3. Ministry of Environment and Forestry of the Republic of Indonesia. Memanfaatkan Bambu sebagai Salah Satu Potensi Hutan Rakyat. 18 October 2018**.** Available online: https://www.menlhk.go.id/site/single_post/1444 (accessed on 24 October 2020).
4. Han, S.W.; Park, Y.M.; Kee, S.H. Stiffness Reduction Factor for Flat Slab Structures under Lateral Loads. *J. Struct. Eng.* **2009**, *135*, 743.
5. ACI Committee 318 Standard. Building Code Requirements for Structural Concrete; American Concrete Institute, Farmington Hills, Michigan, 2014.
6. Gunasti, A.; Dewi, I.C.; Dasuki, M.; Ariyani, S.; Mahmudi, I.; Abadi, T.; Rahman, M.; Hidayatullah, S.; Nilogiri, A.; Galuh, S.D.; et al. The Prediction of Stiffness of Bamboo-Reinforced Concrete Beams Using Experiment Data and Artificial Neural Networks (ANNs). *Crystals* **2020**, *10*, 757.
7. Muhtar; Dewi, S.M.; Wisnumurti; Munawir, A. Enhancing bamboo reinforcement using a hose-clamp to increase bond-stress and slip resistance. *J. Build. Eng.* **2019**, *26*, 100896.
8. Muhtar; Dewi, S.M.; Wisnumurti; Munawir, A. The flexural behavior model of bamboo reinforced concrete beams using a hose clamp. *Proc. Mater. Sci. Eng. Chem*. **2019**, *276*, 1033.
9. Zhang, K.; Zhang, J.; Jin, W.; Mao, J.; Long, J. Stiffness degradation for the fatigue of reinforced concrete beams after electrochemical rehabilitation. *Constr. Build. Mater.* **2020**, *260*, 120455.
10. Salam, A.S.A.; Debra, L.F. Use of negative stiffness in failure analysis of concrete beams. *Eng. Struct.* **2016**, *126*, 187–199.
11. Hu, H.S.; Nie, J.G.; Wang, Y.H. Effective stiffness of rectangular concrete-filled steel tubular members Hong-Song. *J. Constr. Steel Res.* **2016**, *116*, 233–246.
12. Patel, K.A.; Bhardwaj, A.; Chaudhary, S.; Nagpal, A. Explicit expression for effective moment of inertia of RC beams. *Lat. Am. J. Solids Struct.* **2015**, *12*, 542–560.
13. Fu, C.; Wang, Y.; Tong, D. Stiffness Estimation of Cracked Beams Based on Nonlinear Stress Distributions Near the Crack. *Math. Probl. Eng.* **2018**, *2018*, 1–12.
14. Pique, J.R.; Burgos, M. Effective rigidity of reinforced concrete elements in seismic analysis and design. In Proceedings of the 14 World Conference on Earthquake Engineering, Beijing, China, 12–17 October 2008.
15. Akmaluddin; Pathurahman. Effective Moment of Inertia Approach for Predicting Displacement of Concrete Beams Reinforced with Twisted Bamboo Cables. *Int. J. Civ. Environ. Eng. IJCEE-IJENS* **2012**, *12*, 6–13.
16. Kalkan, İ. Displacement Prediction for Reinforced Concrete Beams through Different Effective Moment of Inertia Expressions. *Int. J. Eng. Res. Dev.* **2013**, *5*, 1.
17. Fu, C.; Tong, D.; Wang, Y. Assessing the Instantaneous Stiffness of Cracked Reinforced Concrete Beams Based on a Gradual Change in Strain Distributions. *Adv. Mater. Sci. Eng.* **2020**, *2020*, 1–10.

Comment [M17]: American Concrete Institute, Farmington Hills, Michigan.

18. Feng, X.; Shen, M.; Sun, C.; Chen, J.; Luo, P. Research on flexural stiffness reduction factor of the reinforced concrete column with equiaxial shaped section. In Proceedings of the 13th COTA International Conference of Transportation Professionals (CICTP 2013), Shenzhen, China, 13-16 August 2013; pp. 168–174.
19. Muhtar; Dewi, S.M.; Wisnumurti; Munawir, A. The stiffness and cracked pattern of bamboo reinforced concrete beams using a hose clamp. *Int. J. Civ. Eng. Technol.* **2018**, *9*, 273–284.
20. Agarwal, A.; Nanda, B.; Maity, D. Experimental investigation on chemically treated bamboo reinforced concrete beams and columns. *Constr. Build. Mater.* **2014**, *71*, 610–617.
21. Muhtar. Experimental data from strengthening bamboo reinforcement using adhesives and hose-clamps. *Data Brief* **2019**, *27*, 104827.
22. Rahman, M.M.; Rashid, M.H.; Hossain, M.A.; Hasan, M.T.; Hasan, M.K. Performance evaluation of bamboo reinforced concrete beam. *Int. J. Eng. Technol. IJET-IJENS* **2011**, *11*, 113–118.
23. Muhtar. Precast Bridges of Bamboo Reinforced Concrete in Disadvantaged Village Areas in Indonesia. *Appl. Sci.* **2020**, *10*, 7158.
24. Ghavami, K. Bamboo as reinforcement in structural concrete elements. *Cem. Concr. Compos.* **2005**, *27*, 637–649.
25. Javadian, A.; Wielopolski, M.; Smith, I.F.C.; Hebel, D.E. Bond-behavior study of newly developed bamboo-composite reinforcement in concrete. *Constr. Build. Mater.* **2016**, *122*, 110–117.
26. Muhtar, M.; Dewi, S.; Wisnumurti; Munawir, A. Bond-slip improvement of bamboo reinforcement in the concrete beam using hose clamps. In Proceedings of the 2nd International Multidisciplinary Conference, Jakarta, Indonesia, 15 November 2016; pp. 385–393.
27. Gunasti, A.; Manggala, A.S.; Nusant, A.F.P.; Nilogiri, A. Effect of Reinforcement Details on Precast Bridge Frames of Bamboo Reinforced Concrete to Load Capacity and Crack Patterns. *Int. J. Eng. Res. Technol.* **2020**, *13*, 631–636.
28. Muhtar. Cracked Pattern of Bamboo Reinforced Concrete Beams Using Double Reinforcement with the Strengthening on Tensile Reinforcement. *Int. J. Eng. Res. Technol.* **2020**, *13*, 608–612.
29. ASTM C 39 Standard. *Standard Test Method for Compressive Strength of Cylindrical Concrete Specimens*; ASTM International, West Conshohocken, PA, USA, 2003.
30. PT SIKA Indonesia. Sikadur®-752. 02, 2-3. 2016. Available online: https://www.scribd.com/document/374071630/Sikadur-752 (accessed on 24 October 2020).
31. ASTM C 09 Standard. Standard Test Method for Flexural Strength of Concrete (Using Simple Beam with Third-Point Loading); ASTM International, West Conshohocken, PA, USA, 2002.
32. Muhtar. Numerical validation data of tensile stress zones and crack zones in bamboo reinforced concrete beams using the Fortran PowerStation 4.0 program. *Data Brief* **2020**, *29*, 105332.
33. Avram, C.; Facaoaru, I.; Filimon, I.; Mirsu, O.; Tertea, I. *Concrete Strength and Strain*; Elsvier S.P. Company, New York, Developments in Civil Engineering 3; 1981.
34. Naderpour, H.; Kheyroddin, A.; Amiri, G.G. Prediction of FRP-confined compressive strength of concrete using artificial neural networks. *Compos. Struct.* **2010**, *92*, 2817–2829.
35. Ahmadi, M.; Naderpour, H.; Kheyroddin, A. Utilization of artificial neural networks to prediction of the capacity of CCFT short columns subject to short term axial load. *Arch. Civ. Mech. Eng.* **2014**, *14*, 510–517.
36. Khademi, F.; Akbari, M.; Nikoo, M. Displacement determination of concrete reinforcement building using data-driven models. *Int. J. Sustain. Built Environ.* **2017**, *6*, 400–411.
37. Kaczmarek, M.; Szymanska, A. Application of Artificial Neural Networks to Predict the Displacements of Reinforced Concrete Beams. *Studia Geotech. Mech.* **2016**, *38*, 37–46.
38. Abd, A.M.; Salman, W.D.; Ahmed, Q.W. ANN, and Statistical Modelling to Predict the Displacement of Continuous Reinforced Concrete. *Diyala J. Eng. Sci.* **2015**, 08, 134–143.
39. Ya Tuan, T.M.Y.S.; Alebrahim, R.; Fitri, N.; Alebrahim. M. Analysis of Cantilever Beam Displacement under Uniformly Distributed Load using Artificial Neural Networks. In Proceedings of the MATEC Web of Conferences, Los Angeles, USA, 3–4 February 2018.
40. Khademi, F.; Akbari, M.; Mohammadmehdi, S.; Nikoo, M. Multiple linear regression, artificial neural network, and fuzzy logic prediction of 28 days compressive strength of concrete. *Front. Struct. Civ. Eng.* **2017**, *11*, 90–99.

Comment [M18]: Shenzhen, China, 13-16 August 2013.

Comment [M19]: ASTM International.

Comment [M20]: ASTM International

Comment [M21]: Elsvier S.P. Company, New York.

Comment [M22]: 08

Comment [M23]: Los Angeles.

41. Li, X.; Khademi, F.; Liu, Y.; Akbari, M.; Wang, C.; Bond, P.L.; Keller, J.; Jiang, G. Evaluation of data-driven models for predicting the service life of concrete sewer pipes subjected to corrosion. *J. Environ. Manag.* **2019**, *234*, 431–439.
42. Dewi, S.M.; Nuralinah, D. The Recent Research on Bamboo Reinforced Concrete. In Proceedings of the MATEC Web of Conferences, EDP Sciences, Indonesia, 9 March 2017; Volume 103, p. 2001.
43. Nathan, S. Application of Bamboo for Flexural and Shear Reinforcement in Concrete Beams. Clemson University, Clemson, South Carolina, United States, 2014.
44. Khare, L. Performance Evaluation of Bamboo Reinforced Concrete Beams; UT Arlington, Arlington, Texas, United States, 2005.
45. Mishra, M.; Agarwal, A.; Maity, D. Neural-network-based approach to predict the displacement of plain, steel-reinforced, and bamboo-reinforced concrete beams from experimental data. *SN Appl. Sci.* **2019**, *1*, 584.
46. FEMA 356 Standard. Prestandard and Commentary for the Seismic Rehabilitation of Buildings; American Society of Civil Engineers, 1801 Alexander Bell Drive, Reston, Virginia, November 2000.
47. New Zealand Standard. *Code of Practice for the Design of Concrete Structures*; Part 1; Standards New Zealand, Wellington, New Zealand, 1995.
48. Paulay, T.; Priestley, M.J.N. *Seismic Design of Reinforced Concrete and Masonry Buildings*; Wiley Interscience: New York, 1992.

Publisher's Note: MDPI stays neutral with regard to jurisdictional claims in published maps and institutional affiliations.

© 2020 by the authors. Submitted for possible open access publication under the terms and conditions of the Creative Commons Attribution (CC BY) license (http://creativecommons.org/licenses/by/4.0/).

Comment [M24]: EDP Sciences, Indonesia.

Comment [M25]: Clemson, South Carolina, United States.

Comment [M26]: UT Arlington, Arlington, Texas, United States.

Comment [M27]: American Society of Civil Engineers, 1801 Alexander Bell Drive, Reston, Virginia.

Comment [M28]: Standards New Zealand.

Comment [M29]: New York.